NACA RM A54F14

Superceded by TN 3790

NACA

RESEARCH MEMORANDUM

ANALYSIS OF WIND-TUNNEL TESTS AT LOW SPEEDS OF A
FOUR-ENGINE PROPELLER-DRIVEN AIRPLANE
CONFIGURATION HAVING A WING WITH
40° OF SWEEPBACK

By George G. Edwards and Donald A. Buell

Ames Aeronautical Laboratory
Moffett Field, Calif.

CLASSIFICATION CHANGED TO *Unclassified*
BY AUTHORITY OF *NASA RA # 94*
ON *12/14/55* OF *OSC*

NATIONAL ADVISORY COMMITTEE
FOR AERONAUTICS
WASHINGTON
October 8, 1954

RM-A54F14

CO█████████L
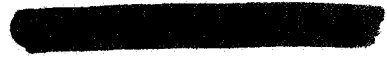
NATIONAL ADVISORY COMMITTEE FOR AERONAUTICS

RESEARCH MEMORANDUM

ANALYSIS OF WIND-TUNNEL TESTS AT LOW SPEEDS OF A
FOUR-ENGINE PROPELLER-DRIVEN AIRPLANE
CONFIGURATION HAVING A WING WITH
40° OF SWEEPBACK

By George G. Edwards and Donald A. Buell

SUMMARY

An investigation has been conducted to determine the effects of operating propellers on the longitudinal characteristics of a four-engine tractor airplane configuration having a 40° swept wing with an aspect ratio of 10. Results of wind-tunnel tests of a model representing such an airplane configuration (recently published) have shown these effects to be of most concern in the low-speed high-thrust flight regime. In the present report these data are analyzed to determine the source of the various effects and to indicate how the adverse effects can be reduced. The data on which the analysis is based were obtained in tests of a semispan model with reflection-plane mounting, representing the right-hand side of a hypothetical airplane. Single-rotation, right-hand propellers were operated at values of thrust coefficient ranging from 0 to 0.9 per propeller. The thrust coefficient was sufficient to simulate 10,000 horsepower per engine at sea level at speeds down to 120 miles per hour, assuming the model to be 1/12 scale. Variations in the model geometry included several heights and incidences of the horizontal tail as well as tail removed, two arrangements of extended split flaps, several propeller-blade angles, and independent as well as simultaneous operation of the inboard and outboard propellers.

The analysis indicates that the large variations of longitudinal stability with angle of attack resulted primarily from passage of the tail into and out of the slipstream. The slipstreams also created large lift increments on the wing, particularly with flaps deflected, which resulted in increases in stability (with increasing thrust coefficient) from the outboard propeller and decreases in stability from the inboard propeller. It was concluded that the longitudinal stability characteristics of the model could be improved by moving the nacelles outward, increasing the tail height, and reducing the tail span. Estimates of the stability with nacelles moved 0.1 of the semispan outboard of their original position are shown, along with estimates of rolling and yawing moments resulting from loss of thrust on an outboard engine.

CO█████AL

The propulsive characteristics of the model are presented and compared with those of the isolated propeller.

INTRODUCTION

The potentialities of the turbine-propeller propulsion system, particularly with regard to take-off and range characteristics of multiengine airplanes, have stimulated interest in the long-range turboprop airplane designed to fly at high subsonic speeds. A practical airplane configuration for this application appears to be one utilizing a sweptback wing of high aspect ratio in combination with tractor-mounted supersonic propellers. The effects of these highly loaded propellers on the flow over the swept wing and tail surfaces and the consequent effects on the longitudinal characteristics of the airplane cannot be estimated with confidence on the basis of existing experimental data or by theoretical methods. Applicable experimental data are meager, and existing theoretical methods, developed for airplanes with low propeller-disc loadings and unswept wings, are of doubtful validity for the arrangement considered.

An investigation has been conducted in the Ames 12-foot pressure wind tunnel to determine the longitudinal characteristics of a representative multiengine airplane configuration with sweptback wing of high aspect ratio. The investigation included wind-tunnel tests of a model with and without supersonic-type propellers. The power-off longitudinal characteristics of several combinations of the components of this airplane configuration have been presented in references 1 to 4. The characteristics of the propeller are reported in reference 5. The results of power-on tests at high subsonic speeds have been presented and analyzed in reference 6 and the results obtained at low speeds have been presented in reference 7, the latter without analysis.

The present report is concerned with an analysis of the low-speed data presented in reference 7. The sources of the large effects of operating propellers indicated in the low-speed data are traced in an effort to indicate those design features which would reduce adverse effects of operating propellers on the longitudinal characteristics of this type of airplane. Calculated static longitudinal stability characteristics are presented for a revised airplane configuration. Also investigated is the propulsive efficiency of the configuration tested and its relation to the efficiency of the isolated propeller.

NOTATION

A　　　upflow angle, average angle of local flow at the 0.7 propeller radius on the horizontal center line of the propeller plane, measured with respect to the thrust axis in a plane parallel to the plane of symmetry

a　　　mean-line designation, fraction of chord over which design load is uniform

a_t　　lift-curve slope of the isolated tail

a_w　　lift-curve slope of the model, tail off

$b/2$　　wing semispan perpendicular to the plane of symmetry

b'　　propeller-blade width

C_L　　lift coefficient, $\dfrac{\text{lift}}{qS}$

C_l　　rolling-moment coefficient,
$$\frac{\text{rolling moment (for complete airplane)}}{q(2S)b}$$

C_m　　pitching-moment coefficient about the quarter point of the wing mean aerodynamic chord, $\dfrac{\text{pitching moment}}{qS\bar{c}}$

$C_{m_{cg}}$　　pitching-moment coefficient about the center of gravity, $\dfrac{\text{pitching moment}}{qS\bar{c}}$ (See fig. 1(a).)

C_N　　propeller normal-force coefficient, $\dfrac{N}{q\,\dfrac{\pi D^2}{4}}$

C_n　　yawing-moment coefficient, $\dfrac{\text{yawing moment (for complete airplane)}}{q(2S)b}$

C_P　　power coefficient, $\dfrac{P}{\rho n^3 D^5}$

$C_{P_{total}}$　　sum of the power coefficients for both propellers

C_T　　thrust coefficient, $\dfrac{T}{\rho n^2 D^4}$

$C_{T_{total}}$ propulsive thrust coefficient for complete model (both propellers operating), $-\dfrac{SJ^2}{2D^2}\left(C_{X_{props\ on}} - C_{X_{props\ off}}\right)_{\alpha=constant}$

C_X longitudinal force coefficient, $\dfrac{X}{qS}$

c local wing chord parallel to the plane of symmetry

c' local wing chord normal to the reference sweep line (See table I.)

$\bar{c}$ wing mean aerodynamic chord, $\dfrac{\int_0^{b/2} c^2 dy}{\int_0^{b/2} c\ dy}$

c_{l_i} wing-section design lift coefficient

D propeller diameter

h maximum thickness of propeller-blade section

i_t incidence of the horizontal tail with respect to the wing-root chord

J propeller advance ratio, $\dfrac{V}{nD}$

l_t tail length, distance between the quarter points of the mean aerodynamic chords of the wing and the horizontal tail, measured parallel to the plane of symmetry

M free-stream Mach number

N normal force per propeller, perpendicular to the propeller shaft in a vertical plane

n propeller rotational speed

P shaft power per motor

q free-stream dynamic pressure, $\dfrac{\rho V^2}{2}$

q_t effective dynamic pressure at the tail

q_{ss} local dynamic pressure in the slipstream at the tail

R Reynolds number, based on wing mean aerodynamic chord

R' propeller-tip radius

r propeller-blade-section radius

S   area of the semispan wing, flaps off

S_t area of semispan tail

T   thrust per propeller, parallel to free stream

T_c thrust coefficient per propeller, $\dfrac{T}{\rho V^2 D^2}$

t   wing-section thickness

V   free-stream velocity

$\bar{V}$ tail volume, $\dfrac{l_t S_t}{\bar{c}S}$

X   longitudinal force, parallel to stream and positive in a drag-
            wise direction

Δx longitudinal distance from the quarter point of the mean aero-
            dynamic chord to a more rearward moment center

y   lateral distance from the plane of symmetry

α angle of attack of the wing chord at the plane of symmetry
            (referred to herein as the wing-root chord)

α_t angle of attack of the tail

β propeller-blade angle measured at 0.70 tip radius

β' propeller-blade-section angle

ϵ effective downwash angle

δ flap angle, measured relative to the local chord in planes
            normal to the reference sweep line

η propeller or propulsive efficiency

$\eta_t \dfrac{q_t}{q}$ tail-efficiency factor (ratio of the lift-curve slope of the
            horizontal tail when mounted on the model to the lift-curve
            slope of the isolated horizontal tail)

ρ mass density of air

φ   angle of local wing chord relative to the wing-root chord,
               positive for washin, measured in planes parallel to the plane
               of symmetry

$\dfrac{dC_m}{di_t}$ tail effectiveness parameter, measured at a constant angle of
               attack

                              Subscripts

av   average

trim   indicates condition of C_m or $C_{m_{cg}} = 0$

                           SELECTION OF MODEL

     Design of the model was based on some of the requirements of an
assumed airplane capable of long-range operation at a cruising speed
of 550 miles per hour at an altitude of 40,000 feet (M = 0.83) with wing
loadings of the order of 75 to 100 pounds per square foot ($C_L = 0.4$
to 0.5). This section of the report will be devoted to a brief discussion
of the factors which were considered in the design of the model. More
detailed discussion of this subject will be found in reference 1 (wing,
fuselage, fences), reference 2 (all-movable tail), reference 4 (nacelles),
reference 5 (propellers), and reference 7 (flaps).

     A semispan model was used in preference to a sting-mounted, full-
span model primarily because of the larger size permissible with the
semispan model, which resulted in increased Reynolds number as well as
more space within the model for oil, water, electric, and air lines.
Limitations of this arrangement are that only longitudinal characteris-
tics can be determined and that the direction of rotation of the pro-
pellers of the image wing is always opposite to that on the semispan
wing itself. The semispan model was designed to represent to 1/12 scale
the right-hand side of a hypothetical four-engine airplane having right-
hand propellers on the right wing and left-hand propellers on the left
wing. Details of the model are presented in figure 1 and in table I.
Photographs of the model mounted in the wind tunnel are presented in
figure 2.

     The wing incorporates a number of features designed to alleviate the
longitudinal stability difficulties usually associated with flow separa-
tion on sweptback wings of high aspect ratio. These features include
cambered wing sections having NACA four-digit thickness distribution
(comparatively large leading-edge radius), twist to reduce the load on
the outer portions of the wing, and chordwise fences on the upper surface

to reduce spanwise flow of the boundary layer and improve the spanwise distribution of load. The spanwise variation of twist and of section maximum thickness ratio shown in figure 1(b) was determined by the requirement that spanwise elements on the wing surfaces be linear. The wing design is therefore not necessarily optimum from an aerodynamic standpoint.

The fuselage (coordinates given in table I) was a half-body of revolution composed of a cylindrical midsection with simple fairings fore and aft. The wing was mounted high on the fuselage at 3° incidence as shown in figure 1(a). Compared to a lower position, this wing position is favorable in that it results in a higher thrust axis relative to the airplane center of gravity (more negative pitching moments due to thrust) while maintaining an under-wing mounting of the nacelle. The all-movable horizontal tail was arranged for testing at various heights (fig. 1(a)).

The shape and size of the nacelles (fig. 1(c)), as well as their locations with respect to the plane of the wing-root chord and leading edge, were governed to a considerable extent by considerations other than aerodynamic. These considerations included space requirements for electric motors and gear boxes for driving model propellers, and provisions for access and removal of these units without impairing the strength of the wing. The aerodynamic qualities of the nacelles in regard to drag and interference effects are probably adversely affected by the previously mentioned requirements which resulted in somewhat larger nacelles than would be required by the engines of the assumed airplane. As may be observed from figure 1(c), the nacelles were inclined downward at a considerable angle with respect to the wing (inboard nacelle -6.5° and outboard nacelle -7.0°). The resulting inclination of the thrust axes was intended to minimize the forces exciting first-order vibratory stresses in the propeller since, if the angles are properly selected, taking into account upwash from the wing, fuselage, and nacelles, the positive upflow angles induced at the low-speed high-gross-weight condition result in excitation forces equal in magnitude to those resulting from the negative upflow angles at the high-speed low-gross-weight condition. For the speed range of a modern high-performance airplane, this inclination of the thrust axis will result in about zero excitation for the design cruise condition. The thrust axis inclination for the model was calculated in accordance with the theoretical method described in Appendix B of reference 8 to provide zero upflow at the assumed cruise condition ($C_L = 0.40$, $M = 0.83$). The adequacy of such calculations was subsequently verified in the investigation of reference 9 wherein the actual upflow angles were measured on the model.

A three-blade supersonic propeller, designated the NACA 1.167-(0)(03)-058 and having right-hand rotation, was used in the high Mach number tests of the model, reported in reference 6. This propeller was a 1/12-scale model of a propeller for the assumed airplane, designed to absorb 5000 horsepower with an efficiency of 75 percent at a forward

Mach number of 0.83 and an altitude of 40,000 feet. The high-speed tests reported in reference 6 were conducted with propellers operating at approximately full-scale Mach numbers, blade angles, and advance ratios. For the low-speed tests reported in reference 7 and analyzed herein, however, a thicker propeller was necessary because of the very high blade loadings accompanying operation in the wind tunnel at an air density of 6 atmospheres. This propeller, designated the NACA 1.167-(0)(05)-058, was identical to the NACA 1.167-(0)(03)-058 propeller except that the blade thicknesses were increased by a factor of 5/3 at all radial stations. Blade-form curves for this propeller are presented in figure 3. The low-speed tests reported in reference 7, herein discussed, were conducted with propellers operating at approximately full-scale blade angles and advance ratios, but at reduced forward speed due to load limitations of the propeller and power limitations of the model motor and gear box. It should be pointed out that in consequence the model propeller operated with section Mach numbers which were everywhere subsonic during these tests at low speeds, whereas, the full-scale constant-speed, propeller would operate with supersonic local Mach numbers near the blade tip even at zero forward speed. More complete details and results of calibration tests of these propellers are given in reference 5.

Two arrangements of extended split flaps were tested on the model, as illustrated in figure 1(d). In the arrangement designated "inboard flaps," the flaps extended from the fuselage to the outer nacelle, and in the second arrangement, designated "outboard flaps," they extended from the inboard nacelle to 70 percent of the semispan. The gaps between the flaps and the wing trailing edge, nacelles, and fuselage were sealed. The outboard-flap arrangement was devised after tests with inboard flaps showed severe destabilizing effects due to propeller operation.

TESTS

Test Conditions and Procedure

The majority of the tests upon which the data analysis is based were made at a Mach number of 0.082, a Reynolds number of 4,000,000, and a propeller-blade angle β of $26°$. The corresponding dynamic pressure q of the air stream was approximately 57 pounds per square foot. Other tests were made at Mach numbers of 0.082 to 0.165, Reynolds numbers of 4,000,000 to 8,000,000, and with propeller-blade angles from $21°$ to $36°$. The angle-of-attack range was $2°$ to $18°$. The model was tested both with and without the horizontal tail, flaps, and propellers. The model was tested with the tail at various angles of incidence and at heights of the hinge axis of 0, 0.05, 0.10, or 0.15 of the wing semispan (see fig. 1(a)). Both the inboard flaps and the outboard flaps (fig. 1(d)) were attached at $30°$ of deflection δ for all of the tests discussed herein.

At each angle of attack, the Mach number and the Reynolds number were held constant while data were obtained for several propeller rotational speeds from windmilling to the maximum attainable, the latter being limited by either the maximum power or the maximum rotational speed of the electric motor.

Propeller Calibration

The propeller was calibrated on a specially constructed calibration nacelle as described in reference 5. With this equipment the thrust characteristics of the propeller in the presence of the spinner and nacelle forebody were measured at several angles of attack for the range of test conditions covered in the tests of the complete model. Also measured, but not heretofore published, were the normal force characteristics of the propeller which included an increment of normal force due to the effect of slipstream on the nacelle forebody.

REDUCTION OF DATA

The shaft thrust (parallel to the propeller shaft) and the normal force (perpendicular to the propeller shaft) were determined from the propeller calibration (ref. 5) at Mach numbers, Reynolds numbers, propeller-blade angles, advance ratios, and upflow angles A corresponding to the complete-model test conditions. The upflow angle for the complete model without flaps and with power off was the average at the 0.7 propeller radius on the horizontal center line of the propeller plane and was based on the measured values presented in reference 9. These propeller forces were used to determine the thrust parallel to the free stream and hence the thrust coefficient T_c used herein. This thrust coefficient is essentially constant with upflow angle. Typical variations of thrust coefficient T_c with advance ratio J are shown in figure 4.

The results of the propeller normal-force measurements (which include the increment of normal force due to slipstream effect on the nacelle forebody) obtained during the calibration of the propeller (ref. 5) are presented in figure 5. The conditions for matching these data to those for the complete model were similar to those for matching T_c, except that in this case, the direct use of the measured values of A presented in reference 9 for the complete model without flaps and power off was not sufficiently accurate because of the close dependence of normal force on the value of A. Modification of these measured values of A was made to allow for changes in upwash due to lift changes caused by slipstream on the wing and by deflection of the flaps. The correction was made using

a theoretical value of the rate of change of upwash angle with lift coef-
ficient at the propeller planes, along with the increments of lift due to
slipstream and due to flaps on the wing as deduced from the force data.

In several instances, data are presented herein for a constant power
condition, based on an assumed model scale of 1/12. The relationships
between T_c and C_L shown in figure 6 were derived on the assumption of
a 200,000-pound airplane in level flight at sea level with constant-
speed propellers turning at 1715 rpm. Also shown in figure 6 are the
variations of propeller efficiency and blade angle with velocity, deter-
mined from the propeller calibration reported in reference 5.

TEST RESULTS

The basic data obtained in low-speed tests of the powered model
have been presented in reference 7. Figure 7 of this report is an example
of the basic data, that is, lift, longitudinal force, and pitching-moment
coefficients, plotted in conventional form for constant values of thrust
coefficient, T_c. The range of configurations and test conditions for
which data are available is indicated in table II of this report.

Increases in Reynolds number (to obtain flow conditions more nearly
like those at full scale) and in Mach number (to increase the stream
dynamic pressure and thus the accuracy of measurements) reduced the thrust
coefficient which could be obtained with the model motor power available
at any given propeller-blade angle. In figure 8 the longitudinal char-
acteristics of the model (tail off) at various Reynolds numbers and Mach
numbers are compared. The effects of changes in propeller-blade angle
on the longitudinal characteristics of the model are shown in figure 9.
It is apparent that within the range of these tests the effects of changes
in Reynolds number and Mach number are of secondary importance. The data
of figure 9 indicate somewhat larger effects of changes in propeller-blade
angle. The differences in pitching-moment characteristics of the model
may be attributed primarily to changes in propeller normal force and slip-
stream rotation accompanying changes in propeller-blade angle. The indi-
cated differences in longitudinal-force coefficient C_X, however, are
believed to be largely scatter resulting from inaccuracies in establishing
the thrust coefficient T_c. Most of the discussion will concern data
obtained at a Reynolds number of 4,000,000, a Mach number of 0.082, and a
propeller-blade angle of 26°, for which conditions the highest thrust
coefficients could be obtained.

DISCUSSION

The results presented in reference 7 show some rather large effects of operating propellers on the longitudinal characteristics of this airplane configuration at low speeds. In order to indicate the factors which caused the over-all observed effects, the discussion will begin with the results of an analysis of the data in terms of the various increments of lift and pitching moment derived from direct propeller forces, slipstream effects on the wing, and slipstream effects on the tail. Direct comparisons of the data are then presented to show the influence of configuration changes on the pitching-moment characteristics, followed by an analysis of static longitudinal stability in terms of several well-known parameters. The objective of this analysis is, of course, to indicate not only the magnitude of the various effects, but also the means whereby the adverse effects of propellers on static longitudinal stability can be reduced.

Components of the Lift Changes Due to Operating Propellers

The operating propellers create components of lift, either directly from the shaft thrust and normal force of the propeller or indirectly as a result of the effects of the propeller slipstream on the wing and the horizontal tail. These components of lift are important because not only do they affect the total lift but they usually influence the longitudinal stability and trim of the airplane.

Increments of lift from direct propeller forces.- The shaft-thrust and normal-force data measured in the propeller calibration were resolved into incremental lift coefficients, taking account of the upflow angles prevailing on the complete model as compared to those on the calibration nacelle (see section entitled "REDUCTION OF DATA"). The calculated incremental lift coefficients from each propeller operating on the model at several constant thrust coefficients are shown in figure 10 for a range of angles of attack. Since the over-all effect on lift is small, the data shown may be considered to apply to either the inboard or the outboard propeller operating with wing flaps up or with either of the two flap configurations. A check showed the differences in lift-coefficient increment for these various conditions to amount to less than 0.01.

Increment of lift from slipstream on the wing.- The increments of lift coefficient attributable to the effects of the propeller slipstream on the wing and rear portion of the nacelles have been calculated from the data for various model configurations and are shown in figures 11 and 12. The method of obtaining this incremental lift coefficient, $\Delta C_{L_{wing}}$, was as follows:

$$\Delta C_{L_{wing}} = C_{L_1} - C_{L_2} - \Delta C_{L_{propeller-nacelle \atop normal\ force}} - \Delta C_{L_{propeller\ shaft \atop thrust}}$$

where

C_{L_1} lift coefficient of the model with tail off and with propellers operating at given thrust coefficient

C_{L_2} lift coefficient of the model with tail off and with propellers off

This increment in lift coefficient includes power effects on the rear portion of the nacelle and all wing-nacelle interference resulting from the slipstream. Referring to figure 11, it may be seen that with flaps up, $\Delta C_{L_{wing}}$ was negative at angles of attack below 4° or 5°, despite the fact that portions of the wing immersed in the slipstream were operating at section lift coefficients of the order of 0.35, power off. Comparison of $\Delta C_{L_{wing}}$ for both propellers operating (flaps up or flaps down) with the sum of values of $\Delta C_{L_{wing}}$ measured for inboard and outboard propellers operated independently generally shows some positive interference lift. In regard to figure 12, it is noted that changing from inboard flaps to outboard flaps decreased $\Delta C_{L_{wing}}$ but had little effect on the rate of change of $\Delta C_{L_{wing}}$ with angle of attack.

Increment of lift from tail.- For a constant tail incidence the increment of lift due to the effects of power on the tail is dependent upon tail height and incidence as well as on flap configuration. However, the increment of lift due to the effects of power on the tail can hardly be discussed without reference to the pitching-moment changes involved, since the lift on the tail must be that to balance the airplane. This will be discussed in succeeding paragraphs.

Components of the Pitching-Moment Changes Due to Operating Propellers

The application of power results in changes of pitching moment, due in a large measure to the fact that the centers of the lift increments previously discussed are at some distance from the reference center of moments. The various components of the change in pitching moment can therefore be classified in the same manner as the lift changes of the previous section, that is, according to whether they arise from the direct forces of the propeller (normal force and thrust), or whether they result from the effects of the propeller slipstream on the wing or on the tail. The components will be considered in that order.

Increments of pitching moment from direct propeller forces.- The normal force of the propeller (including the increment in normal force

due to slipstream effect on the nacelle forebody) can be considered to
act in the plane of the propeller[1] and the pitching moment from this
source is simply the normal force times the distance to the moment center.
The increments of pitching-moment coefficient due to normal forces created
by the operating propellers are shown in figure 13. The swept-wing con-
figuration with tractor propellers inherently has larger pitching-moment
increments from propeller normal force than a corresponding straight-
wing configuration because the propeller must be farther forward to
maintain a given clearance between the wing and the inboard propeller tip.

The increments of pitching-moment coefficient due to shaft thrust
of the operating propellers (thrust parallel to the shaft times the dis-
tance to the moment center) are shown in figure 14. It is obvious that
changes in the vertical location of the propellers with respect to the
center of gravity can materially affect the magnitude of these increments
in pitching-moment coefficient.

Increment of pitching moment from slipstream on the wing.- The incre-
ments of pitching-moment coefficient attributable to the effects of the
propeller slipstream on the wing and on the rear portion of the nacelles
have been calculated from the data for various model configurations and
are shown in figures 15 and 16. The method of obtaining this incremental
pitching-moment coefficient, $\Delta C_{m_{wing}}$, was as follows:

$$\Delta C_{m_{wing}} = C_{m_1} - C_{m_2} - \Delta C_{m_{propeller-nacelle}} - \Delta C_{m_{propeller \ shaft}}$$
$$\text{normal force} \qquad \text{thrust}$$

where

C_{m_1} pitching-moment coefficient of the model with tail off and with
propellers operating at the given thrust coefficient

C_{m_2} the pitching-moment coefficient of the model with tail off and with
propellers off

and all pitching-moment coefficients are referred to the 1/4 point of the
mean aerodynamic chord.

The increments of pitching-moment coefficient due to the effects of
the slipstream on the wing are closely related to the local lift changes
which occur and their location along the span of the wing. Hence, such
configuration characteristics as spanwise position of the nacelles and
spanwise extent of the flaps are dominant factors affecting the magnitude
of this increment of pitching-moment coefficient. Referring to figure 15,
it is noted that with flaps up $\Delta C_{m_{wing}}$ is positive, due almost entirely
to the influence of the inboard propeller. There were no large changes
in the variation of $\Delta C_{m_{wing}}$ with α due to lowering the inboard flaps.

---

[1]The pitching moment of the propeller-nacelle combination (ref. 5)
about the intersection of the thrust axis with the plane of the propeller
was found to be negligible.

In figure 16 it can be seen that the change from inboard to outboard flaps made $\Delta C_{m_{wing}}$ much more negative but had little effect on its variation with α.

Increment of pitching moment from tail.- The increments of pitching-moment coefficient attributable to the effects of operating propellers on the tail (at constant incidence) were calculated as follows:

$$\Delta C_{m_{tail}} = \left(C_{m_{tail\ on}} - C_{m_{tail\ off}} \right)_{power\ on} -$$

$$\left(C_{m_{tail\ on}} - C_{m_{tail\ off}} \right)_{power\ off}$$

Figure 17 gives values of the increment for one tail incidence, flaps up, and demonstrates the large moments that are incurred from this source. These data also illustrate the importance of the vertical location of the horizontal tail on $\Delta C_{m_{tail}}$.

The pitching moment contributed by the tail can be expressed as

$$C_{m_{tail}} = - a_t\ \overline{V}(\alpha + i_t - \epsilon)\ \eta_t\ \frac{q_t}{q} \tag{1}$$

For a given tail incidence, the lift on the tail, and thus the pitching moment due to the tail, is dependent on the downwash and the dynamic pressure at the tail, both of which will be affected by operation of the propellers. A study of the effects of propeller slipstream on the parameters ϵ and $\eta_t(q_t/q)$ provides some insight into the flow changes at the tail which produce pitching-moment changes.

The parameter $\eta_t(q_t/q)$, calculated from the force data by means of the equation

$$\eta_t\ \frac{q_t}{q} = - \frac{dC_m}{di_t}\ \frac{1}{a_t\overline{V}} \tag{2}$$

is presented in figure 18 as a function of angle of attack for various constant thrust conditions and for propellers off. (The value of a_t was taken as 0.059 per degree based on experimental data for the isolated tail presented in reference 2.) Data are compared for two different tail heights (0 and 0.10 b/2), approximately one propeller radius apart, with flaps up and with either the inboard or the outboard flaps deflected. The data in figure 18 are useful for ascertaining the approximate location of the slipstream relative to the tail. It is observed that deflection of the inboard flaps moved the slipstream downward to the extent that it missed the high tail even at high angles of attack; whereas, deflection of the outboard flaps moved it down only a small amount in the region of the tail.

CO█████L

The effective angles of downwash ϵ, calculated from the force data by means of the equation

$$\epsilon = \alpha + i_t - \frac{\left(C_{m_{tail\ on}} - C_{m_{tail\ off}}\right)_{\alpha=constant}}{\dfrac{dC_m}{di_t}} \qquad (3)$$

are presented in figure 19. The variation of ϵ is affected by a number of factors, some of which have opposing effects, and the relative importance of each is difficult to ascertain from the data available. The data in figures 18 and 19 indicate that the variation of ϵ with α at constant T_c and the variation of ϵ with T_c at constant α are greatly dependent on the location of the tail relative to the slipstream. Also very important in its effect on ϵ is the location of the tail in the field of downwash from the wing itself. Over most of the angle-of-attack range, an increase of T_c increased the lift on the wing (see fig. 11) which by itself would increase the downwash and also move downward the point of maximum downwash. However, it can be seen in figure 19 that there is a general reduction in the effect of increasing T_c on ϵ for those instances where the tail is in the slipstream (see fig. 18).

Comparison of pitching-moment increments.- The relative magnitude of the various pitching-moment-coefficient increments due to the effects of power and an indication of the effects on static longitudinal stability are shown in figure 20 (flaps up) and figure 21 (inboard flaps deflected). In these figures only, the pitching-moment coefficients have been referred to a new moment center which is more representative of the vertical height of the center of gravity for the assumed full-scale airplane. The longitudinal location of this assumed center of gravity is maintained at the quarter point of the mean aerodynamic chord but its vertical location is lowered $0.10\bar{c}$ (see fig. 1(a)). The effect of this change of moment center is to nearly eliminate the shaft thrust contribution to pitching moments without materially changing any of the other increments. From figures 20 and 21 it may be observed that the propeller normal force contributed a general increase in slope of the pitching-moment-coefficient curve, even at zero thrust, and the effect was, as might be expected, essentially independent of changes of flap configuration or tail height. For constant T_c the slipstream on the wing contributed an increase in moment, but no general change in slope of the pitching-moment-coefficient curve. The tail contribution as a function of angle of attack was extremely variable compared to the other components. This was, of course, due to the variation in tail lift as the tail moved into or out of the slipstream. Changes of tail height and deflection of flaps strongly influenced the pitching moment contributed by the tail.

In figures 22 and 23 similar data are presented with the inboard and the outboard propellers operating independently (that is, with one propeller removed). These data show that the inboard propeller caused most

of the effects of power on the pitching-moment coefficient (flaps up or
flaps down), due primarily to the effects of the slipstream on the wing
and on the tail.

<div align="center">Effect of Configuration Changes on the Pitching-
Moment Characteristics of the Model</div>

The various components of pitching-moment and lift coefficients
discussed in the previous sections combine to give the characteristics
evident in the basic data (ref. 7). In the following discussion the
over-all effects of configuration changes on the pitching-moment char-
acteristics will be considered in the light of what is known concerning
the component effects.

Effects of variations of tail height and incidence.- The position of
the horizontal tail with respect to the slipstream is an important factor
affecting the tail contribution to the pitching moment, as was evident
from figures 20 through 23. The effects of changes in tail height on
the over-all pitching-moment characteristics of the model with flaps up
and propellers operating at several constant thrust coefficients are
shown in figure 24. Observing the changes in the pitching-moment-
coefficient curves for the tail-off condition (fig. 24), it is seen that
an increase in thrust coefficient resulted in a moderate positive increase
in dC_m/dC_L. The linearity of these curves was, however, little affected
by an increase in power. With the tail on, the pitching-moment charac-
teristics were decidedly nonlinear at thrust coefficients above zero, due
to passage of the outer portion of the tail into and out of the slipstream
(refer to fig. 18(a)). The abrupt change in the slope dC_m/dC_L to a more
negative value indicates entry of the tail into the slipstream. Increas-
ing the tail height increased the lift coefficient at which this reduction
in dC_m/dC_L began.

The pitching-moment characteristics of the model with the horizontal
tail at various heights are further compared in figure 25 where the
pitching-moment curves are arranged to show the effect of increasing
thrust coefficient for each tail height. The constant-power curve super-
imposed thereon shows how dC_m/dC_L for constant power differed from that
for constant thrust coefficient.

While comparable data for all four tail heights were obtained at
thrust coefficients T_c to only 0.4 (figs. 24 and 25), the range of
thrust coefficients was extended to 0.80 for two tail heights, 0 and
0.10 b/2. Figure 26(a) compares the pitching-moment characteristics for
the model with the flaps up and figure 26(b) compares the data for the
model with the inboard flaps deflected. The chief effect of the inboard
flaps was to deflect the slipstream downward (see fig. 18), resulting in

pitching-moment characteristics with the low tail that resemble those with the higher tail, flaps up.

The various factors affecting the tail contribution to dC_m/dC_L will now be examined to provide the basis for explaining and interpreting the large changes in power-on pitching-moment characteristics accompanying changes in tail height or deflection of the flaps. Using the relation expressing the pitching-moment coefficient due to the tail, equation 1, the following expression can be written (for a constant thrust or power condition and a constant angle-of-tail incidence):

$$\frac{dC_{m_{tail}}}{dC_{L_w}} = \frac{1}{a_w} \frac{dC_{m_{tail}}}{d\alpha} = -\frac{a_t}{a_w} \overline{V} \left\{ \left(1 - \frac{d\epsilon}{d\alpha} \right) \eta_t \frac{q_t}{q} + \alpha_t \frac{d[\eta_t(q_t/q)]}{d\alpha} \right\} \quad (4)$$

where

$$\alpha_t = \alpha + i_t - \epsilon$$

and the subscript w refers to the complete model less tail. It is ordinarily assumed that $\dfrac{dC_{m_{tail}}}{dC_L} \approx \dfrac{dC_{m_{tail}}}{dC_{L_w}}$; that is, the tail lift is neglected. A more accurate expression is

$$\frac{dC_{m_{tail}}}{dC_L} = \frac{\dfrac{dC_{m_{tail}}}{dC_{L_w}}}{1 - \left[\dfrac{\overline{c}}{l_t} \left(\dfrac{dC_{m_{tail}}}{dC_{L_w}} \right) \right]} \quad (5)$$

The values of a_t/a_w, $1-(d\epsilon/d\alpha)$, and $\eta_t(q_t/q)$ which appear in equation 4 and are assumed independent of tail incidence, are presented in figure 27 for various thrust conditions, flaps up. Similar information is given in figures 28 and 29 for two cases of flaps deflected. The effect of power-induced lift changes on $\dfrac{dC_{m_{tail}}}{dC_L}$ was significant as shown by the changes in a_t/a_w with T_c (which reflect the changes in a_w). For example, at an angle of attack of $5°$, flaps up, a_t/a_w decreased from 0.74 to 0.52 as T_c increased from 0 to 0.80. By itself, this represents a 30-percent change in $\dfrac{dC_{m_{tail}}}{dC_L}$. The value of a_t/a_w with flaps up was about the same as that with flaps deflected except at high angles of attack.

The effect of power on the effective-downwash term, $1-(d\epsilon/d\alpha)$, was erratic (figs. 27, 28, and 29), depending as it does on such diverse factors as changes in wing-generated downwash, changes in downwash from

the propeller, changes in velocity of the slipstream, and changes in the position of wing wake and slipstream relative to the tail. An indication of the location of the slipstream with respect to the tail is provided by the curves of $\eta_t(q_t/q)$ vs. α presented in figure 18 and repeated for convenience in figures 27, 28, and 29. It is important to note that with the high tail and with the inboard flaps deflected (a condition for which the curves of $\eta_t(q_t/q)$ indicate that the tail was out of the slipstream except at the higher angles of attack) the value of $1-(d\epsilon/d\alpha)$ decreased with increasing thrust coefficient at angles of attack up to about 10° (a destabilizing effect). With the low tail, the opposite effect occurred in that $1-(d\epsilon/d\alpha)$ increased.

The term $d[\eta_t(q_t/q)]/d\alpha$ which expresses the dependency of the tail contribution to stability on the tail load (eq. 4), has been evaluated from the test data and is presented in figures 30, 31, and 32 as a function of α. The value of α_t is also shown since it is the product of the terms α_t and $d[\eta_t(q_t/q)]/d\alpha$ which affects $dC_{m_{tail}}/d\alpha$ (eq. 4). The magnitude of the effect is dependent not only on thrust coefficient and tail position relative to the slipstream (these factors affecting $d[\eta_t(q_t/q)]/d\alpha$ primarily) but also on tail incidence through its effect on α_t. The effect of tail incidence on the pitching-moment curves is shown in figure 33 for tail heights of 0 b/2 and 0.10 b/2, flaps up. Similar data for the model with the flaps deflected are presented in figures 34 and 35. The effect of tail incidence is important at moderate to high thrust coefficients but only when the tail is entering or leaving the propeller slipstream where $d[\eta_t(q_t/q)]/d\alpha$ assumes the largest numerical values (figs. 30, 31, and 32). For such cases, the constant tail incidence pitching-moment curve is obviously a poor indicator of the longitudinal stability except at the trim lift coefficient.

Effects of changing flap configuration.- The power-on pitching-moment characteristics of the model with two arrangements of flaps and a tail height of 0.10 b/2 are presented in figure 36. Note that test data are compared at different tail incidences for the two flap configurations in order that similar trim conditions exist in the two cases. It is observed that with inboard flaps, the pitching-moment curves are nearly linear over the greater portion of the lift-coefficient range, but there is a progressive increase in dC_m/dC_L with increasing T_c. The linear portions of these curves extend over a lift range for which the curves of $\eta_t(q_t/q)$ vs. α (fig. 28) indicate that there was little, if any, direct contact of the slipstream with the tail surfaces. The increase in dC_m/dC_L with increasing T_c was due largely to the propeller normal forces (see fig. 13(b)).

The pitching-moment curves for the model with outboard flaps (fig. 36) are not linear, showing a distinct change of slope dC_m/dC_L

at lift coefficients well below the maximum. Comparison of these data
with the curves of $\eta_t(q_t/q)$ vs. α (fig. 29) indicates that dC_m/dC_L
became more negative because the tail entered the slipstream. Moving
the flaps from the inboard to the outboard location moved the effective
center of pressure of wing sections affected by them out along the span,
which not only produced more negative pitching moments at a given C_L
and T_c (apparent in fig. 36 in spite of the change of tail incidence) but
also, at a given C_L, reduced the change of pitching moment with increas-
ing T_c. The latter effect can be explained on the basis of the data in
figure 16 which show that the pitching-moment increment due to slipstream
on the wing with outboard flaps became more negative with increasing T_c;
whereas, with inboard flaps, it became more positive. Moving the flaps
outboard also caused a large reduction in effective downwash ϵ at all
thrust coefficients (as may be seen from fig. 19). This effect in com-
bination with the more negative pitching moments from the wing caused the
large negative tail incidence required to trim the model at moderate lift
coefficients.

Effect of single-propeller operation.- The data obtained with the
inboard and the outboard propellers operating independently are of con-
siderable interest, not only because they help to explain the large
effects of operating propellers on the model as tested, but because they
can be used as the basis for estimating the effects of configuration
changes such as moving the nacelles to other spanwise positions.

In figure 37 the pitching-moment characteristics of the model with
the tail off and both propellers operating are compared with similar data
with the inboard and outboard propellers operating independently. Data
are presented for the model with the flaps up and with the inboard flaps
deflected. The translation of the pitching-moment curves with increas-
ing T_c, evident in all of these data, is primarily the result of positive
pitching moments contributed by the propeller thrust. (As may be seen
from fig. 14, this increment of pitching-moment coefficient was essen-
tially independent of angle of attack at a given thrust coefficient.)
The data of figure 37 for the case of only the inboard propeller operating
show an increase in dC_m/dC_L with increasing T_c. This effect was caused
by the contributions of propeller normal force and slipstream effect on
the wing (see figs. 13 and 15). With outboard propeller only, the slope
of the pitching-moment curves decreased with increasing T_c. In this
case the portion of the wing affected by the slipstream lies behind the
moment center. Consequently, the moment due to slipstream effect on the
wing opposed the moment created by the outboard propeller normal force,
the latter moment being of considerably less magnitude than that from
the inboard propeller because of the more rearward location of the pro-
peller disc (see figs. 13 and 15). The changes in slope of the pitching-
moment curves caused by inboard and outboard propellers appear to be

approximately compensating since the data of figure 37 for both propellers
operating show little change in slope with increasing T_c and are nearly
linear.

Data similar to those in figure 37 are presented in figure 38 for
the model with tail at 0.10 b/2. It is seen that with outboard propeller
only, the pitching-moment curves were linear and dC_m/dC_L did not change
with T_c. On the other hand, with inboard propeller only, the linearity
and slope of the pitching-moment curves were greatly affected by increases
in T_c. Comparison of the data in figures 37 and 38 leads to the con-
clusion that the major part of the adverse effects of propeller operation
on the pitching-moment characteristics of the model was due to the
effects of the slipstream from the inboard propeller on the flow at the
tail.

Stick-Fixed Longitudinal Stability of the Model

The discussion up to this point has been concerned only with the
changes in lift and pitching moment due to power at arbitrary angles of
tail incidence. However, stick-fixed longitudinal stability is a function
of the lift and pitching moment for the particular tail incidence which
will trim the model at a given lift coefficient. In the ensuing dis-
cussion the effects of operating propellers on the longitudinal stability
will be presented for trim conditions.

Unless the subscript cg is used with the various parameters, it
is to be understood that the center of moments is at the quarter point of
the mean aerodynamic chord.

Effects of power on various longitudinal stability parameters.- Each
of the stability parameters in general use portrays the effects of power
in varying degrees depending on which parameter is used. The longitudinal
stability of the model with flaps up is presented in figure 39 in terms
of three of these parameters. The tail incidence for trim $(i_t)_{trim}$
was determined from the test data by straight-line fairing of C_m vs. i_t
for constant lift coefficient, extrapolating where necessary. The slope
of the pitching-moment curve $(dC_m/dC_L)_{trim}$ and the static margin (i.e.,
the distance in mean aerodynamic chords from the center of moments to the
neutral point) were determined by means of straight-line fairings of
dC_m/dC_L vs. C_m/C_L at constant lift coefficient, following the method
of reference 10 for the neutral point. In some instances data were not
available at a sufficient number of tail incidences in the proper range
to avoid some rather long extrapolations. Although the order of accuracy
under such circumstances is not high, the results are considered adequate
for discerning gross effects.

The variation of $(i_t)_{trim}$ with C_L, figure 39(a), shows effects of power similar to the pitching-moment curves (fig. 26(a), for example). A negative slope of the curves in figure 39(a) indicates positive stability; thus, at high T_c, the model was marginally stable at high lift coefficients with the low tail and at low lift coefficients with the high tail. The sources of the power effects are indicated by the following expressions developed from elementary considerations:

$$(i_t)_{trim} \equiv (\alpha_t - \alpha + \epsilon)_{trim} \tag{6}$$

and since

$$(\alpha_t)_{trim} = \frac{(C_m)_{tail\ off}}{\eta_t(q_t/q)\ a_t\overline{V}} \tag{7}$$

$$(i_t)_{trim} = \frac{(C_m)_{tail\ off}}{\eta_t(q_t/q)\ a_t\overline{V}} - (\alpha - \epsilon)_{trim} \tag{8}$$

The parameter $(dC_m/dC_L)_{trim}$ shown in figure 39(b), is the slope of the pitching-moment curve with the tail incidence for trim. It gives the same information as the $(i_t)_{trim}$ curve of figure 39(a) but is more directly associated with the pitching-moment curves and is thus somewhat easier to use when discussing pitching-moment components. A negative value indicates positive stability, as did the slope of the $(i_t)_{trim}$ curve. The sources of the power effects on this parameter may be observed in the terms of the following expressions for $(dC_m/dC_L)_{trim}$ which neglect the lift from the tail.

$$\left(\frac{dC_m}{dC_L}\right)_{trim} = \left(\frac{dC_m}{dC_L}\right)_{tail\ off} + \frac{dC_{m_{tail}}}{dC_L} \tag{9}$$

and using equations 4 and 7,

$$\left(\frac{dC_m}{dC_L}\right)_{trim} = \left(\frac{dC_m}{dC_L}\right)_{tail\ off} - \frac{a_t}{a_w}\left\{\overline{V}\left(1 - \frac{d\epsilon}{d\alpha}\right)\eta_t(q_t/q) + \right.$$

$$\left. \frac{C_{m_{tail\ off}}\dfrac{d[\eta_t(q_t/q)]}{d\alpha}}{a_t[\eta_t(q_t/q)]}\right\} \tag{10}$$

It is evident from equation (10) that the magnitude of the pitching-moment coefficient, tail off, can affect the tail contribution to stability if $d[\eta_t(q_t/q)]/d\alpha$ is not negligible. Figures 27 to 32 show the quantities making up the tail contribution as they are affected by power changes while figures 10 to 16 indicate the effects of power on the tail-off components of stability. The nonlinearities in the variation of $(dC_m/dC_L)_{trim}$ with C_L, shown in figure 39(b), are due largely to changes in the tail-load term.

The static margin, shown in figure 39(c), represents the maximum distance the center of gravity may be moved rearward without making the airplane unstable. It is normally the most convenient stability parameter where center-of-gravity travel is to be considered. It may be noted from figures 39(b) and 39(c) that for this configuration there were in some cases large differences between $(dC_m/dC_L)_{trim}$ and the static margin. The differences can be explained by means of the following equations which describe the moment relationship between the existing center of moments and a more rearward center of moments (indicated by a prime) separated by the distance Δx:

$$C_m' \cong C_m + \frac{\Delta x}{\bar{c}} C_L \tag{11}$$

$$\frac{dC_m'}{dC_L} \cong \frac{dC_m}{dC_L} + \frac{\Delta x}{\bar{c}} \tag{12}$$

It is understood that all derivatives are for constant tail incidence. If the model were trimmed about the original center of moments, these become:

$$C_m' \cong \frac{\Delta x}{\bar{c}} C_L \tag{13}$$

$$\frac{dC_m'}{dC_L} \cong \left(\frac{dC_m}{dC_L}\right)_{trim} + \frac{\Delta x}{\bar{c}} \tag{14}$$

Thus, $\Delta x/\bar{c}$ is the change in slope of the pitching-moment curve at the original tail incidence. Now, an additional increment of slope may occur when the model is retrimmed since this involves a change in α_t which, as may be seen from equation 4, can change the tail contribution to the slope of the pitching-moment curve if $d[\eta_t(q_t/q)]/d\alpha$ is not zero. Neglecting tail lift, this increment may be expressed

$$\Delta\left(\frac{dC_m'}{dC_L}\right) = -\Delta\alpha_t \frac{a_t}{a_w} \bar{V} \frac{d[\eta_t(q_t/q)]}{d\alpha} \tag{15}$$

but since

$$\Delta\alpha_t = \frac{C_m{}'}{\eta_t(q_t/q)\ a_t\overline{V}} = \frac{C_L(\Delta x/\overline{c})}{\eta_t(q_t/q)\ a_t\overline{V}} \tag{16}$$

$$\Delta\left(\frac{dC_m{}'}{dC_L}\right) = -\frac{C_L}{a_w}\frac{\Delta x}{\overline{c}}\frac{\dfrac{d[\eta_t(q_t/q)]}{d\alpha}}{\eta_t(q_t/q)} \tag{17}$$

For trimmed conditions about the new moment center

$$\left(\frac{dC_m{}'}{dC_L}\right)_{trim} \cong \left(\frac{dC_m}{dC_L}\right)_{trim} + \frac{\Delta x}{\overline{c}} - \frac{C_L}{a_w}\frac{\Delta x}{\overline{c}}\frac{\dfrac{d[\eta_t(q_t/q)]}{d\alpha}}{\eta_t(q_t/q)} \tag{18}$$

Setting $(dC_m{}'/dC_L)_{trim}$ equal to zero makes $\Delta x/\overline{c}$ the static margin, expressed as follows:

$$\text{static margin} = \left(\frac{\Delta x}{\overline{c}}\right)_{\substack{neutral \\ point}} \cong \frac{-(dC_m/dC_L)_{trim}}{1 - \dfrac{C_L}{a_w}\dfrac{\dfrac{d[\eta_t(q_t/q)]}{d\alpha}}{\eta_t(q_t/q)}} \tag{19}$$

This expression illustrates why the degree of longitudinal stability indicated by the static margin was at times much larger than that indicated by the slope of the pitching-moment curve (see data for the high tail, figs. 39(b) and 39(c)). For example, figures 39(b) and 39(c) indicate that $C_L = 1.1$ and $T_c = 0.6$, the value of $(dC_m/dC_L)_{trim}$ is -0.31 whereas the static margin is 0.80.

<u>Effects of flaps on the longitudinal stability</u>.- The stability characteristics of the model with various flap configurations are presented in terms of $(dC_m/dC_L)_{trim}$ in figure 40 for tail heights of 0 b/2 and 0.10 b/2. The stability changes due to deflection of flaps (at constant thrust coefficient T_c) indicated in figure 40 can be correlated with changes in the various parameters appearing in equation (10) by reference to figures 27 to 32 and to the $C_{m_{tail\ off}}$ data in figures 33, 34, and 35. For example, consider the stability curves of figure 40 for a tail height of zero. With flaps up, there was a decrease of stability with increasing lift coefficient at lift coefficients above 0.4 (and thrust coefficients other than zero) due primarily to a decrease in $\eta_t(q_t/q)$ (fig. 27) as the tail moved out of the slipstream, and to

the negative values of $d[\eta_t(q_t/q)]/d\alpha$ (fig. 30) combined with increasing values of $C_{m_{tail\ off}}$ (fig. 33(a)).

With deflection of the inboard flaps, the slipstream was moved down-ward. Reference to figures 28 and 31 reveals that in this case $\eta_t(q_t/q)$ increased with increasing lift coefficient and $d[\eta_t(q_t/q)]/d\alpha$ became positive as the tail moved into the slipstream, both trends tend-ing to increase stability according to equation (10).

Considering next the stability curves in figure 40 for the model with a tail height of 0.10 b/2, it may be noted that with flaps up, the sta-bility increased with increasing lift coefficient (at constant thrust coefficients other than zero). This increase in stability was due pri-marily to the increase in $\eta_t(q_t/q)$ (fig. 27) and the positive value of $d[\eta_t(q_t/q)]/d\alpha$ (fig. 30) combined with positive values of $C_{m_{tail\ off}}$ (fig. 33). With inboard flaps deflected, the slipstream was deflected downward so that the tail remained out of the slipstream over most of the angle-of-attack range. Consequently, $\eta_t(q_t/q)$ did not change with lift coefficient and $d[\eta_t(q_t/q)]/d\alpha$ approached zero. There was also a sizeable reduction in $1-(d\epsilon/d\alpha)$ due to deflection of the flaps as may be seen in figures 27 and 28. The result was a loss of stability due to deflection of the inboard flaps (fig. 40, 0.10 b/2).

The stability curves in figure 40 for the model with outboard flaps may be interpreted in a manner similar to that outlined for the other cases, noting that in this case, $C_{m_{tail\ off}}$ was negative according to figure 35. It should be observed that with the outboard flaps deflected, a large negative angle of tail incidence (i_t to $-14°$) was required to trim the model at high angles of attack.

<u>Effects of vertical movement of the center of moments on the longi-tudinal stability</u>.- The effects on longitudinal stability of displacing the center of moments, or center of gravity, a distance $0.1\bar{c}$ below the original moment center (located at $\bar{c}/4$) are shown in figure 41 for the case of flaps up. It is observed that with the low tail the effect of lowering the center of gravity was to increase the longitudinal stability; whereas, with the high tail, the effect was either much reduced or actu-ally destabilizing. In both instances a change of tail incidence was required to retrim about the new center of gravity. The influence of tail height results from differences in the effect of tail load changes on stability which, as may be seen in equation (10), are in turn depend-ent upon the values of $d[\eta_t(q_t/q)]/d\alpha$.

Reduction of Adverse Effects of Propellers on Longitudinal Stability

The longitudinal characteristics of the subject model demonstrate some of the undesirable effects of propeller operation which should be suppressed or eliminated. There is, of course, a need for theoretical methods of calculating these effects of operating propellers on the longitudinal stability. However, the results of attempts to calculate power effects for this model entirely by means of existing theory have been discouraging. Such calculations may be considered in three parts which treat separately the effects due to direct propeller forces normal to and along the thrust axis, those due to slipstream action on the wing and nacelles, and those due to slipstream action on the flow at the tail. It is obvious that the pitching moment due to propeller thrust can be calculated accurately. The propeller normal force, and therefore the pitching moment due to it, can be calculated with fair accuracy for the isolated propeller, as has been demonstrated in reference 11. Note that the normal force of the isolated propeller (ref. 11) was in many instances very much less than the normal force indicated in figure 5 of this report for the combination of propeller and forward portion of the nacelle. The difference represents the normal force due to slipstream effect on the forward portion of the nacelle. Predictions of this normal force were not in good agreement with experiment.

An attempt was made to calculate the pitching moments arising from slipstream effects on the wing by consideration of the lift increments on the portions of the wing immersed in the slipstream. The calculations followed the method of reference 12 in which the propeller is regarded as an actuator disc (no rotation in the slipstream). Lift due to slipstream on the nacelles was neglected. The total lift increment due to propeller slipstream effects was predicted with adequate accuracy but the pitching-moment increment, which depends on the center of pressure of the lift increments on portions of the wing behind each propeller, was not predicted satisfactorily. The latter result is not surprising in view of the experimental pressure-distribution results presented in reference 13 which show a large effect of slipstream rotation on the distribution of incremental lift due to slipstream on the wing. Some of the discrepancy was, of course, due to neglect of slipstream effects on the nacelles.

Finally, with regard to prediction of the pitching-moment contribution of the tail, a strictly theoretical approach seems quite impractical for configurations such as considered herein where the tail passes into and out of the slipstream with changing angle of attack. Such predictions would require not only satisfactory estimates of the dynamic pressure and of the flow angles in the slipstream, but equally as important and probably more difficult, satisfactory estimates of the location of the slipstream relative to the tail. On the other hand, the longitudinal stability changes associated with slipstream effects on the tail have

been shown to be so serious that a more practical approach indicates the need for configuration changes to prevent the slipstream from striking the tail.

Assuming that the basic nature of the configuration (that is, a swept wing, four-engine tractor type) is to be retained, it appears that there are three ways of reducing or eliminating direct contact of the propeller slipstream with the horizontal tail and the associated large changes in longitudinal stability. The tail could be moved to a very high or a very low position, or the propellers could be moved farther outboard, or the tail span could be reduced. Since there are limitations on all three, a combination of these might be required.

When inboard flaps are used, a high tail position is more favorable than a low position from the standpoint that the flaps deflect the slip-stream downward, and in the case of the high tail, away from it. With the high tail it is also possible that the tail would remain out of the slipstream when the airplane is yawed. No large increase in the direc-tional and lateral control problems would be anticipated from increased tail height. However, a simple increase in the height of the tail will not in itself correct all deficiencies of this configuration. The tail operates in a downwash field which, even though the slipstream does not strike the tail, is responsive to power changes. It has been shown that the effect of power on the effective downwash was quite destabilizing in those instances when there were no compensating effects due to slipstream striking the tail. Additional configuration changes are therefore indicated.

An outward shift of the nacelles (with an accompanying rearward shift) produces favorable changes in the pitching moments arising from the propeller normal forces and from wing lift due to the slipstream (as well as decreasing the likelihood that the slipstream will strike the horizontal tail). For the tractor configuration considered, the pitching moment due to propeller normal force increases with angle of attack (at constant T_c) to produce a destabilizing effect and this can be reduced by outward shift of the nacelles. The pitching moment result-ing from wing lift due to slipstream is approximately a linear function of α (at constant T_c) but is stabilizing or destabilizing, depending upon the location of the effective center of pressure of this lift rel-ative to the moment center. If the nacelles are moved sufficiently far outward, the effect of power on the pitching moment arising from slip-stream on the wing can be made stabilizing and thus can be used as a means of counteracting the destabilizing effects from other sources. The amount that the nacelles can be moved outward is restricted by the accompanying increase in the lateral and directional control requirements needed in event of engine failure.

Estimate of longitudinal stability with the nacelles moved outward.- In the absence of flow surveys at the position of the tail, some rough

approximations were used to establish the position of the slipstream with
respect to the tail. This was necessary in order to judge how far out-
ward the nacelles need be moved to prevent the slipstream from striking
the tail. The calculations involved the determination of how much of
the outer portion of the tail would have to be immersed in the slip-
stream to produce the observed increase in the maximum value of $\eta_t(q_t/q)$
from $T_c = 0$ to $T_c = 0.8$. The assumption was made that the dynamic-
pressure distribution in the slipstream could be approximated with suf-
ficient accuracy for this purpose by that given in reference 14 for a
counter-rotating propeller ahead of a straight wing. It was further
assumed that the dynamic pressure due to the slipstream at each spanwise
station of the tail influenced the over-all effective value of $\eta_t(q_t/q)$
in proportion to the tail loading at that station as determined by the
Weissinger method. (Note that η_t is assumed to be independent of T_c.)
The results of these rough calculations are given in figure 42 for high
angles of attack where the slipstream effect is indicated to extend
farthest inboard. The figure indicates that an outward movement of the
nacelles of 0.1 b/2 would result in a small effect of power on $\eta_t(q_t/q)$
even with no alterations to the plan form of the horizontal tail. Further
improvement could be gained by a reduction of tail span.

Even though the slipstream does not actually strike the tail when the
nacelles are moved outward, it is likely that there would be some changes
in effective downwash due to power. The nature of these changes is illus-
trated in figure 43 where calculated effective downwash is presented for
inboard and outboard propellers at their original spanwise positions. In
the absence of force data for several tail incidences with propellers
operating independently, values of dC_m/di_t for calculating ϵ were
taken from power-off data for the case of outboard propeller only and
from data with both propellers operating for the case of inboard pro-
peller only. The data of figure 43 indicate that, with the outboard
propeller operating, an increase in thrust coefficient T_c produced a
decrease in the rate of change of ϵ with α. This stabilizing effect
of T_c on ϵ can be attributed partially to the spanwise variations of
wing lift which are caused by propeller operation. The data in refer-
ence 13 show that, for the model used in the present investigation, there
were large increments in normal force on those portions of the wing behind
the propeller due to propeller operation. These increments can be
expected to increase the downwash to the rear of and to decrease the
downwash to the side of the affected wing sections, due to trailing vor-
tices shed as a result of the large and concentrated changes in span
loading. For the present model having right-hand propellers, this effect
would be expected to be largest on the portion of the wing inboard of the
nacelle where the lift increment is the greatest. With the outboard pro-
peller operating, the resultant effect on the tail will depend on the
proximity of the tail to the trailing vortex from the section of the wing
behind the upgoing propeller blades, as well as on other factors such as
the rotation that remains in the slipstream and the interaction of the
slipstream and the wing-downwash field. The fact that a propeller as far

from the tail as the outboard propeller can produce a decrease in ϵ
attests to the possible strength of the effect. This fact also points
up the possibility that a propeller situated between the present inboard
and outboard positions may give a large stabilizing effect of downwash
if the major portion of the tail area lies inboard of the wing sections
immersed in the slipstream and if the rotation of the propeller has the
same direction as those on the model. Since the magnitude of the effect
is uncertain, it is neglected in present estimates of stability with the
nacelles moved outward. However, if the tail is no longer subjected to
the high dynamic pressure of the slipstream and if the tail-off stability
can be improved, the stability contributed by the tail will be a smaller
part of the model stability than was the case with the existing model,
and the importance of the effect of power on downwash will be diminished.

On the basis of the foregoing considerations, the assumption will be
made that if the nacelles are moved to stations 0.35 b/2 and 0.60 b/2,
to a first approximation the effects of power on the tail contribution to
stability can be neglected, leaving only the pitching-moment contributions
of the direct propeller forces and the slipstream effect on the wing to
be considered. It will be assumed that the nacelles are moved outward
to stations 0.35 b/2 and 0.60 b/2, the longitudinal position of the
nacelles being established by maintaining the distance between the pro-
peller planes and the reference sweep line, and the vertical position of
the thrust line being established on the basis of linear variation with
spanwise position. The calculation of the pitching moments due to pro-
peller normal force and shaft thrust for the new nacelle locations was
made simply by changing the previous values in proportion to the changes
in the lengths of the moment arms. These data are presented in figures 44
and 45.

The calculation of the new values of pitching-moment contribution of
the slipstream on the wing involved the use of the increments of lift and
pitching moment due to slipstream derived from the experimental data,
adjusted for changes in the areas of the wing immersed in the slipstream
and for changes in the moment arm resulting from outward movement of the
nacelles. It was assumed that for a given thrust coefficient the distri-
bution of incremental lift over each wing area in the slipstream was
unaltered by moving the propeller outward. The latter assumption implies
that for the case of flaps deflected, the flaps were moved outward with
the nacelles. The estimated pitching-moment contribution of the wing
derived on the above assumptions is presented in figure 46.

The estimated longitudinal stability of the model with nacelles moved
to stations 0.35 b/2 and 0.60 b/2 was calculated using the data in fig-
ures 44 to 46 and equation 10 (the tail lift was not neglected, however).
The slope of the pitching-moment curve, tail off and power off, was
assumed unchanged by movement of the nacelles and flaps. The factors
$1-(d\epsilon/d\alpha)$ and $\eta_t(q_t/q)$ were assumed equal to those measured with power
off, while $d[\eta_t(q_t/q)]/d\alpha$ was taken as zero. The results of these

calculations are given in figure 47 in terms of $(dC_m/dC_L)_{trim}$ for both the new and the original configurations. It is indicated that the revised configuration would have more nearly constant longitudinal stability than the original and would show little variation with thrust. Note that although the model with outboard flaps loses very little stability with increasing thrust, the tail incidence for trim is even more negative than on the original configuration (estimated at approximately -16° at $C_L = 1.6$, $T_c = 0.40$).

Estimates of lateral and directional moments due to asymmetric loss of power.- An outward shift of the nacelles, which has been suggested as one means of alleviating adverse effects of propellers on longitudinal stability, would be detrimental to the lateral and directional characteristics. Within the limitations of the data which have been obtained with the semispan model, estimates have been made of the rolling moments and yawing moments created by loss of thrust on the right outboard nacelle and are shown in figure 48 for an angle of attack of 14°. The lateral center of pressure of the lift increment on each area of the wing affected by slipstream was estimated, on the basis of the pressure data in reference 13, to be located at a distance of one-half the radius of the propeller inboard of the thrust axis. This lateral center of pressure was used for all flap configurations. The direct propeller forces were assumed to act at the thrust axes.

The values of rolling-moment coefficient that are shown in figure 48 are, of course, only part of that which the ailerons may have to counteract in case of engine failure. The large yawing-moment coefficient caused by loss of thrust on an outboard engine (see fig. 48) may be expected to result in additional rolling moment due to yawing. The estimates in figure 48 show that moving the nacelles outward produces an increase of about 15 percent in rolling-moment coefficient for the engine-out condition. The increase in yawing moment amounts to about 20 percent.

Propulsive Characteristics

The propeller thrust, denoted by T_c, was not available in its entirety as propulsive thrust on the model. The propulsive thrust of the two propellers (i.e., the longitudinal force of the semispan model with power on minus the longitudinal force with power off, at a constant angle of attack) was calculated and converted to the propeller-thrust coefficient $C_{T_{total}}$ (note that $C_{T_{total}}$ is for two propellers). Figure 49(a) presents the propulsive-thrust characteristics of the model with flaps up (tail off) at two angles of attack, along with the power characteristics for both propellers. Also shown in figure 49(a) for comparison are the thrust and power characteristics of a pair of isolated propellers operating at approximately zero inclination to the airstream. At the

CO█████AL

lower angle of attack (6.1°) the propellers on the model also operated at approximately zero inclination.

In the calculation of propulsive efficiency, it has been suggested by Betz in reference 15 that the propellers be credited for the lift created by their operation. This can be done in several ways and with varying results. In the present study, the propellers were credited with an increment of thrust equal to the change in induced drag associated with the change in lift attributable to the propellers. This induced drag was calculated for an assumed elliptic span load distribution and was added to the propulsive thrust $C_{T_{total}}$ presented in figure 49(a) (both determined at constant angle of attack). Propulsive efficiencies, calculated using propulsive thrust coefficients with and without this adjustment for lift created by the propellers, are presented in figure 49(b) as functions of advance ratio J. Also shown for comparison is the efficiency of the isolated propeller. Data are presented for three different propeller-blade angles and for two different angles of attack of the model. Note that figure 49(b) also gives the thrust coefficient T_c (used previously in the discussion of stability) in order to relate the efficiency curves to this parameter. At an angle of attack of 6.1°, the propulsive efficiency of the model with flaps up was less than 3 percent below the efficiency of the isolated propellers at thrust coefficients of 0.1 or larger. A larger loss in efficiency is indicated at 14.3° angle of attack, although roughly half is offset by the lift creditable to the propeller.

The variation of the propulsive efficiencies with angle of attack is shown in figure 49(c) for constant values of advance ratio in the higher thrust regime. Data are presented for several flap configurations. Also shown for comparison are the isolated-propeller efficiencies measured at angles of attack corresponding to the upflow angles A existing on the model. It is indicated that the flaps generally caused a loss in efficiency at a given angle of attack, though not necessarily at a given lift coefficient. The general decrease of efficiency with increasing angle of attack is lessened, particularly at the low values of J, by crediting the propellers with lift created by their operation.

CONCLUSIONS

The effects of operating propellers on the longitudinal characteristics of a representative four-engine tractor airplane configuration with a 40° sweptback wing have been investigated in wind-tunnel tests of a semispan model. An analysis of the data for low-speed, high-thrust conditions indicates the following conclusions:

1. The over-all effects of operating propellers on the static longi-
tudinal stability of the model at low speeds were generally large but
varied considerably throughout the lift-coefficient range.

2. Most of the objectionable static longitudinal stability variation
with lift coefficient observed with the configuration tested was due to
large changes in the pitching-moment contribution of the tail originating
from passage of the tail into and out of the slipstream.

3. Large lift increments due to slipstream may be expected on the
sections of the wing which are immersed in the slipstream, particularly
when the sections are equipped with flaps. Because of sweepback, the
lateral disposition of wing areas so affected determines whether the slip-
stream effect on the wing will be stabilizing or destabilizing.

4. Although the effects of propeller normal force and thrust on the
longitudinal stability of this configuration could be predicted with fair
accuracy, available theoretical methods failed to predict satisfactorily
the effects of propeller slipstream on the wing, nacelles, and horizontal
tail. However, for configurations similar to that used in the present
investigation, the available experimental data seem to furnish a good
starting point for making such predictions.

5. To avoid large longitudinal stability variation with lift coef-
ficient, the slipstream should not impinge on the tail. It is indicated
that one way to accomplish this with the configuration tested is by mov-
ing the propellers outward about 0.1 of the wing semispan. This modifica-
tion would also make the effect of propeller slipstream on the wing more
stabilizing and reduce the destabilizing effects of the propeller normal
forces. Calculations indicate great improvement of the longitudinal
stability characteristics both with flaps up and flaps down. The lateral
control required to offset the increase in rolling moment associated with
loss of the outboard propeller is estimated to be 15 percent more than for
the original configuration and the directional control, 20 percent more.

6. Other design changes tending to prevent the slipstream from
striking the tail and which do not affect the lateral and directional
control problem are reduction of the tail span and raising the horizontal
tail. The experimental results indicate that if the tail is placed high
enough to avoid the slipstream, the effect of power on the tail contri-
bution to stability will be destabilizing. This indicates that for the
configuration tested, some outward shift of the propellers would still be
required to produce satisfactory longitudinal stability characteristics.

7. Propulsive efficiencies for the complete configuration were approximately equal to the efficiency of the isolated propeller if, in calculating propulsive efficiency, the propellers were credited with the lift they produced.

Ames Aeronautical Laboratory
    National Advisory Committee for Aeronautics
        Moffett Field, Calif., June 14, 1954

REFERENCES

1. Edwards, George G., Tinling, Bruce E., and Ackerman, Arthur C.:
    The Longitudinal Characteristics at Mach Numbers up to 0.92 of a
    Cambered and Twisted Wing Having 40° of Sweepback and an Aspect
    Ratio of 10. NACA RM A52F18, 1952.

2. Tinling, Bruce E.: The Longitudinal Characteristics at Mach Numbers
    up to 0.9 of a Wing-Fuselage-Tail Combination Having a Wing With
    40° of Sweepback and an Aspect Ratio of 10. NACA RM A52I19, 1952.

3. Boltz, Frederick W., and Shibata, Harry H.: Pressure Distribution
    at Mach Numbers up to 0.90 on a Cambered and Twisted Wing Having
    40° of Sweepback and an Aspect Ratio of 10, Including the Effects
    of Fences. NACA RM A52K20, 1953.

4. Tinling, Bruce E., and Lopez, Armando E.: The Effects of Nacelles
    and of Extended Split Flaps on the Longitudinal Characteristics
    of a Wing-Fuselage-Tail Combination Having a Wing With 40° of
    Sweepback and an Aspect Ratio of 10. NACA RM A53D06, 1953.

5. Demele, Fred A., and Otey, William R.: Investigation of the NACA
    1.167-(0)(03)-058 and NACA 1.167-(0)(05)-058 Three-Blade Propellers
    at Forward Mach Numbers to 0.92 Including Effects of Thrust-Axis
    Inclination. NACA RM A53F16, 1953.

6. Sutton, Fred B., and Demele, Fred A.: The Effects of Operating Pro-
    pellers on the Longitudinal Characteristics at High Subsonic Speeds
    of a Four-Engine Tractor Airplane Configuration Having a Wing With
    40° of Sweepback and an Aspect Ratio of 10. NACA RM A53J23, 1954.

7. Edwards, George G., Buell, Donald A., and Dickson, Jerald K.: The
    Results of Wind-Tunnel Tests at Low Speeds of a Four-Engine
    Propeller-Driven Airplane Configuration Having a Wing With 40°
    of Sweepback and an Aspect Ratio of 10. NACA RM A53I28, 1953.

8. Rogallo, Vernon L.: Effects of Wing Sweep on the Upwash at the
    Propeller Planes of Multiengine Airplanes. NACA TN 2795, 1952.

9. Lopez, Armando E., and Dickson, Jerald K.: The Effects of Compress-
    ibility on the Upwash at the Propeller Planes of a Four-Engine
    Tractor Airplane Configuration Having a Wing With 40° of Sweepback
    and an Aspect Ratio of 10. NACA RM A53A30a.

10. Schuldenfrei, Marvin: Some Notes on the Determination of the Stick-
    Fixed Neutral Point From Wind-Tunnel Data. NACA WRL-344, 1943.
    (Formerly NACA RB 3I20)

11. Demele, Fred A., and Otey, William R.: Investigation of the Normal
    Force Accompanying Thrust-Axis Inclination of the NACA
    1.167-(0)(03)-058 and the NACA 1.167-(0)(05)-058 Three-Blade
    Propellers at Forward Mach Numbers to 0.90. NACA RM A54D22, 1954.

12. Smelt, R., and Davies, H.: Estimation of Increase in Lift Due to
    Slipstream. R. & M. No. 1788, British A.R.C., 1937.

13. Kolbe, Carl D., and Boltz, Frederick W.: Effects of Operating
    Propellers on the Wing-Surface Pressures of a Four-Engine Tractor
    Airplane Configuration Having a Wing With 40° of Sweepback.
    NACA RM A53L29, 1954.

14. Sleeman, William C., Jr., and Linsley, Edward L.: Low-Speed Wind-
    Tunnel Investigation of the Effects of Propeller Operation at
    High Thrust on the Longitudinal Stability and Trim of a Twin-
    Engine Airplane Configuration. NACA RM L52D04, 1952.

15. Betz, A.: Considerations on Propeller Efficiency. NACA TM 481,
    1928.

CO██████L

TABLE I.- GEOMETRIC PROPERTIES OF THE MODEL

Wing

  Reference sweep line: Locus of the quarter chords of sections
    inclined 40° to the plane of symmetry

  Aspect ratio (full-span wing) 10.0
  Taper ratio 0.4
  Sweepback . . . . 40°
  Twist . . . . -5°
  Reference sections (normal to reference sweep line)
    Root . . . . NACA 0014, a=0.8 (modified) c_{l_i}=0.4
    Tip . . . . NACA 0011, a=0.8 (modified) c_{l_i}=0.4
  Area (semispan model) . . . . 6.944 ft^2
  Mean aerodynamic chord . . . . 1.251 ft
  Flaps, extended from trailing edge . . . . 0.20 c'
  Incidence (measured in the plane of symmetry) . . . . 3°

  Fences are located at y/(b/2)=0.33, 0.50, 0.70, and 0.85.

Nacelles

  Frontal area (each) . . . . 0.208 ft^2
  Inclination (see fig. 1(c))
    Inboard . . . . -6.5°
    Outboard . . . . -7.0°

Propellers

  Diameter . . . . 1.167 ft
  Number of blades 3
  Propeller-activity factor (per blade) 188.4
  Propeller-blade thickness-chord ratio (0.70 radius) 0.05
  Solidity (per blade) 0.058
  Blade sections . . . . symmetrical NACA 16 series

Horizontal Tail

  Reference sweep line: Locus of quarter chords of sections inclined
    40° to the plane of symmetry

  Aspect ratio (full-span tail) 4.5
  Taper ratio 0.4
  Sweepback . . . . 40°

TABLE I.- GEOMETRIC PROPERTIES OF THE MODEL - Concluded

Horizontal tail (Continued)

Reference section (normal to reference sweep line) . . . . . NACA 0010
Tail length, l_t . . . . $3.25\bar{c}$
Area (semispan model) . . . . 1.387 ft^2
Mean aerodynamic chord . . . . 0.833 ft
Tail volume, $l_t/\bar{c}$ (S_t/S) 0.65
Tail heights (measured vertically from the fuselage center
  line to the hinge axis of the horizontal tail in wing
  semispans (see fig. 1(a)) 0, 0.05, 0.10, 0.15

Fuselage

Fineness ratio 12.6
Frontal area (semispan model) . . . . 0.273 ft^2
Fuselage coordinates:

Distance from nose, in.	Radius, in.
0	0
1.27	1.04
2.54	1.57
5.08	2.35
10.16	3.36
20.31	4.44
30.47	4.90
39.44	5.00
50.00	5.00
60.00	5.00
70.00	5.00
76.00	4.96
82.00	4.83
88.00	4.61
94.00	4.27
100.00	3.77
106.00	3.03
126.00	0

TABLE II.- RANGE OF TEST VARIABLES

Tail height	Type flaps	δ, deg	M	R, million	β, deg	i_t, deg
tail off	none	---	0.082	4	21	---
		---	.082	4	26	---
		---	.082	4	[a]26	---
		---	.082	4	[b]26	---
		---	.082	4	31	---
		---	.123	4	21	---
		---	.123	4	31	---
		---	.123	4	36	---
		---	.123	6	31	---
		---	.165	8	31	---
		---	.165	8	36	---
0	none	---	.082	4	26	0
		---	.082	4	26	-4
		---	.082	4	26	-8
		---	.123	4	31	-4
0.05 b/2	none	---	.082	4	21	-4
		---	.082	4	31	-4
		---	.123	4	21	-4
		---	.123	4	31	-4
		---	.123	4	36	-4
		---	.123	6	31	-4
		---	.165	8	31	-4
		---	.165	8	36	-4
0.10 b/2	none	---	.082	4	26	-4
		---	.082	4	[c]26	-4
		---	.082	4	[a]26	-4
		---	.082	4	[b]26	-4
		---	.082	4	26	0
		---	.082	4	26	-8
		---	.123	4	26	-4
		---	.123	4	[c]26	-4
		---	.123	4	31	0
		---	.123	4	31	-4
		---	.123	4	31	-8

Tail height	Type flaps	δ, deg	M	R, million	β, deg	i_t, deg
0.15 b/2	none	---	0.123	4	31	-4
tail off	Inbd.	30	.082	4	26	---
			.082	4	[a]26	---
			.082	4	[b]26	---
			.082	4	31	---
			.123	4	31	---
0	Inbd.	30	.082	4	26	0
			.082	4	26	-2
			.082	4	26	-4
0.10 b/2	Inbd.	30	.082	4	26	0
			.082	4	[a]26	0
			.082	4	[b]26	0
			.082	4	26	-2
			.082	4	26	-4
tail off	Outbd.	30	.082	4	26	---
0.10 b/2	Outbd.	30	.082	4	26	0
			.082	4	[a]26	0
			.082	4	[b]26	0
			.082	4	26	-8
tail off	Inbd.	60	.082	4	26	---
			.082	4	31	---
			.123	4	31	---
0.10 b/2	Inbd.	60	.082	4	26	0

[a]Inboard propeller only.
[b]Outboard propeller only.
[c]Negative thrust.
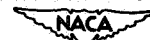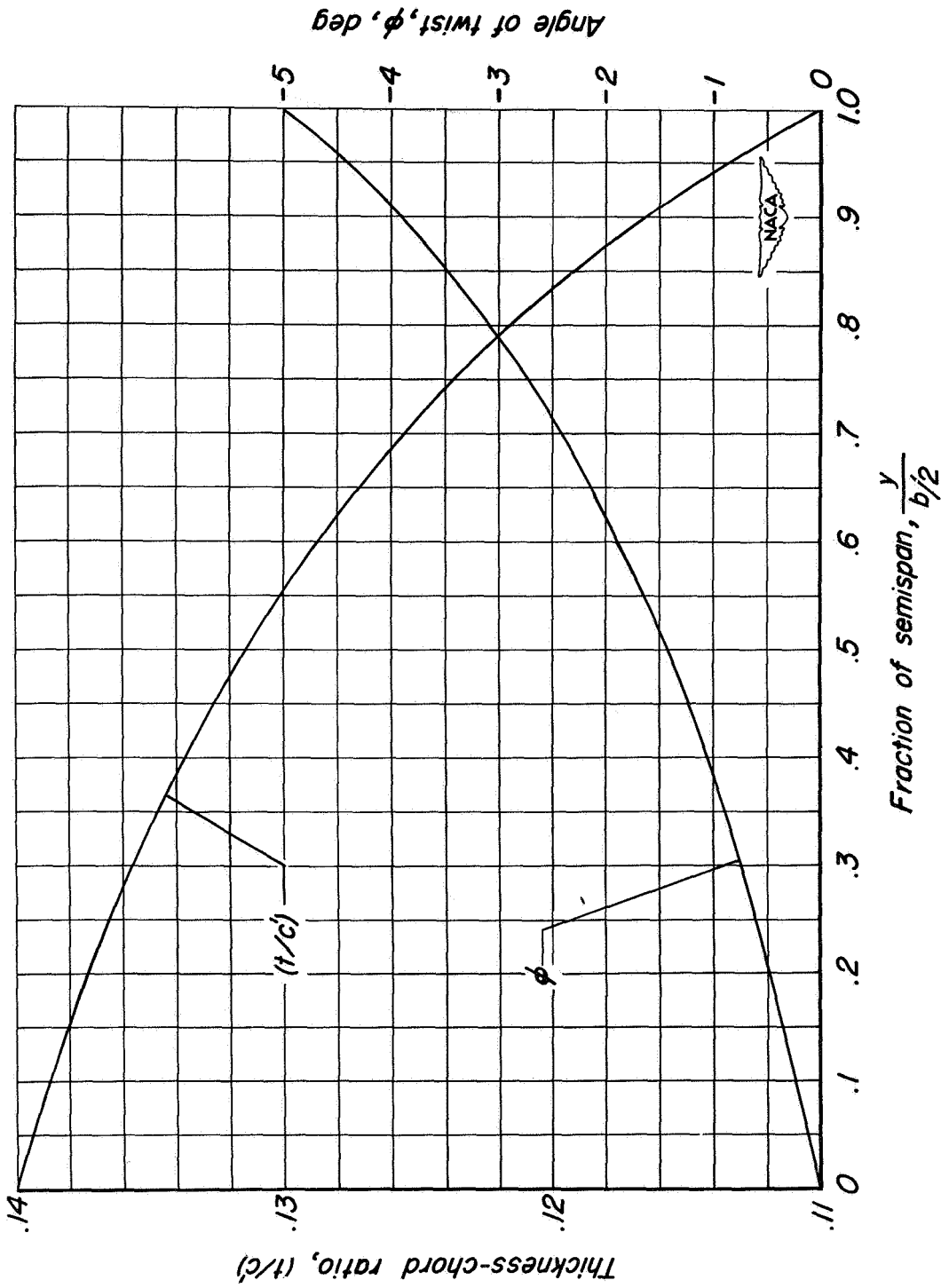
(b) Wing twist and thickness-chord ratio.

Figure 1.- Continued.

Nacelle coordinates

Sta	r_1		Sta	r_2
−5.00	0		2.00	0.350
−4.79	.385		3.00	.419
−4.58	.567		4.00	.616
−4.25	.788		5.00	.919
−3.95	.951		6.00	1.290
−3.25	1.242		7.00	1.685
−2.55	1.472		8.00	2.056
−1.80	1.670		9.00	2.359
−.80	1.871		10.00	2.556
0	1.985		11.00	2.625
2.00	2.100		30.50	2.625
12.00	2.100		32.50	2.450
			34.50	2.220
			36.50	1.825
			38.50	1.270
			40.50	.675
			41.50	.275
			42.25	0

All dimensions are in inches unless otherwise noted.

Plane of root chord and L.E. of wing

Local chord line extended

c̄/4

0.81

Inboard nacelle

−.59°

2.42

1.75

r_1

r_2

14.38

29.32

Prop ℄

+5.00

−6.5°

−1.43°

c̄/4

2.40 (to c̄/4)

Outboard nacelle

2.24

1.75

r_1

r_2

13.79

47.25

Sta 0.0

−7.0°

Sta 0.0

r_1

Sta 6.00

r_1

r_2

Thrust axis

Sta 24.00

r_2

Sta 36.00

r_2

NACA

(c) Dimensions of the nacelles.

Figure 1.- Continued.

Model with outboard flaps

0.125 in.

0.20c'
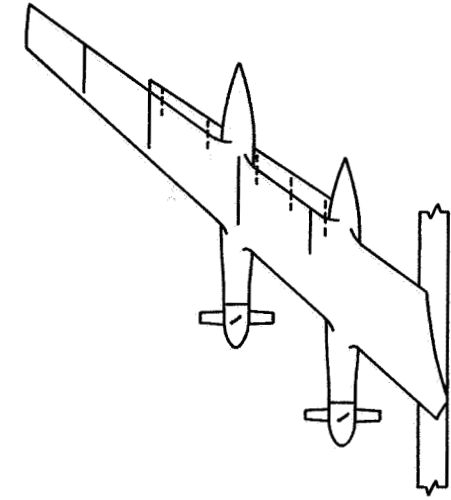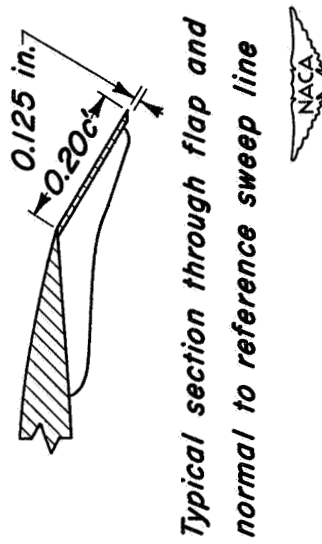
Typical section through flap and
normal to reference sweep line

NACA

0.85 b/2

0.70 b/2

0.50 b/2

0.33 b/2

0.25 b/2

Extended fence

Short fence
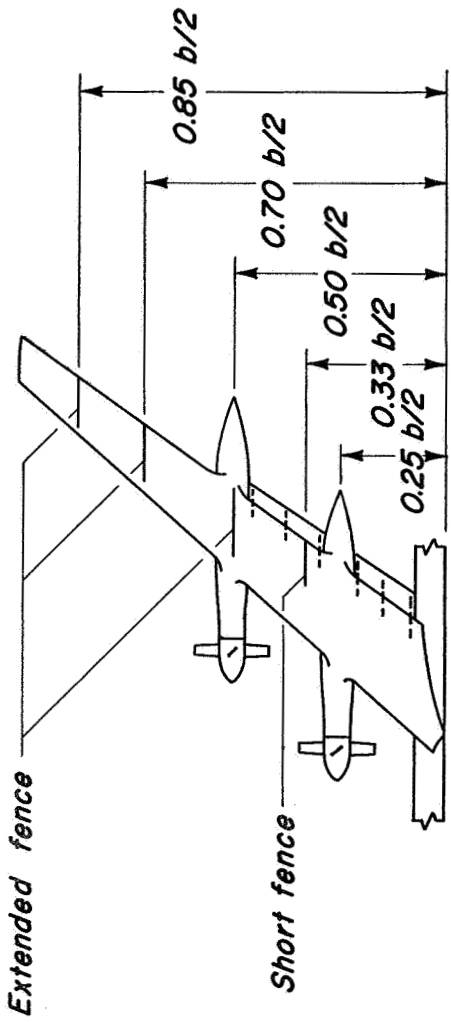
Model with inboard flaps

0.08 c

c

0.42 c

Extended

Short
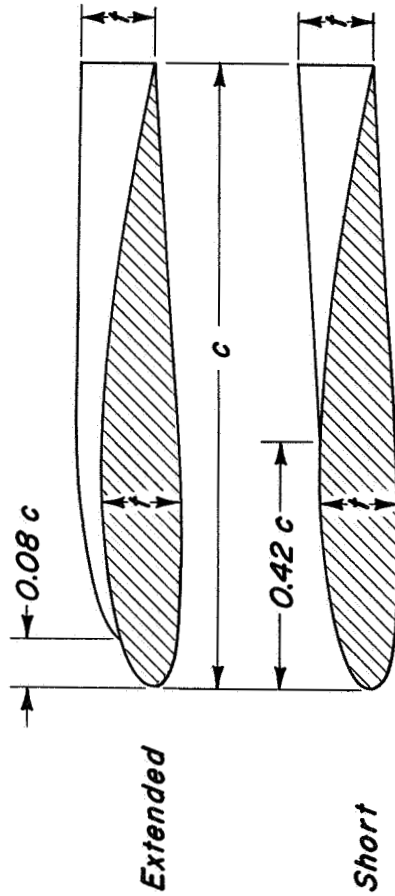
Typical sections through fences

(d) Fence and flap details.

Figure 1.— Concluded.
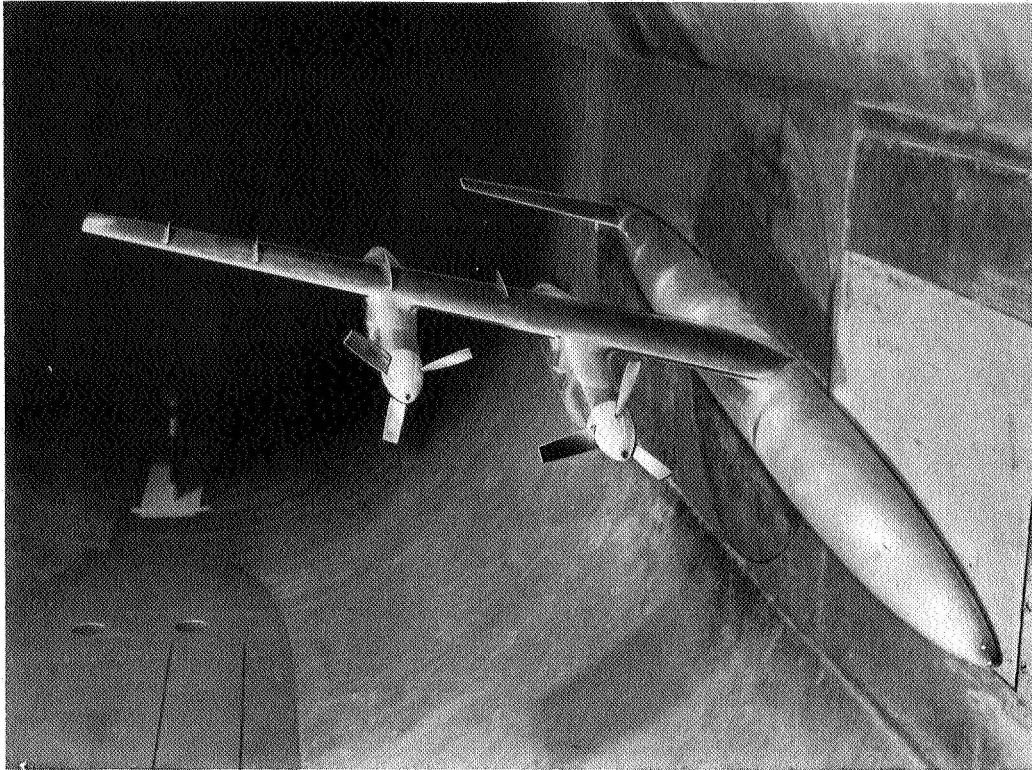
A-17444.1
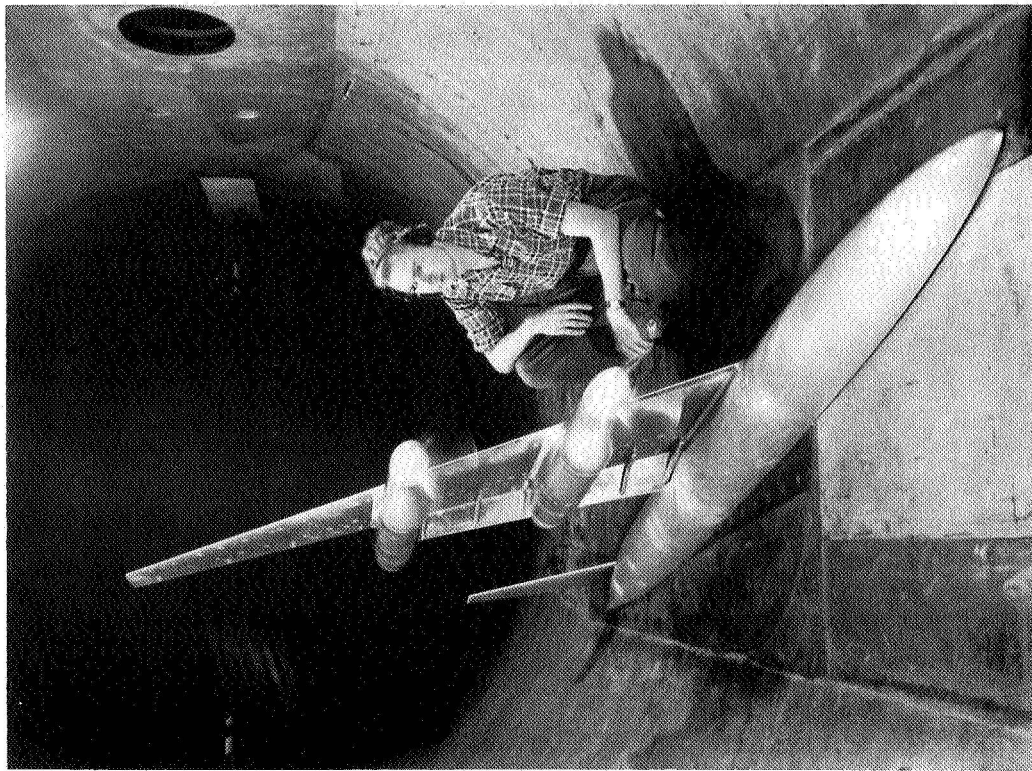
A-17525.3

Figure 2.- Model mounted in the wind tunnel.
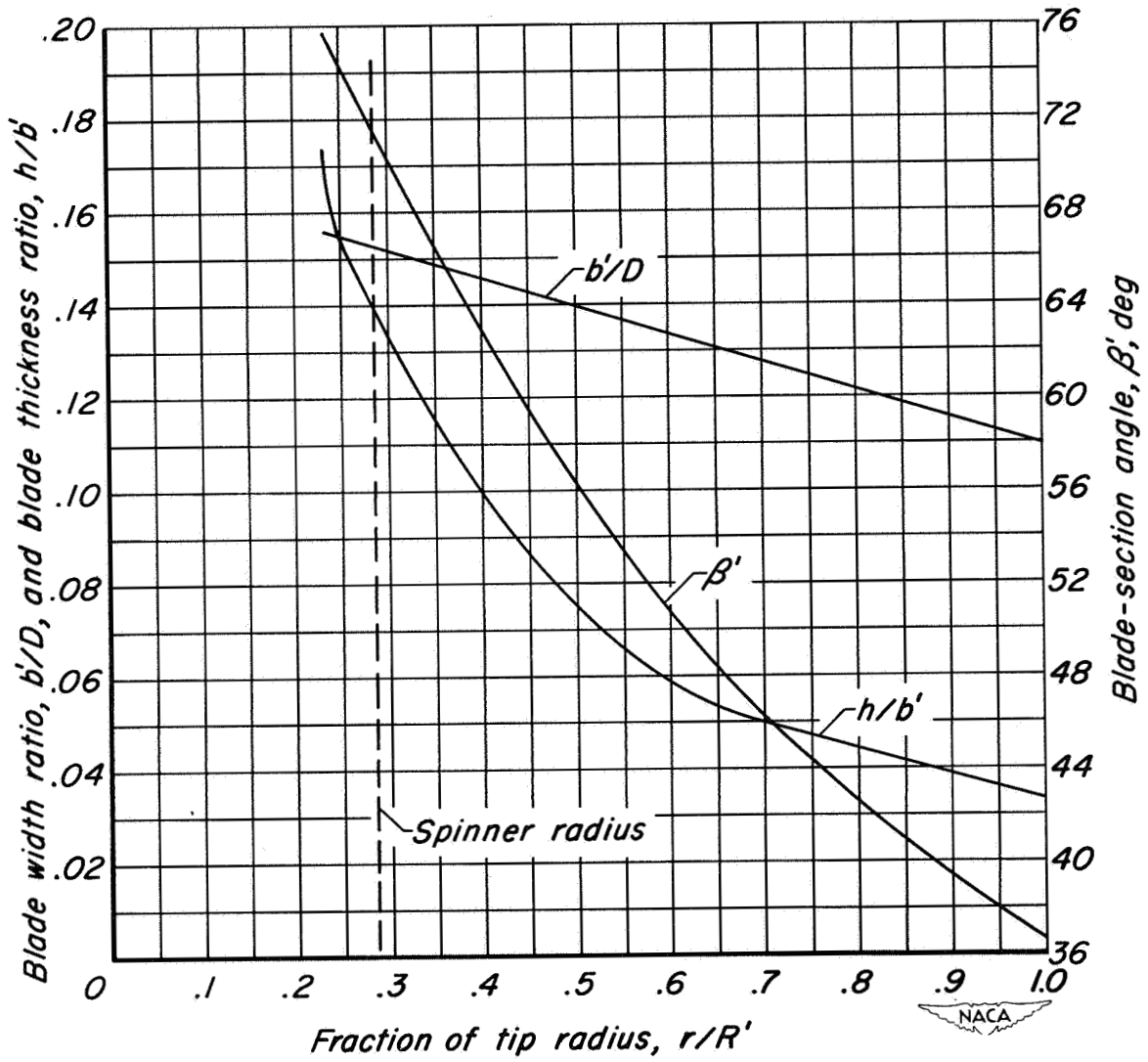
Figure 3.- Blade-form curves for the NACA 1.167-(0)(05)-058
three-blade propeller.
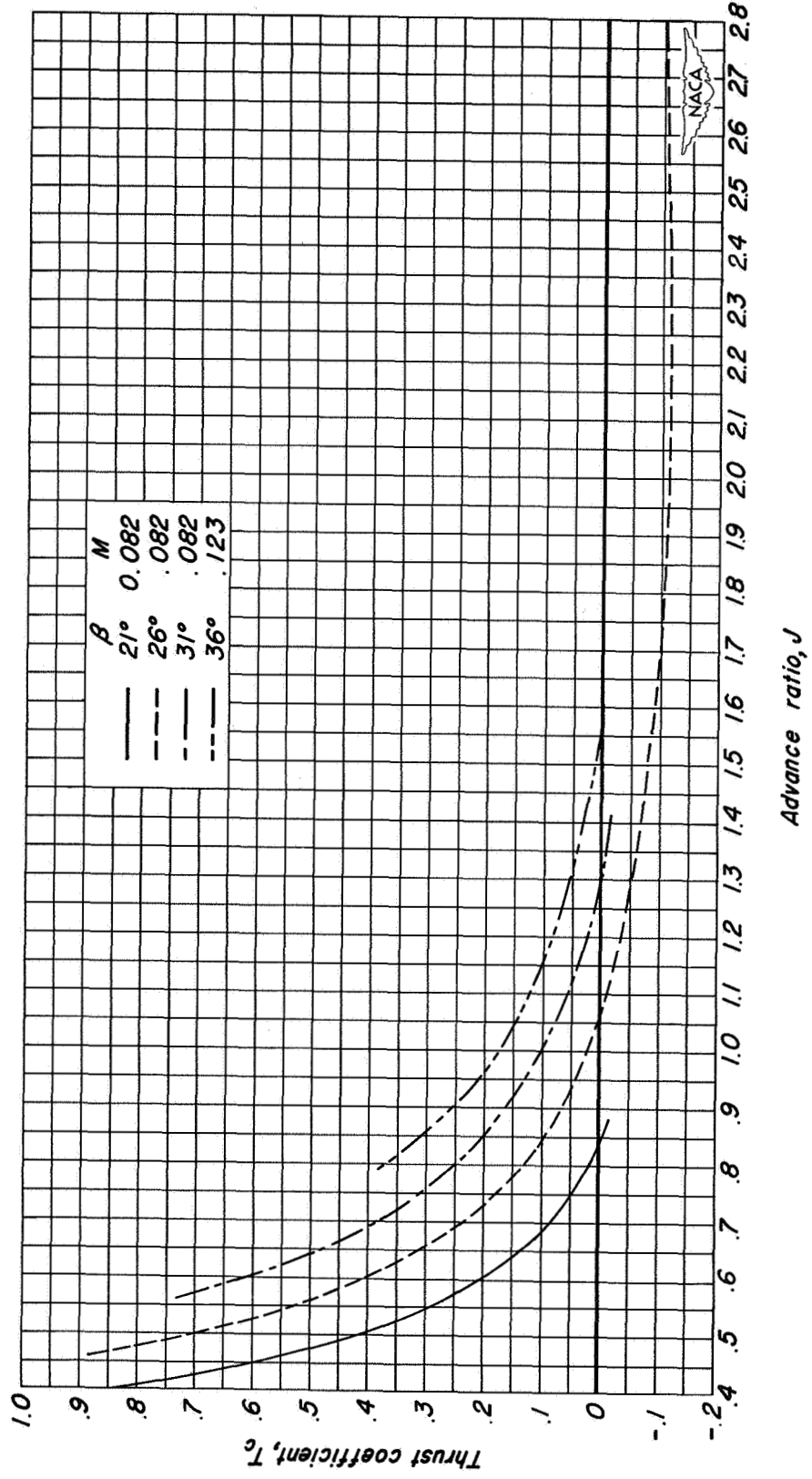
Figure 4.- The variation of T_c with J for the NACA 1.167-(0)(05)-058 propeller; $A = 0°$; $R = 4,000,000$.
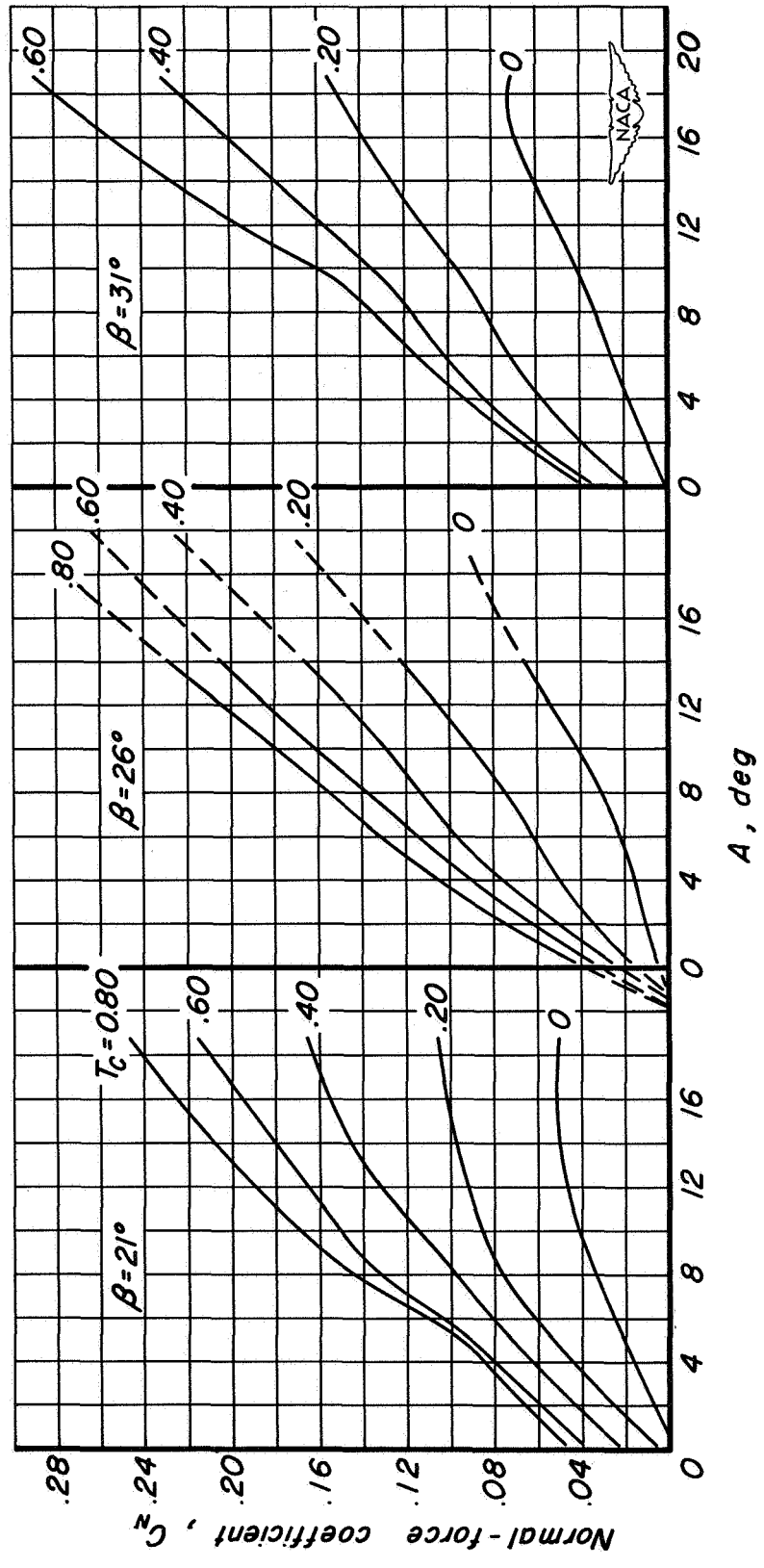
Figure 5.- Normal-force characteristics of the NACA 1.167-(0)(05)-058 propeller;
M = 0.082; R = 4,000,000.
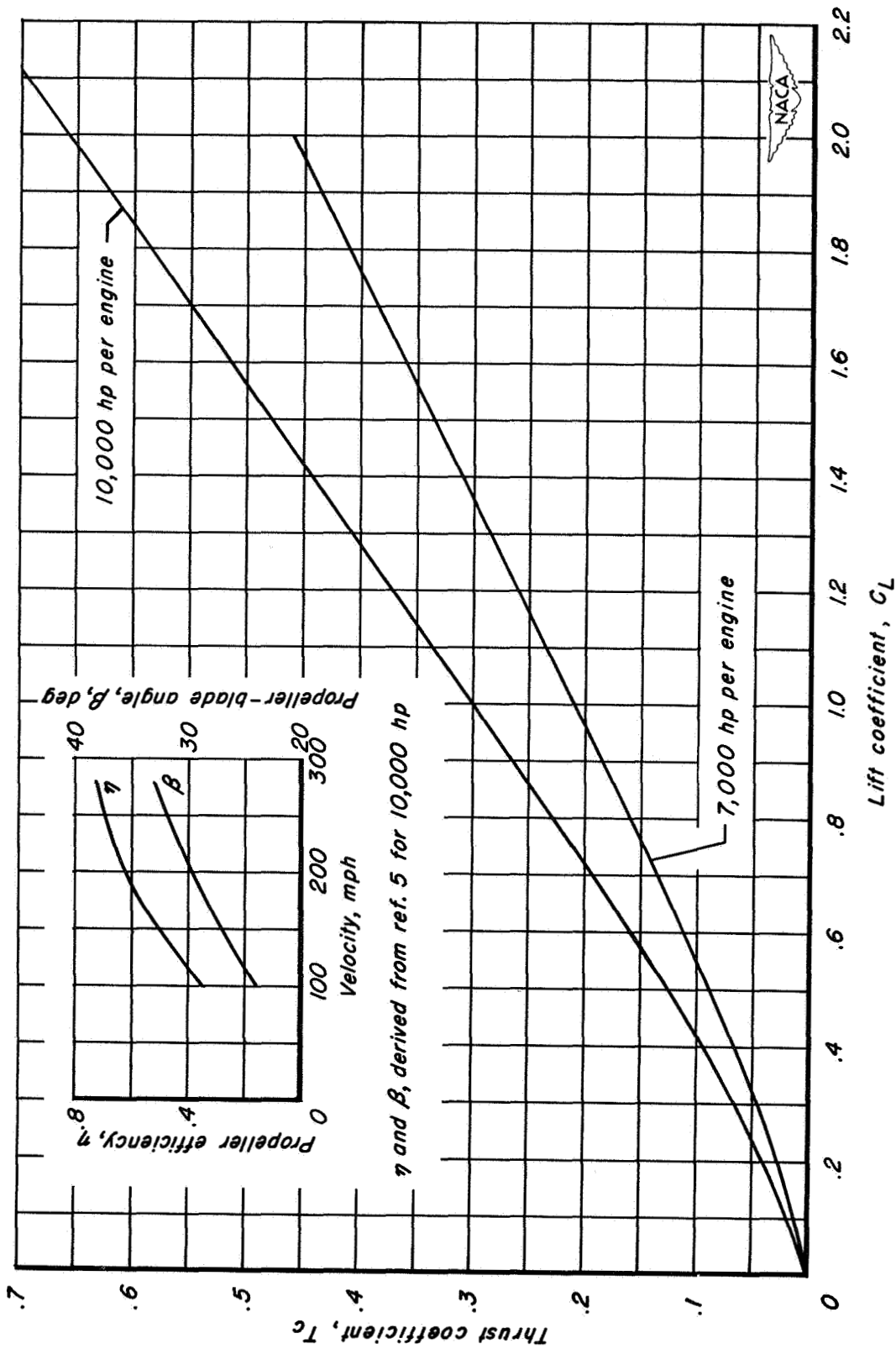
Figure 6.- The T_c vs. C_L relationship for simulated full-scale constant power conditions; wing loading = 100 lb/sq ft; propeller rotational speed = 1715 rpm; propeller diameter = 14 ft; propeller efficiency and blade angle as shown; sea level.
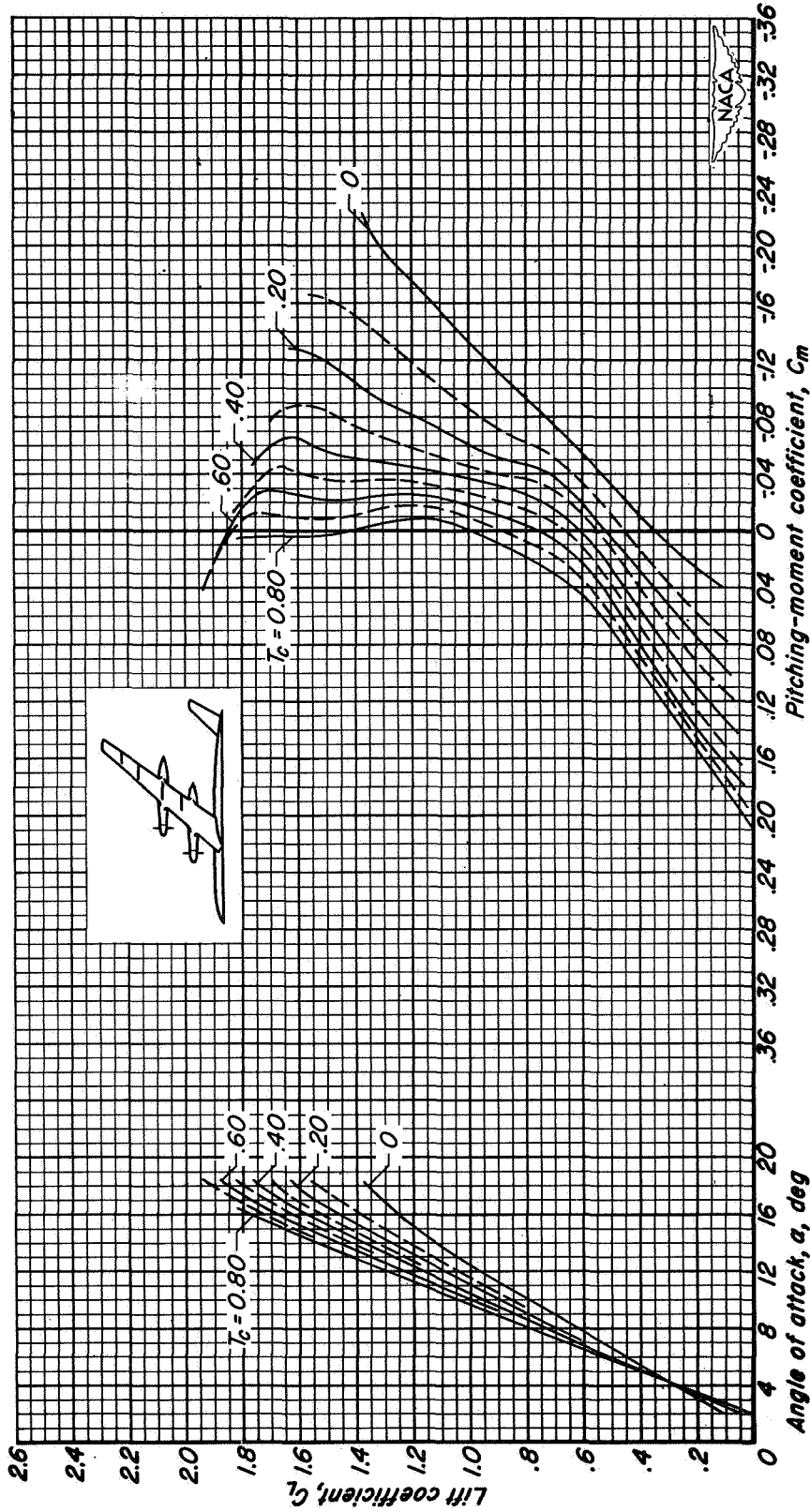
(a) C_L vs. α and C_m

Figure 7.- Example of data from reference 7 showing the longitudinal characteristics of the model; tail height = 0; flaps up; M = 0.082; R = 4,000,000; β = 26°; i_t = -4°.

COᴎFIDEᴎᴛIAL
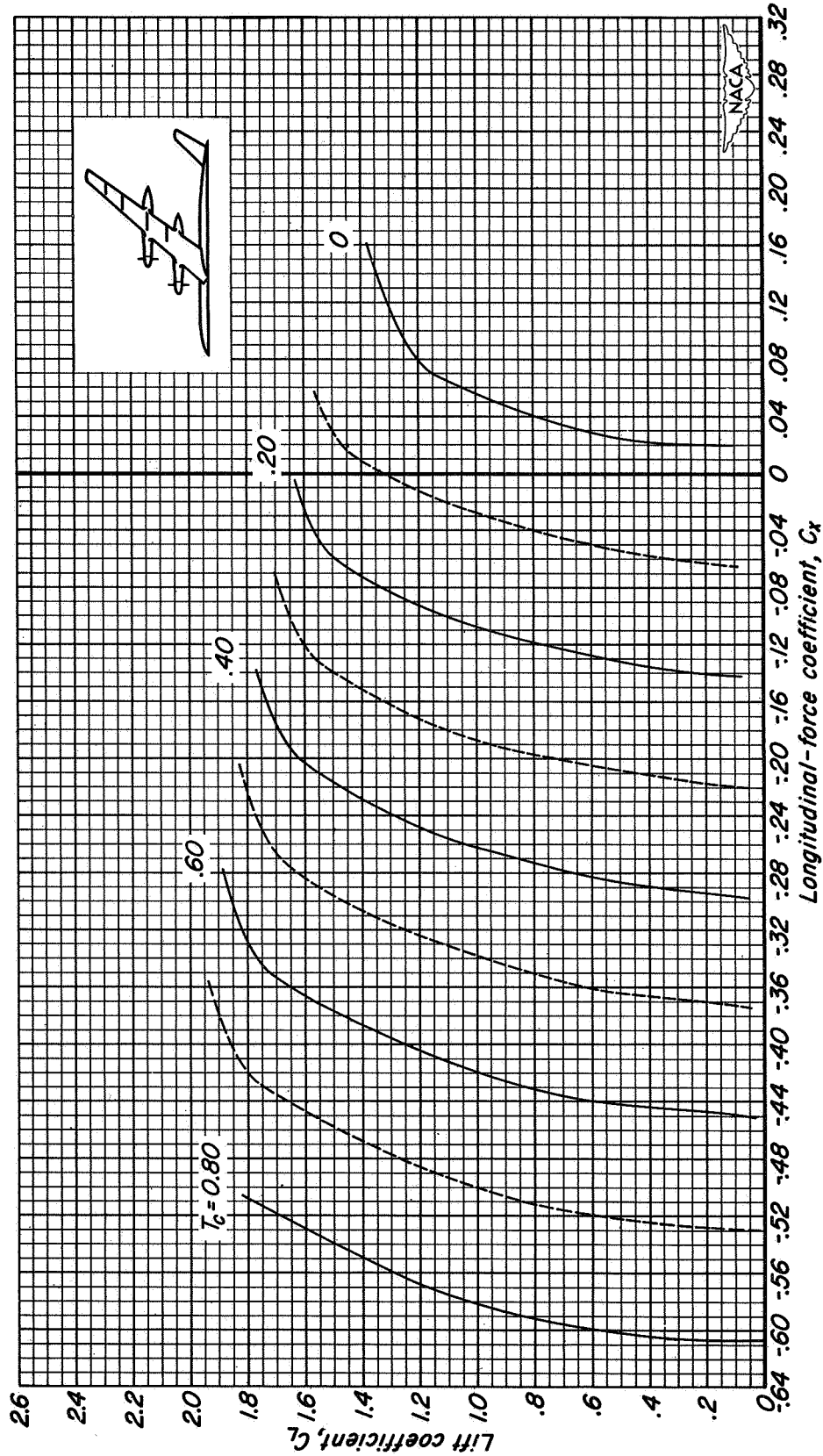
(b) C_L vs. C_X

Figure 7.- Concluded.
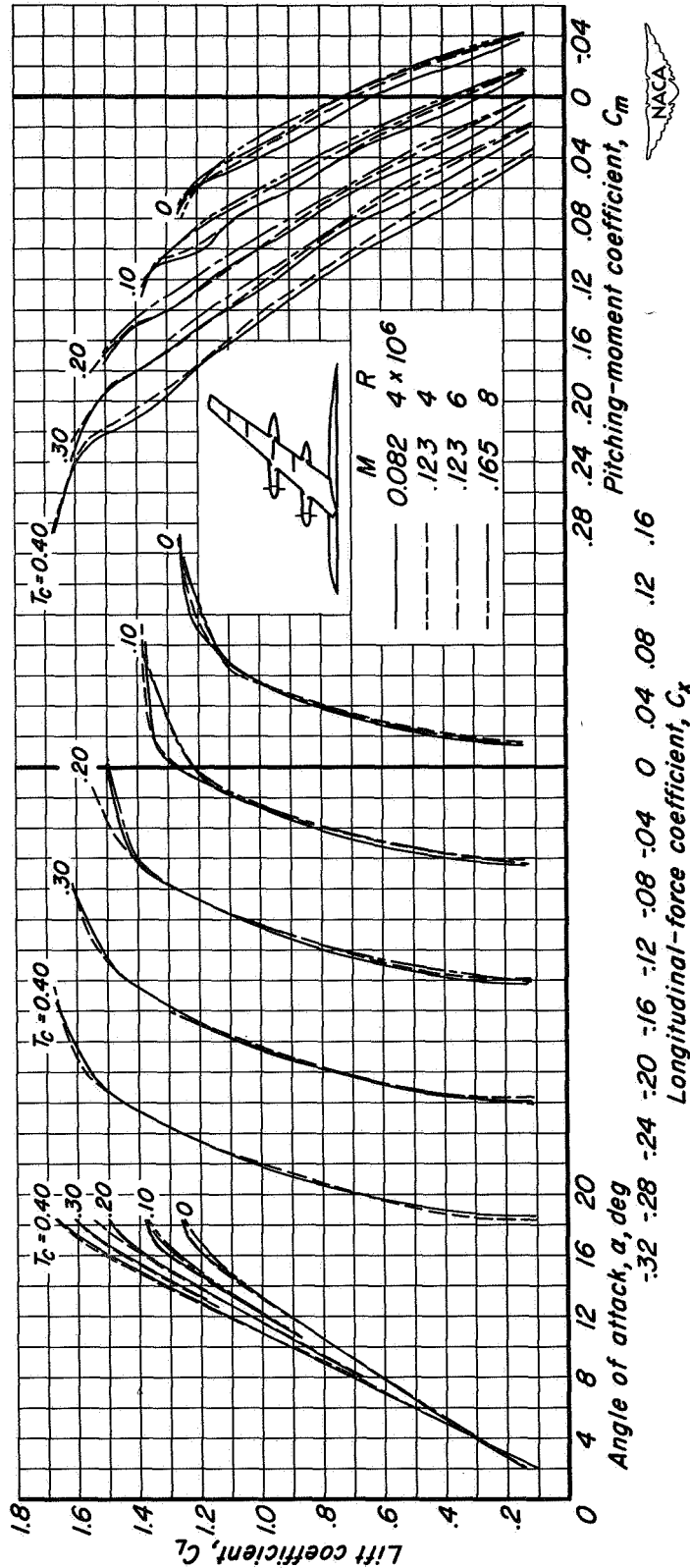
Figure 8.- The effects of Mach number and Reynolds number on the longitudinal characteristics of the model; tail removed; flaps up; β = 31°.
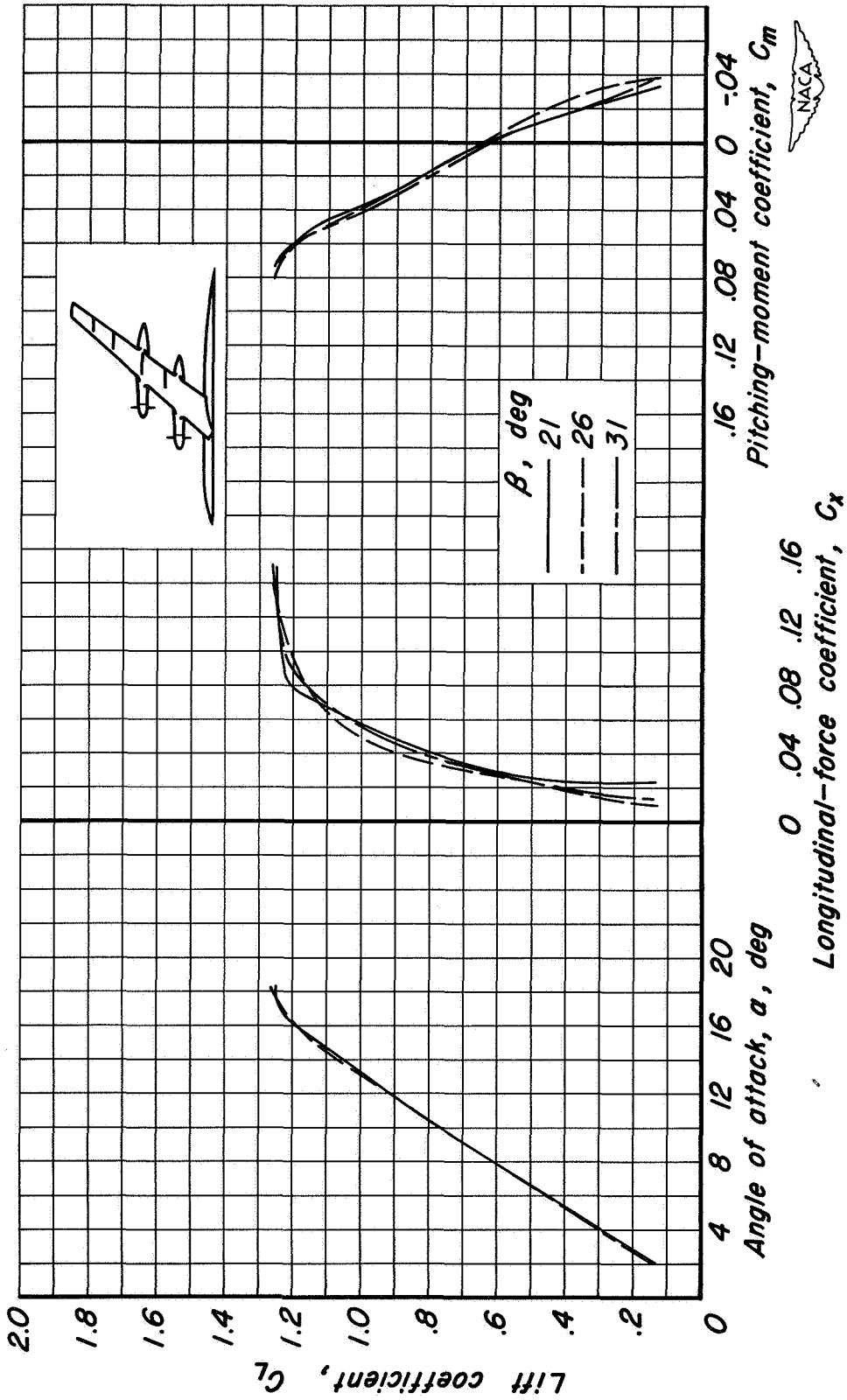
Figure 9.- The effects of propeller-blade angle on the longitudinal characteristics of the model; tail removed; flaps up; M = 0.082; R = 4,000,000.

(a) $T_c = 0$

CO███████L
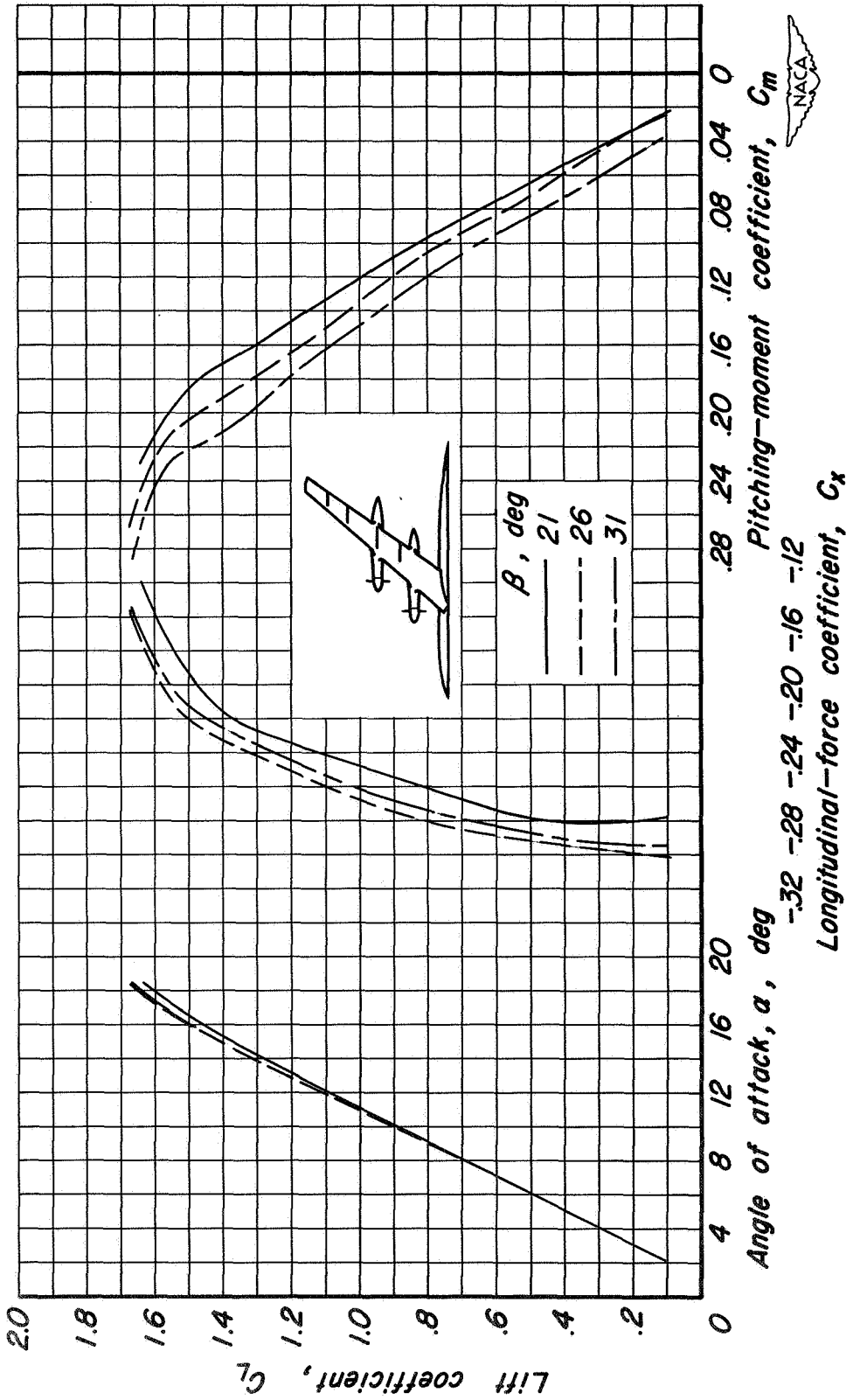
(b) $T_c = 0.40$

Figure 9.- Continued.
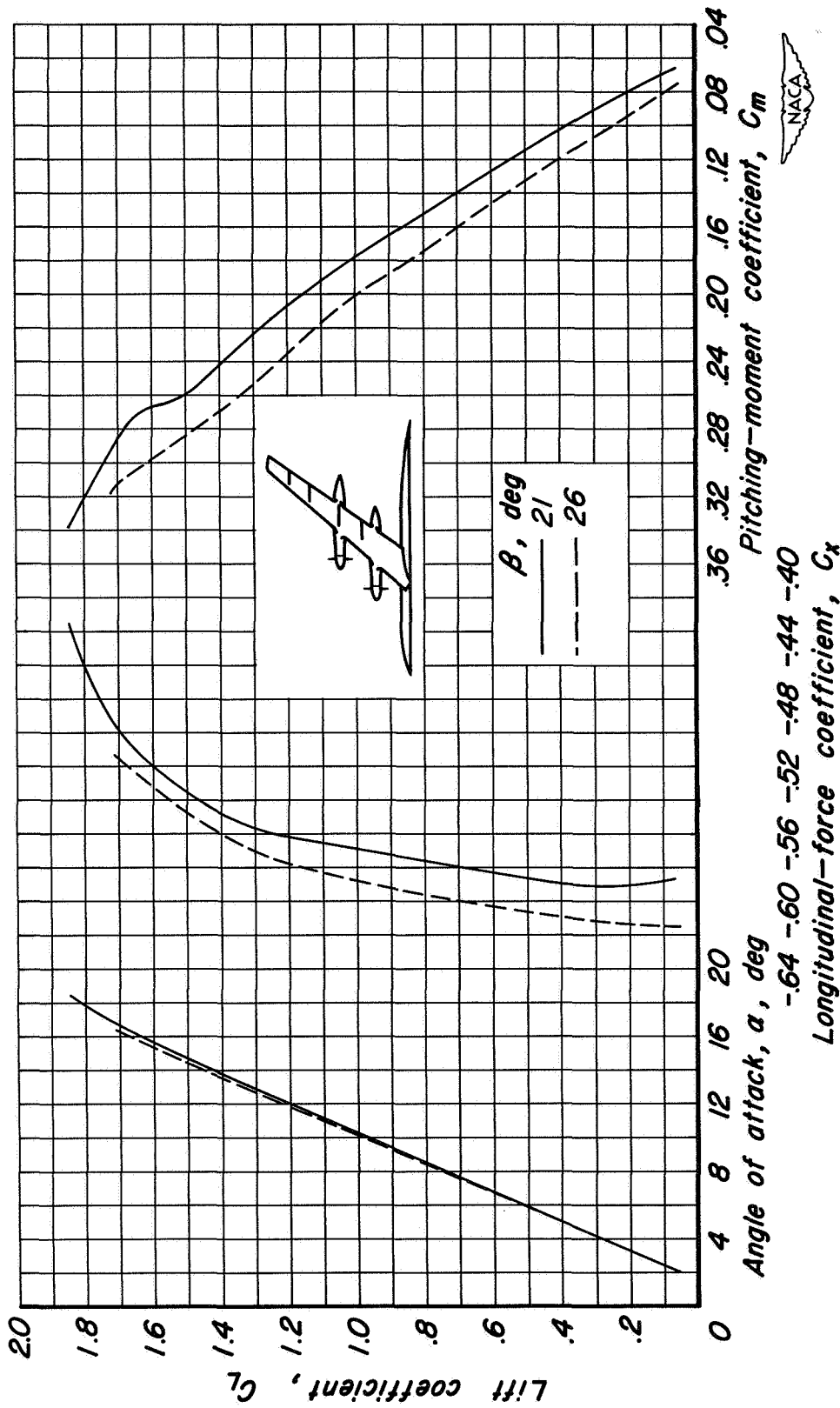
(c) $T_c = 0.80$

Figure 9.- Concluded.
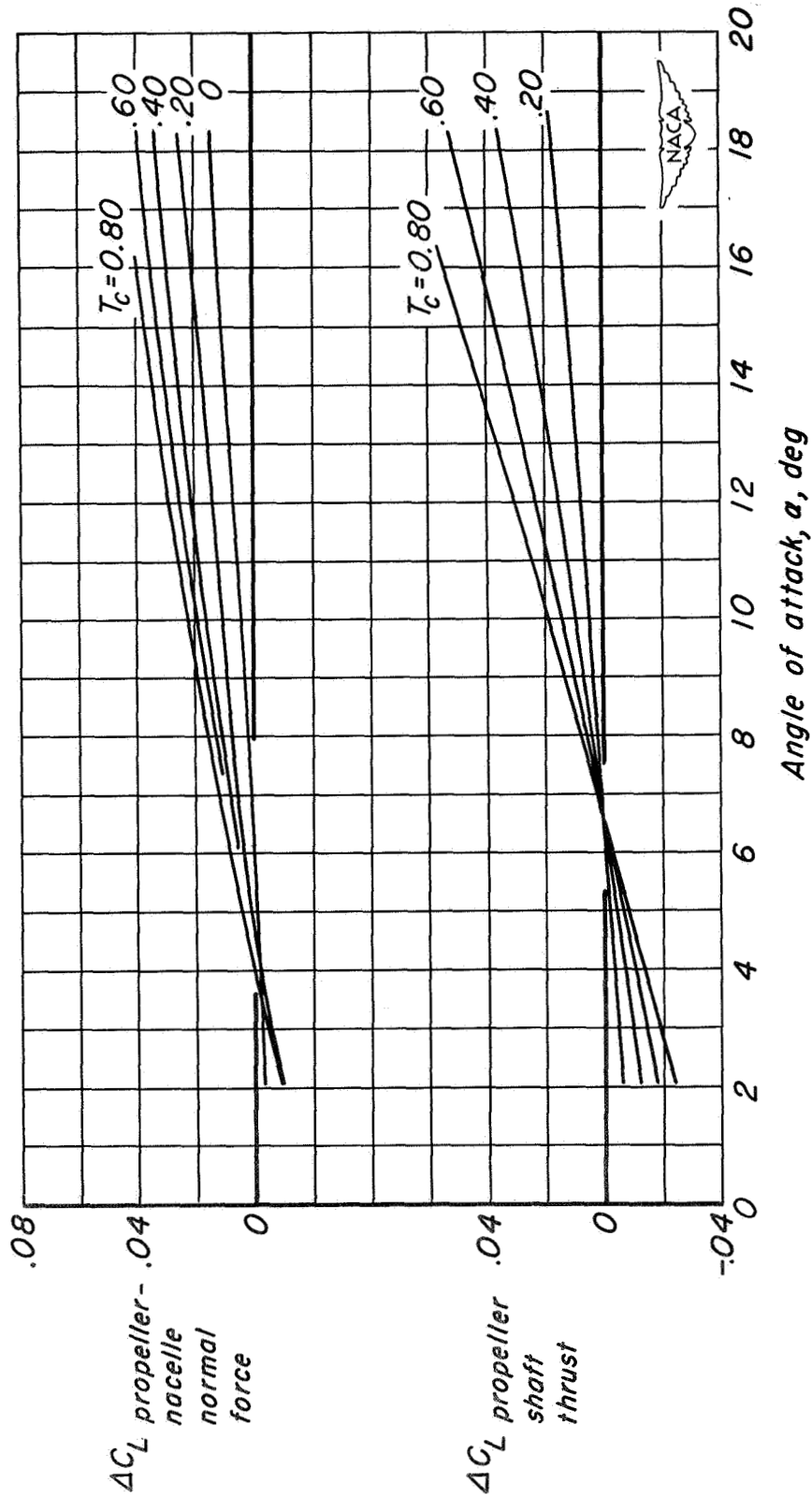
Figure 10.- The increments of lift coefficient of the model due to the normal force and shaft thrust of each propeller, including the effects of slipstream on the nacelle forebody; M = 0.082; R = 4,000,000; β = 26°.
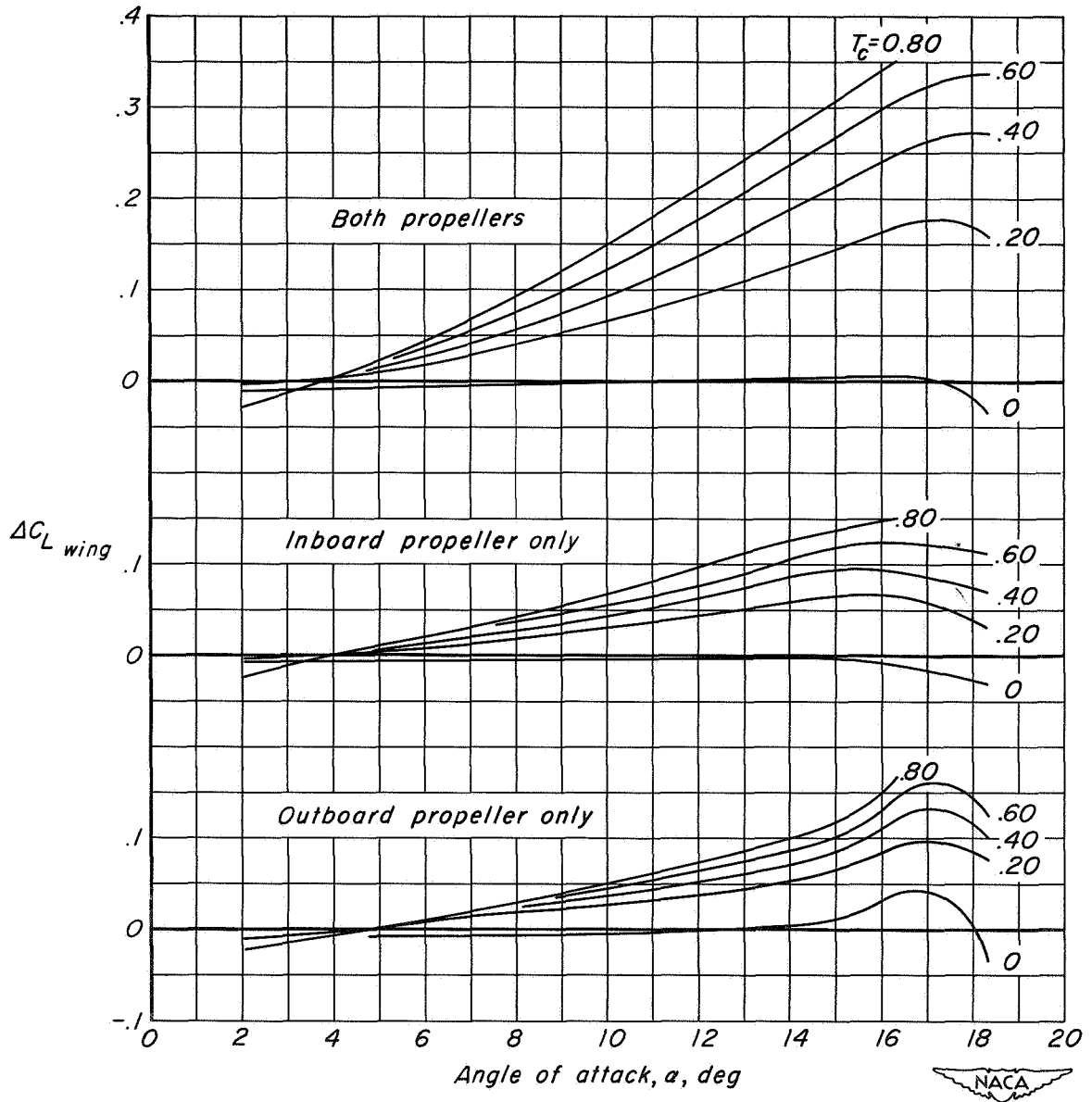
(a) Flaps up.

Figure 11.— The increments of lift coefficient due to the slipstreams on
the wing; M = 0.082; R = 4,000,000; β = 26°.
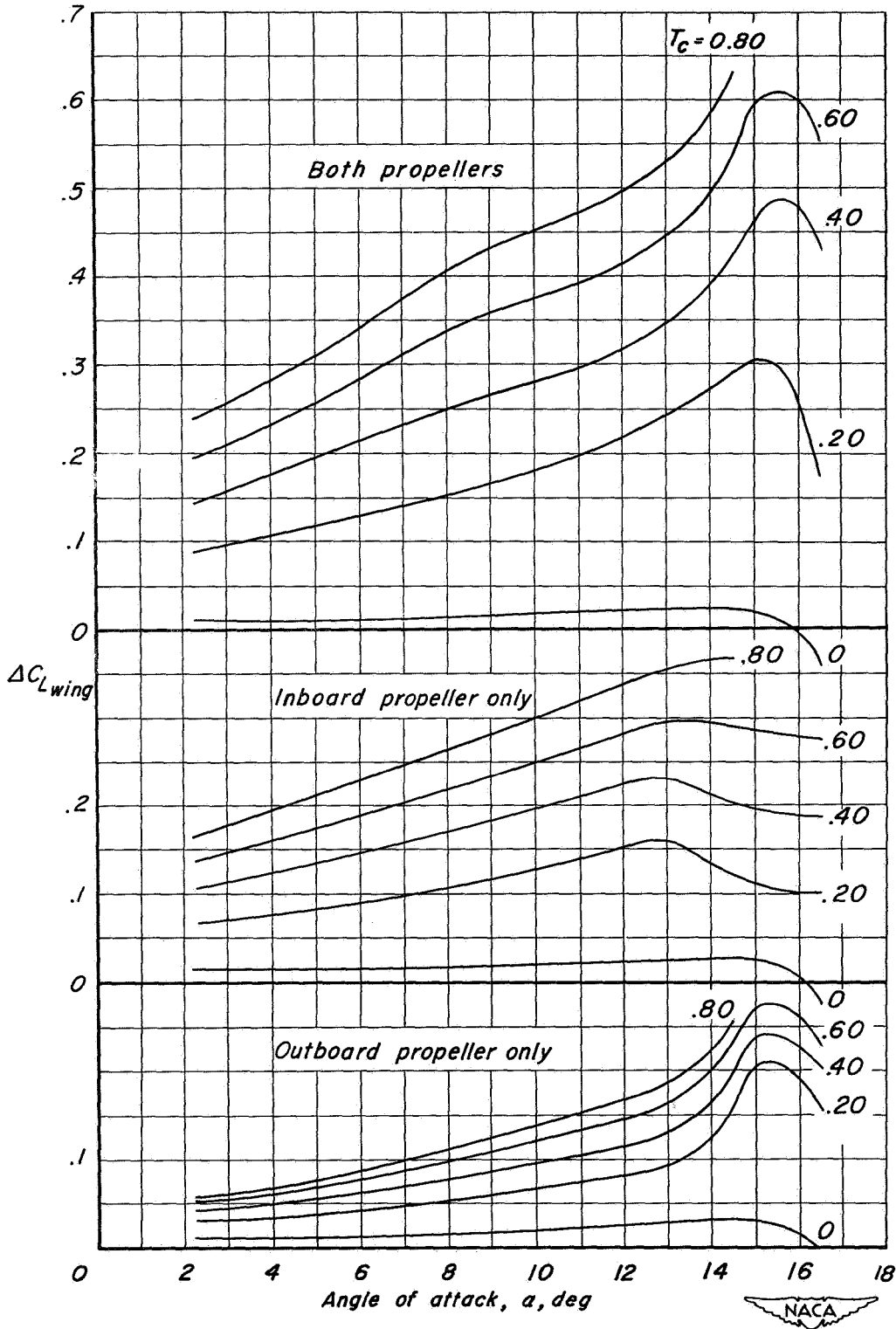
(b) Inboard flaps deflected.

Figure 11.- Concluded.
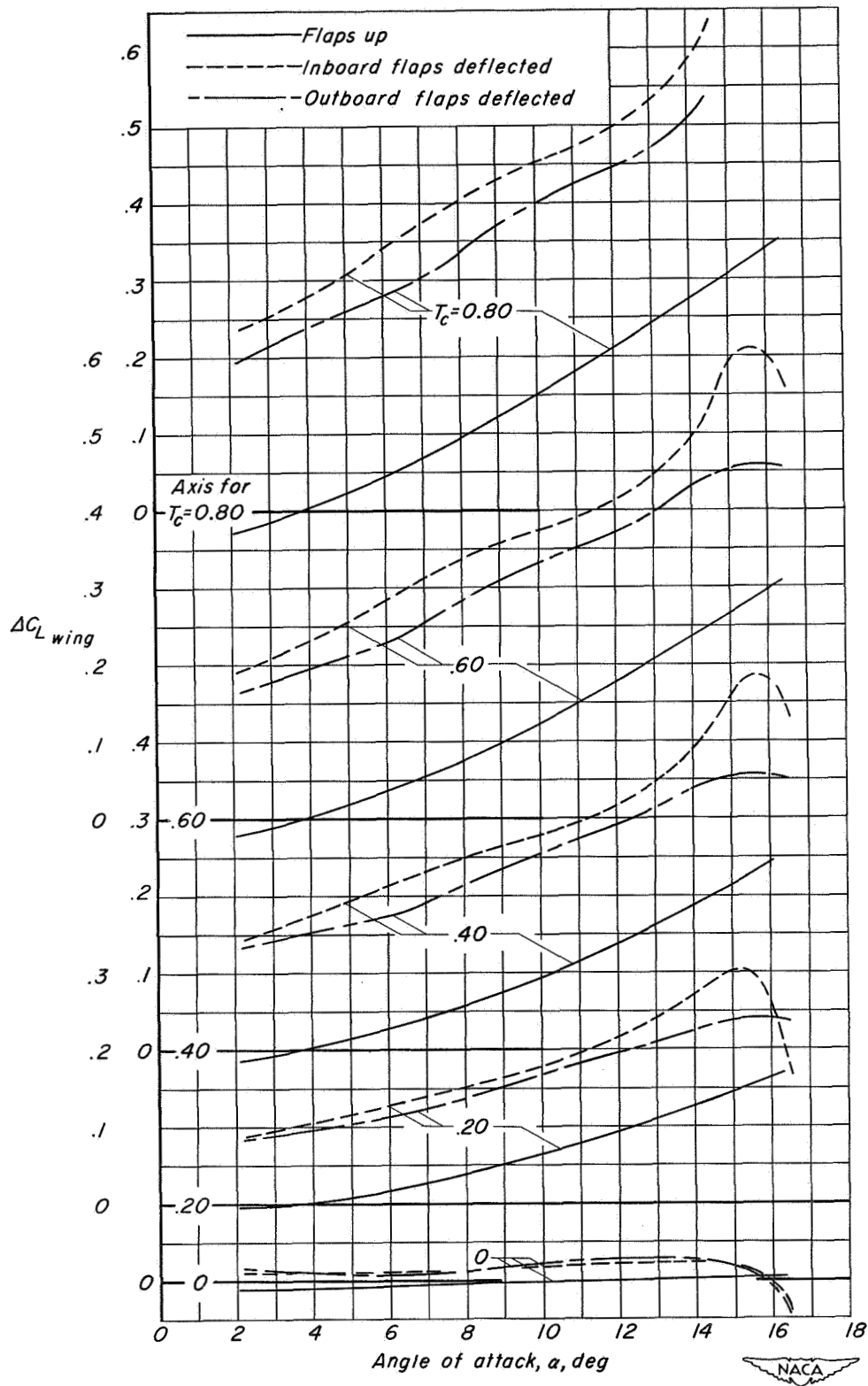
Figure 12.- The effects of flaps on the increments of lift coefficient due to the slipstreams on the wing; M = 0.082; R = 4,000,000; β = 26°.
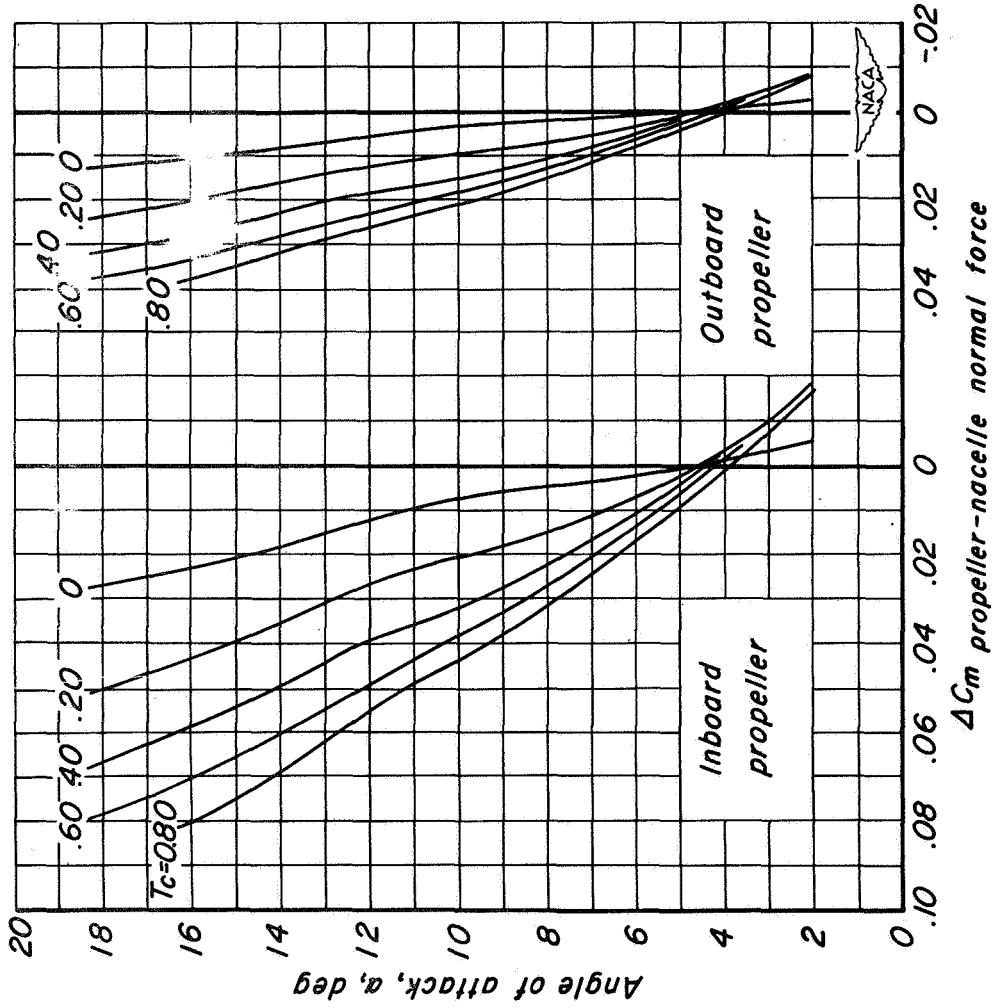
Figure 13.- The increments of pitching-moment coefficient of the model due to the normal force of each propeller, including the effects of slipstream on the nacelle forebody; M = 0.082; R = 4,000,000; β = 26°.
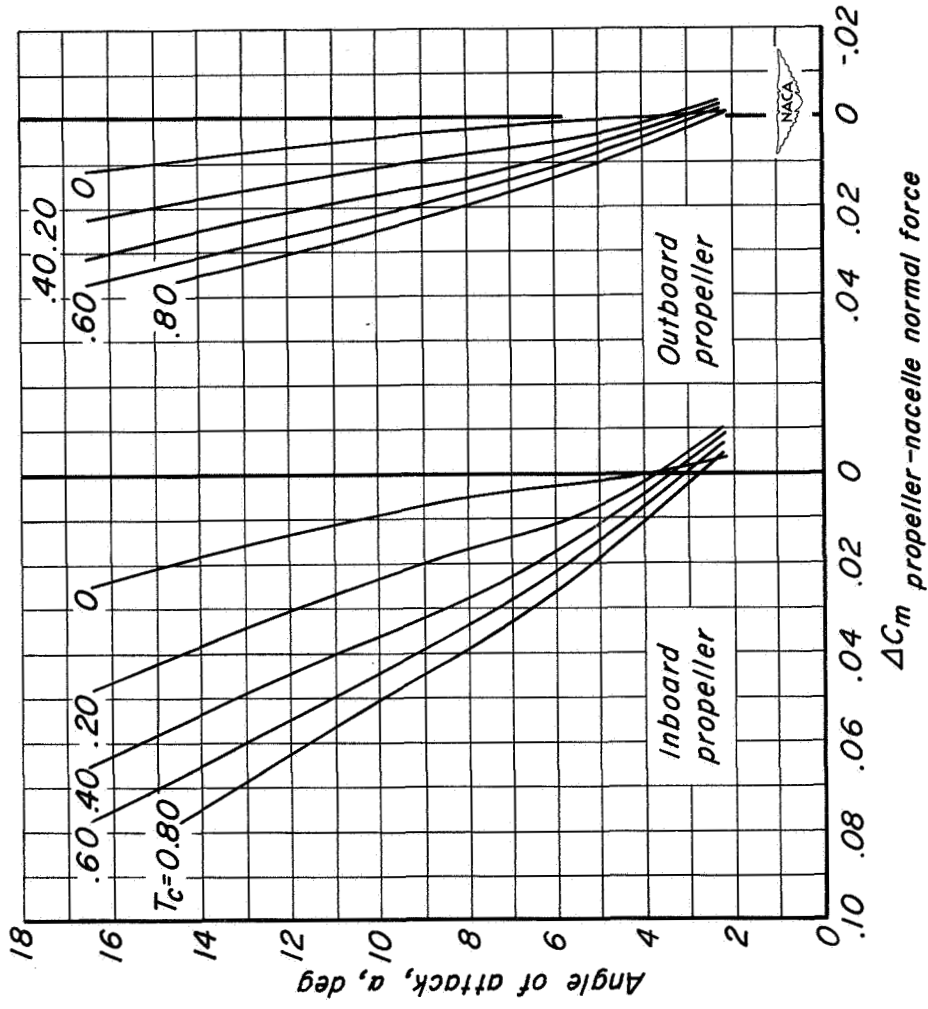
(b) Inboard flaps deflected.

Figure 13.- Concluded.
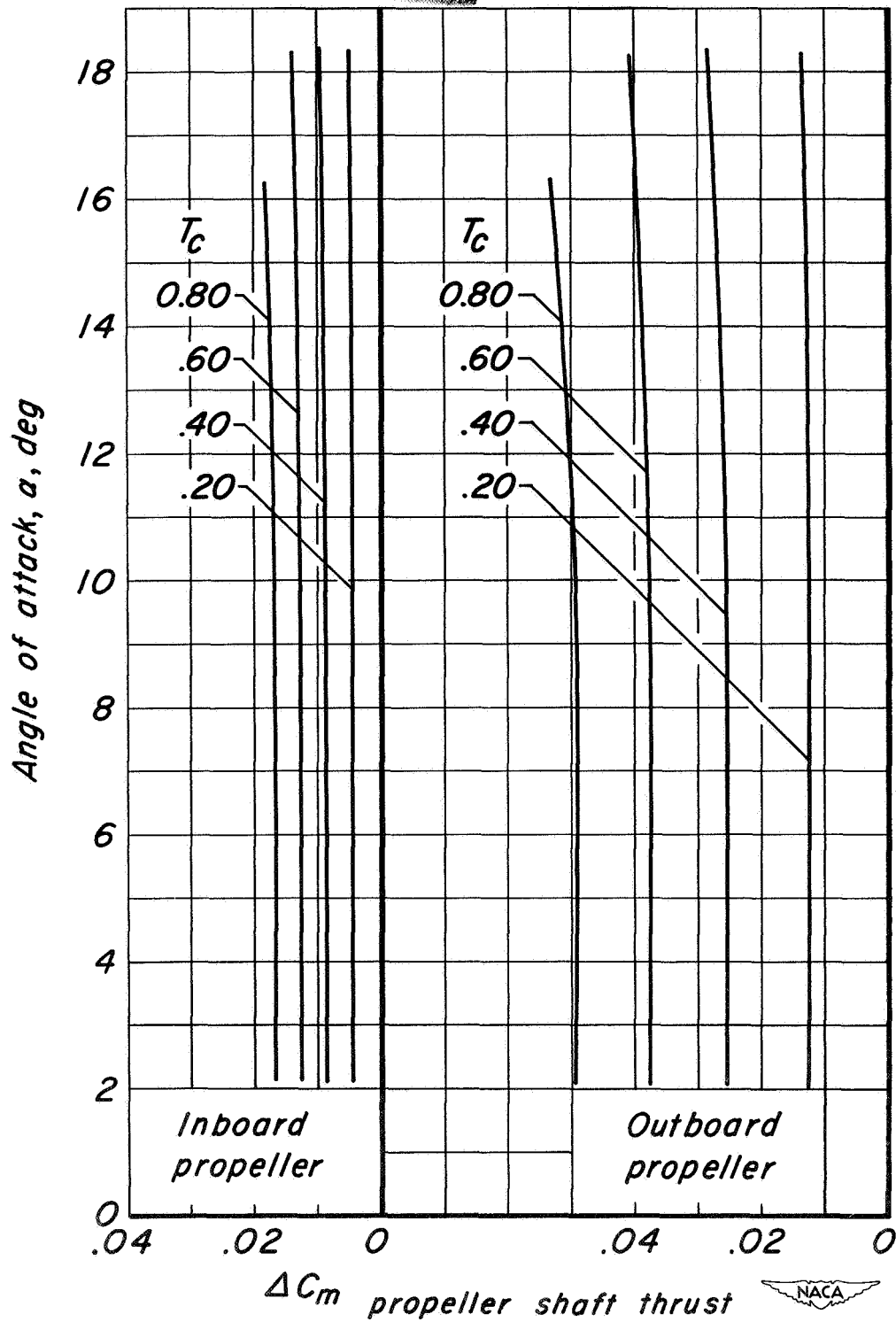
Figure 14.- The increments of pitching-moment coefficient of the model due to the shaft thrust of each propeller, including the effects of slipstream on the nacelle forebody; M = 0.082; R = 4,000,000; β = 26°.
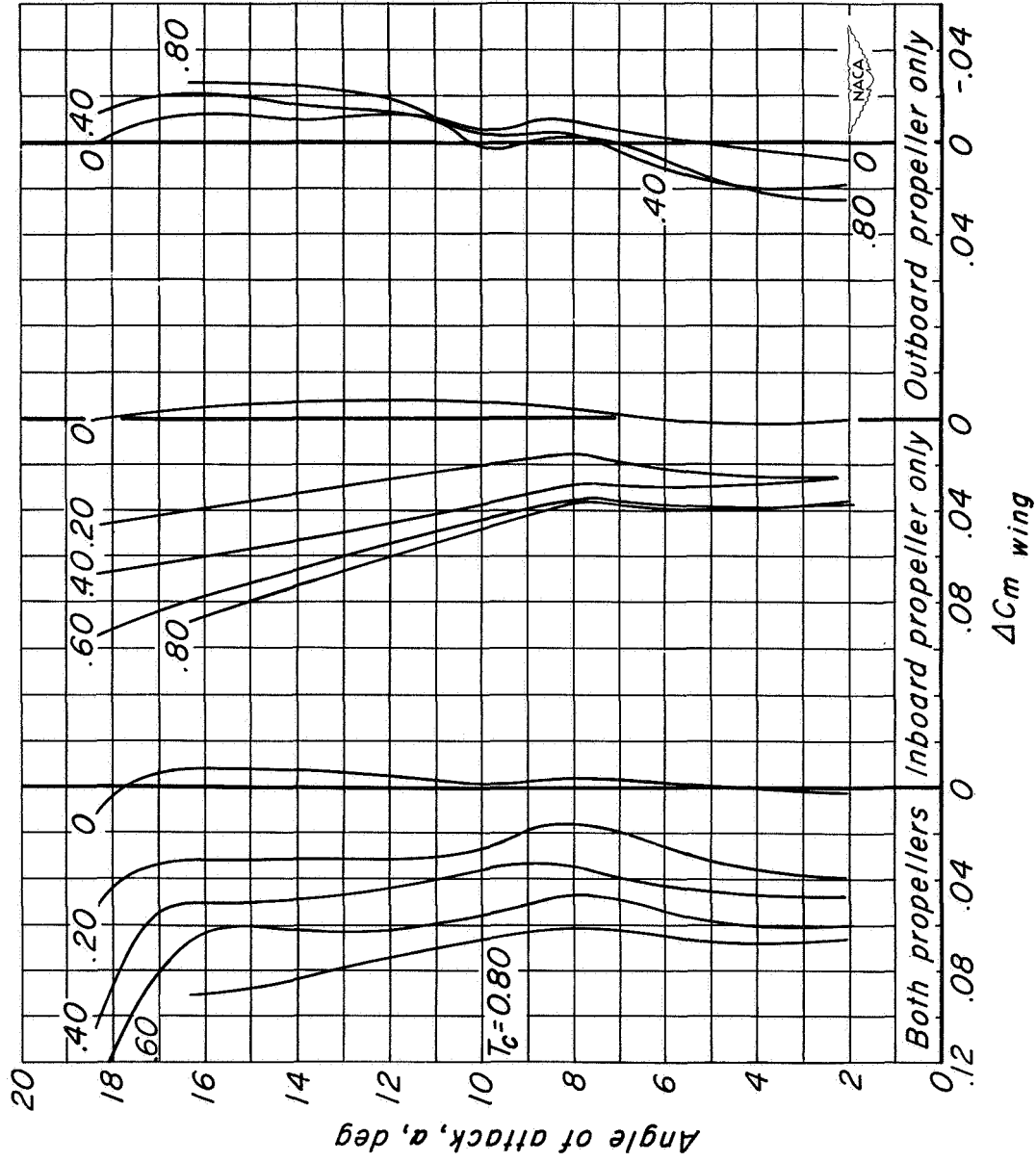
(a) Flaps up.

Figure 15.- The increments of pitching-moment coefficient due to the slipstreams on the wing; $M = 0.082$; $R = 4,000,000$; $\beta = 26°$.
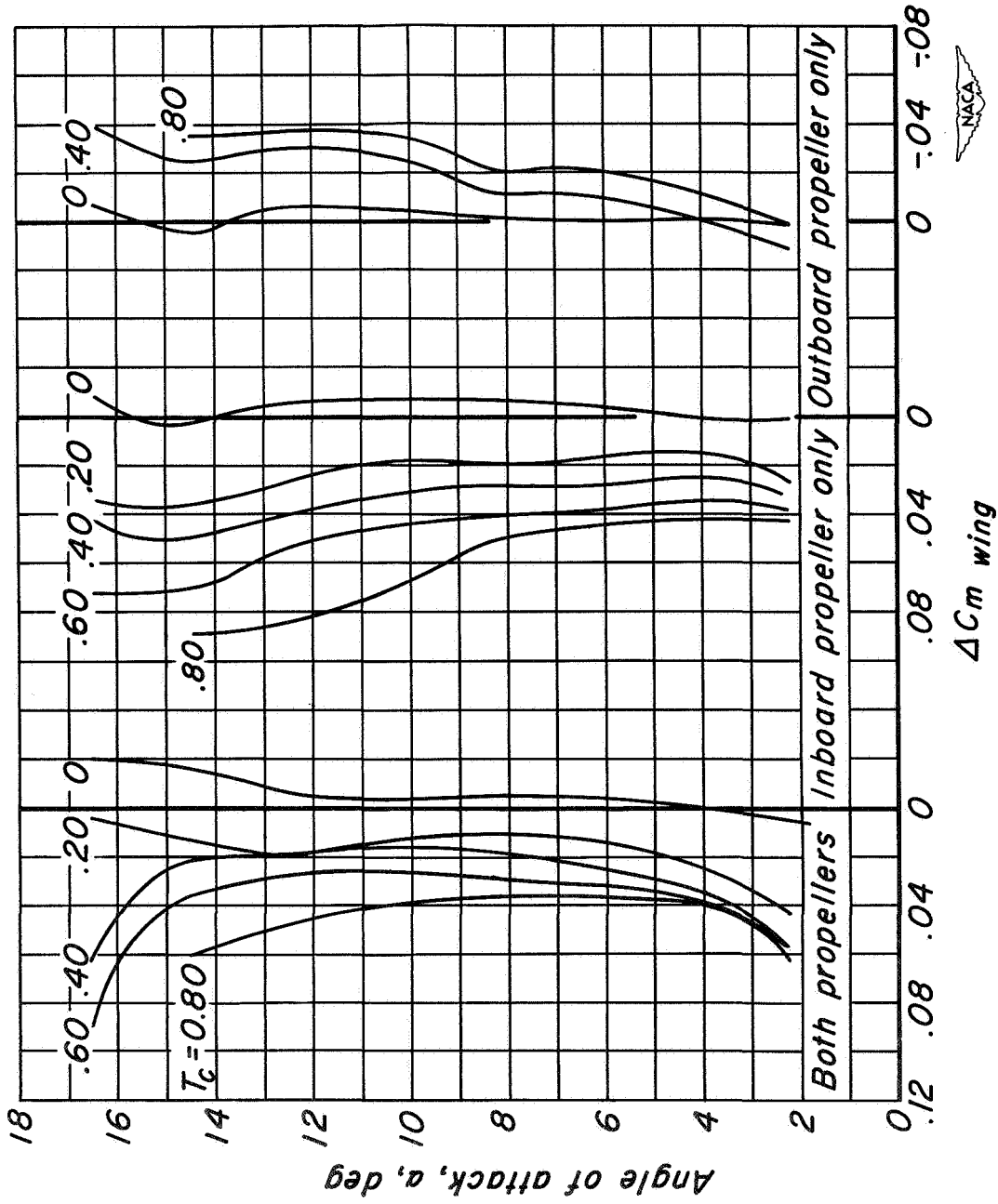
(b) Inboard flaps deflected.

Figure 15.- Concluded.
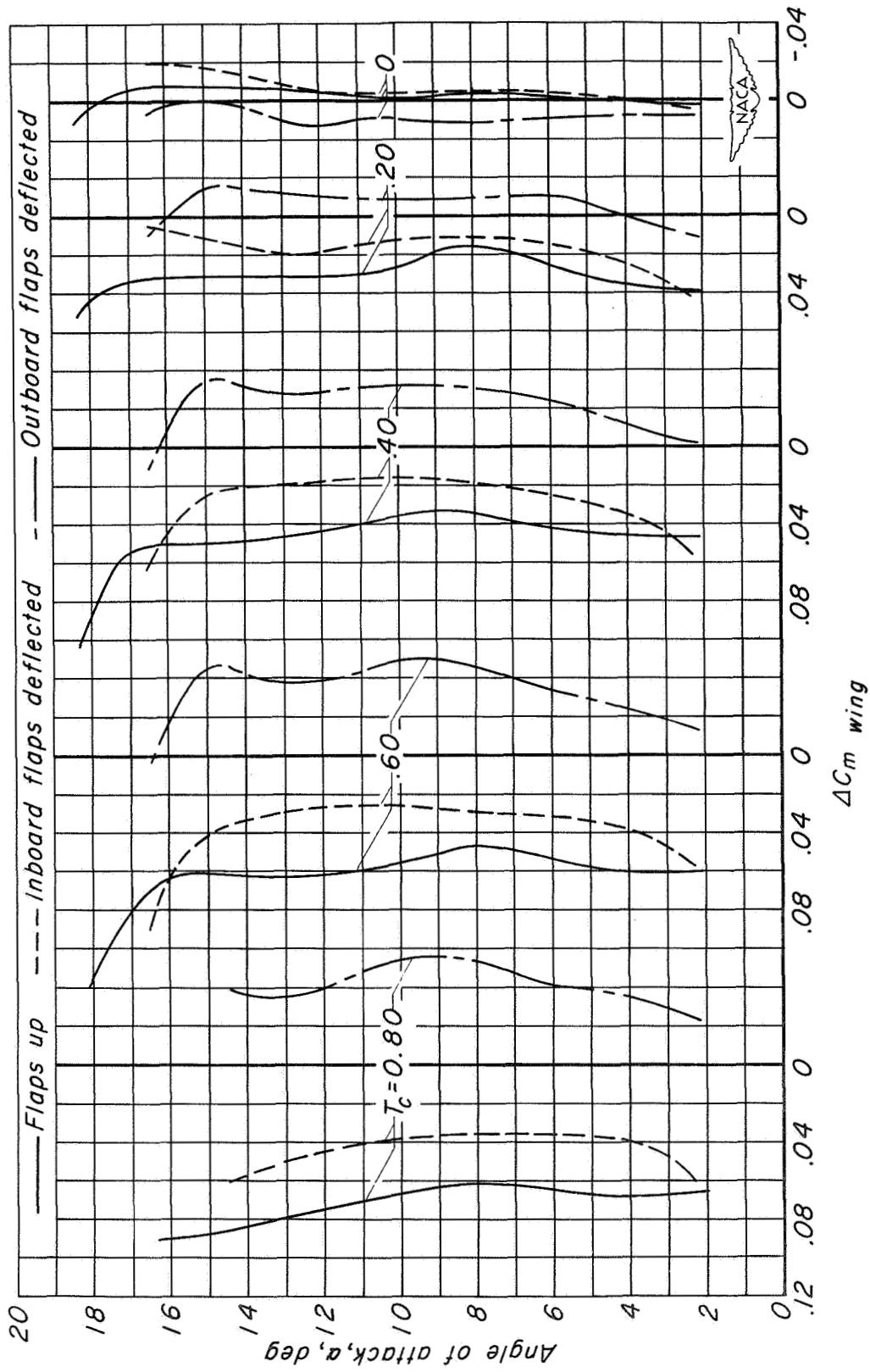
Figure 16.- The effects of flaps on the increments of pitching-moment coefficient due to the slipstreams on the wing; $M = 0.082$; $R = 4,000,000$; $\beta = 26°$.
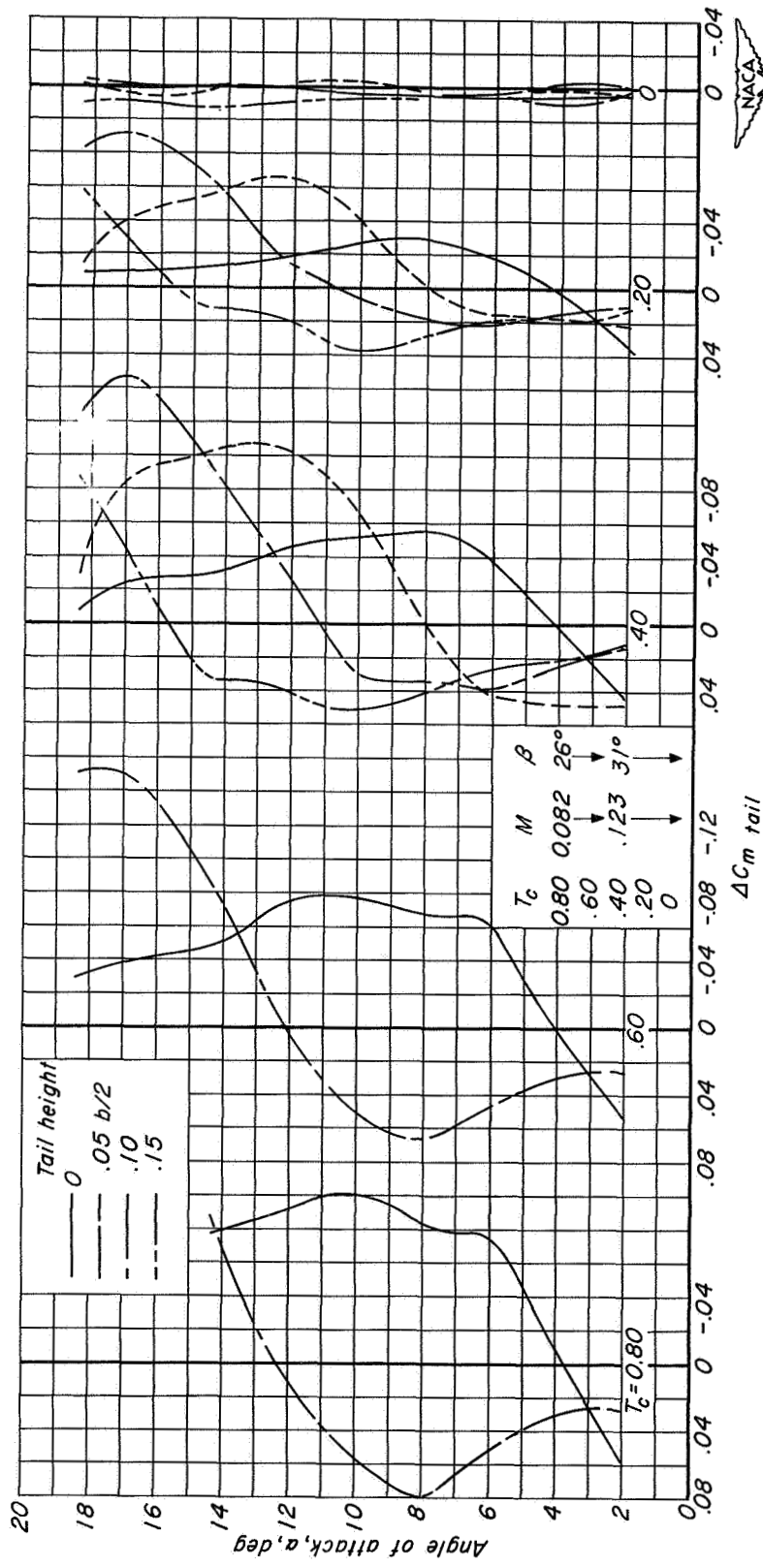
Figure 17.- The increments of pitching-moment coefficient from the tail due to operation of the propellers; flaps up; M and β as noted; R = 4,000,000; $i_t = -4°$.
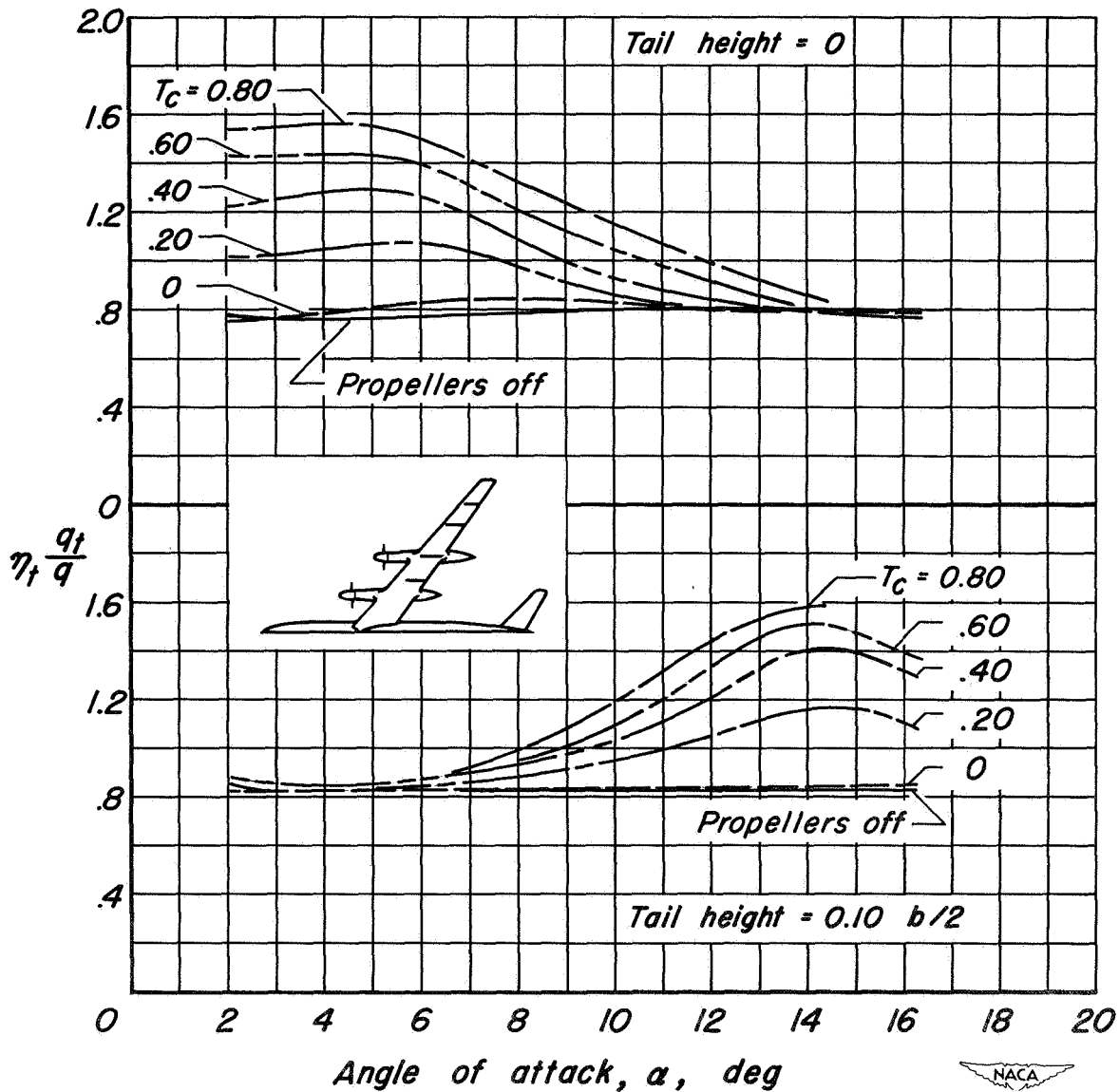
(a) Flaps up.

Figure 18.- The effects of operating propellers on the tail-efficiency factor; M = 0.082; R = 4,000,000; β = 26°.
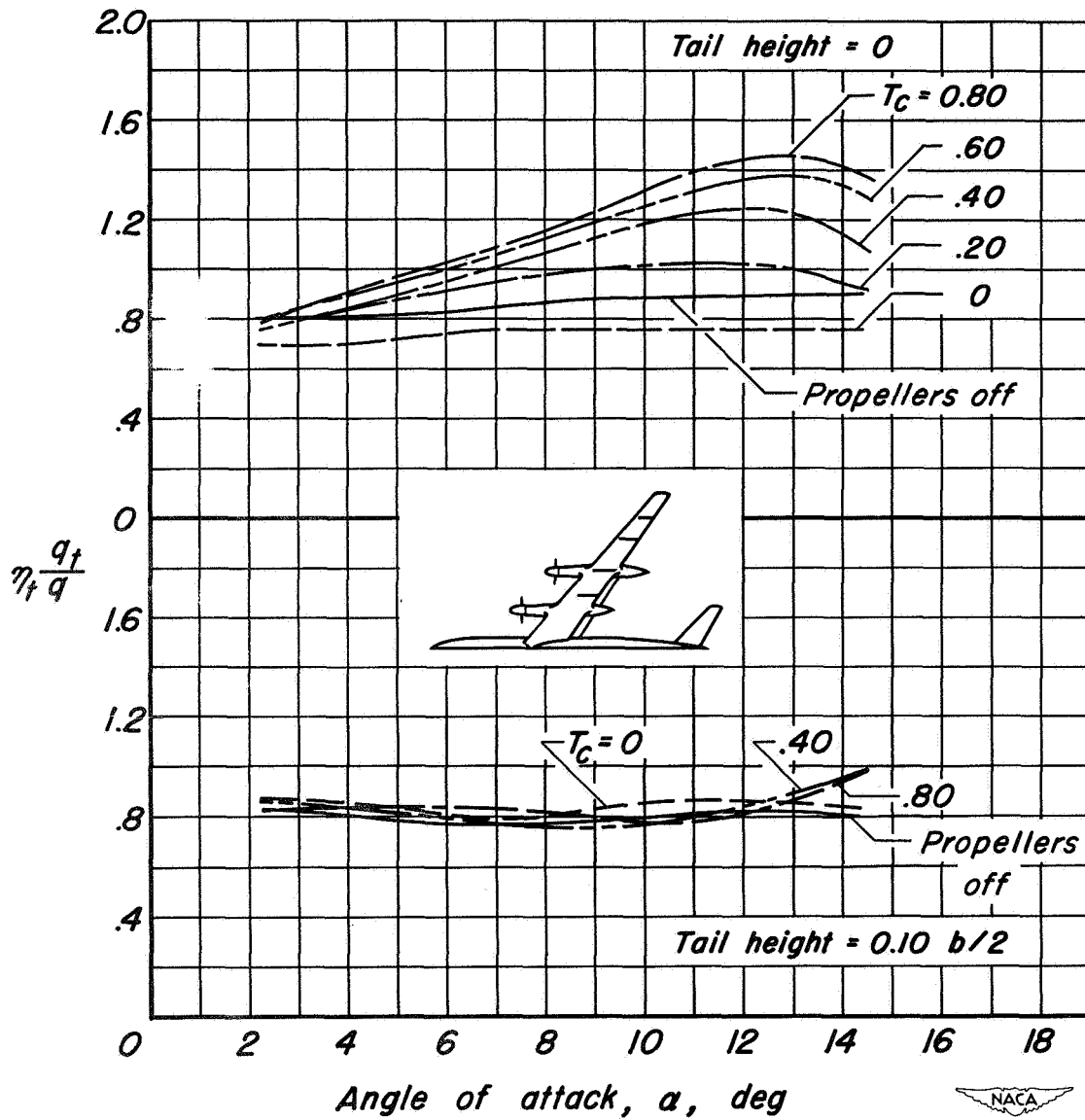
(b) Inboard flaps deflected.

Figure 18.- Continued.
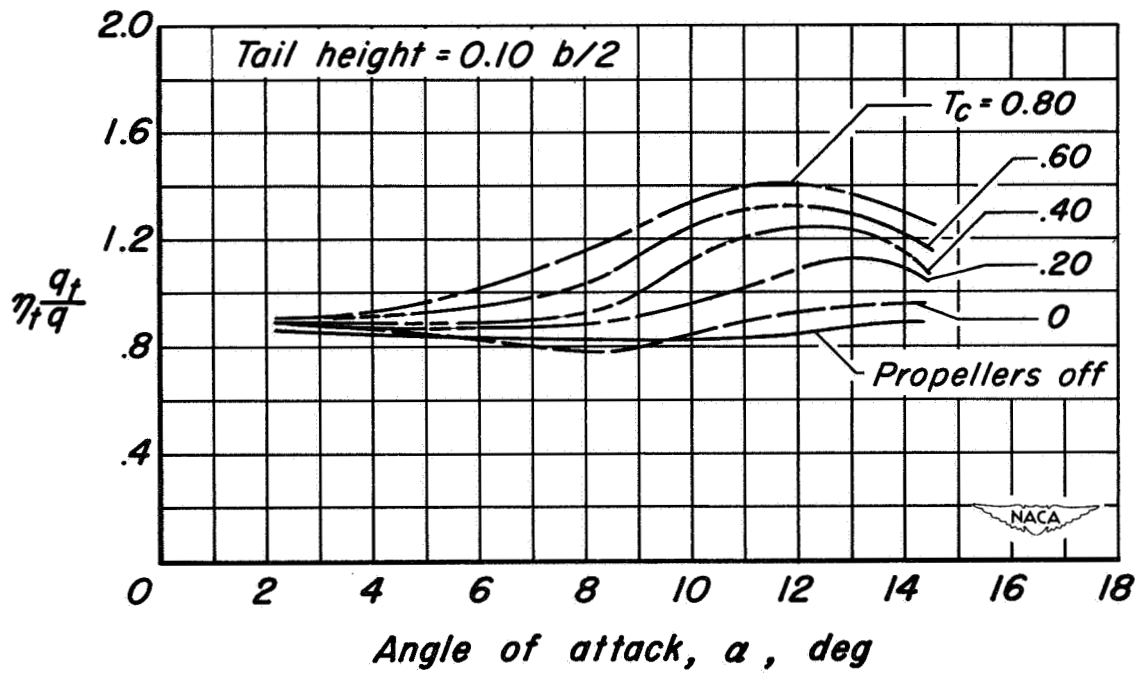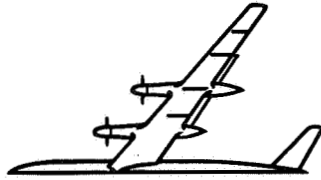
(c) Outboard flaps deflected.

Figure 18.- Concluded.
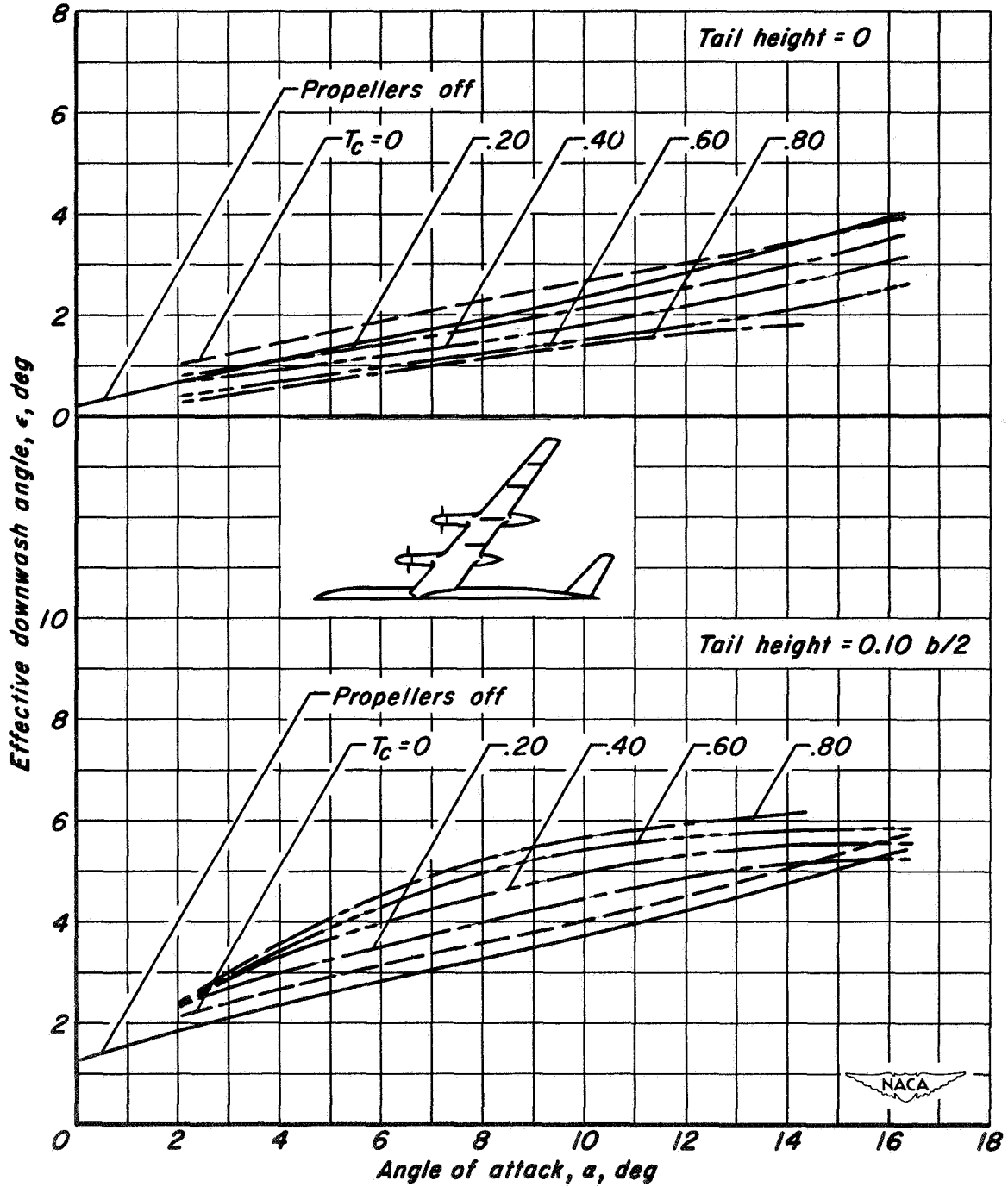
(a) Flaps up.

Figure 19.- The effects of operating propellers on the effective
downwash at the tail; $M = 0.082$; $R = 4,000,000$; $\beta = 26°$.
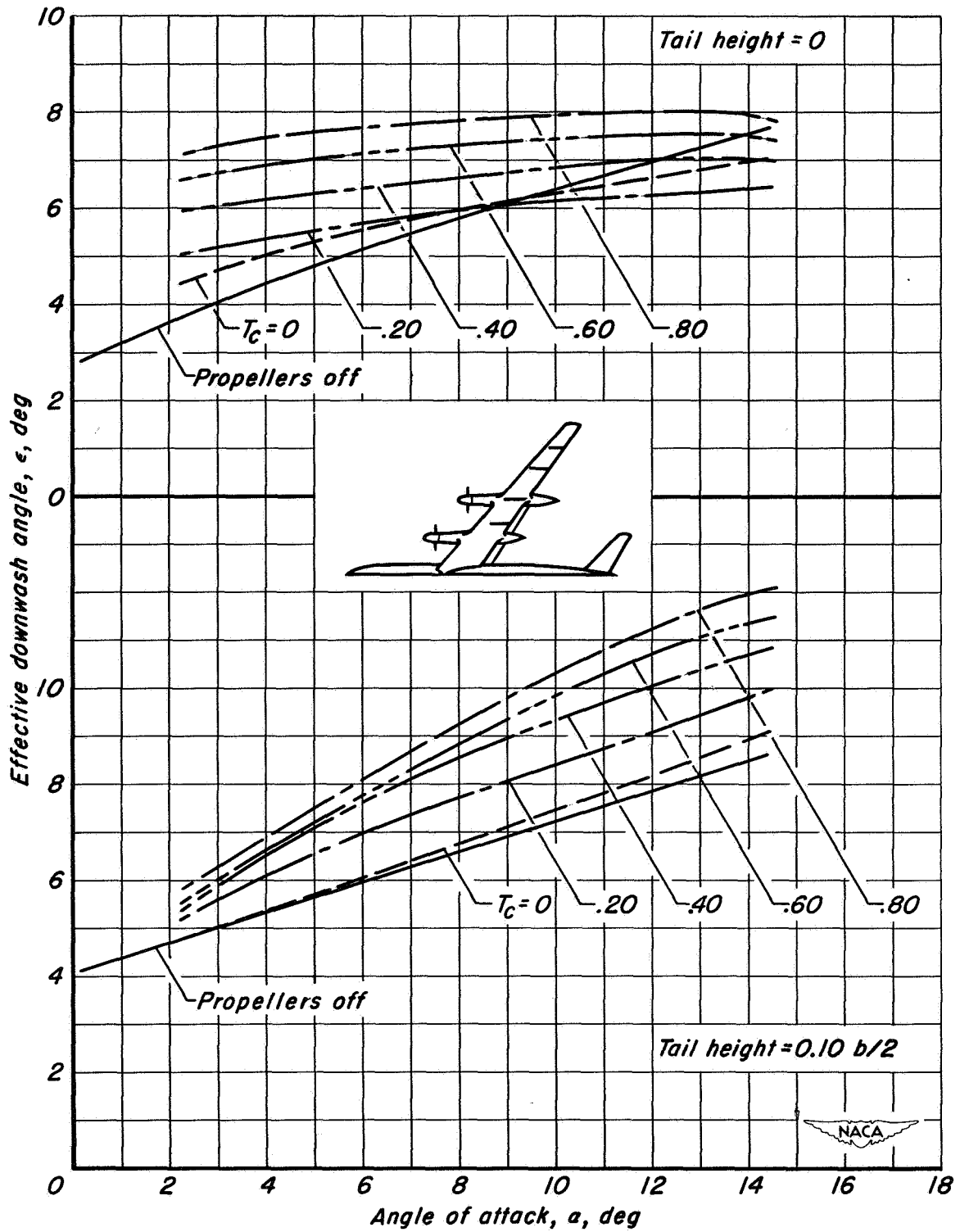
(b) Inboard flaps deflected.

Figure 19.- Continued.
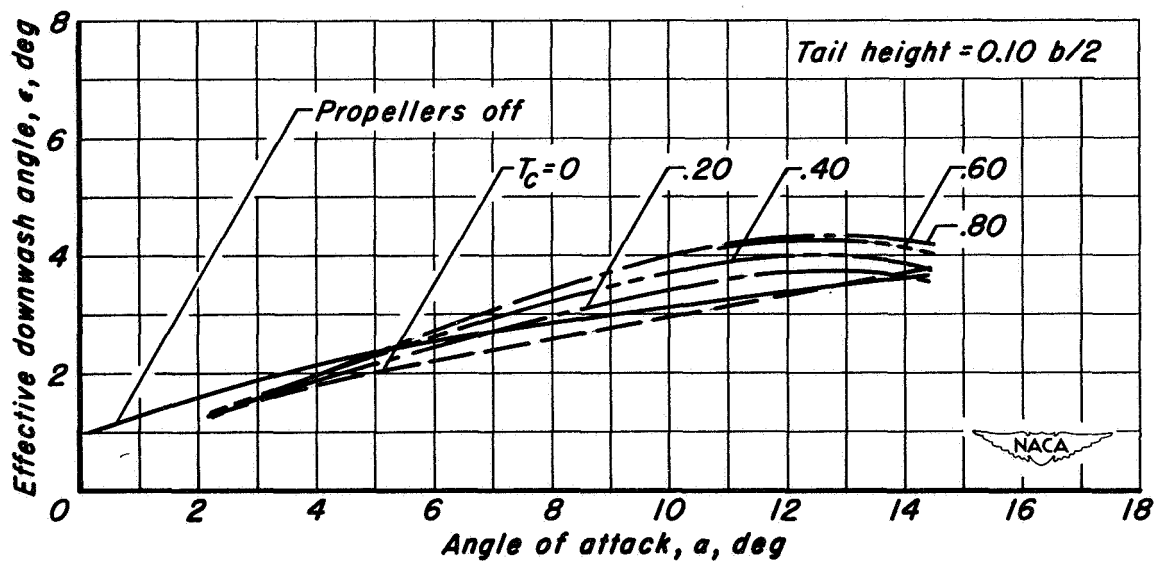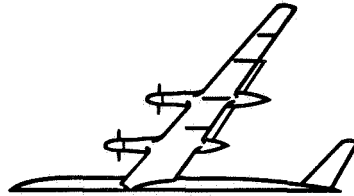
(c) Outboard flaps deflected.

Figure 19.- Concluded.
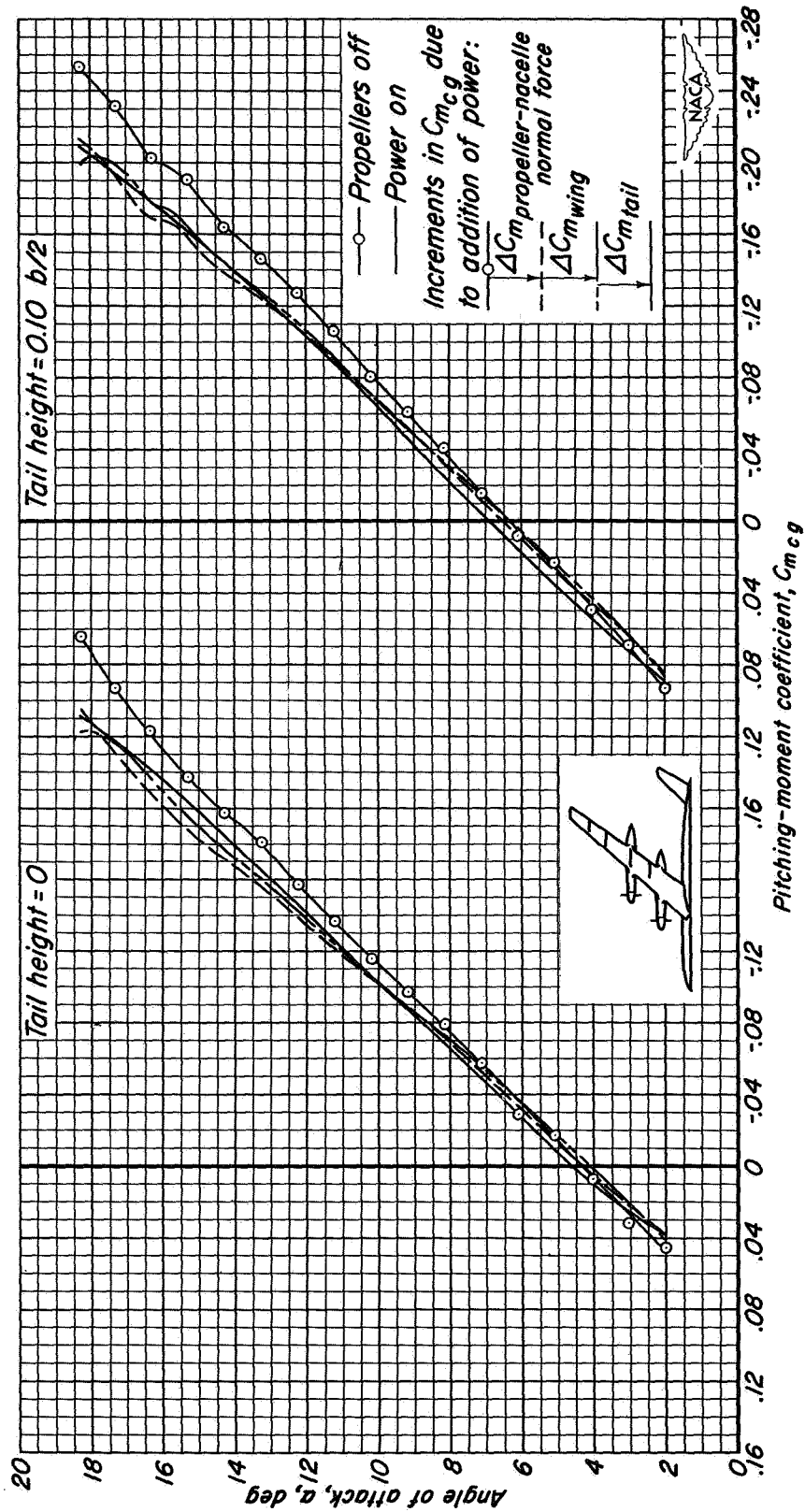
(a) $T_c = 0$

Figure 20.- The various effects of operating propellers on the pitching-moment characteristics of the model; flaps up; M = 0.082; R = 4,000,000; β = 26°; it = -4°.
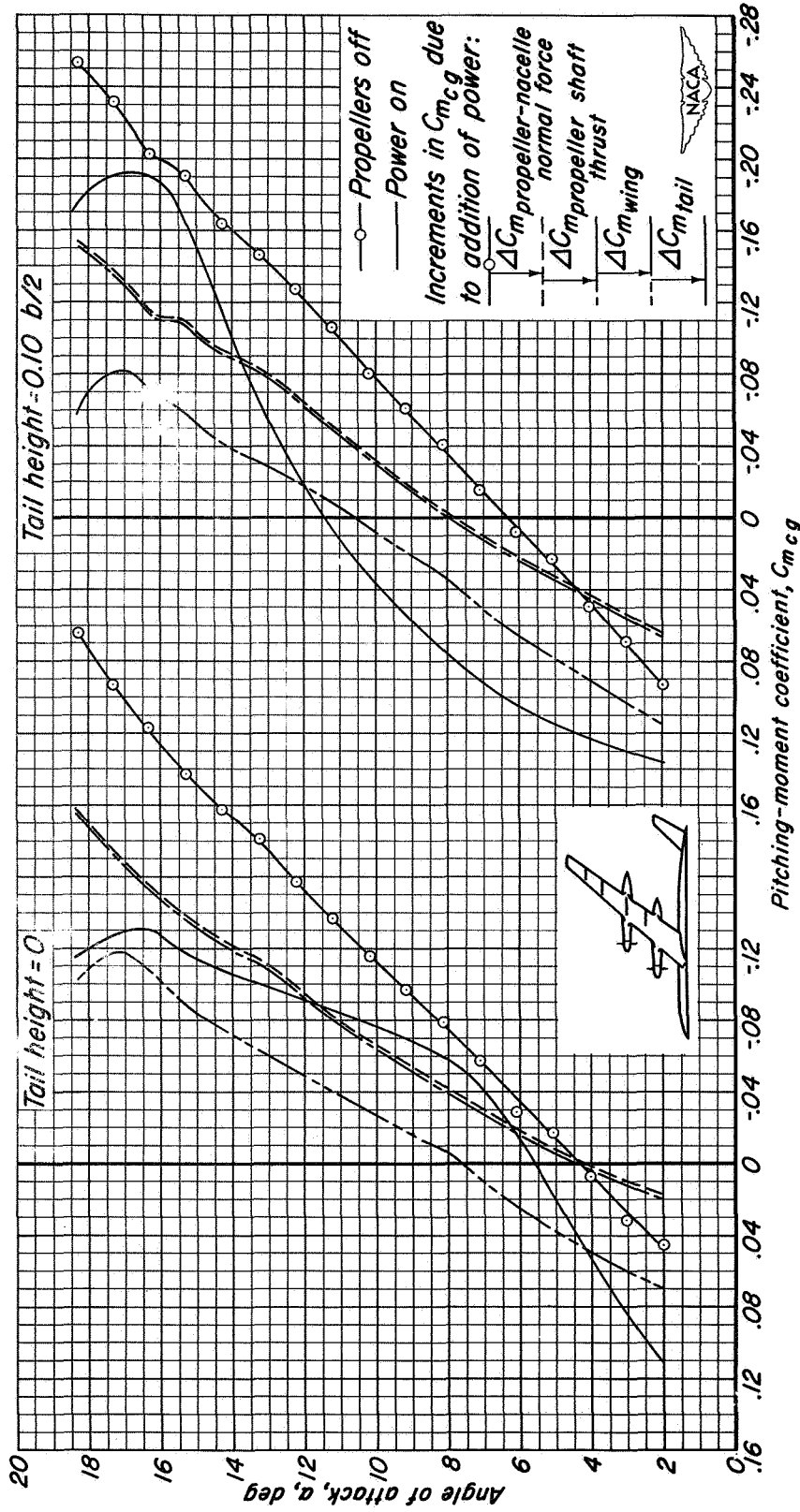
(b) $T_c = 0.40$

Figure 20.- Continued.
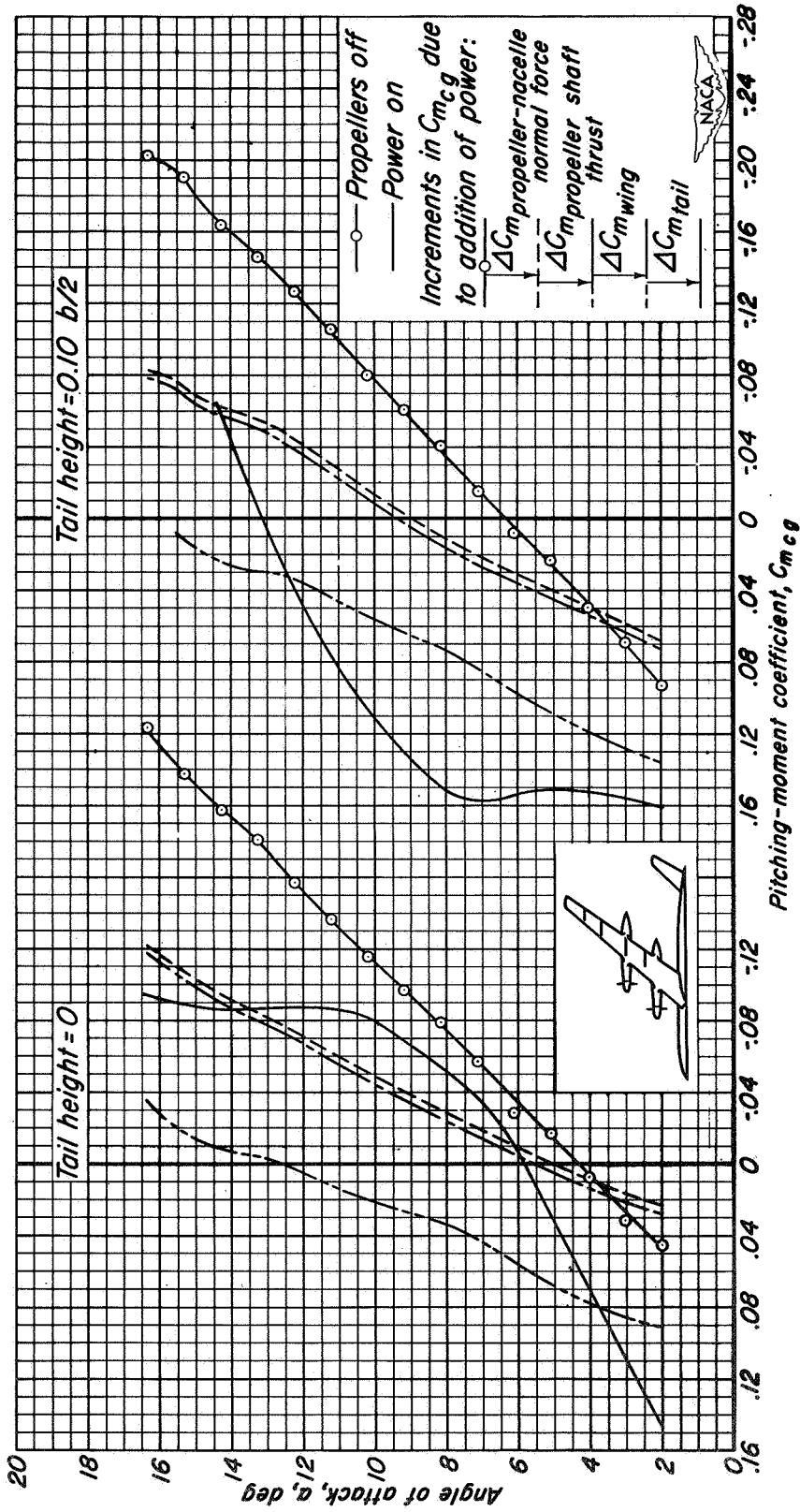
(c) $T_c = 0.80$

Figure 20.— Continued.
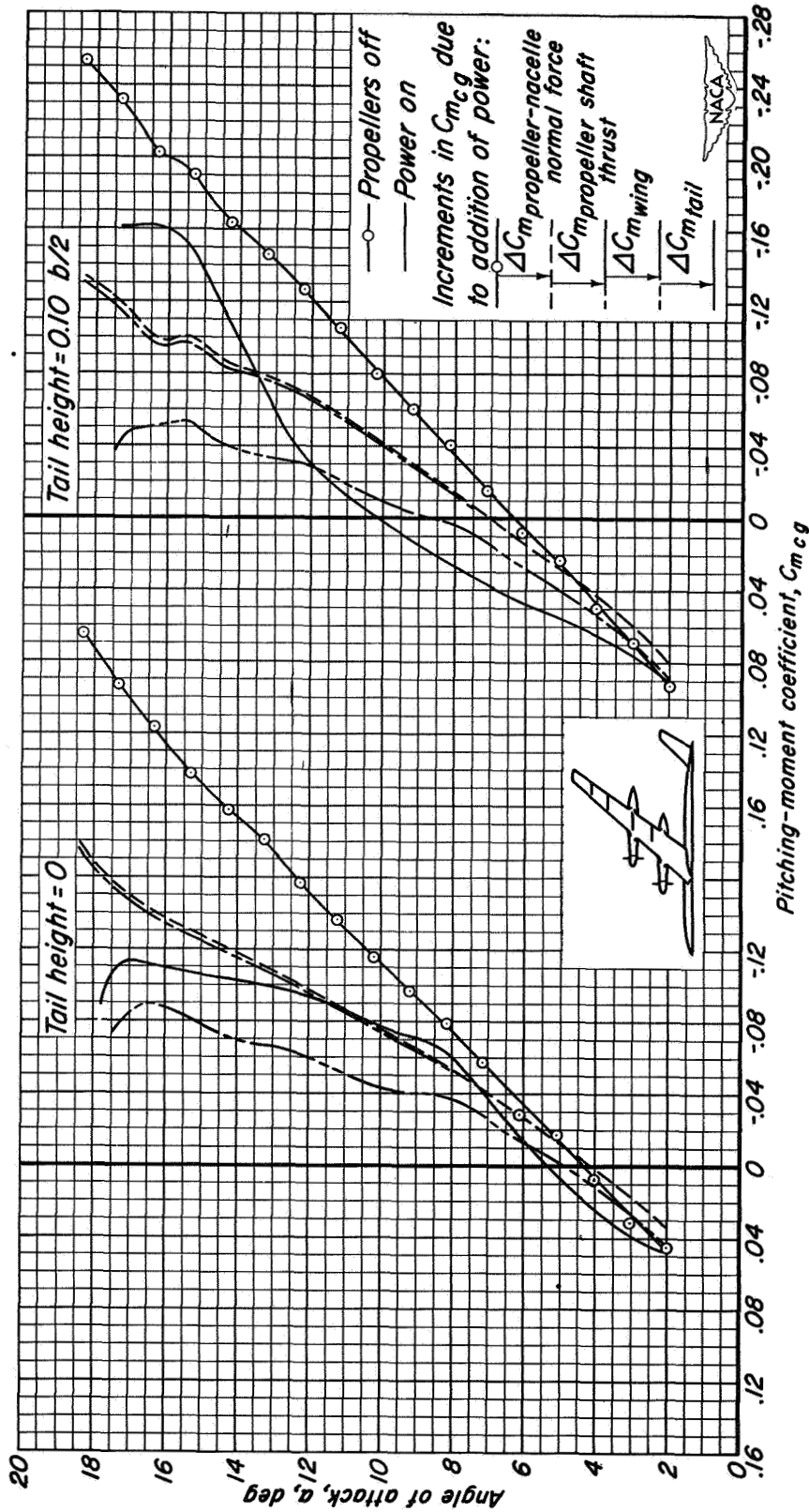
(d) 10,000 simulated hp

Figure 20.- Concluded.
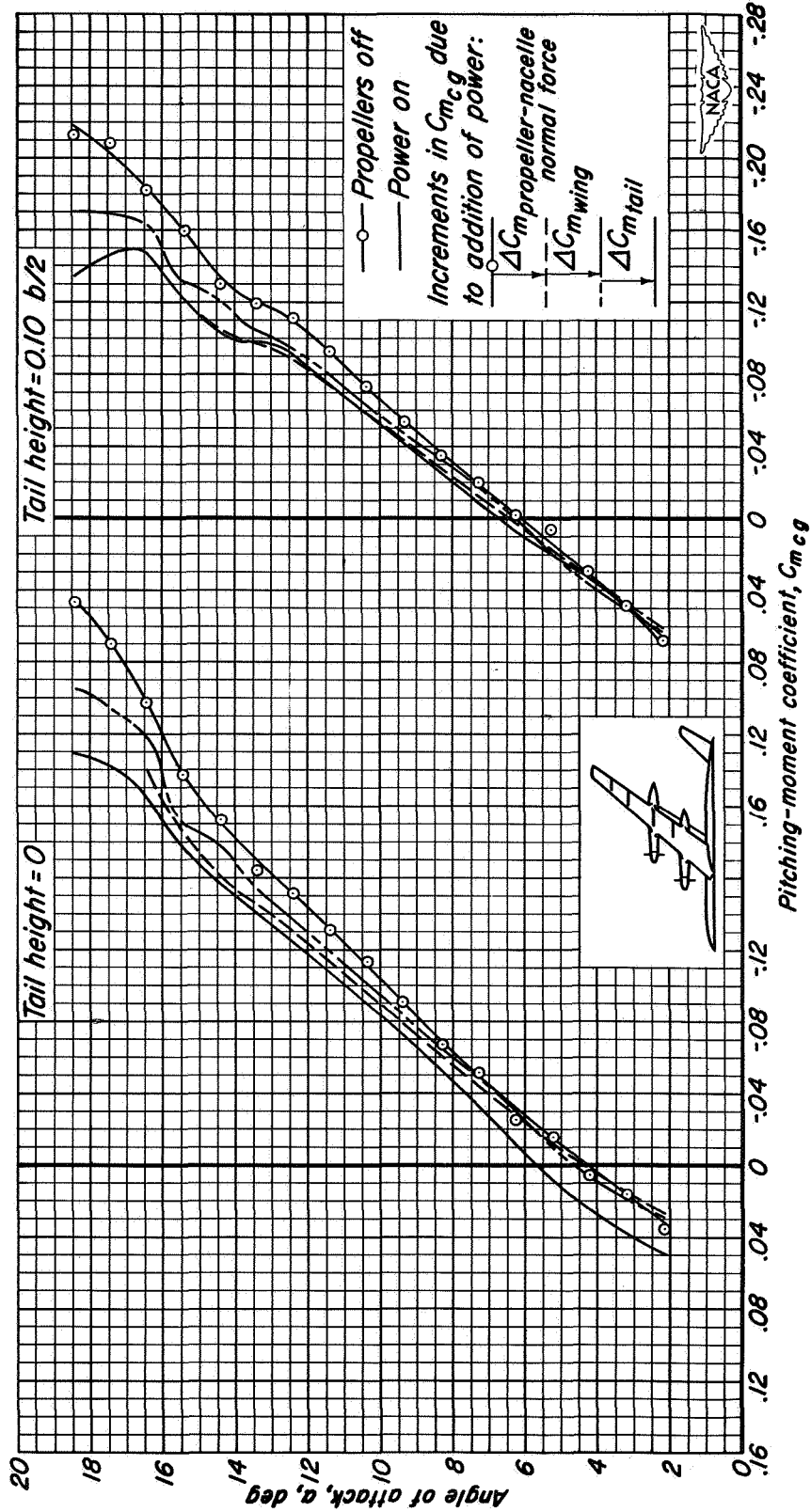
(a) $T_c = 0$

Figure 21.- The various effects of operating propellers on the pitching-moment characteristics of the model; inboard flaps deflected; $M = 0.082$; $R = 4,000,000$; $\beta = 26^{\circ}$; $i_t = 0^{\circ}$.
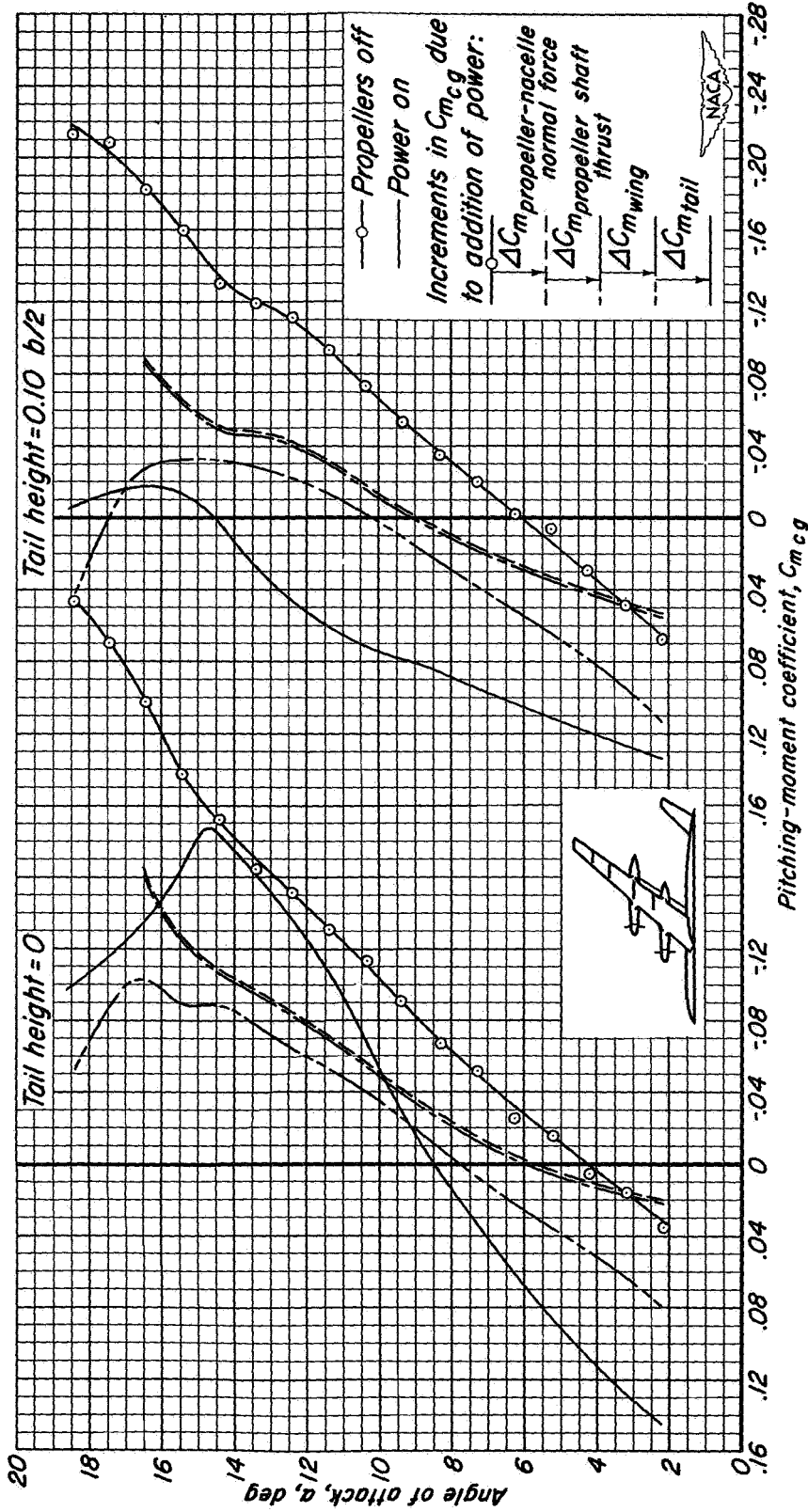
(b) $T_c = 0.40$
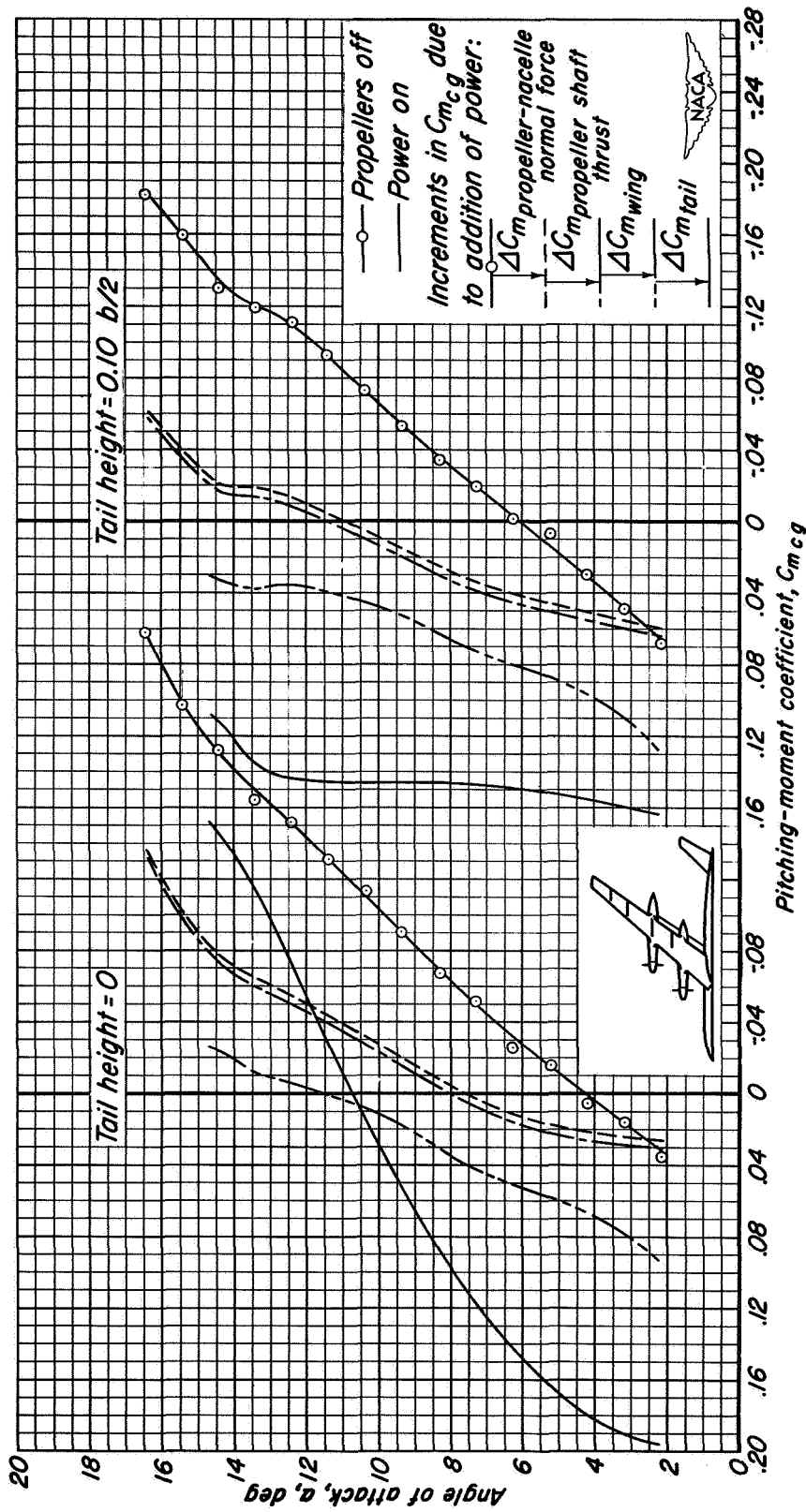
Figure 21.- Continued.

(c) T_c = 0.80

Figure 21.- Continued.
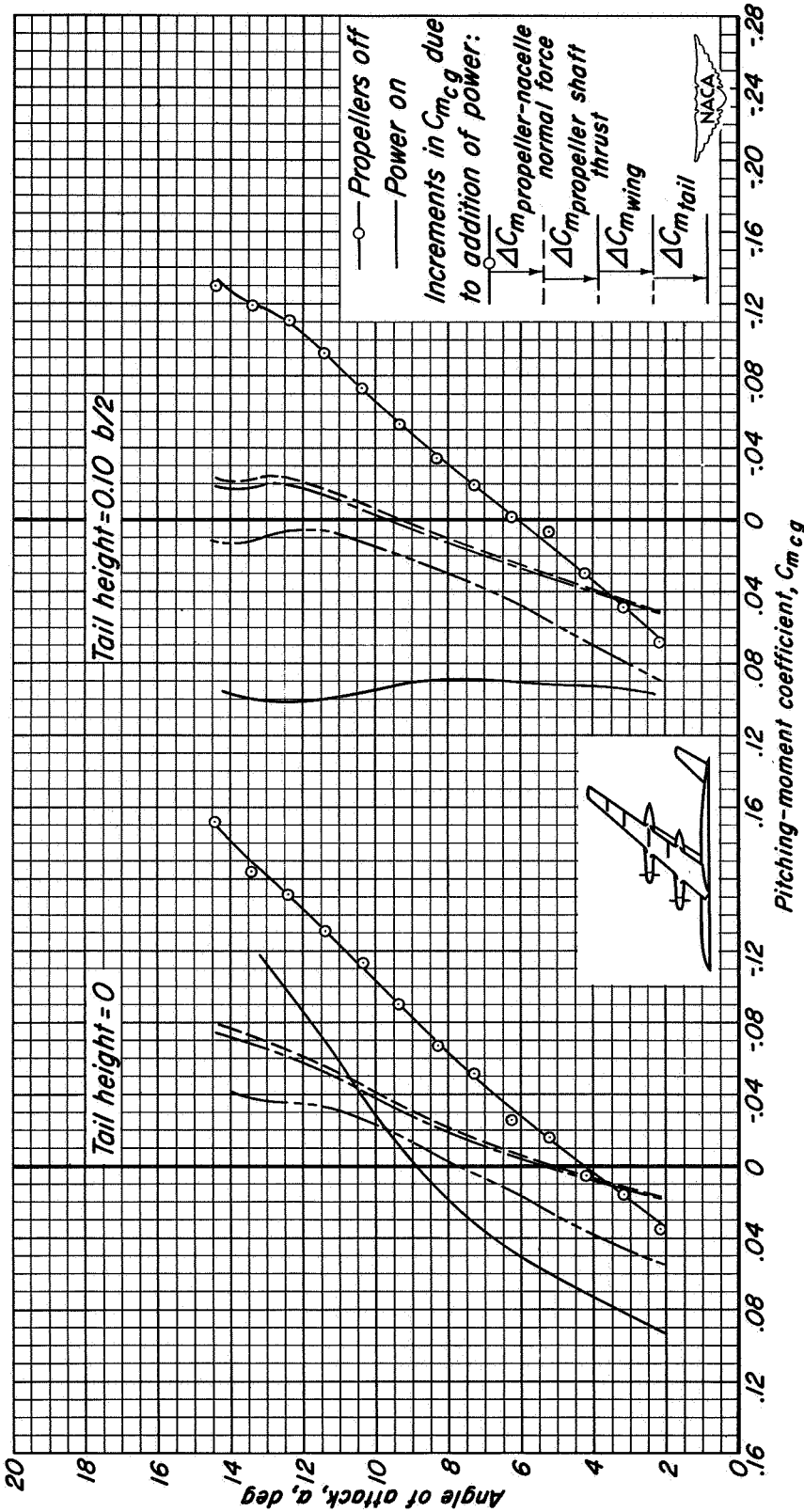
(d) 10,000 simulated hp

Figure 21.- Concluded.
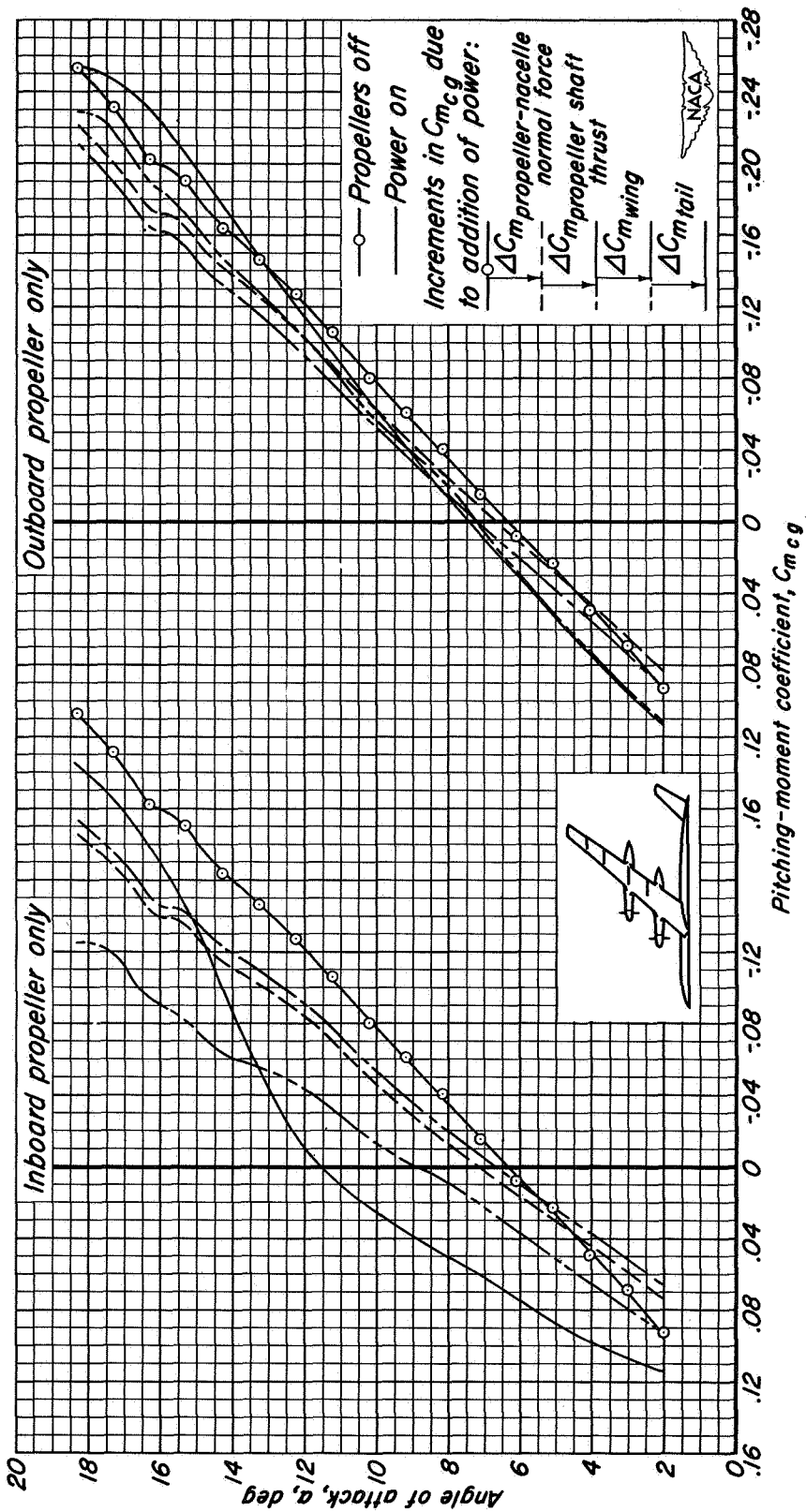
(a) $T_c = 0.40$.

Figure 22.- A comparison of the various effects of the inboard propeller on the pitching-moment characteristics of the model with those of the outboard propeller; tail height = 0.10 b/2; flaps up; M = 0.082; R = 4,000,000; β = 26°; it = -4°.
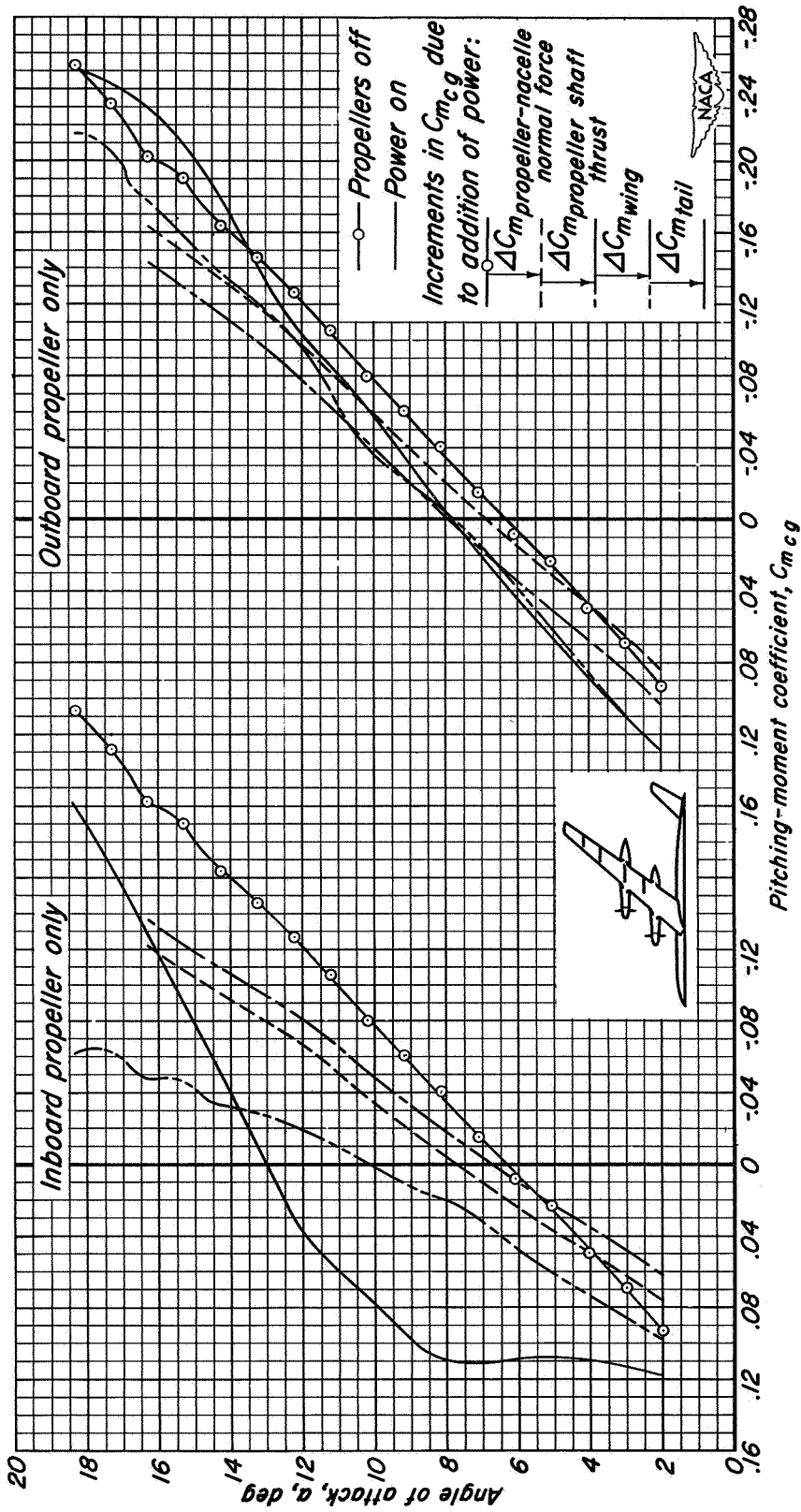
(b) $T_c = 0.80$

Figure 22.- Continued.
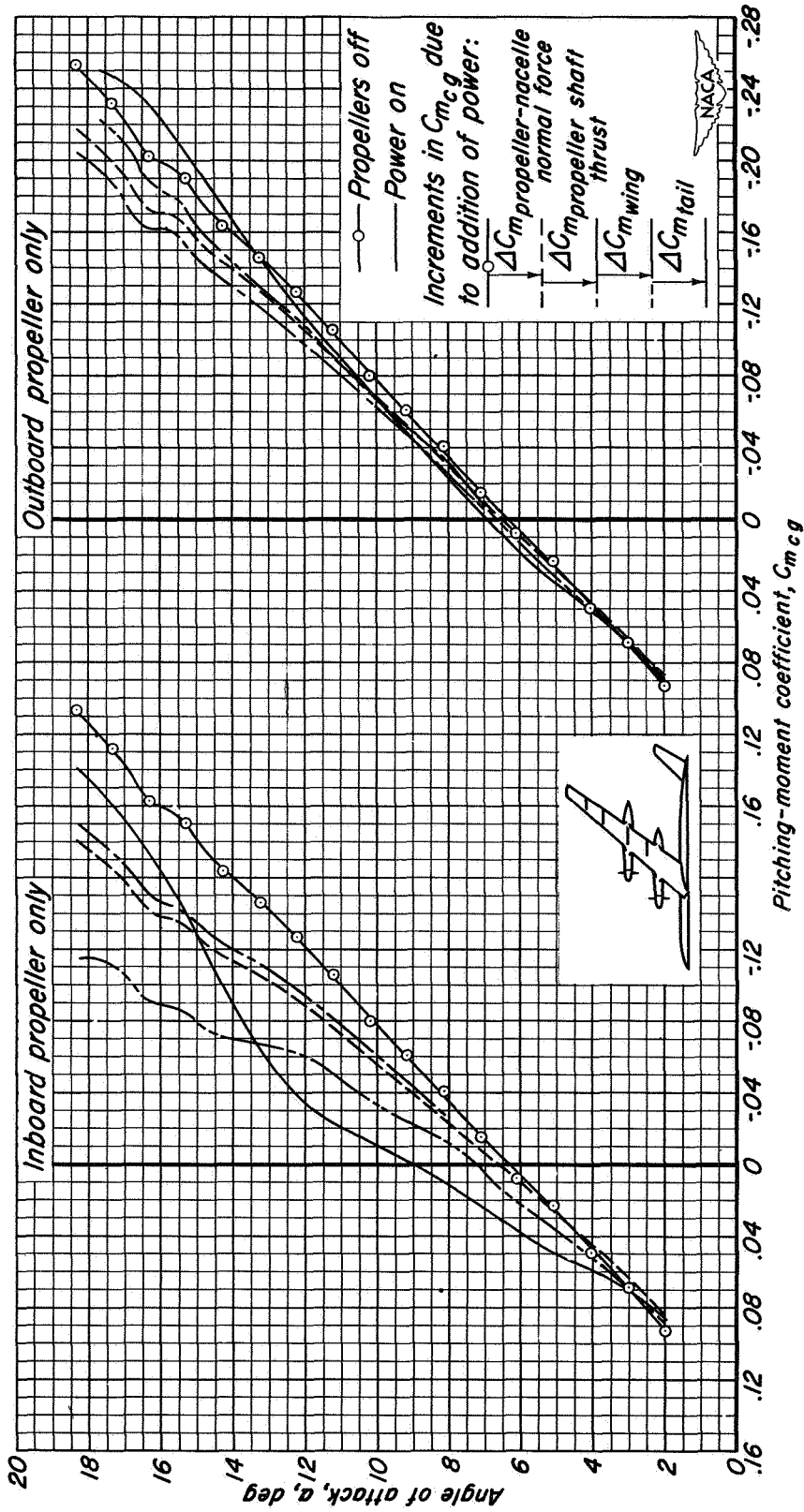
(c) 10,000 simulated hp

Figure 22.- Concluded.
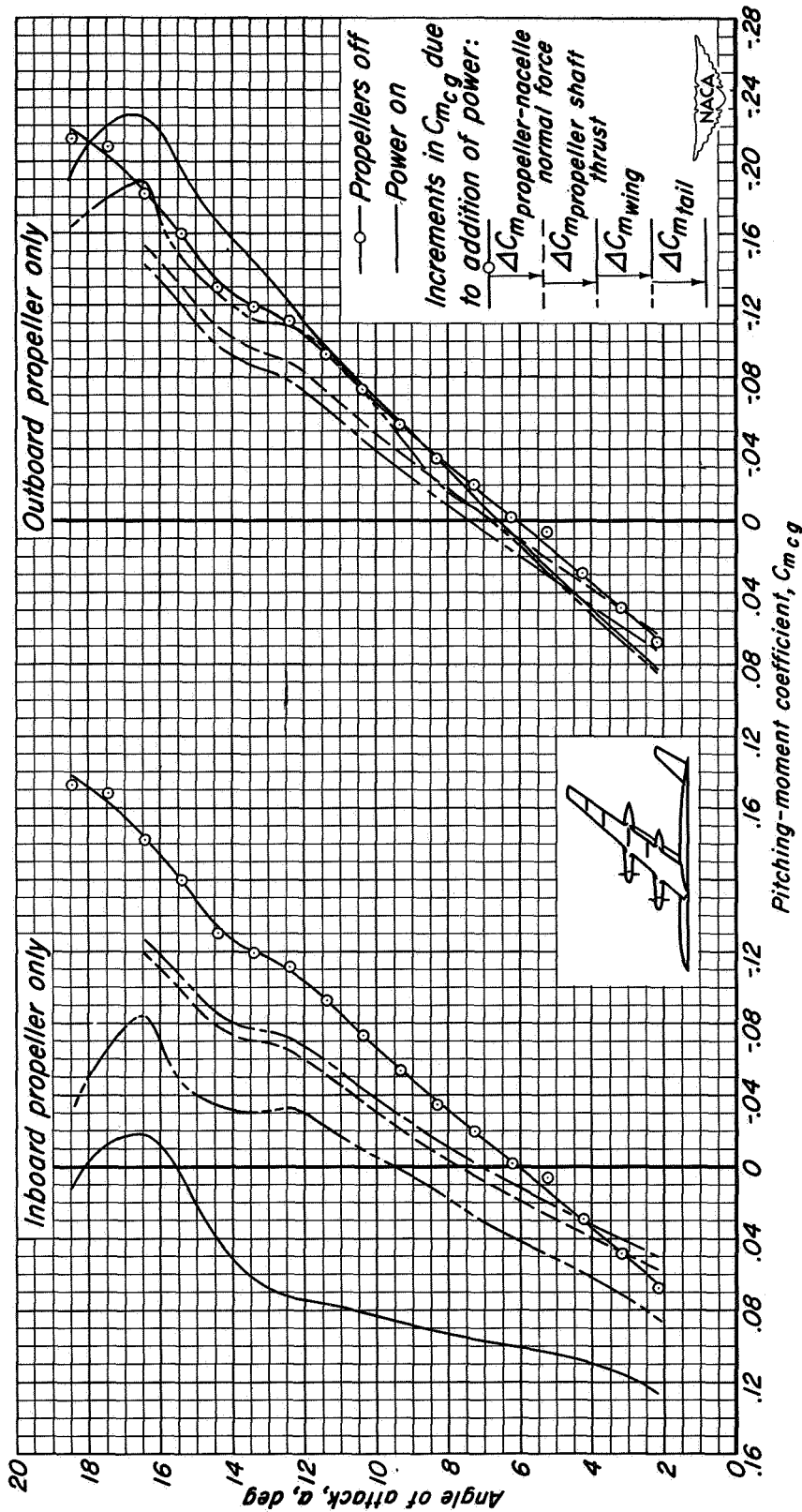
(a) T_c = 0.40

Figure 23.- A comparison of the various effects of the inboard propeller on the pitching-moment characteristics of the model with those of the outboard propeller; tail height = 0.10 b/2; inboard flaps deflected; M = 0.082; R = 4,000,000; β = 26°; it = 0°.
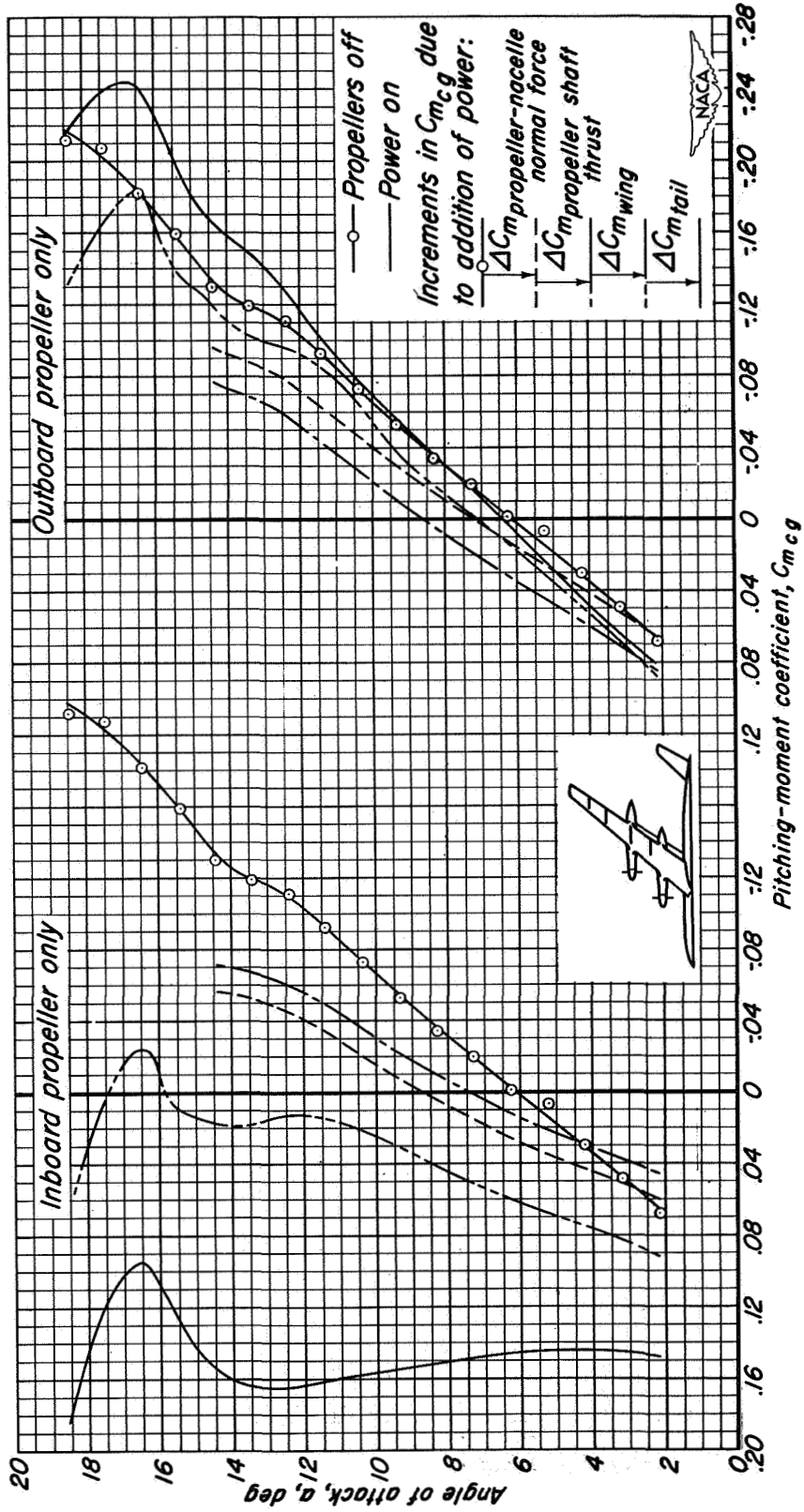
(b) $T_c = 0.80$

Figure 23.- Continued.
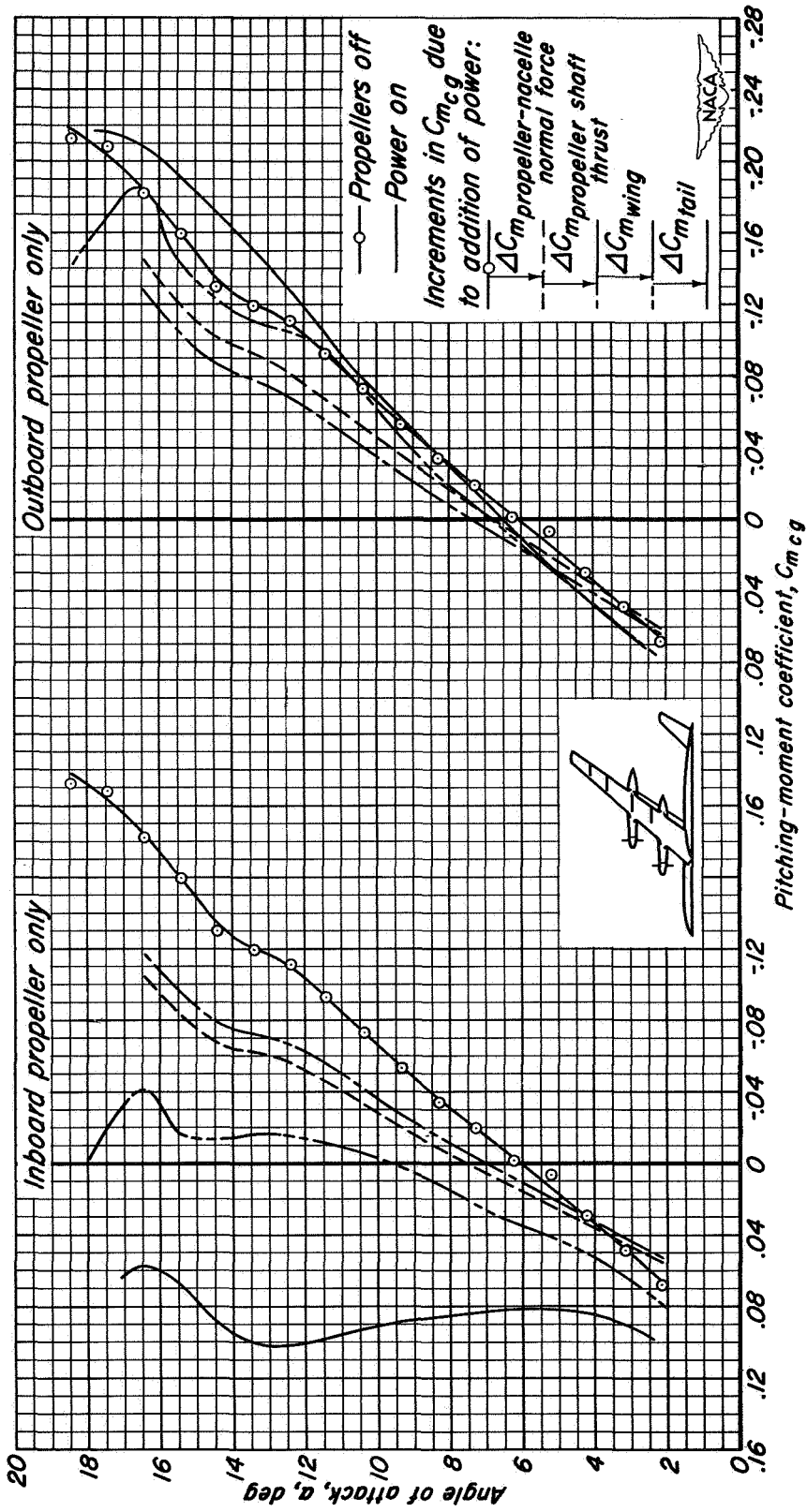
(c) 10,000 simulated hp

Figure 23.- Concluded.
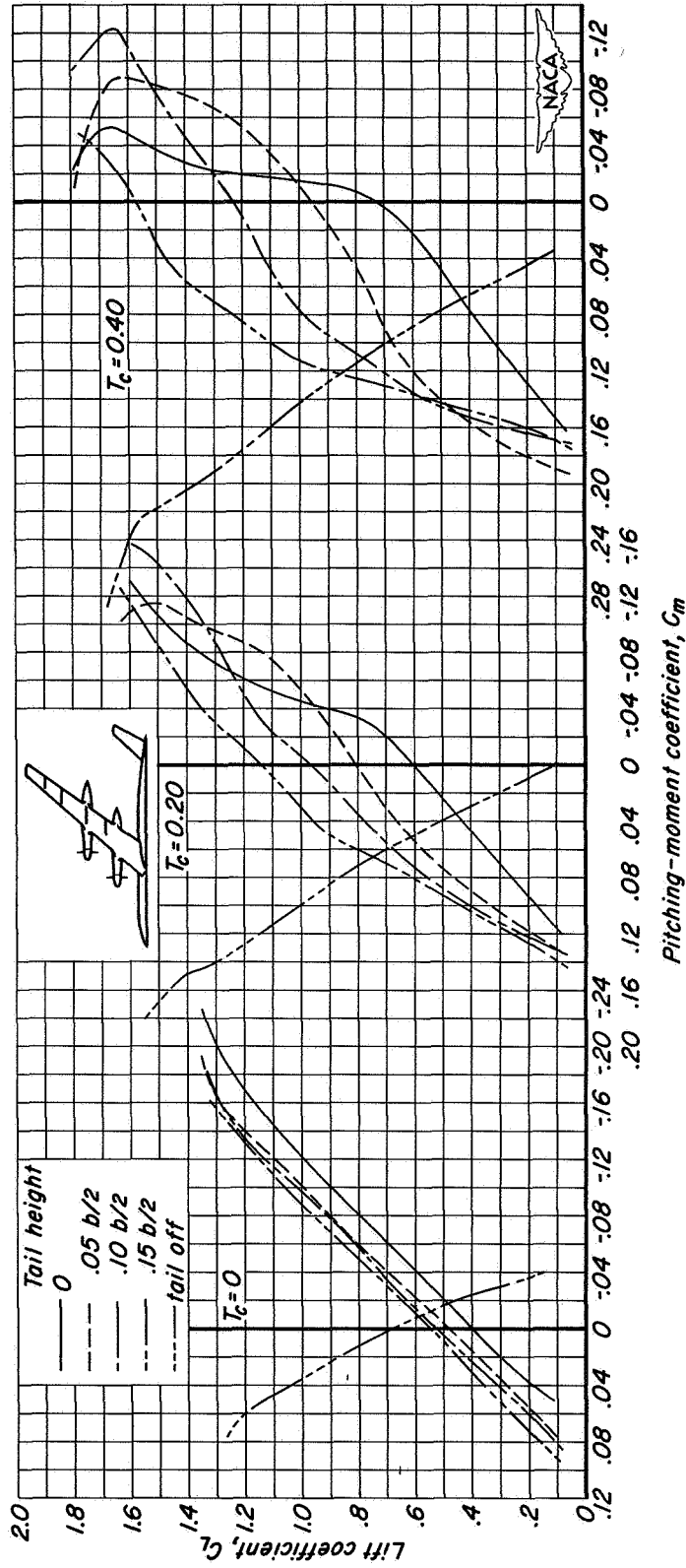
Figure 24.- The effects of tail height on the pitching-moment characteristics of the model; flaps up; $M = 0.123$; $R = 4,000,000$; $\beta = 31°$; $i_t = -4°$.
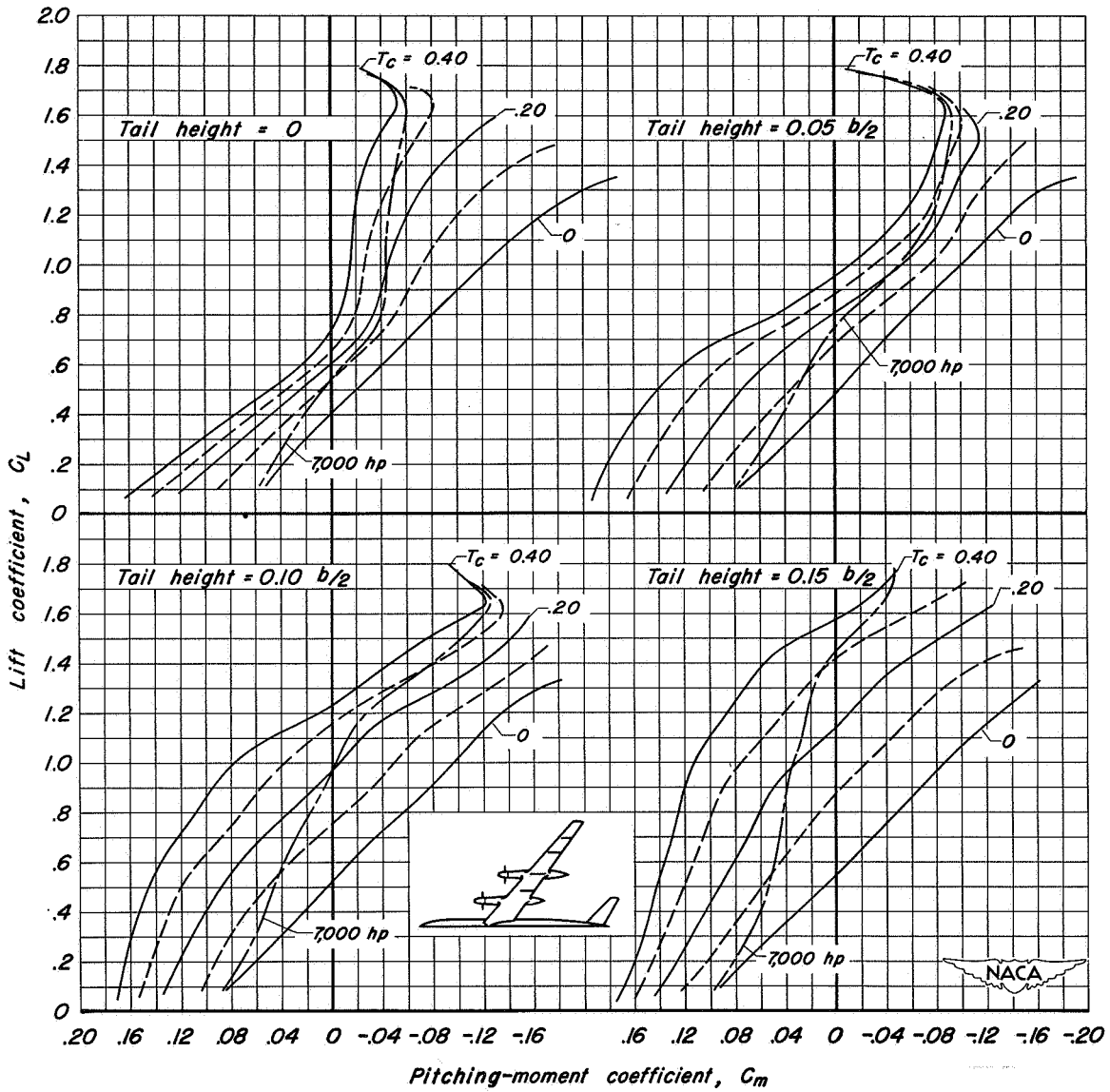
Figure 25.- A comparison at various tail heights of the effects of
operating propellers on the pitching-moment characteristics of the
model; flaps up; M = 0.123; R = 4,000,000; β = 31°; i_t = -4°.
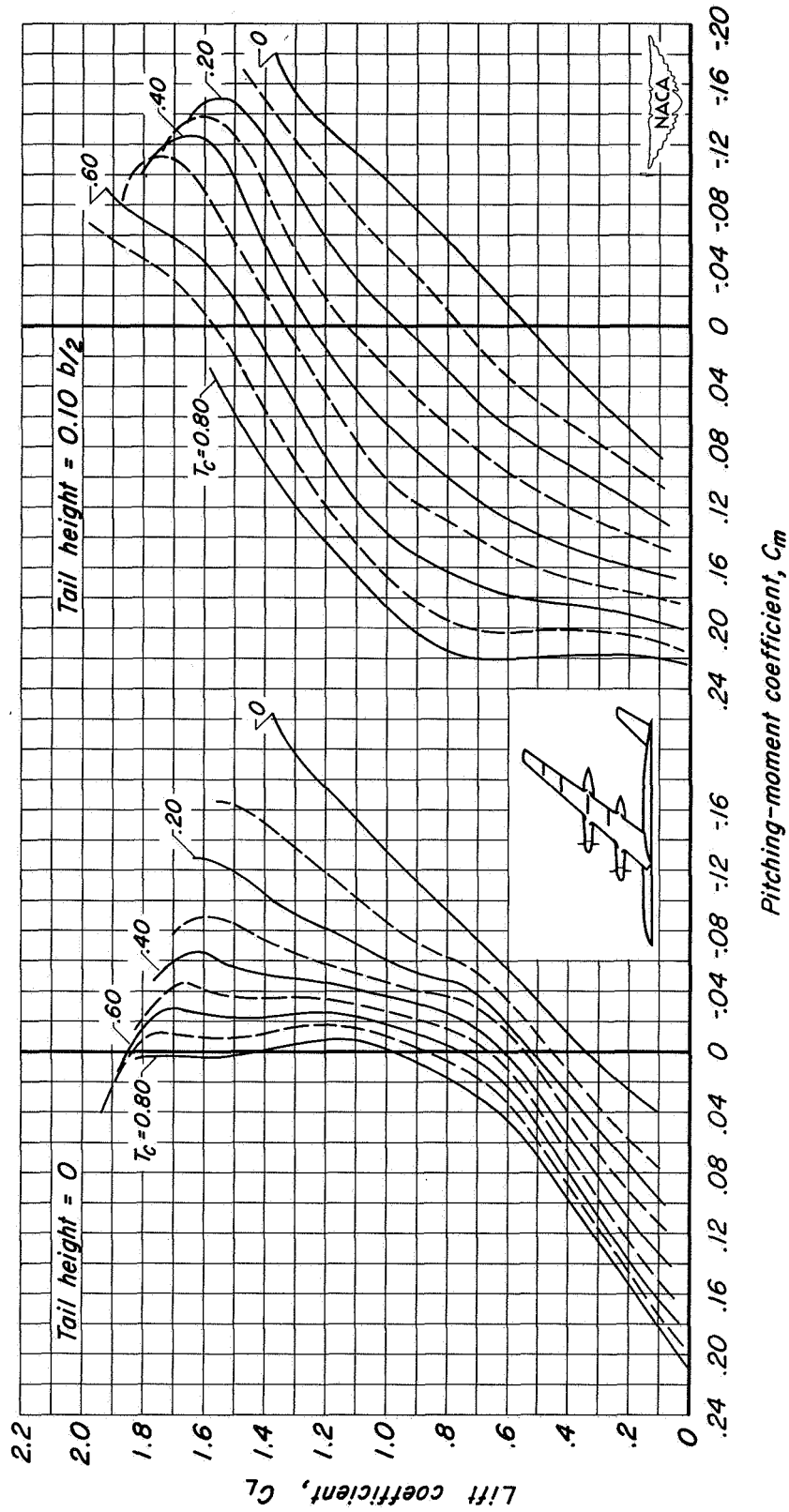
(a) Flaps up; $i_t = -4°$

Figure 26.- A comparison for two tail heights of the effects of operating propellers on the pitching-moment characteristics of the model; M = 0.082; R = 4,000,000; β = 26°.

C█████████   NACA RM A54F14
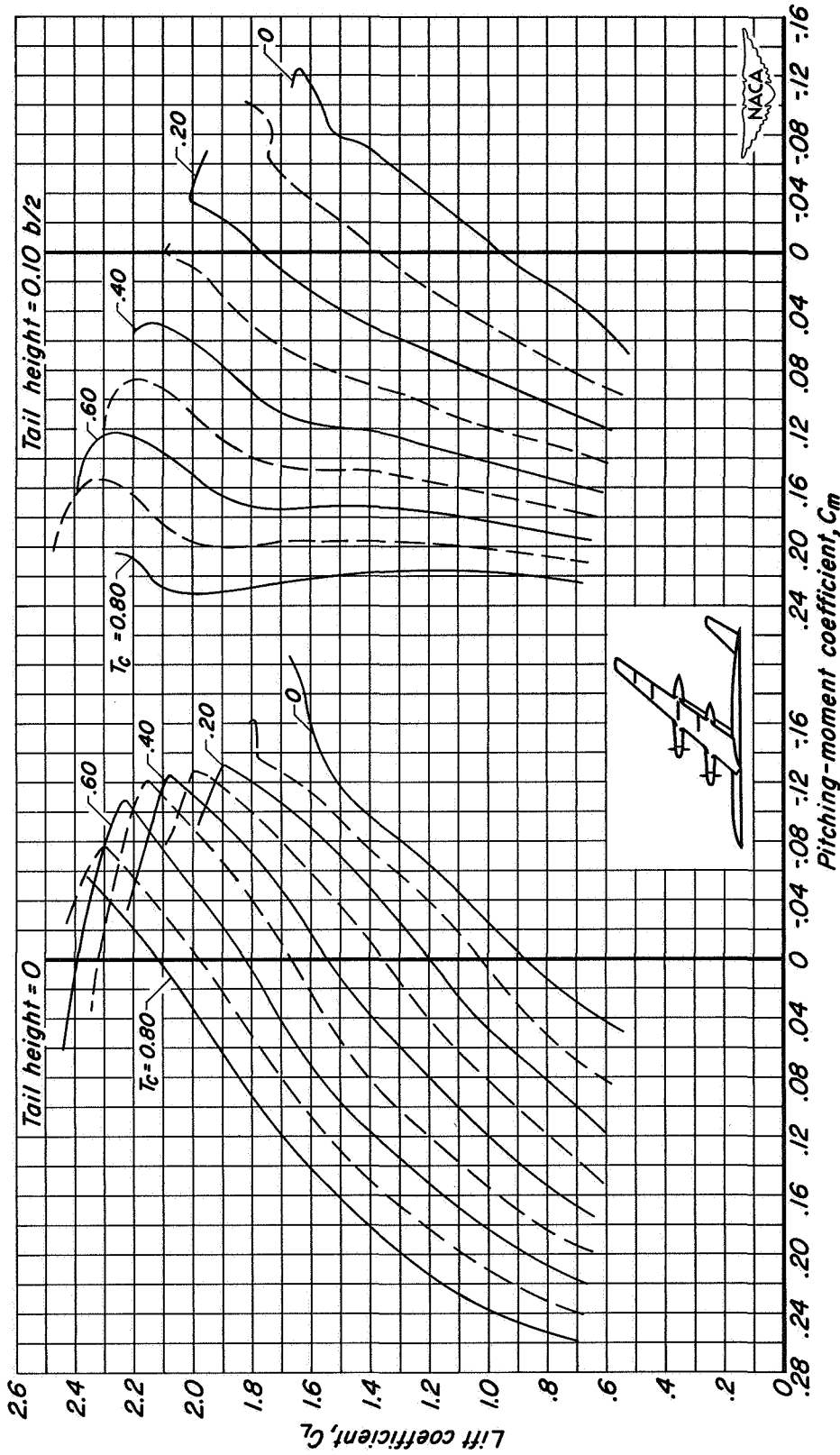
(b) Inboard flaps deflected; $i_t = 0°$

Figure 26.- Concluded.
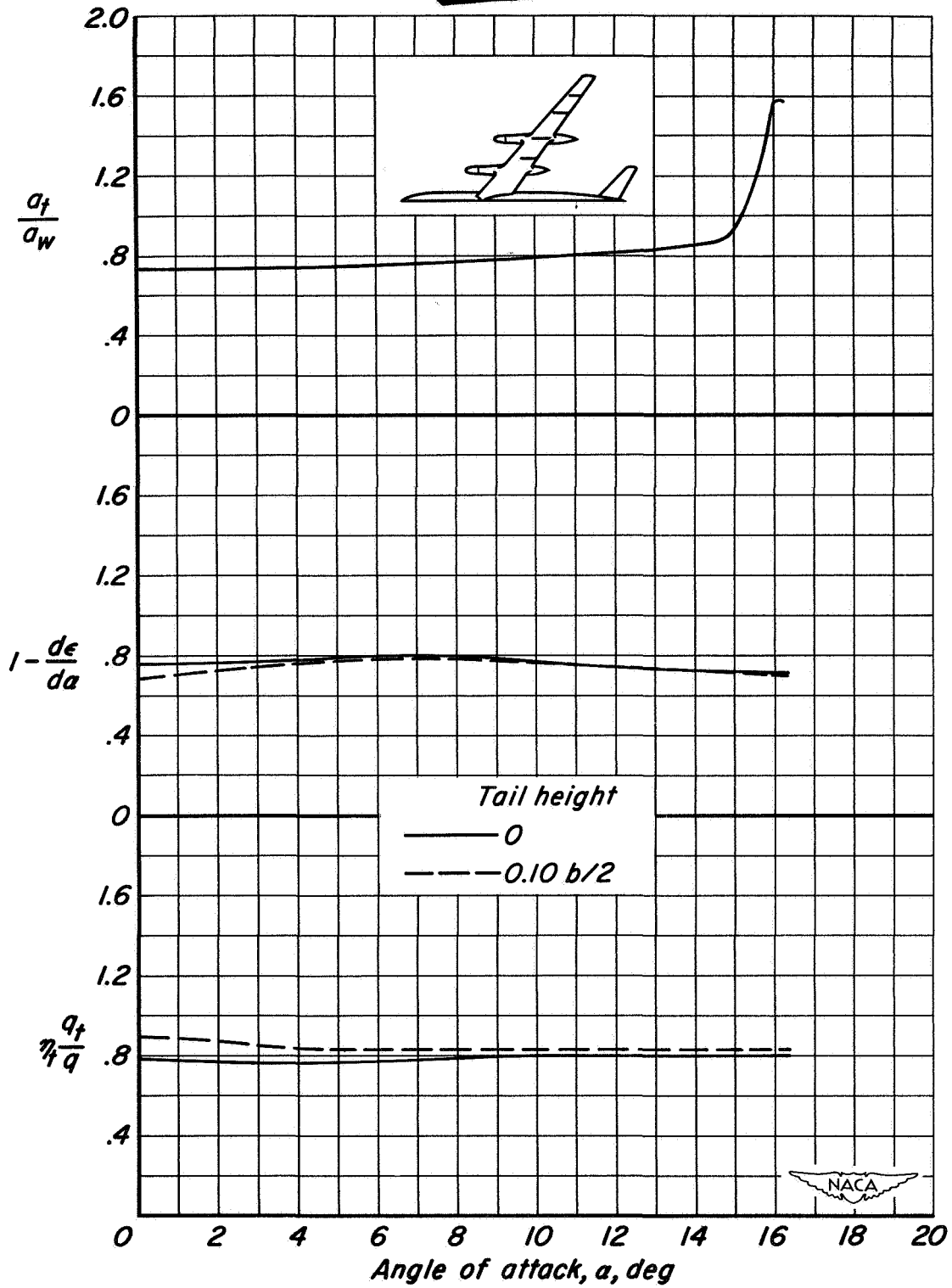
(a) Propellers off.

Figure 27.- The variation of a_t/a_w, $1-(d\epsilon/d\alpha)$, and $\eta_t(q_t/q)$ with α; flaps up; M = 0.082; R = 4,000,000; β = 26°.
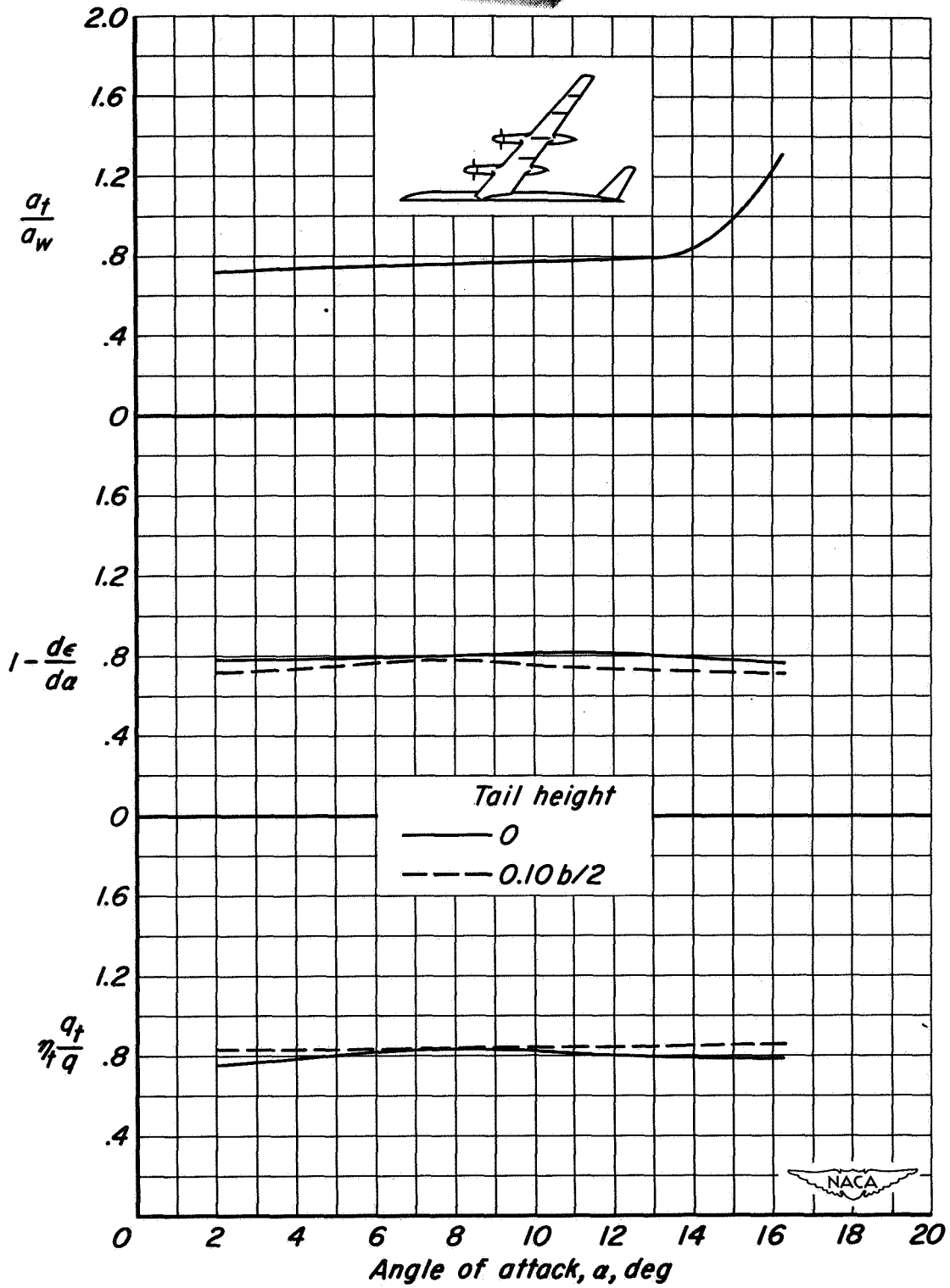
(b) $T_c = 0$

Figure 27.- Continued.
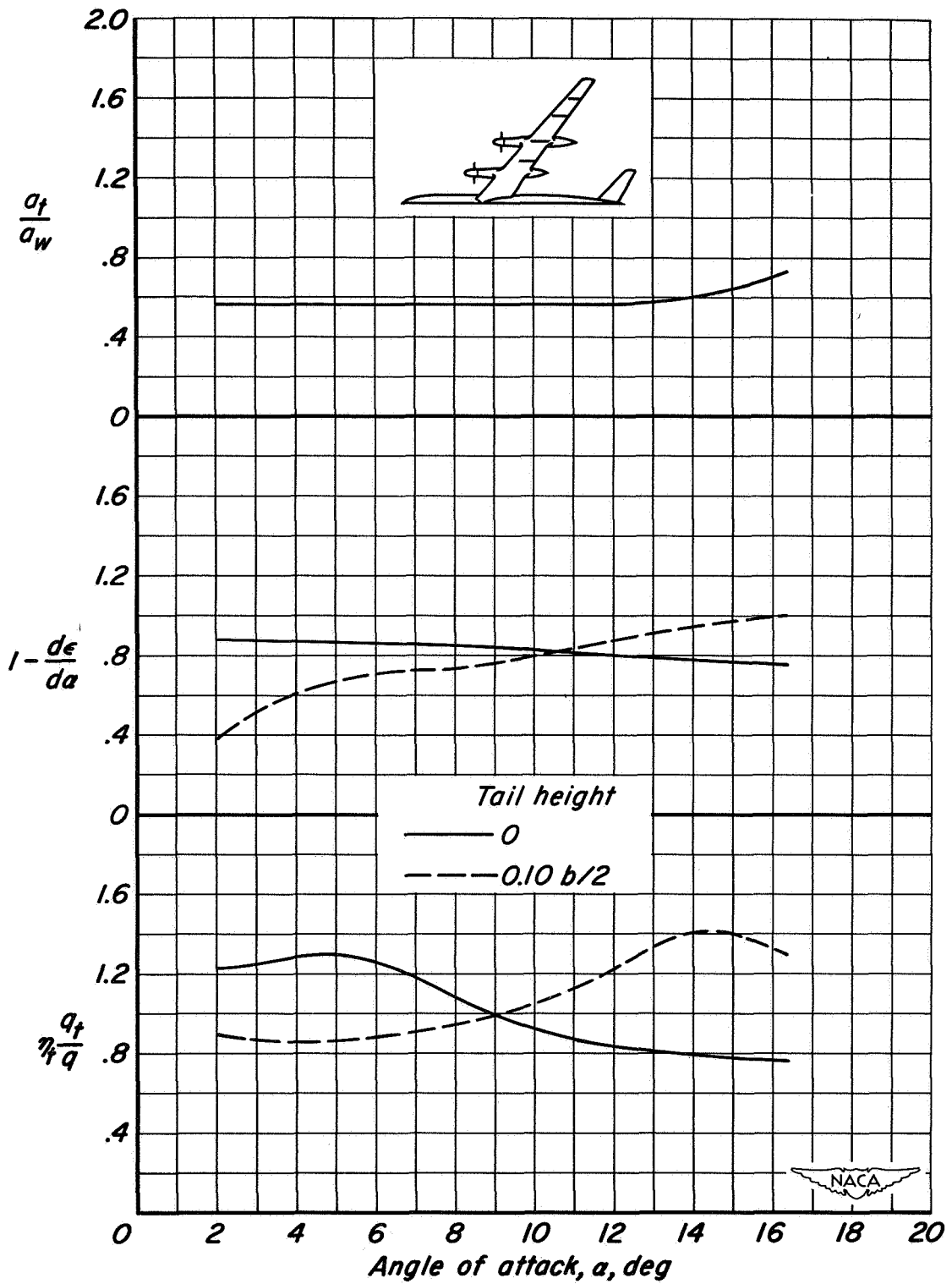
(c) $T_c = 0.40$

Figure 27.- Continued.
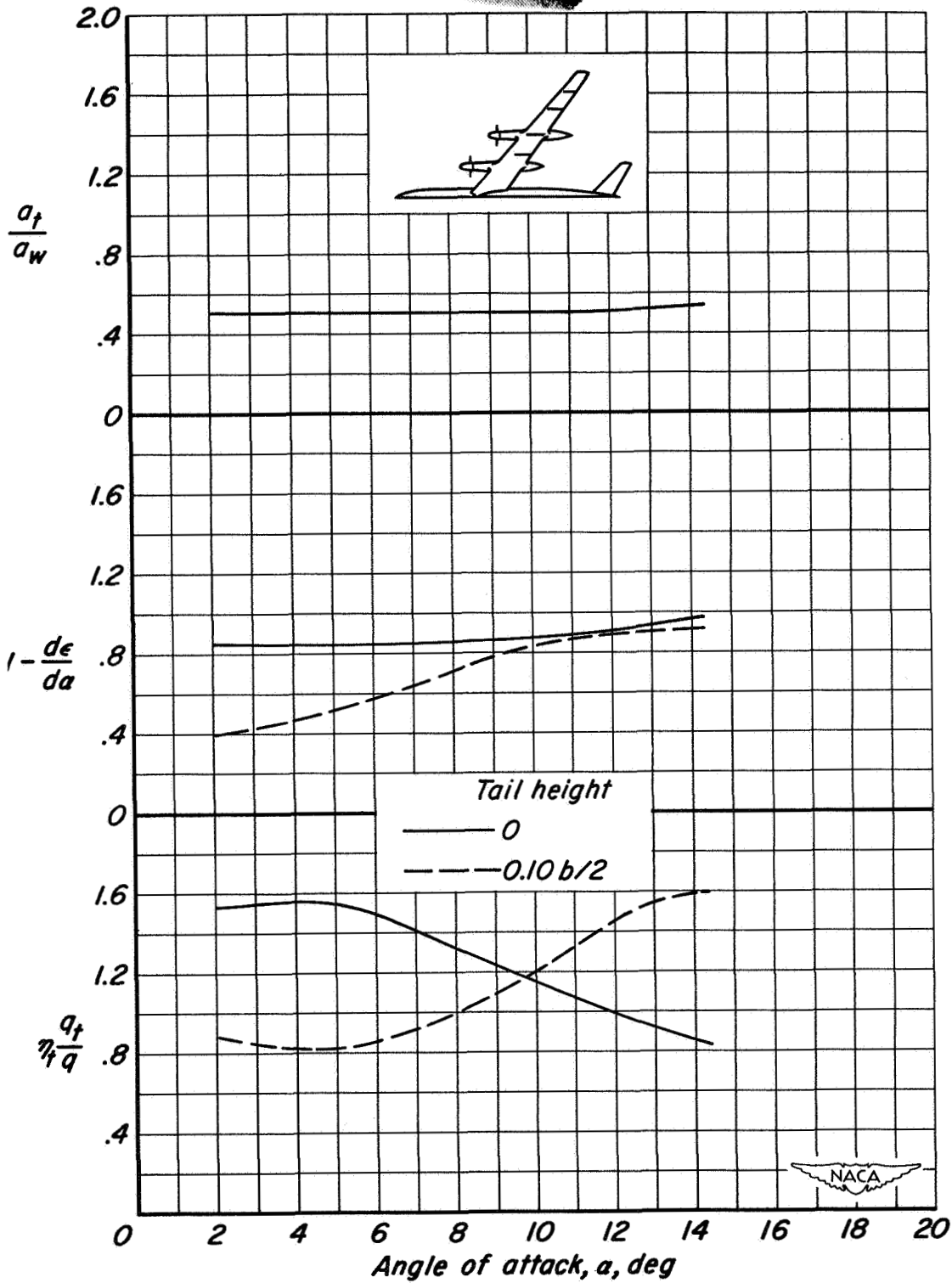
(d) $T_c = 0.80$

Figure 27.- Concluded.
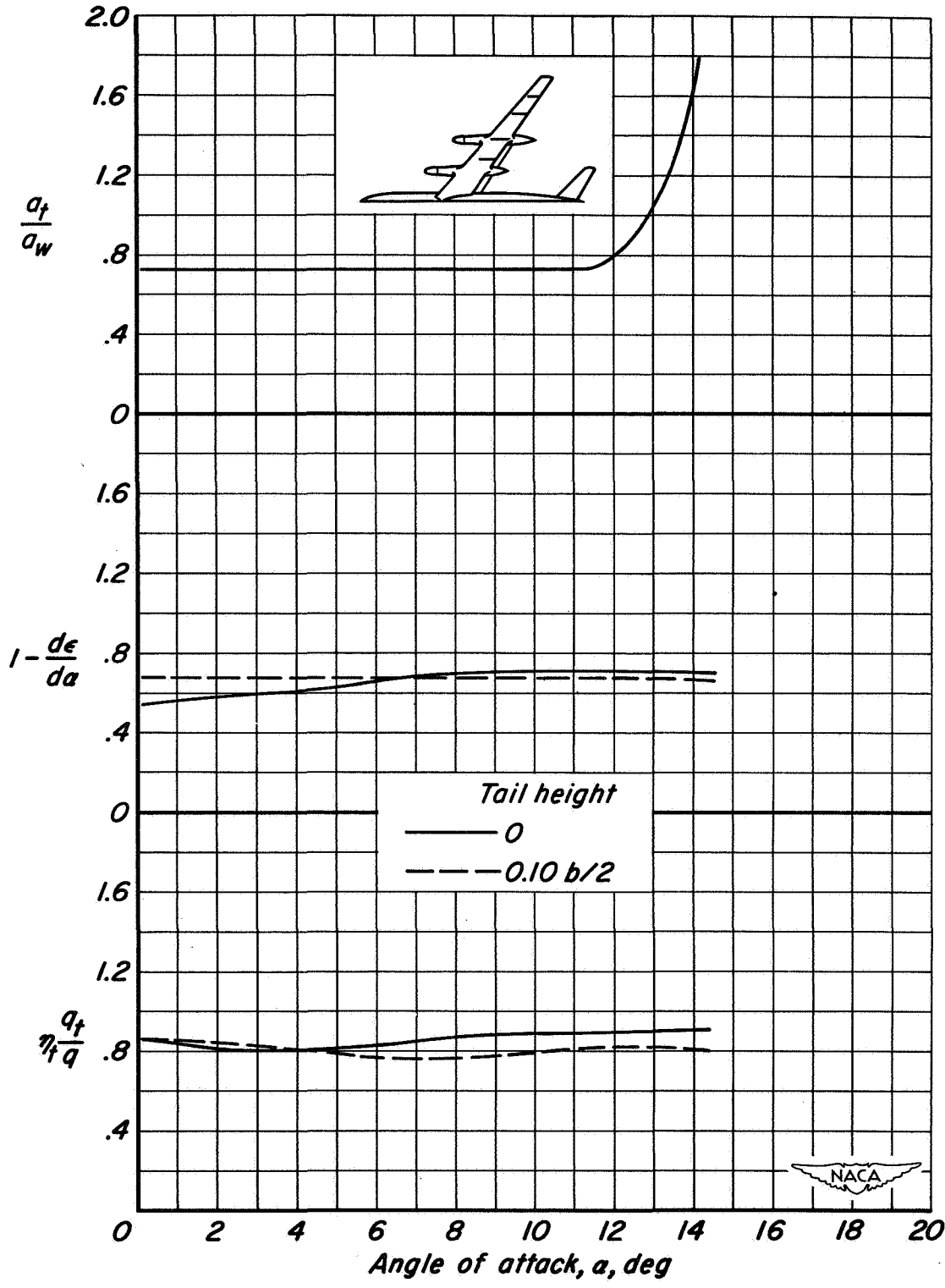
(a) Propellers off.

Figure 28.- The variation of a_t/a_w, $1-(d\epsilon/d\alpha)$, and $\eta_t(q_t/q)$ with α; inboard flaps deflected; $M = 0.082$; $R = 4,000,000$; $\beta = 26°$.
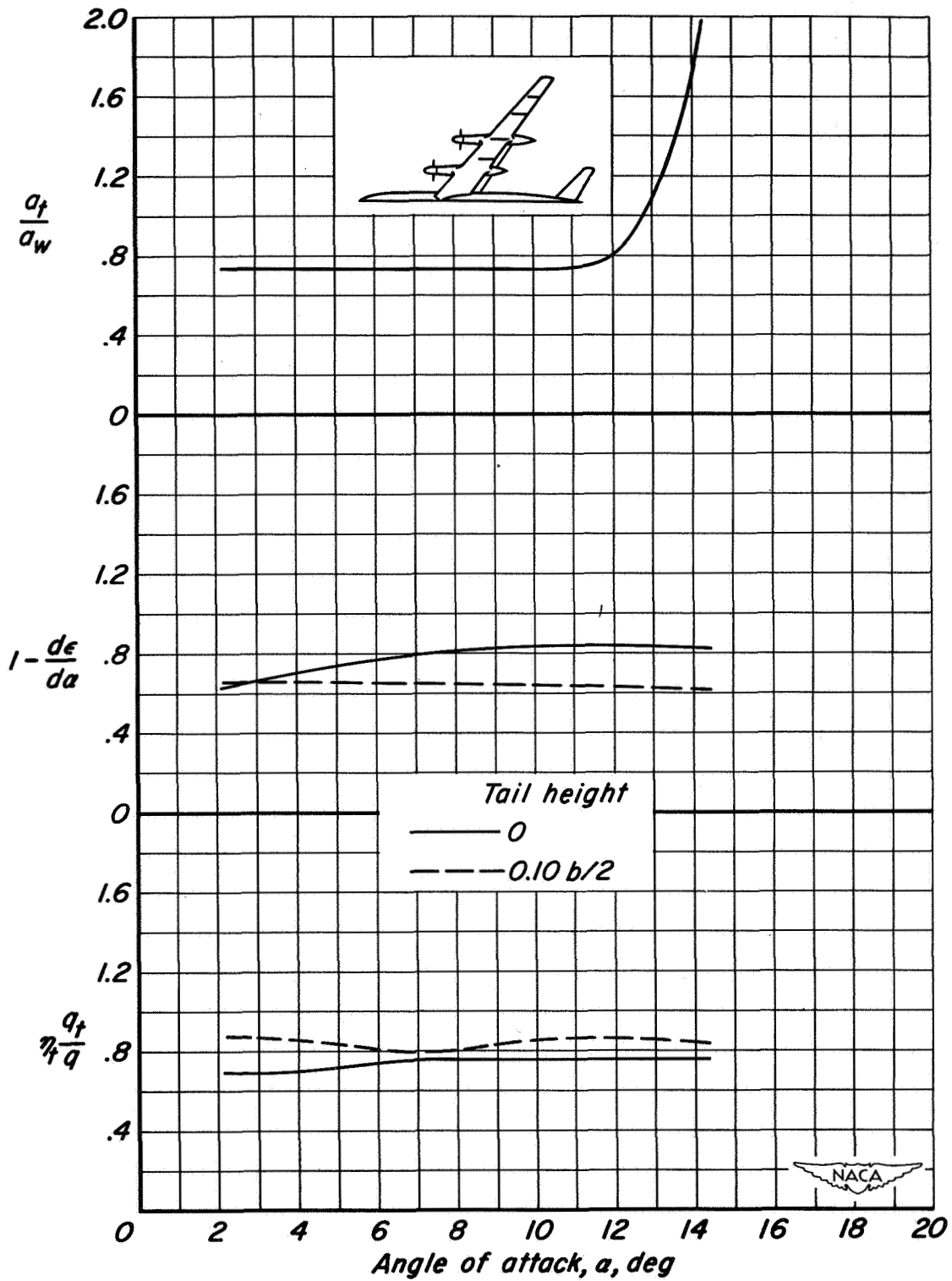
(b) $T_c = 0$

Figure 28.- Continued.
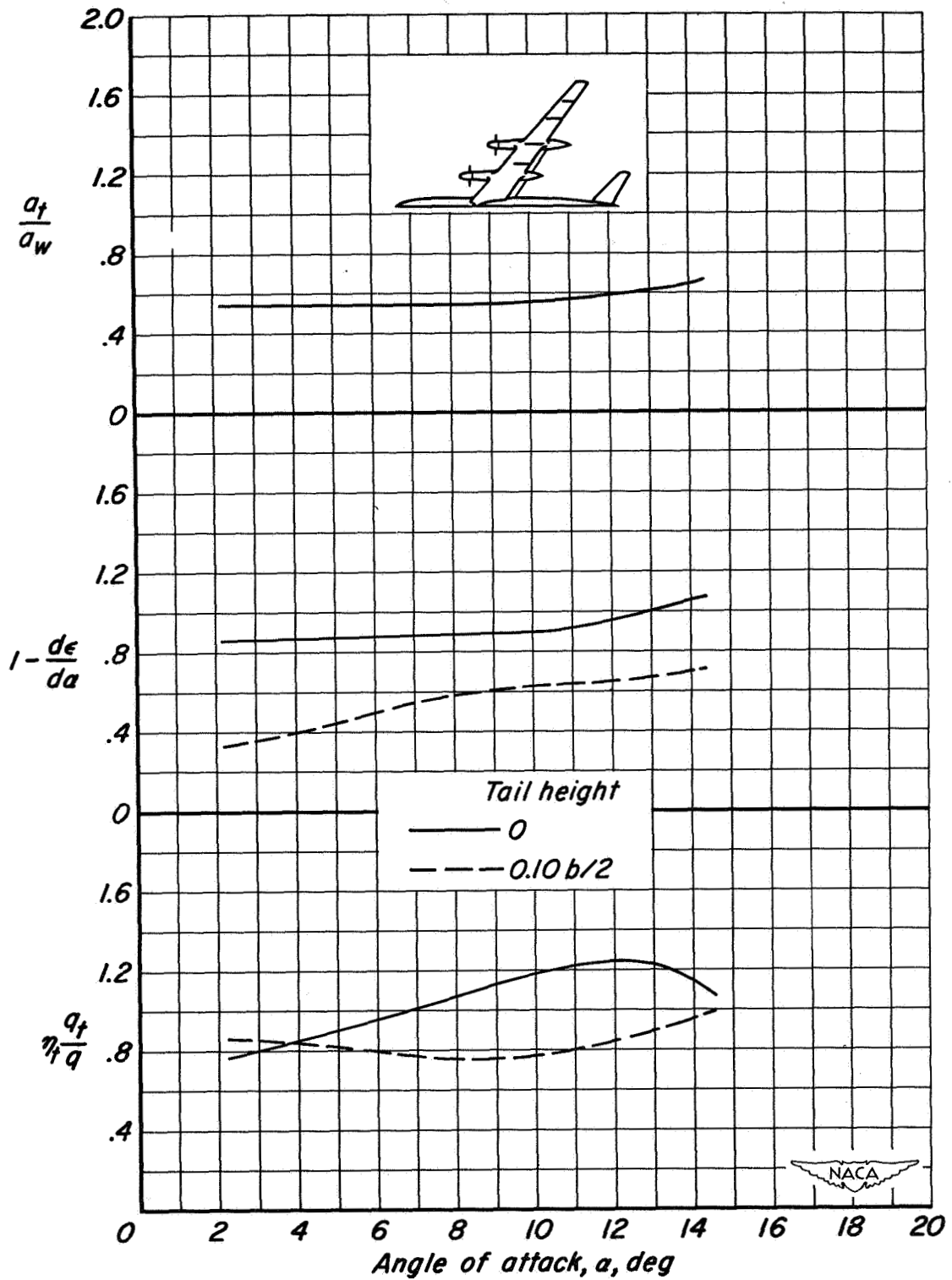
(c) $T_c = 0.40$

Figure 28.- Continued.
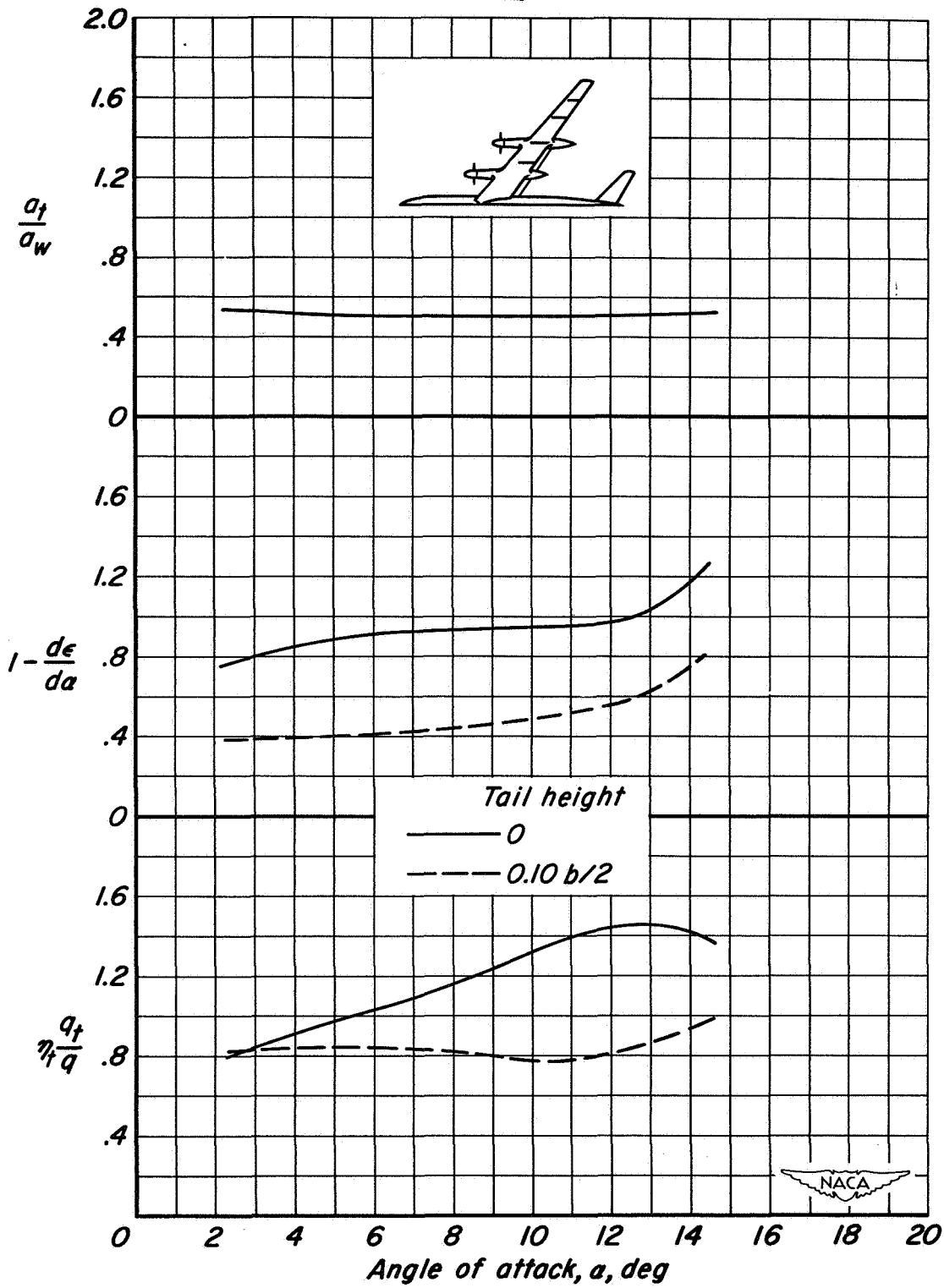
(d) $T_c = 0.80$

Figure 28. - Concluded.
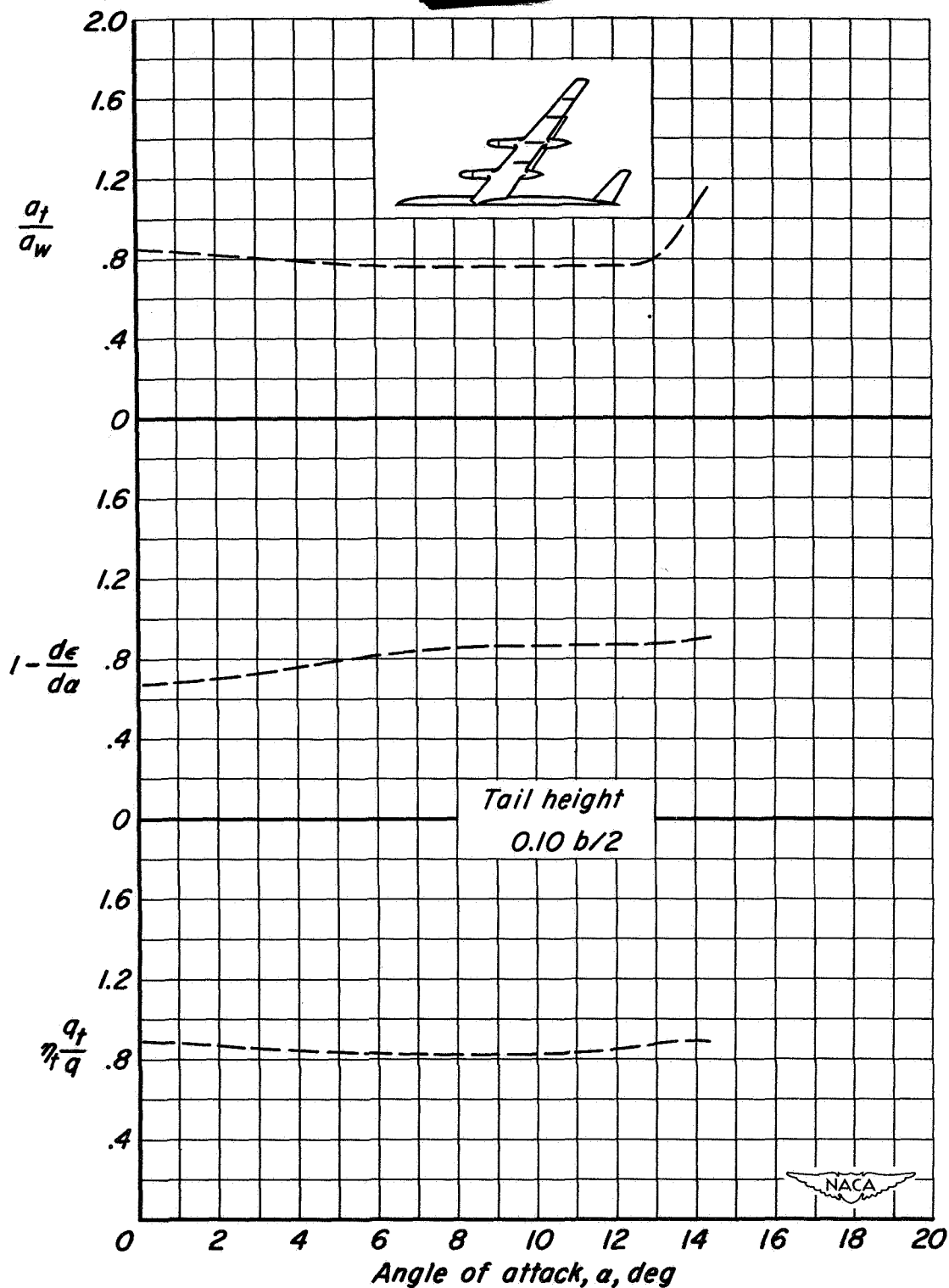
(a) Propellers off.

Figure 29.- The variation of a_t/a_w, $1-(d\epsilon/d\alpha)$, and $\eta_t(q_t/q)$ with α; outboard flaps deflected; M = 0.082; R = 4,000,000; β = 26°.

$\dfrac{a_t}{a_w}$

$1 - \dfrac{d\epsilon}{d\alpha}$

Tail height
0.10 b/2

$\eta_t \dfrac{q_t}{q}$

NACA

Angle of attack, α, deg

(b) $T_c = 0$

Figure 29.- Continued.

$$\frac{a_t}{a_w}$$

$$1 - \frac{d\epsilon}{d\alpha}$$

Tail height
0.10 b/2

$$\eta_t \frac{q_t}{q}$$

Angle of attack, α, deg
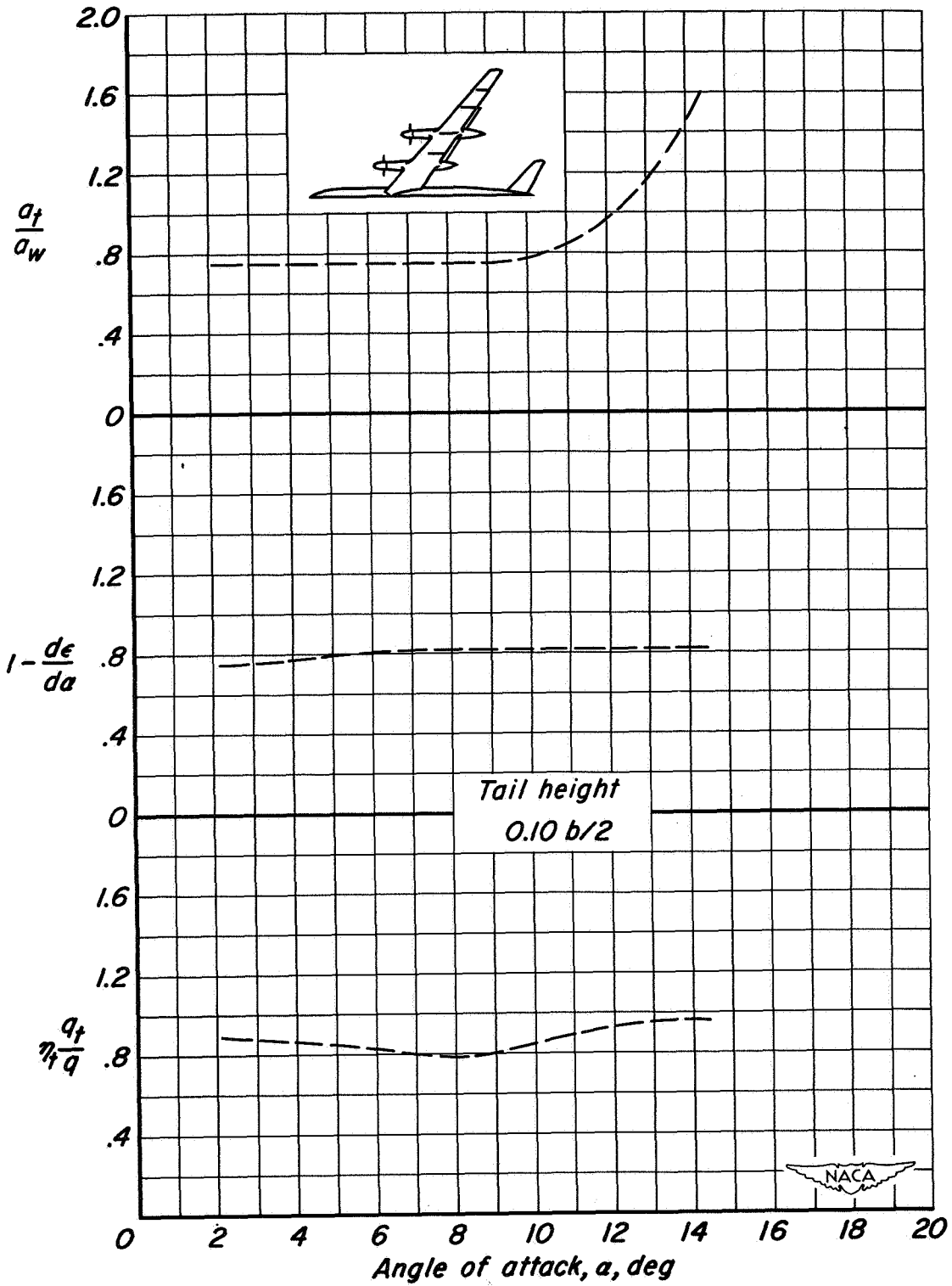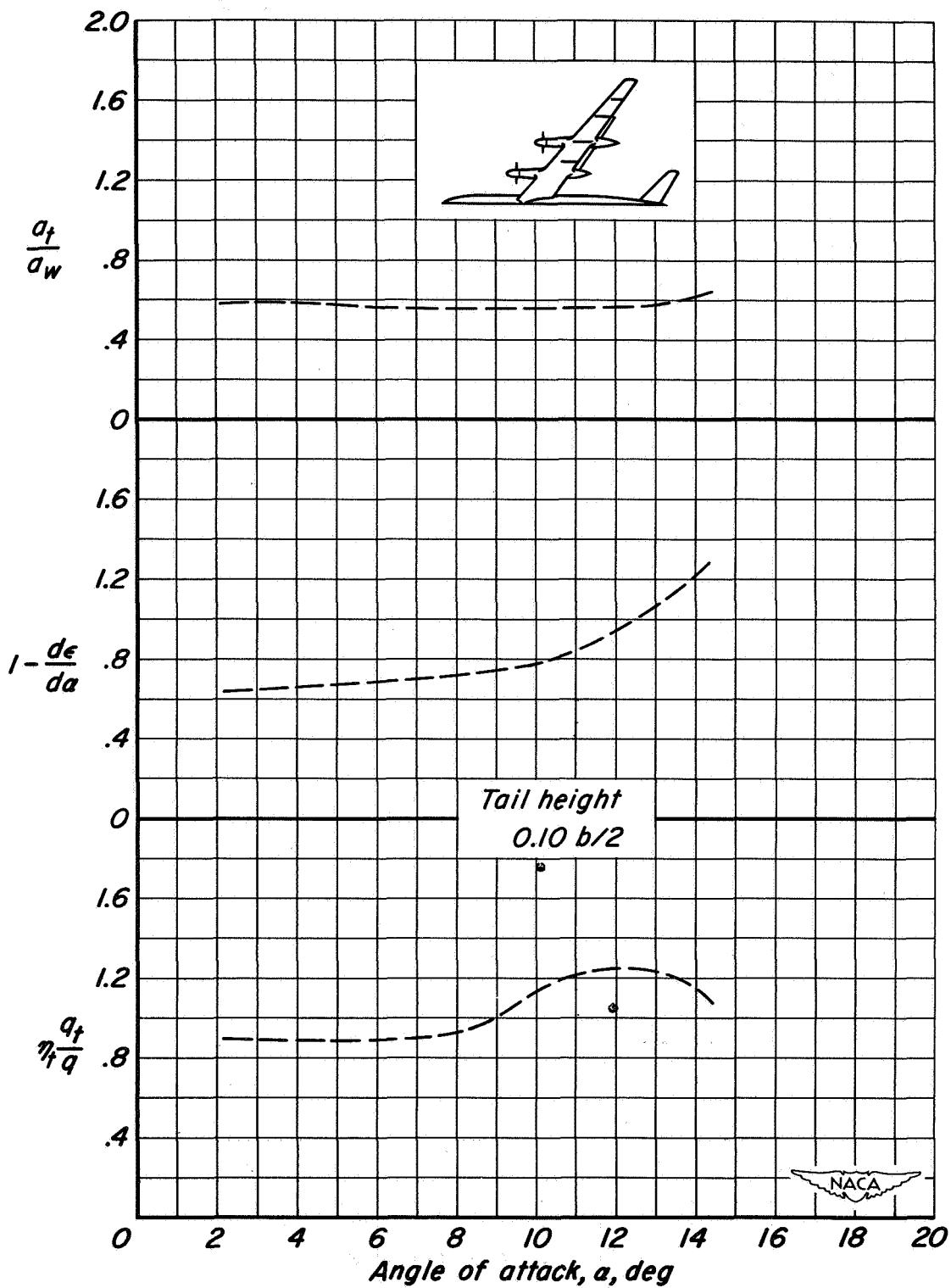
(c) $T_c = 0.40$

Figure 29.- Continued.
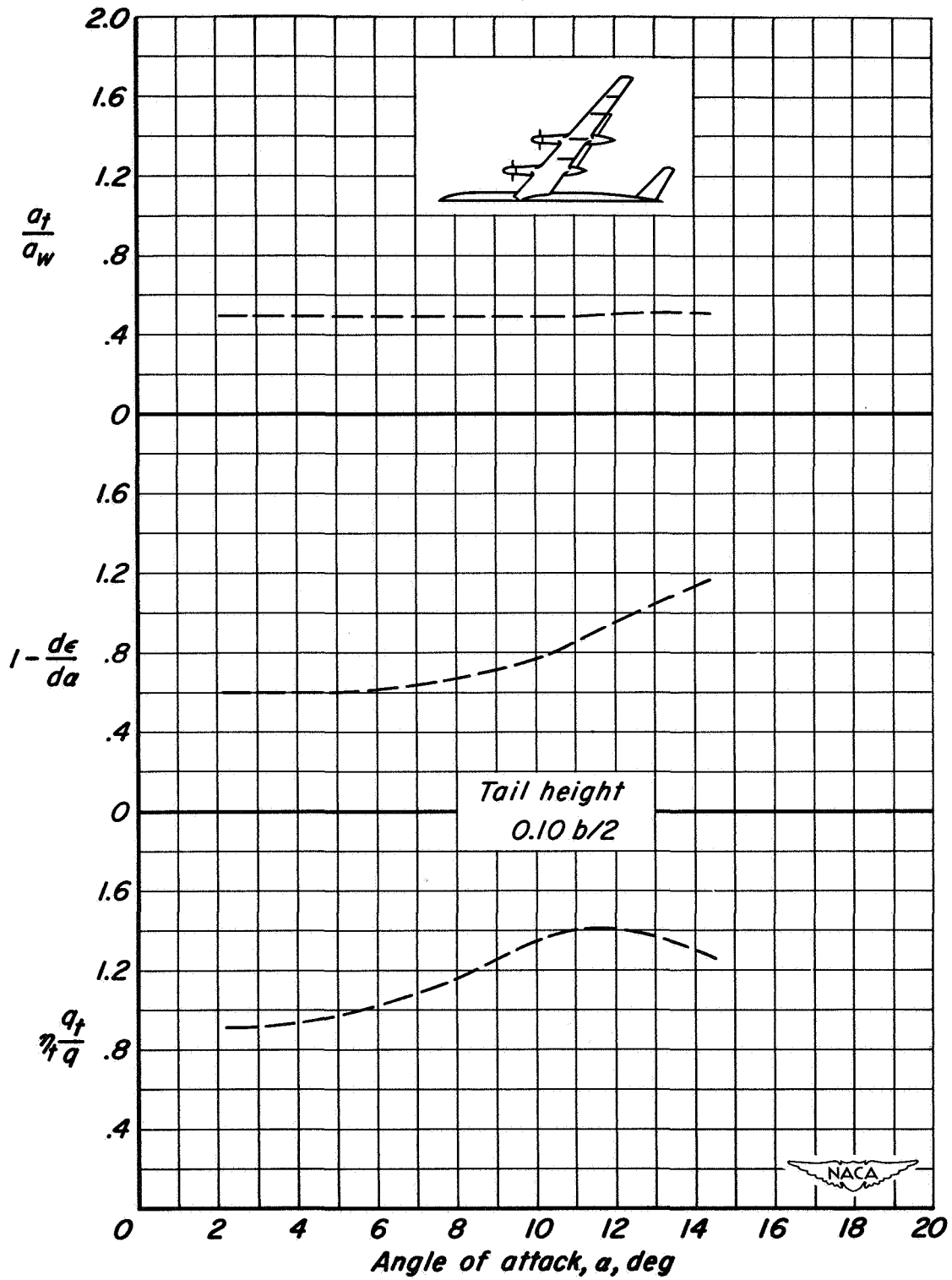
(d) $T_c = 0.80$

Figure 29.- Concluded.
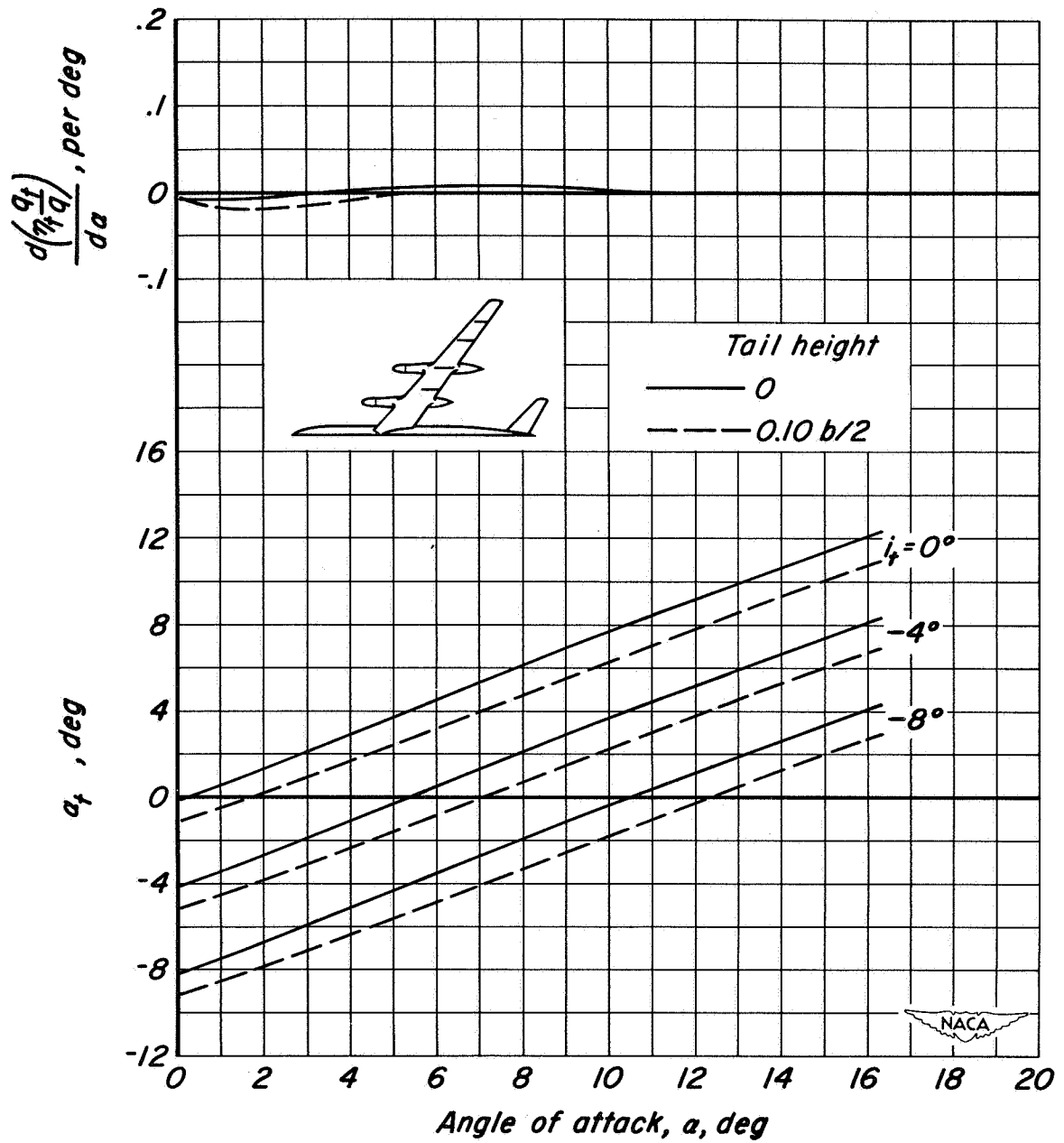
(a) Propellers off.

Figure 30.- The variation of $\dfrac{d(\eta_t q_t/q)}{d\alpha}$ and α_t with α; flaps up;
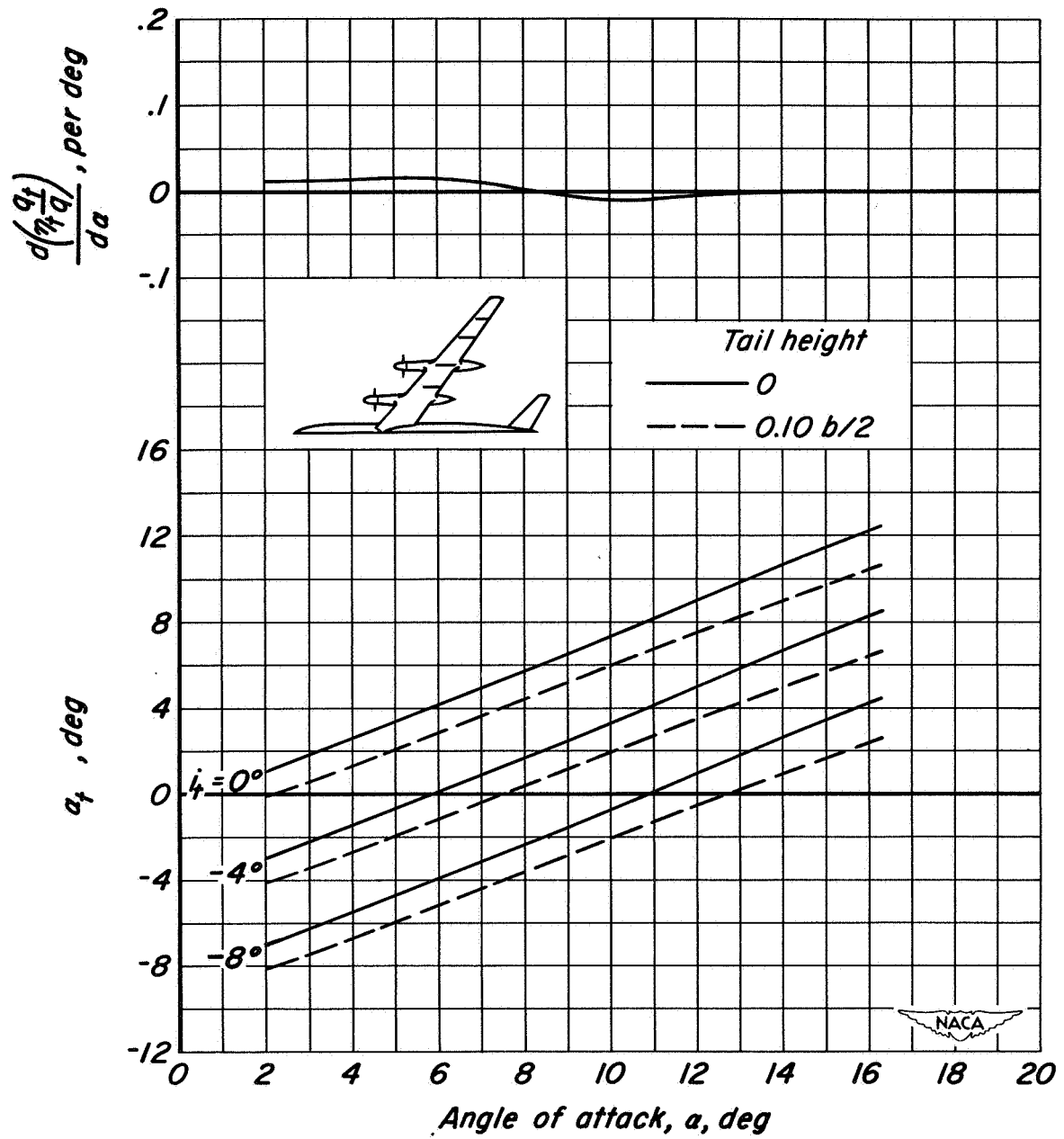
M = 0.082; R = 4,000,000; β = 26°.

(b) $T_c = 0$

Figure 30.- Continued.
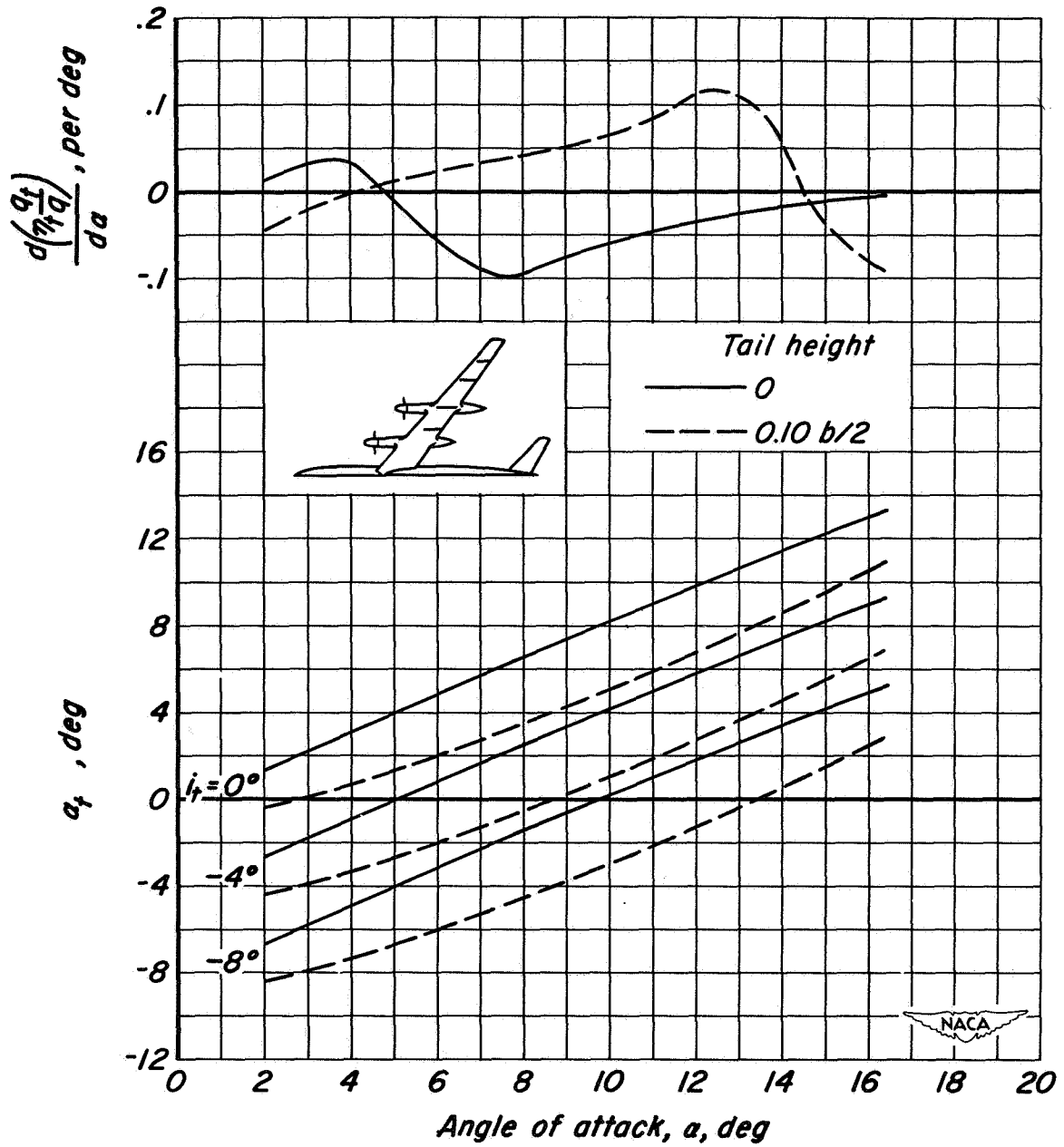
(c) $T_c = 0.40$

Figure 30.- Continued.
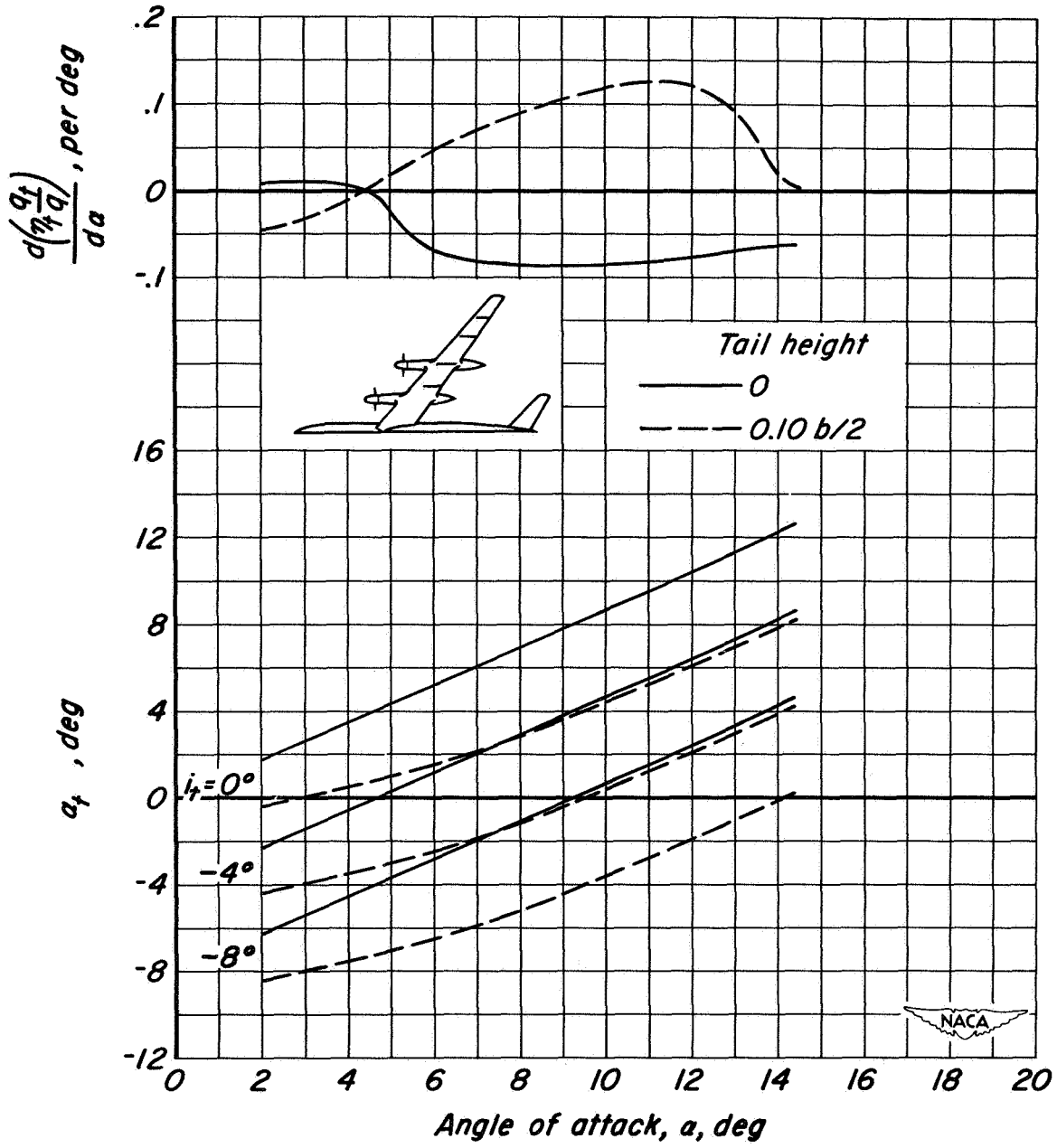
(d) $T_c = 0.80$

Figure 30.- Concluded.
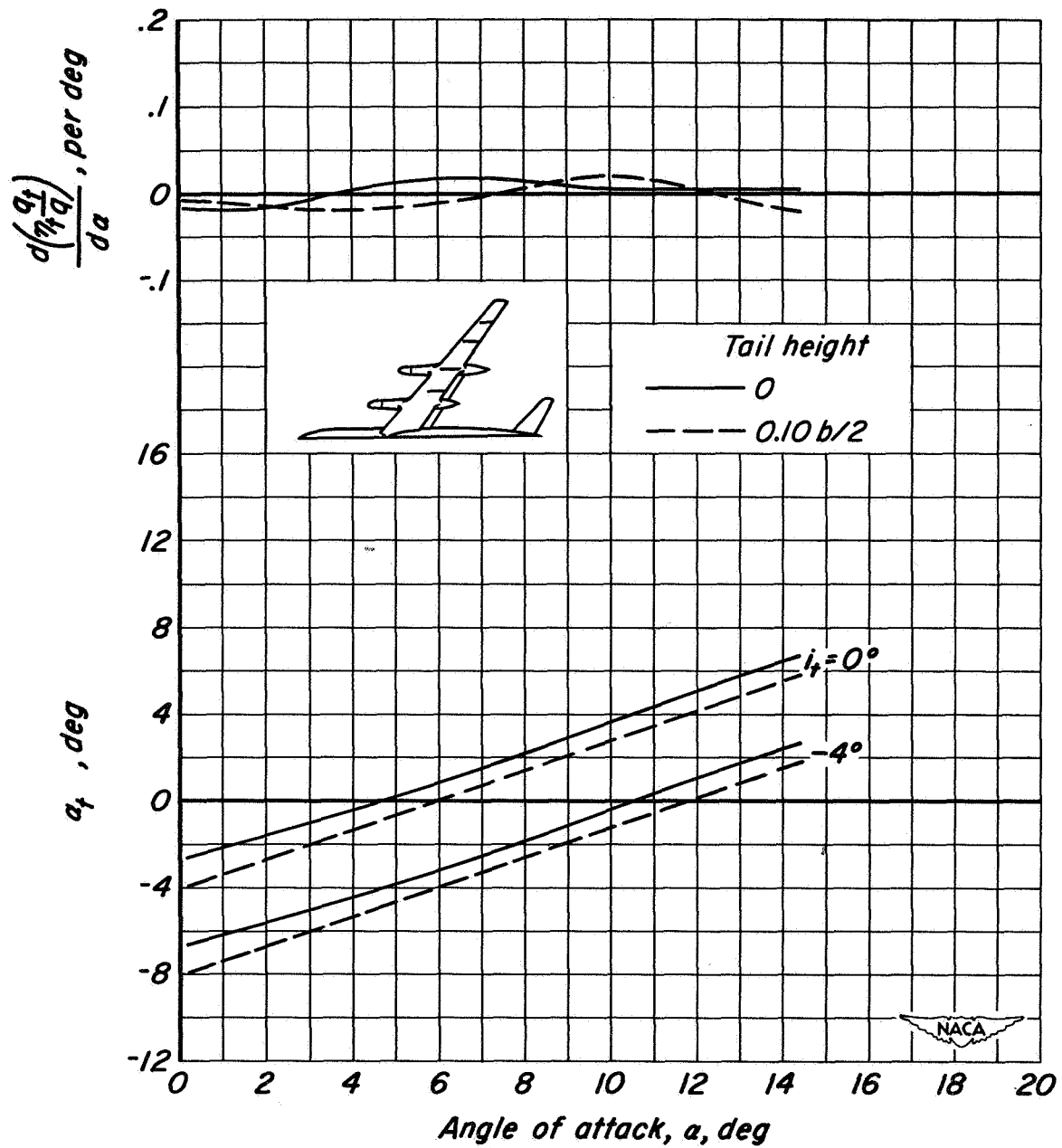
(a) Propellers off.

Figure 31.- The variation of $\dfrac{d(\eta_t q_t/q)}{d\alpha}$ and α_t with α; inboard flaps deflected; M = 0.082; R = 4,000,000; $\beta = 26°$.
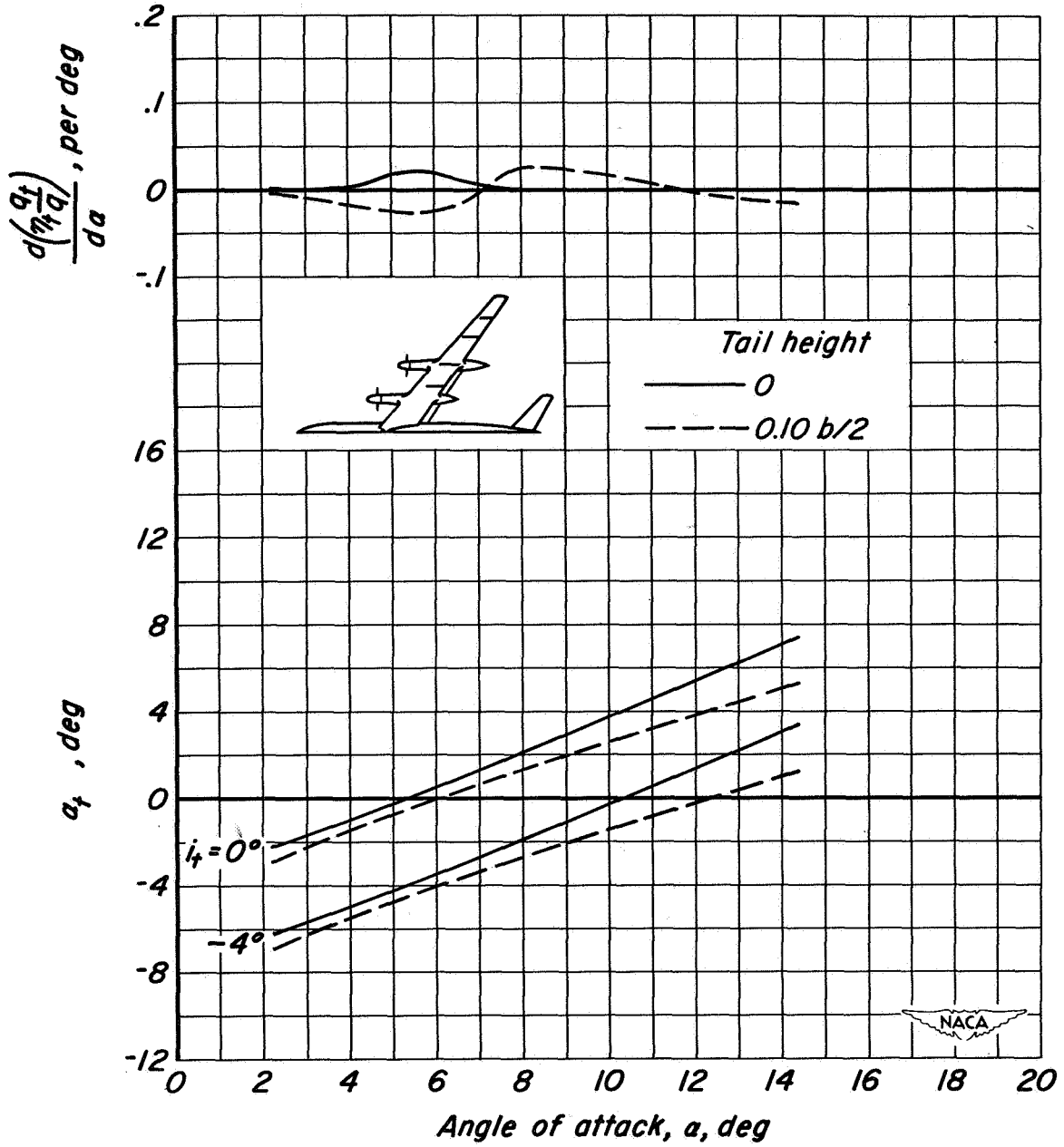
(b) $T_c = 0$

Figure 31.- Continued.
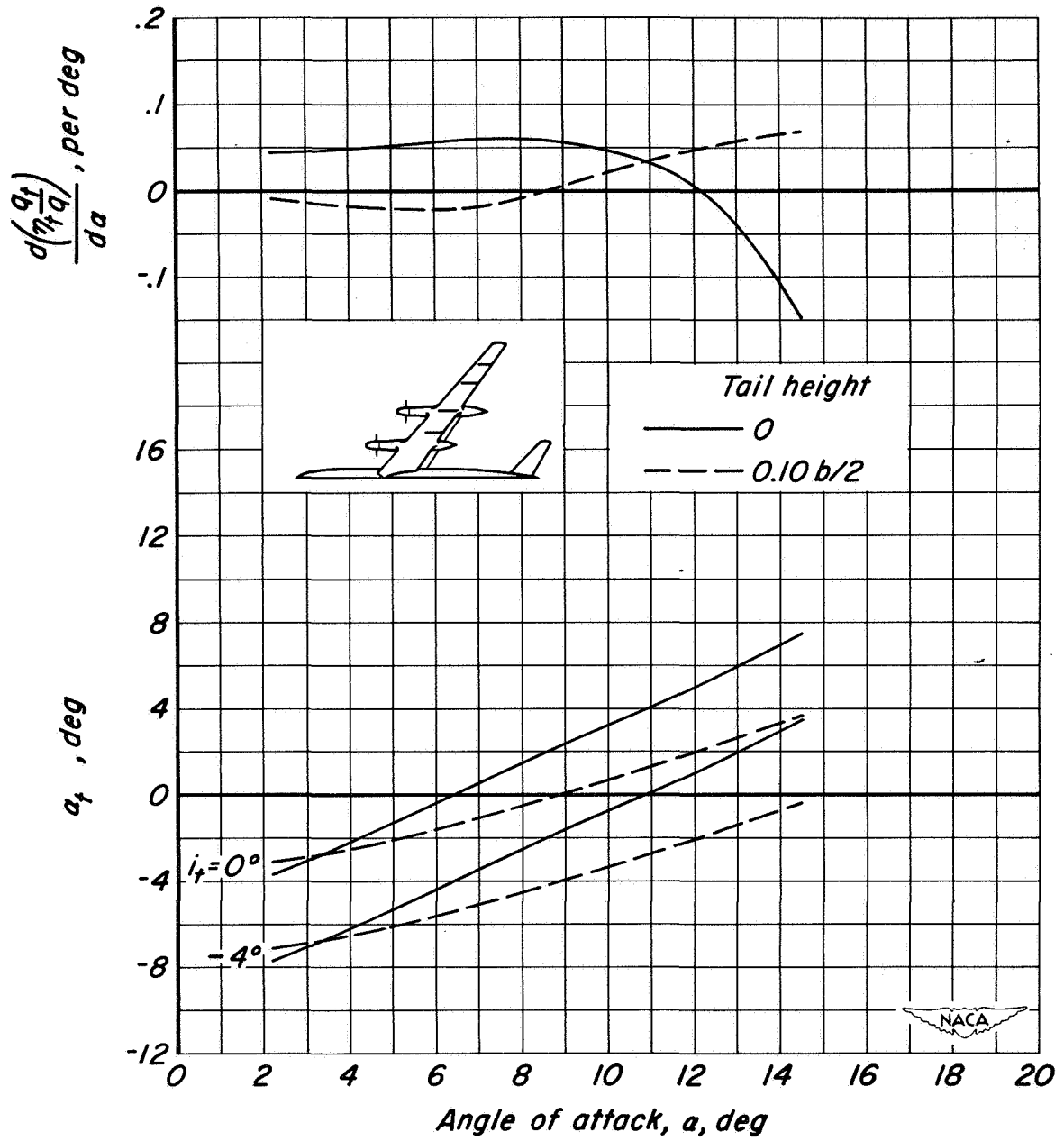
(c) $T_c = 0.40$

Figure 31.- Continued.
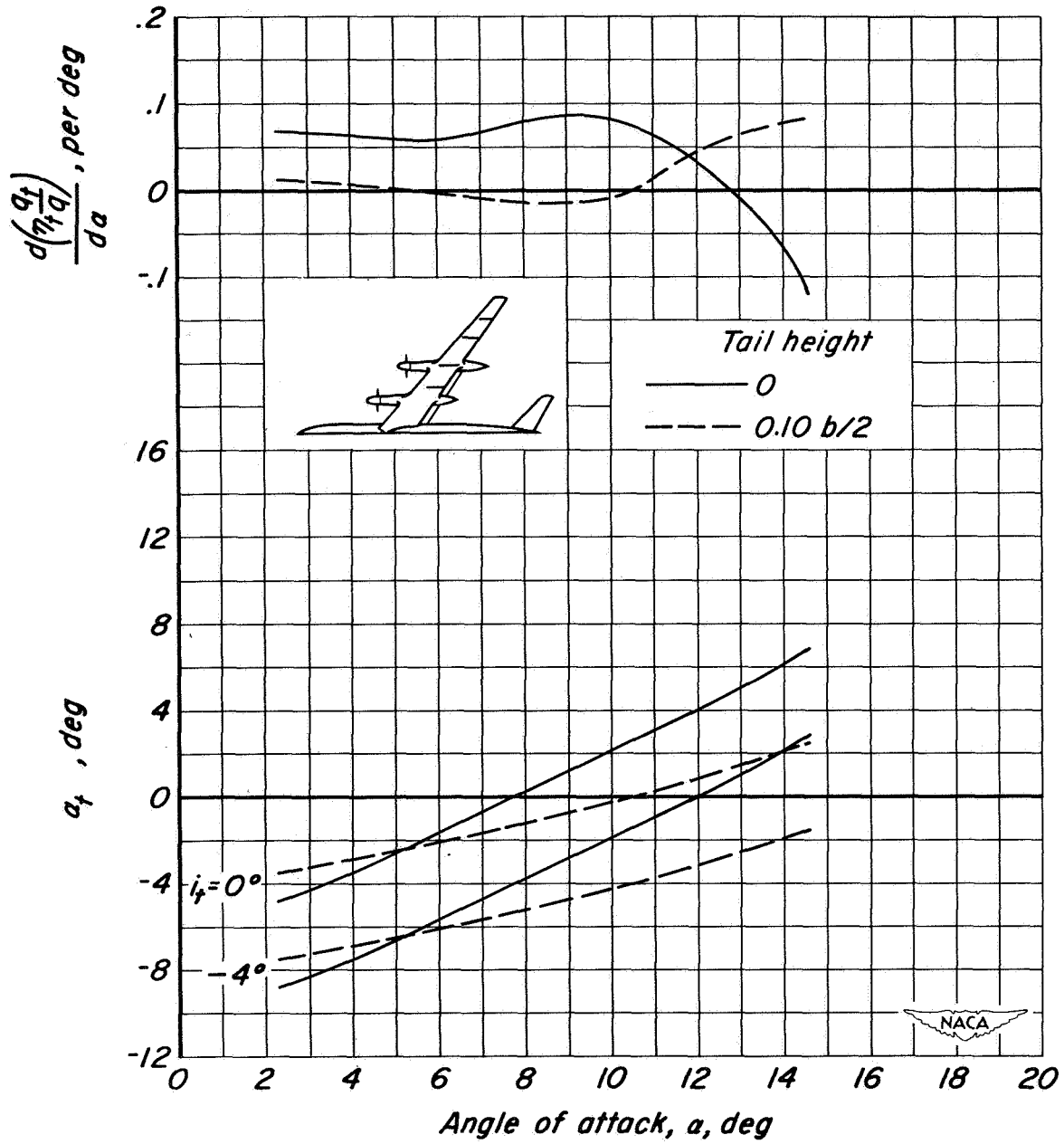
(d) $T_c = 0.80$

Figure 31.- Concluded.
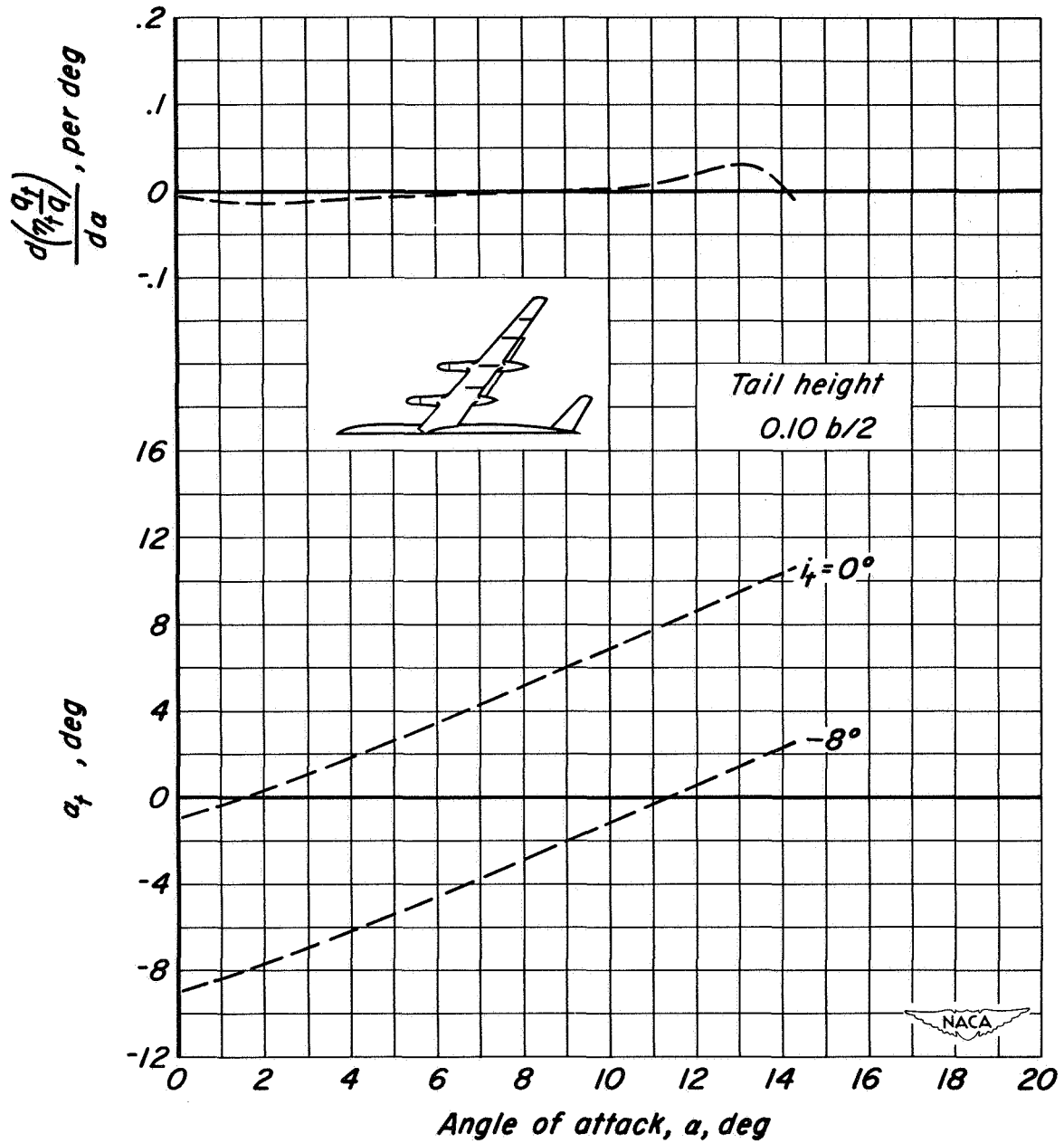
(a) Propellers off.

Figure 32.- The variation of $\dfrac{d(\eta_t q_t/q)}{d\alpha}$ and α_t with α; outboard flaps deflected; M = 0.082; R = 4,000,000; β = 26°.
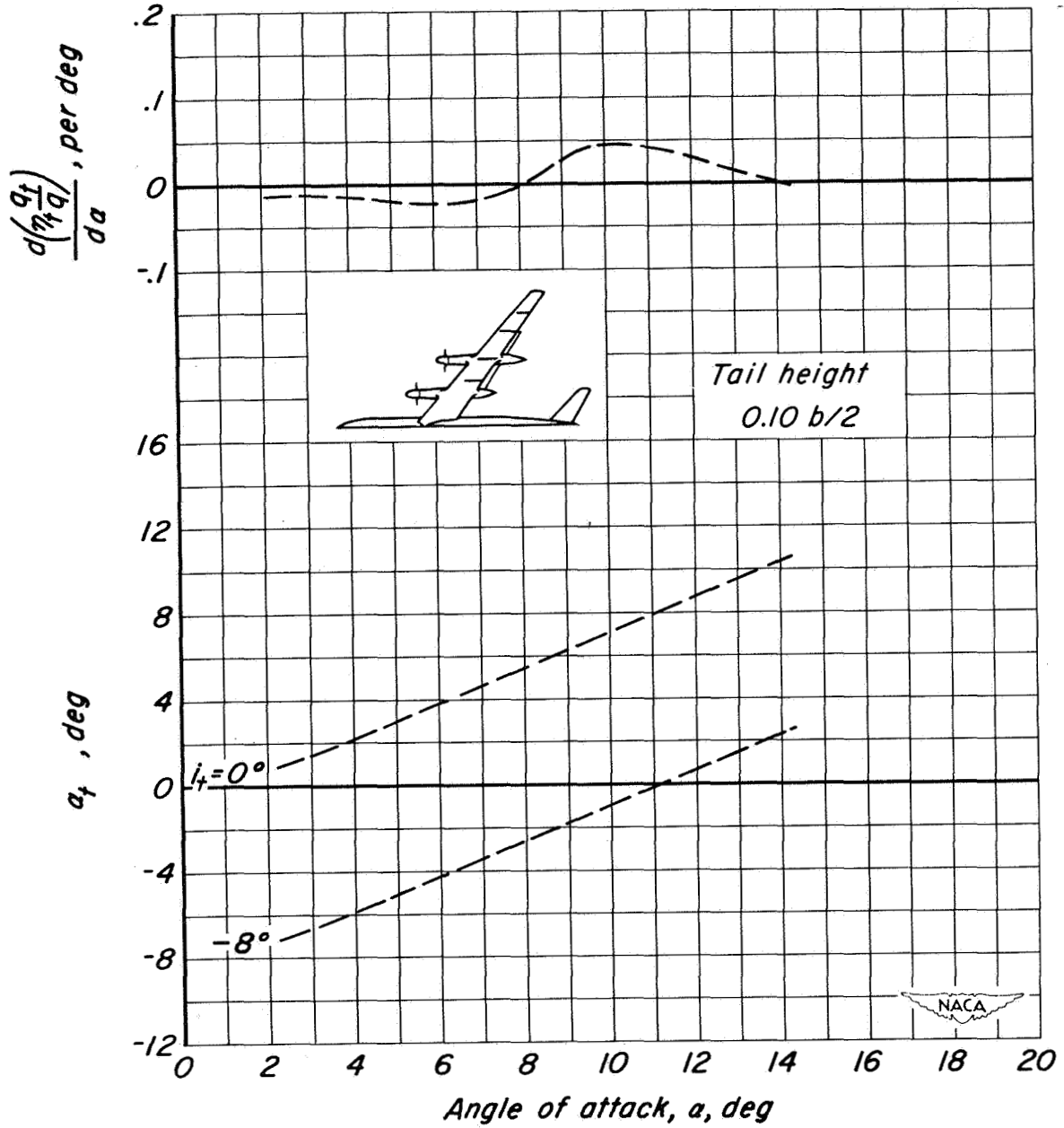
(b) $T_c = 0$

Figure 32.- Continued.
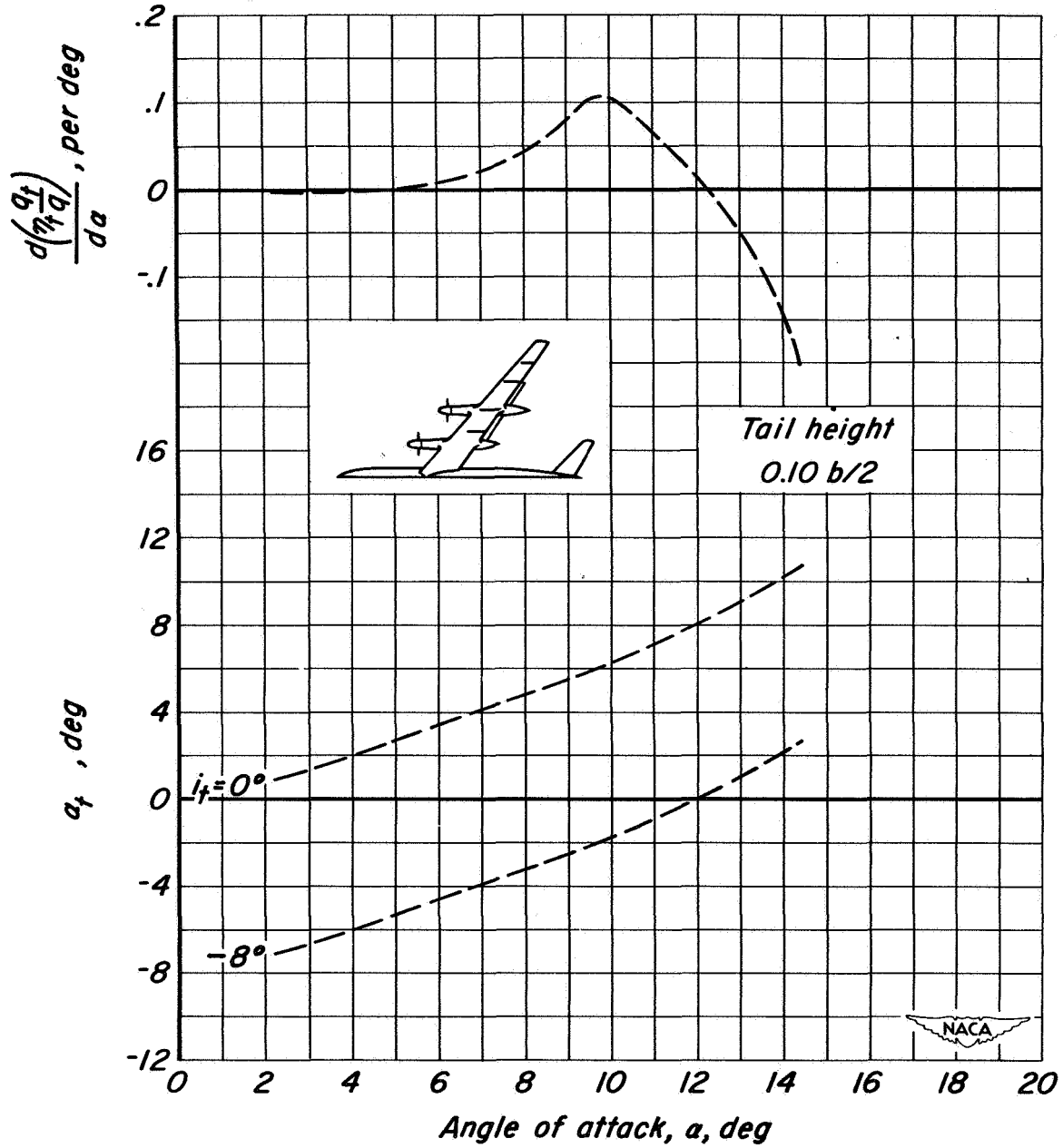
(c) $T_c = 0.40$

Figure 32.- Continued.
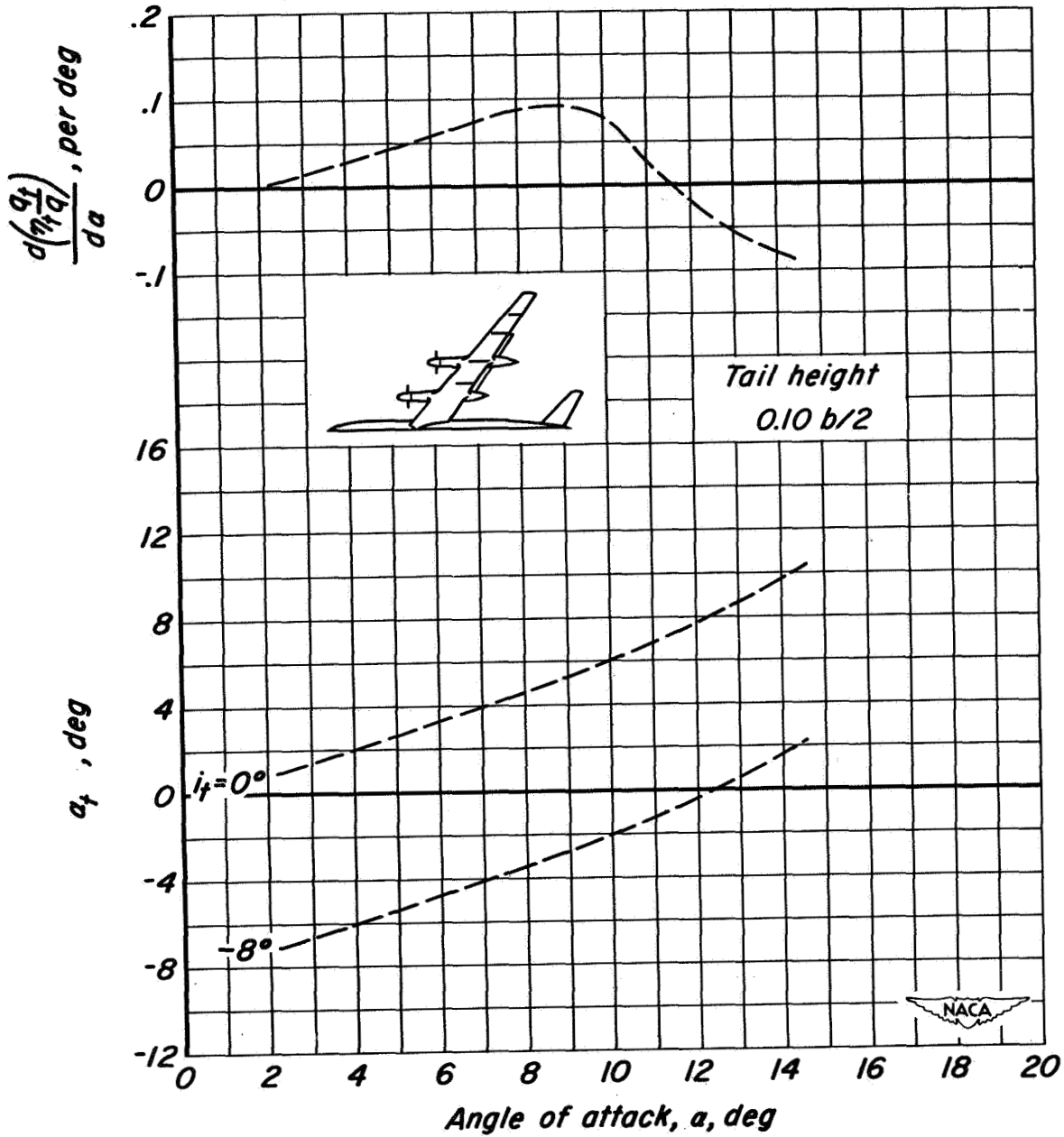
(d) $T_c = 0.80$

Figure 32.- Concluded.
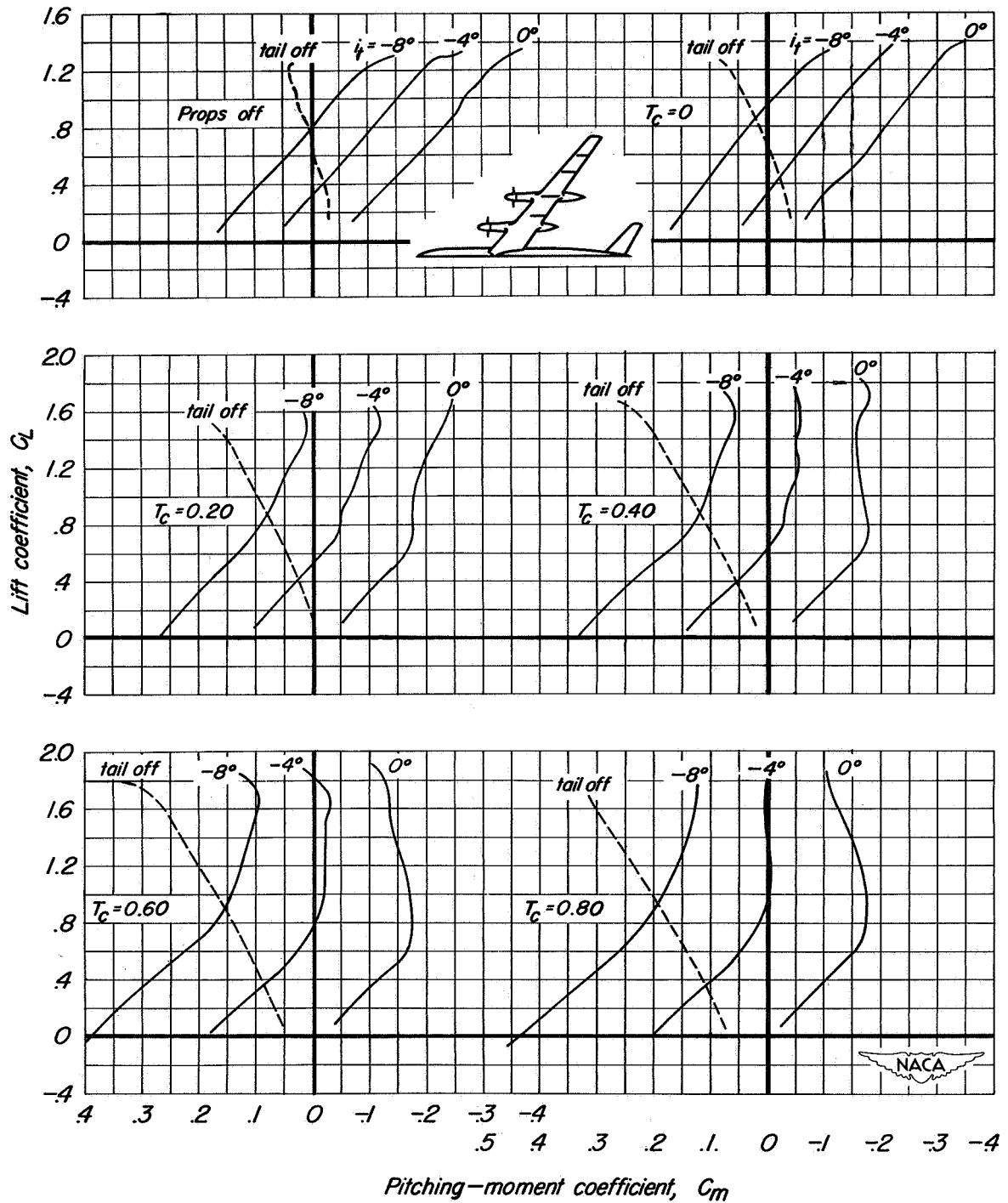
(a) Tail height = 0

Figure 33.- The effects of tail incidence on the pitching-moment charac-
teristics of the model; flaps up; M = 0.082; R = 4,000,000; β = 26°.
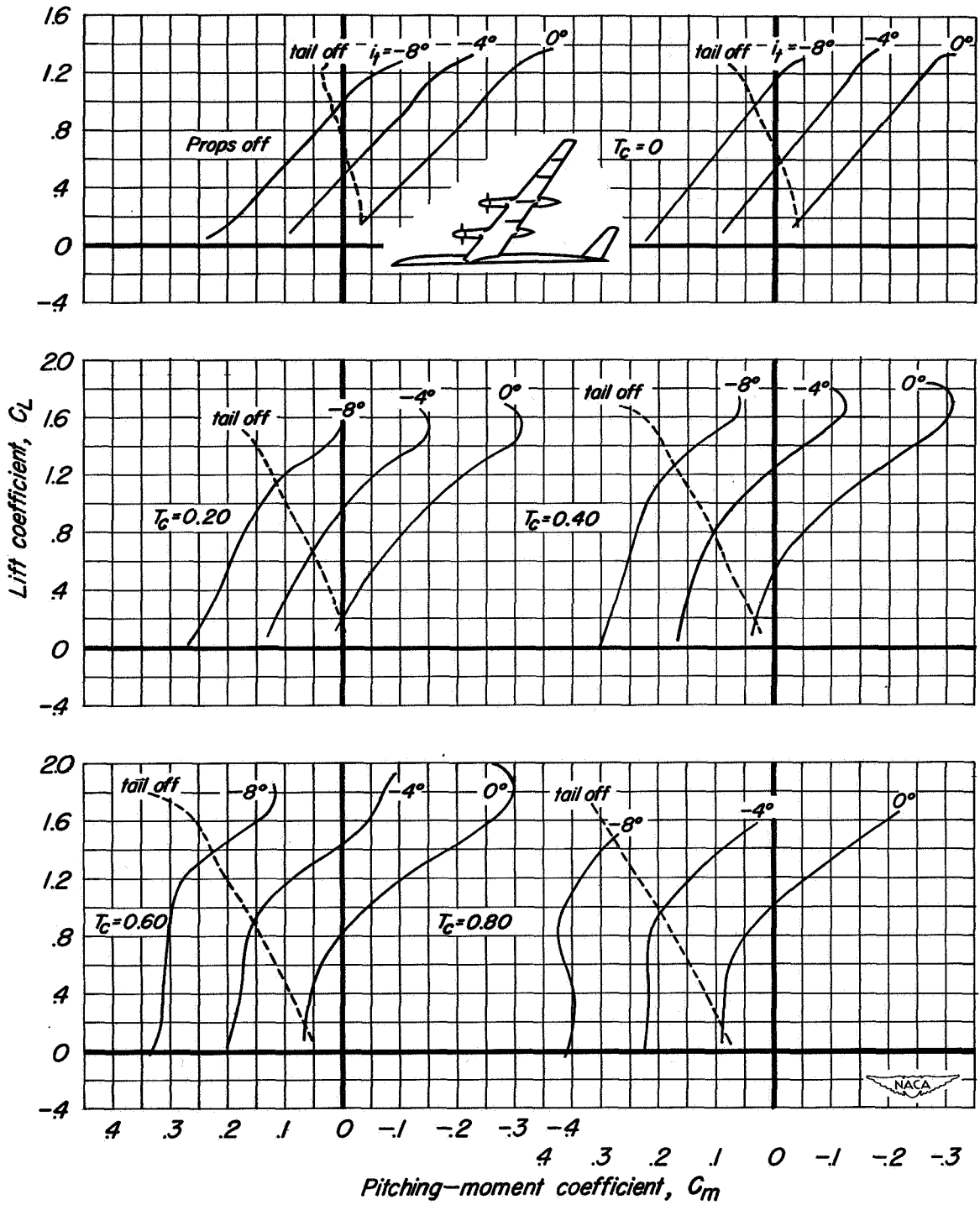
(b) Tail height = 0.10 b/2

Figure 33.- Concluded.

Pitching-moment coefficient, C_m
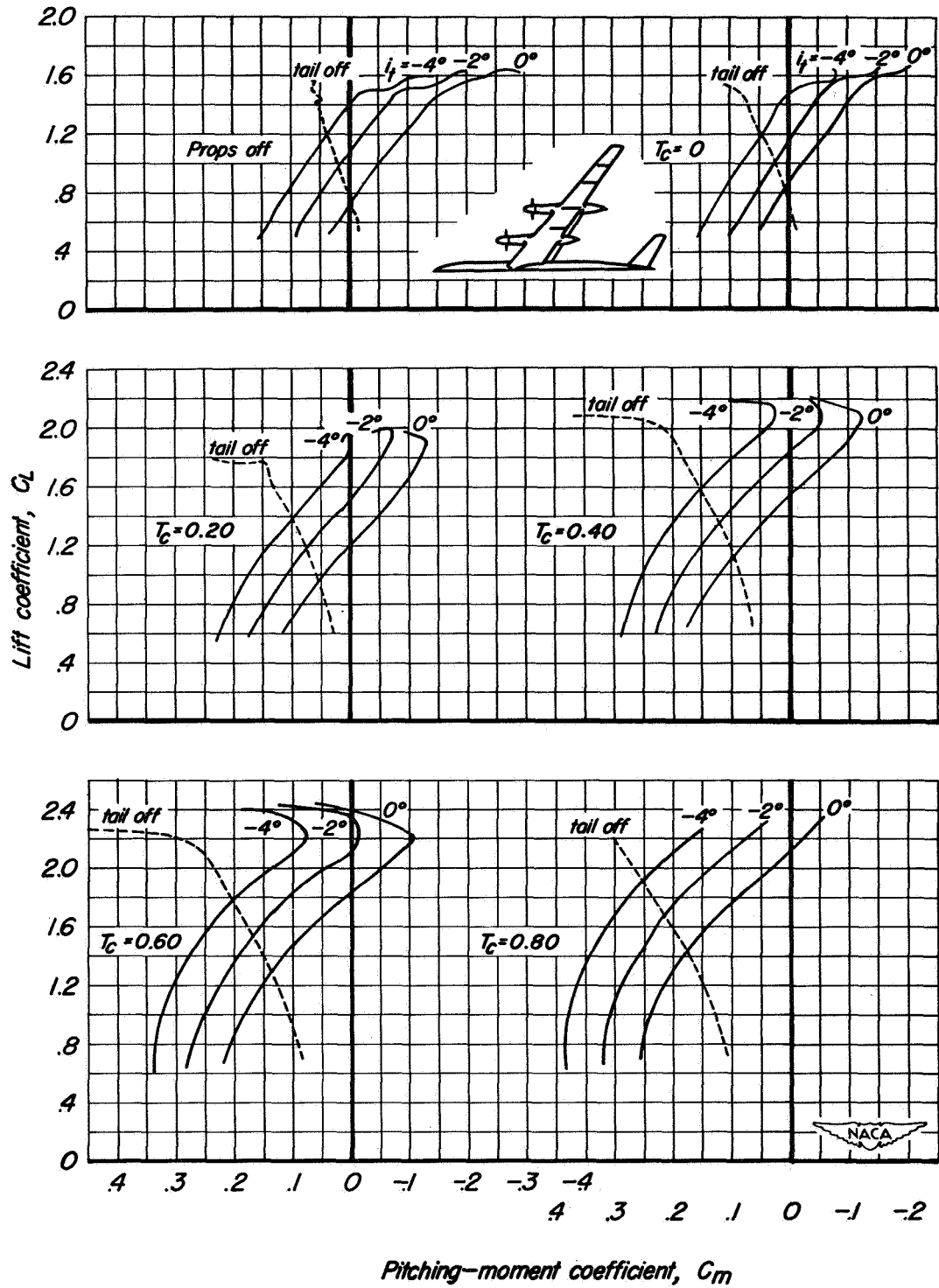
(a) Tail height = 0

Figure 34.- The effects of tail incidence on the pitching-moment charac-
teristics of the model; inboard flaps deflected; M = 0.082;
R = 4,000,000; β = 26°.
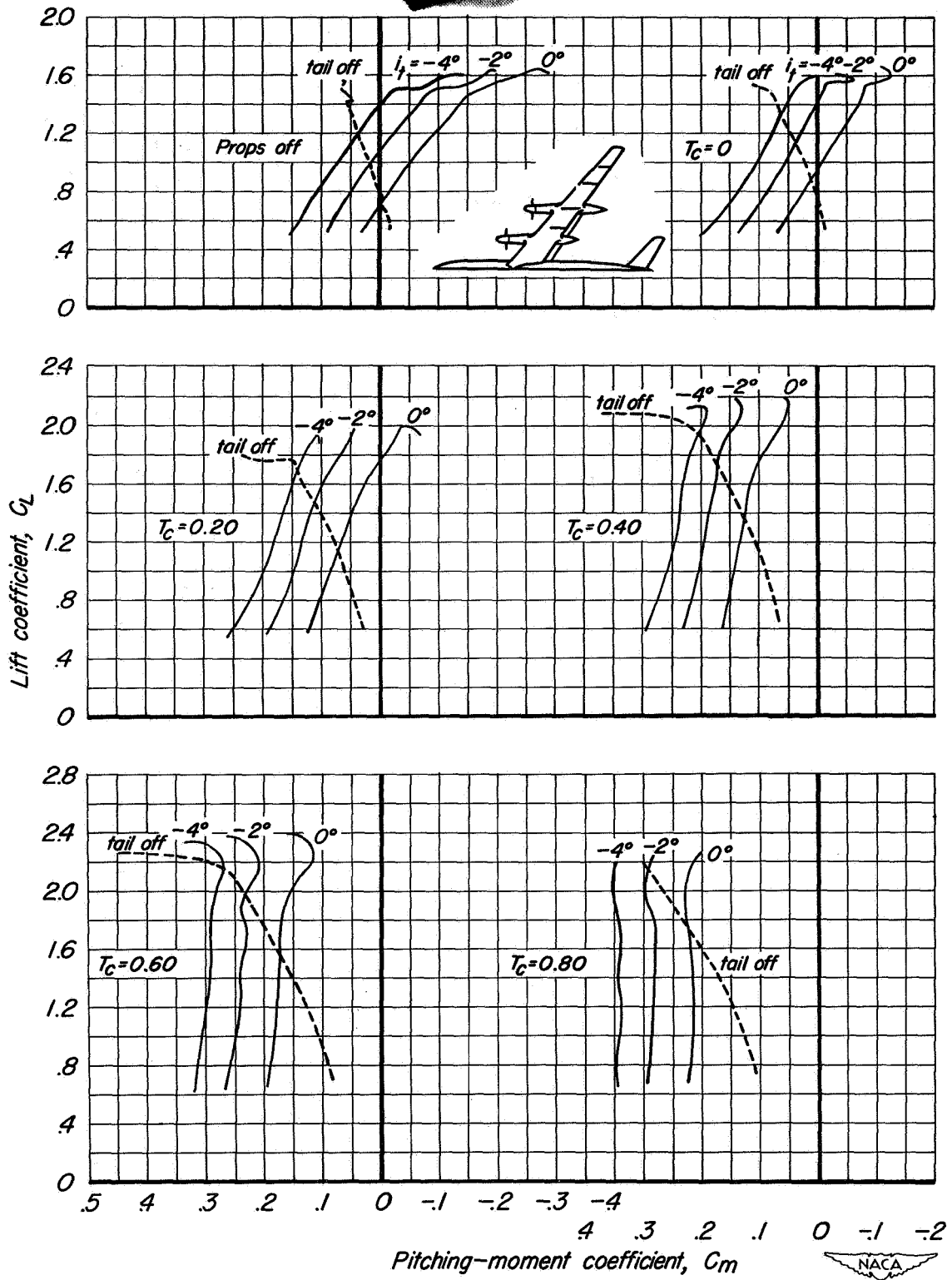
(b) Tail height = 0.10 b/2

Figure 34.- Concluded.
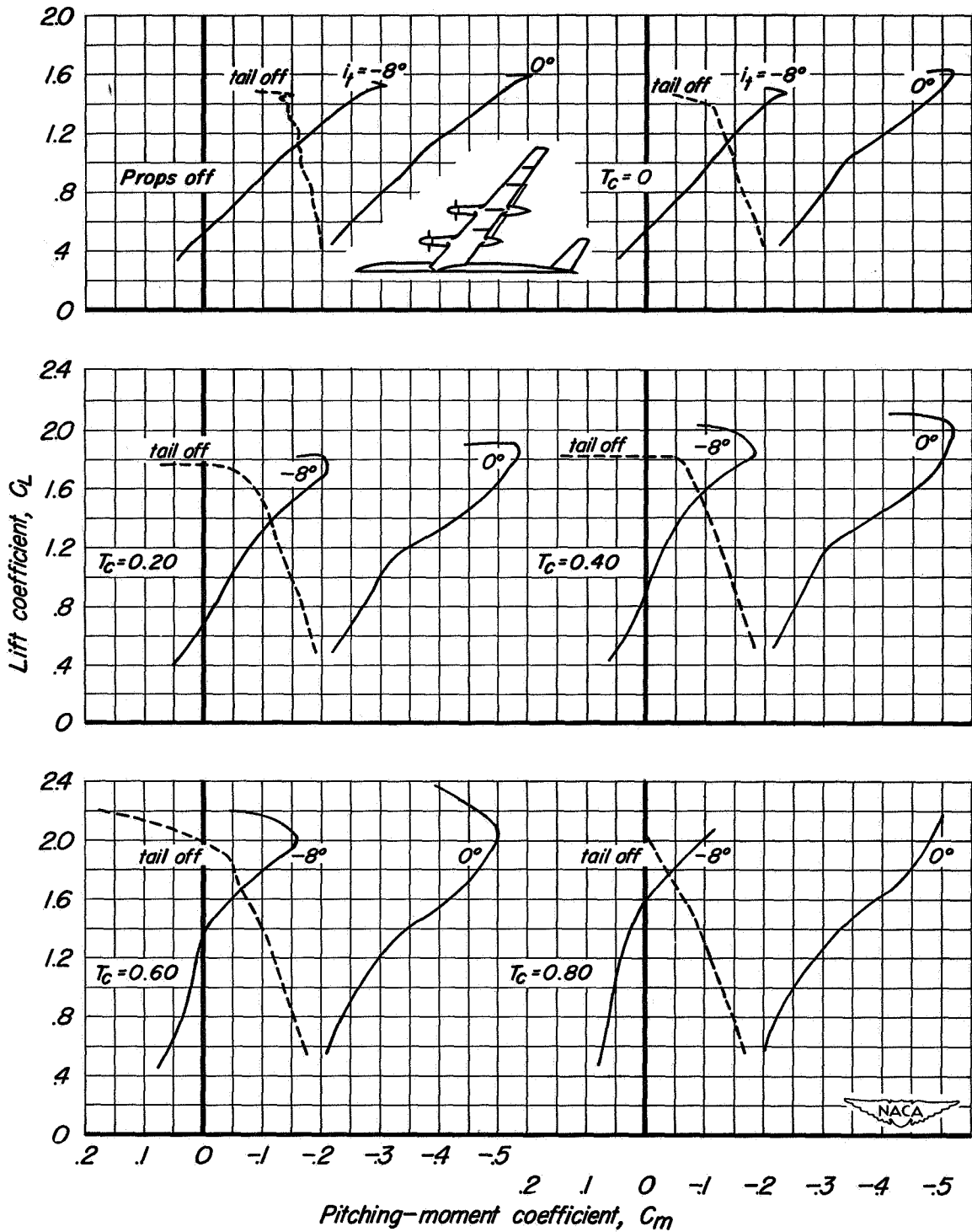
Figure 35.- The effects of tail incidence on the pitching-moment charac-
teristics of the model; tail height = 0.10 b/2; outboard flaps
deflected; M = 0.082; R = 4,000,000; β = 26°.
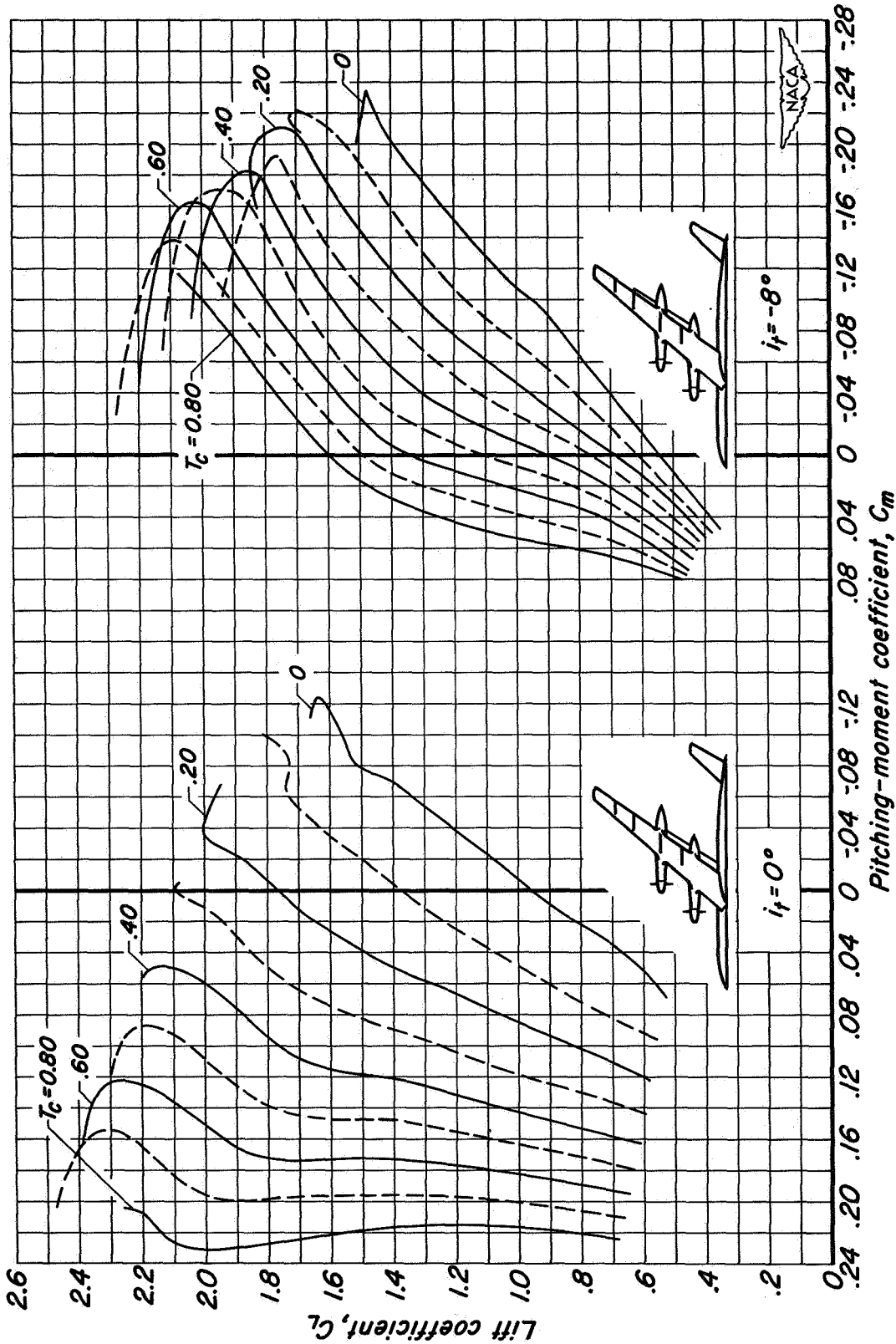
Figure 36.- A comparison of the pitching-moment characteristics of the model having inboard flaps with those of the model having outboard flaps; tail height = 0.10 b/2; M = 0.082; R = 4,000,000; β = 26°.

Figure 37.- A comparison of the pitching-moment characteristics of the model for independent and simultaneous operation of the propellers; tail removed; M = 0.082; R = 4,000,000; β = 26°.

(a) Flaps up.

(b) Inboard flaps deflected.

Figure 37.- Concluded.
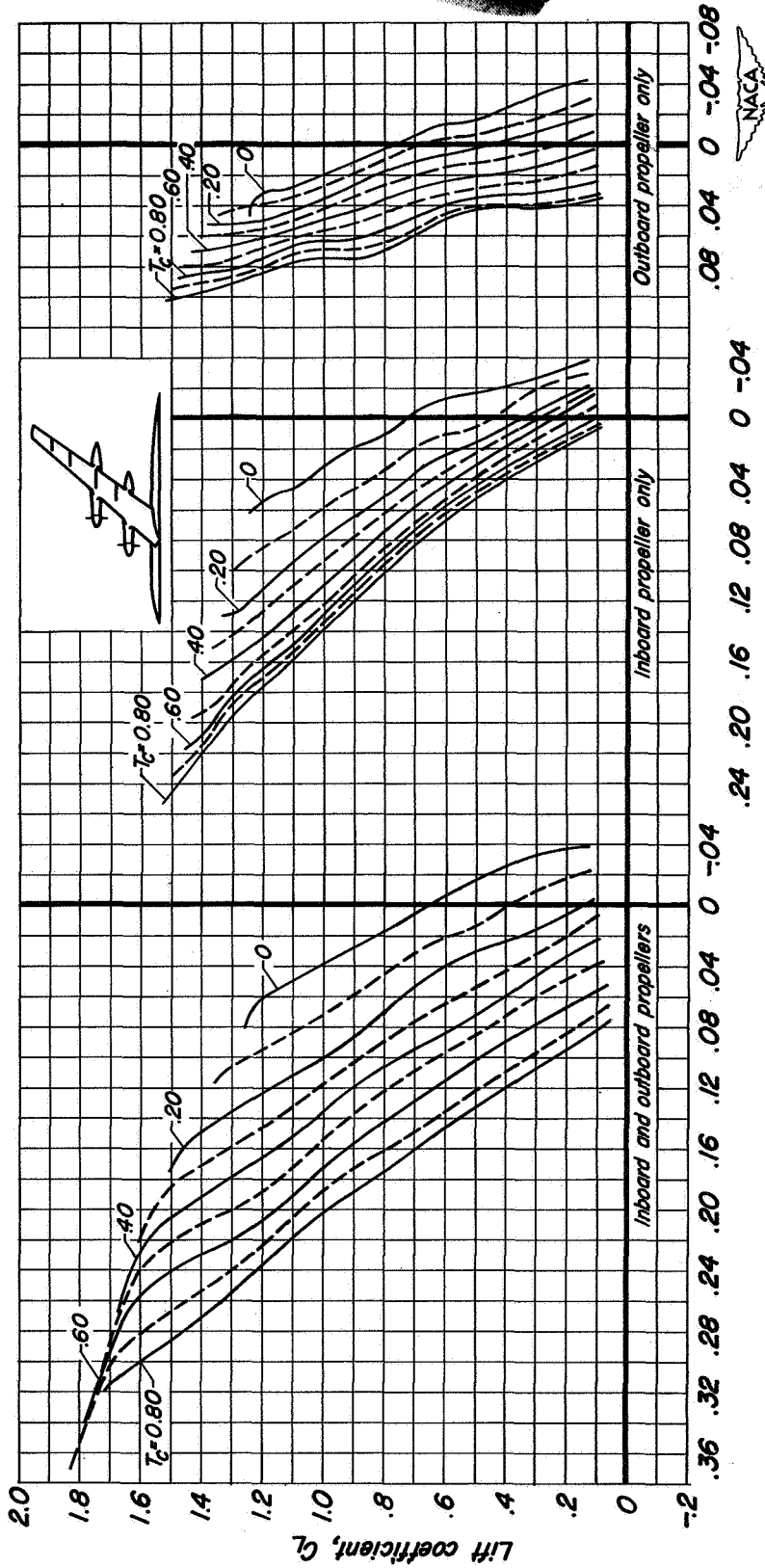
Pitching-moment coefficient, C_m
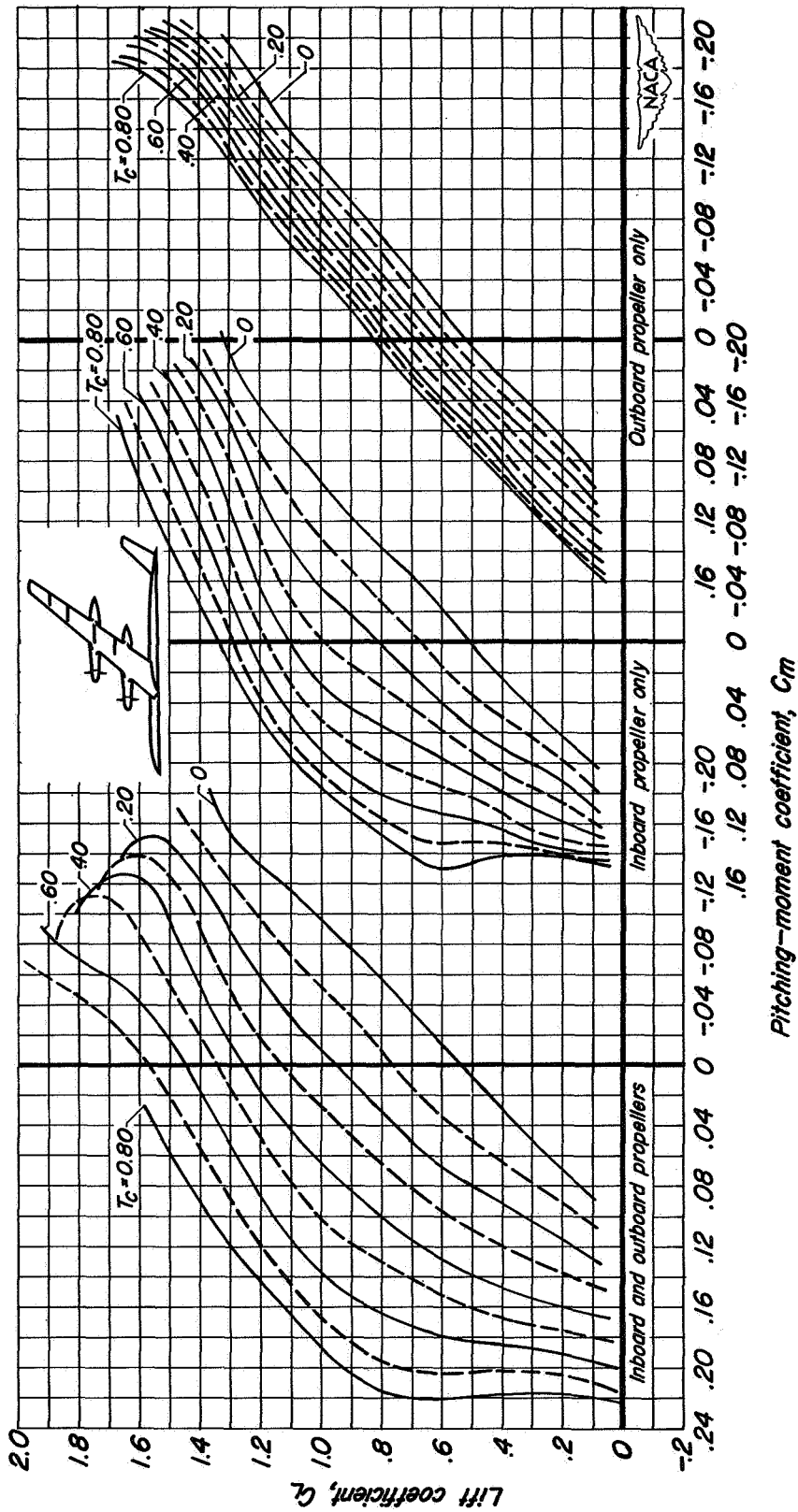
(a) Flaps up; $i_t = -4°$.

Figure 38.- A comparison of the pitching-moment characteristics of the model for independent and simultaneous operation of the propellers; tail height = 0.10 b/2; M = 0.082; R = 4,000,000; B = 26°.
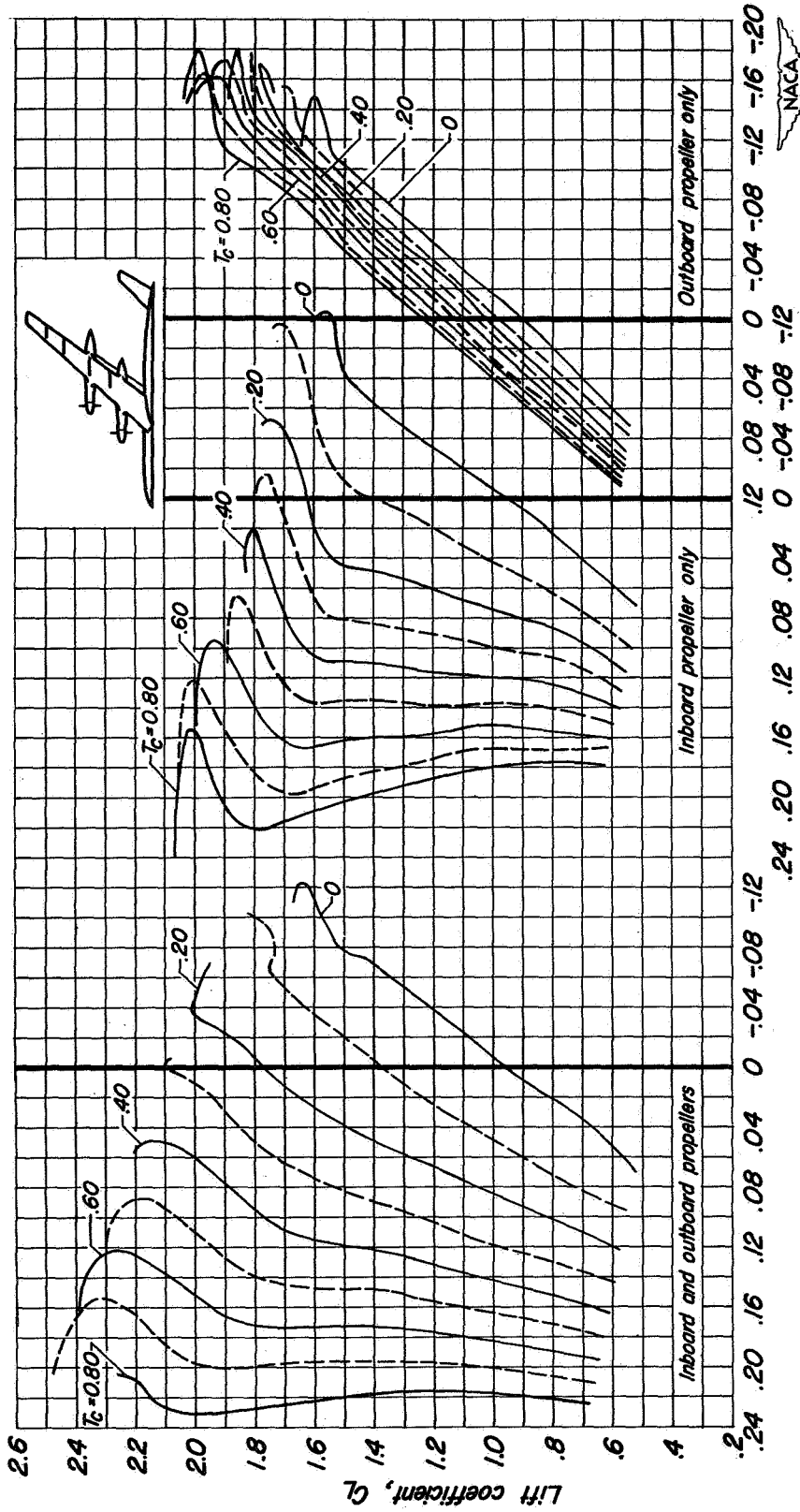
Pitching-moment coefficient, C_m

(b) Inboard flaps deflected; $i_t = 0°$.

Figure 38.- Concluded.
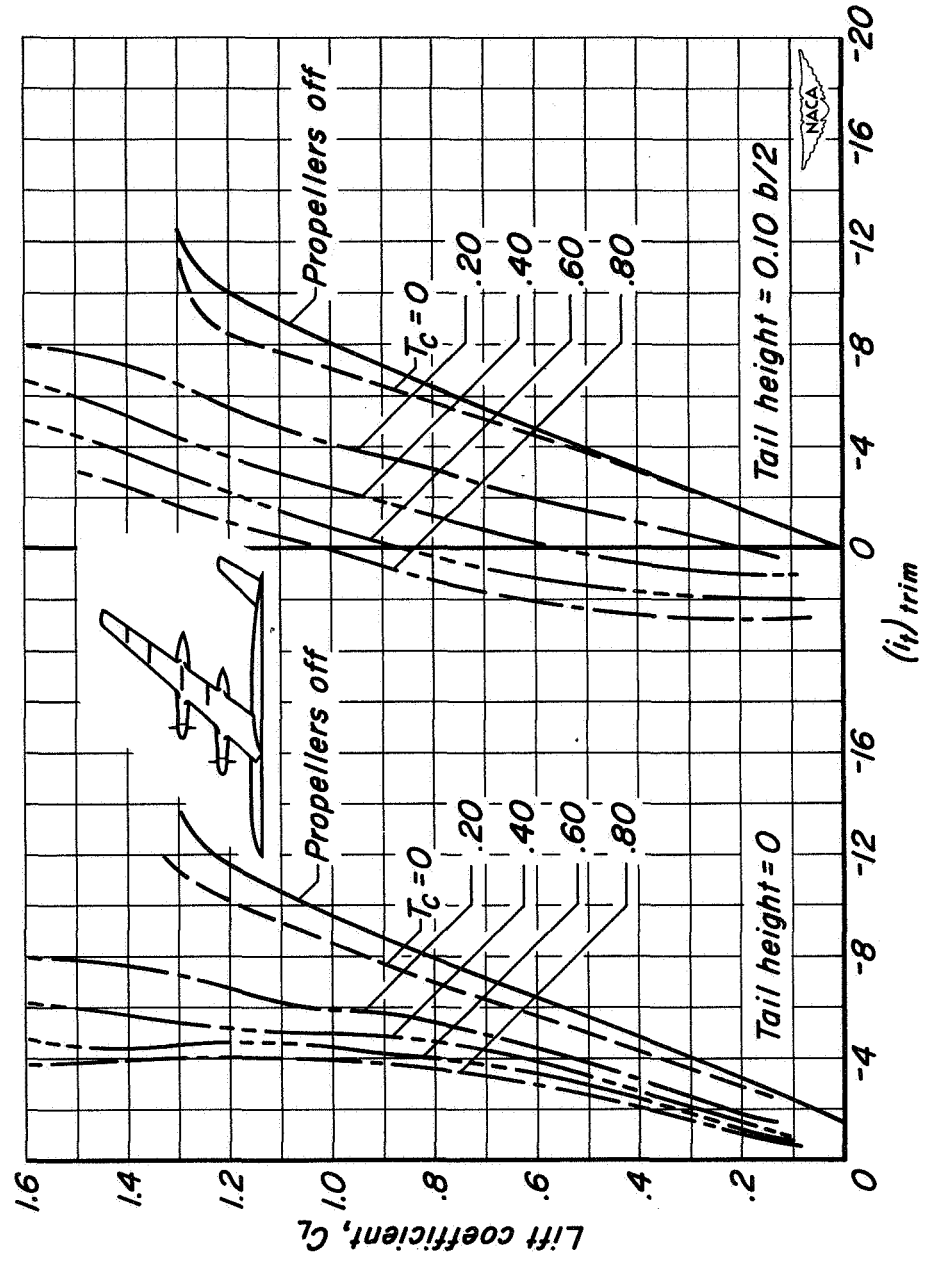
(a) (i_t)trim vs. C_L

Figure 39.- A comparison for two tail heights of the effects of operating propellers on the longi-
tudinal stability of the model; flaps up; M = 0.082; R = 4,000,000; β = 26°.
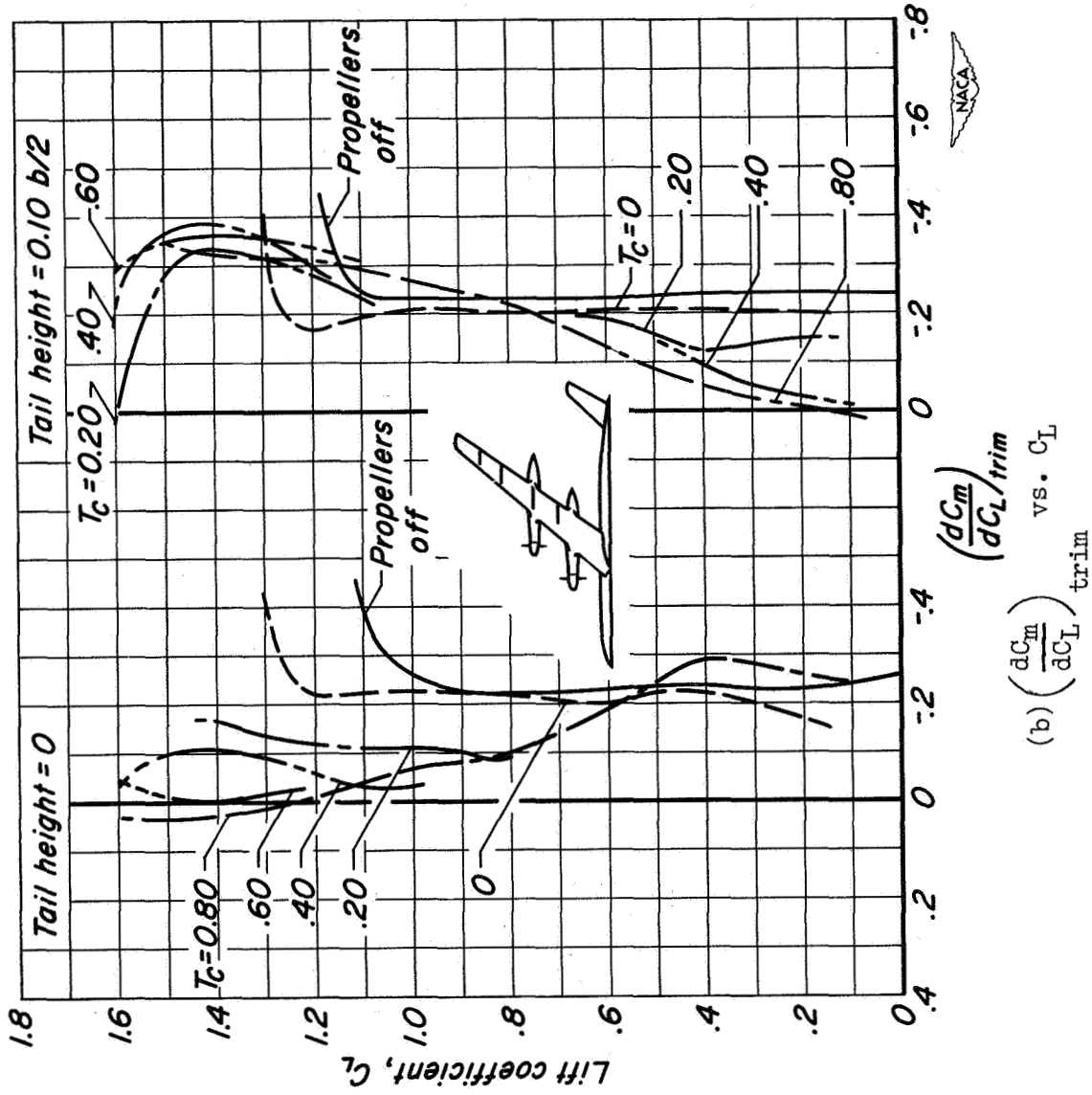
(b) $\left(\dfrac{dC_m}{dC_L}\right)_{trim}$ vs. C_L

Figure 39.- Continued.
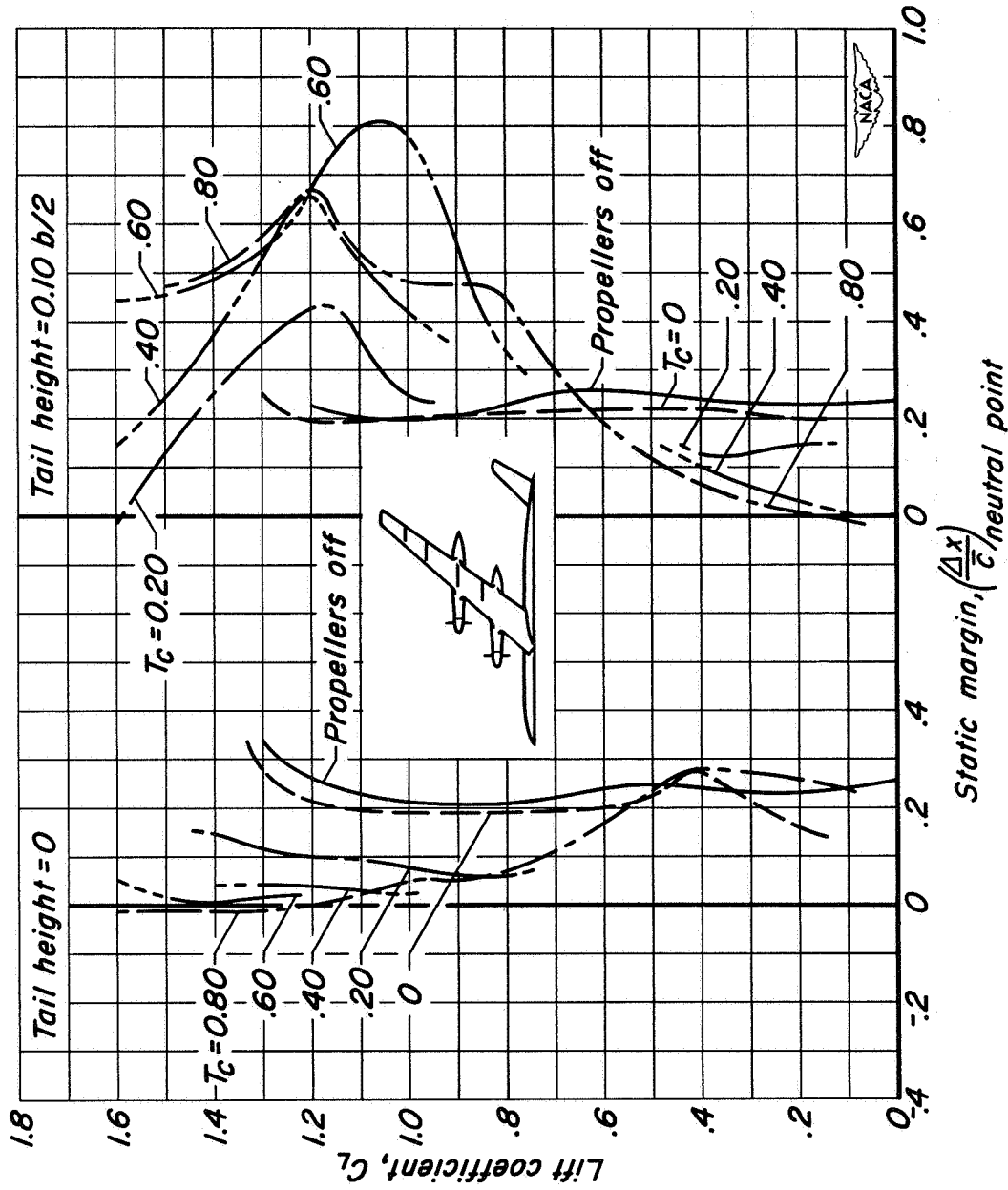
(c) Static margin vs. C_L.

Figure 39.- Concluded.
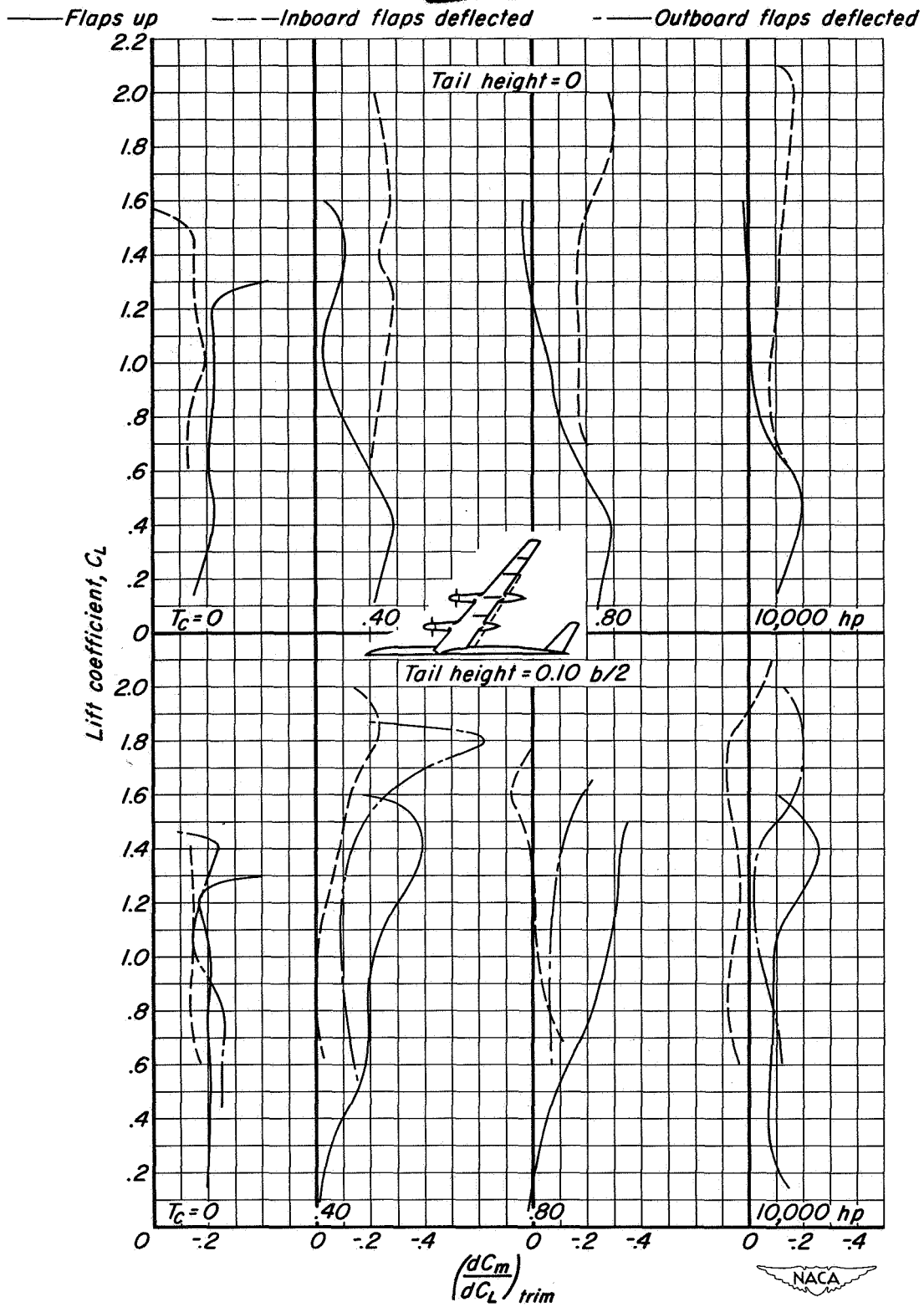
Figure 40.- The effects of flaps on the longitudinal stability of the
model; M = 0.082; R = 4,000,000; β = 26°.
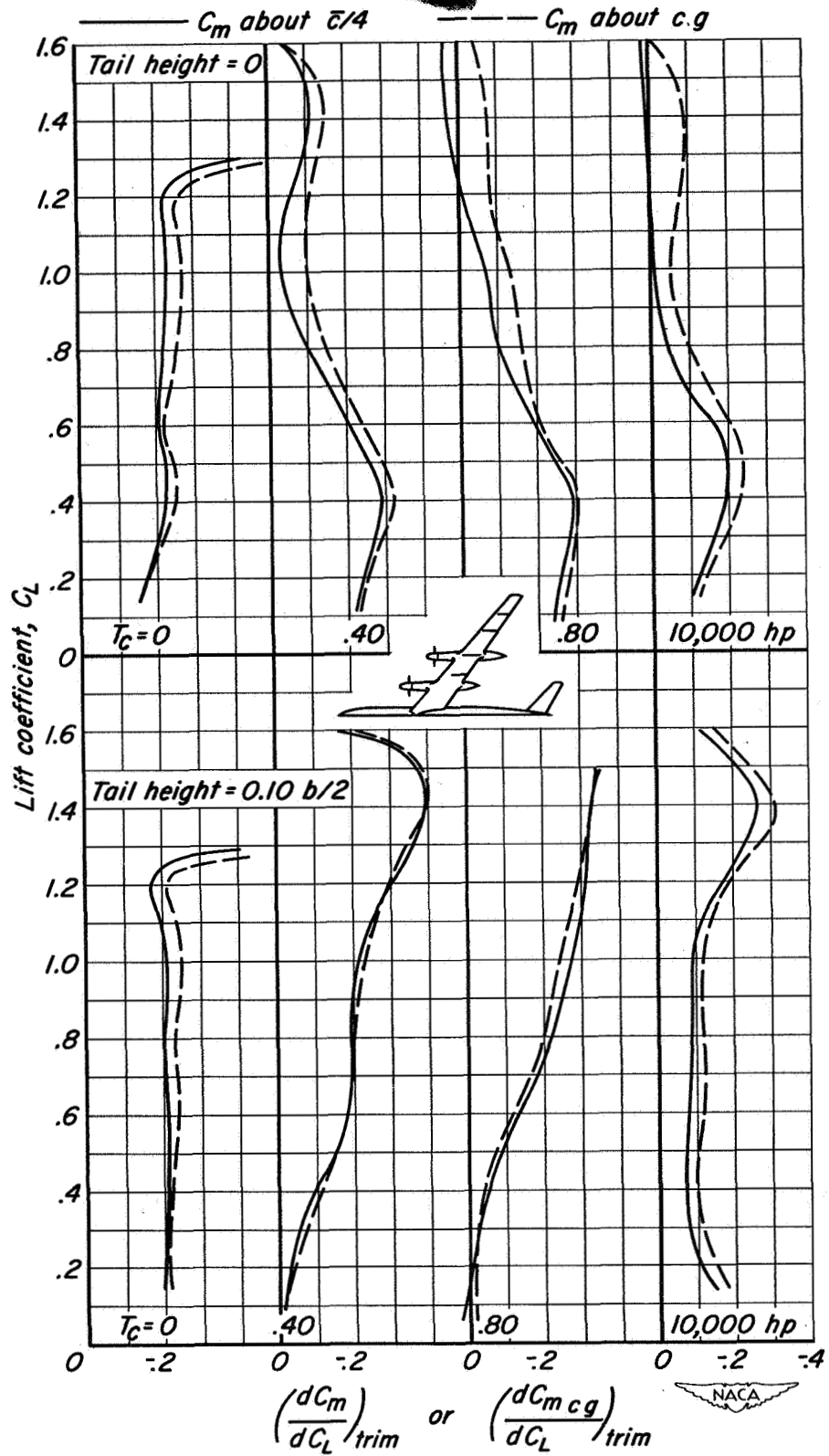
Figure 41.- The effects of vertical displacement of the center of moments on the longitudinal stability of the model; flaps up; M = 0.082; R = 4,000,000; $\beta = 26°$.
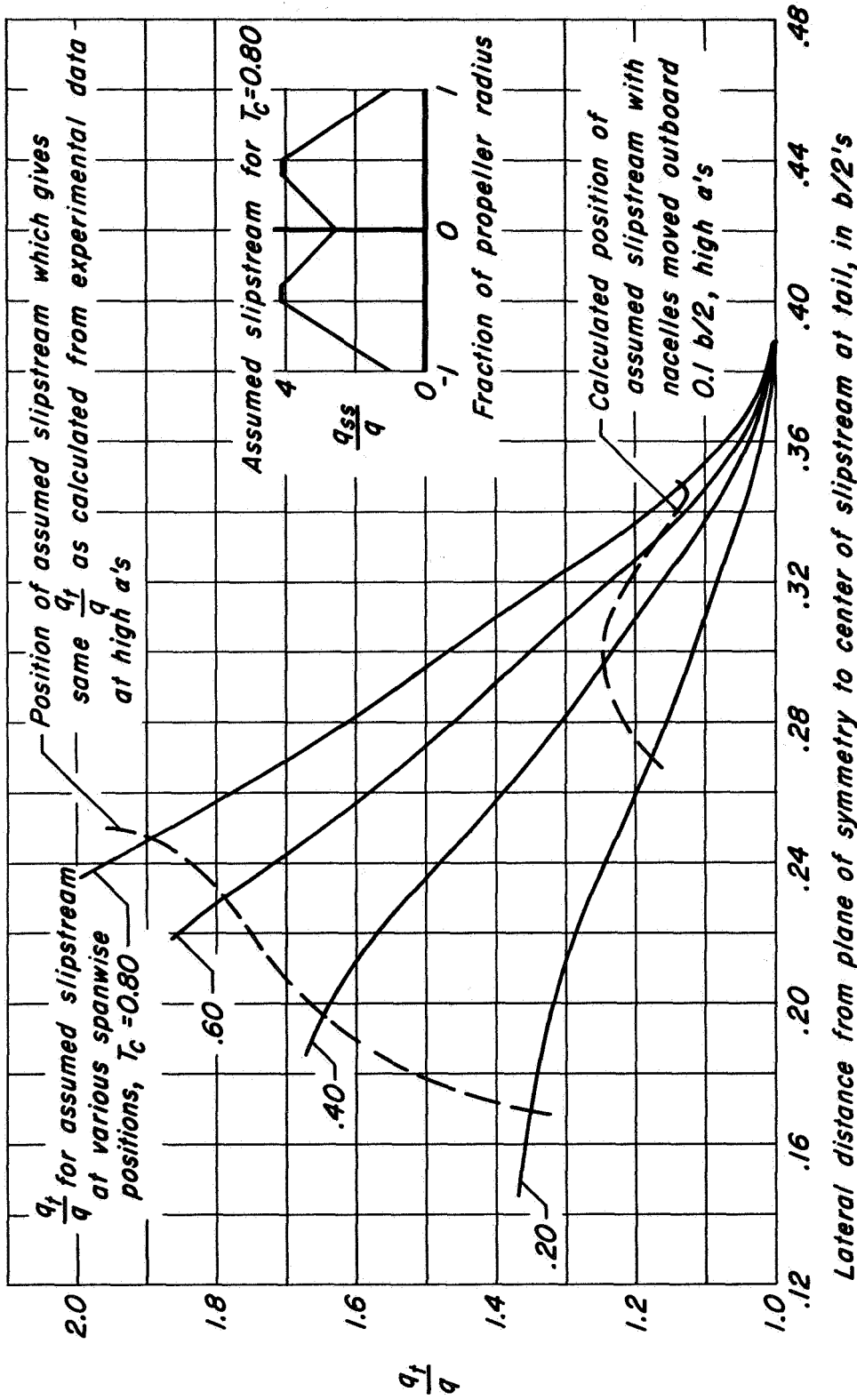
Figure 42.- The estimated maximum effective dynamic pressure at the tail with the nacelles moved outboard; flaps up or inboard flaps deflected; M = 0.082; R = 4,000,000; β = 26°.
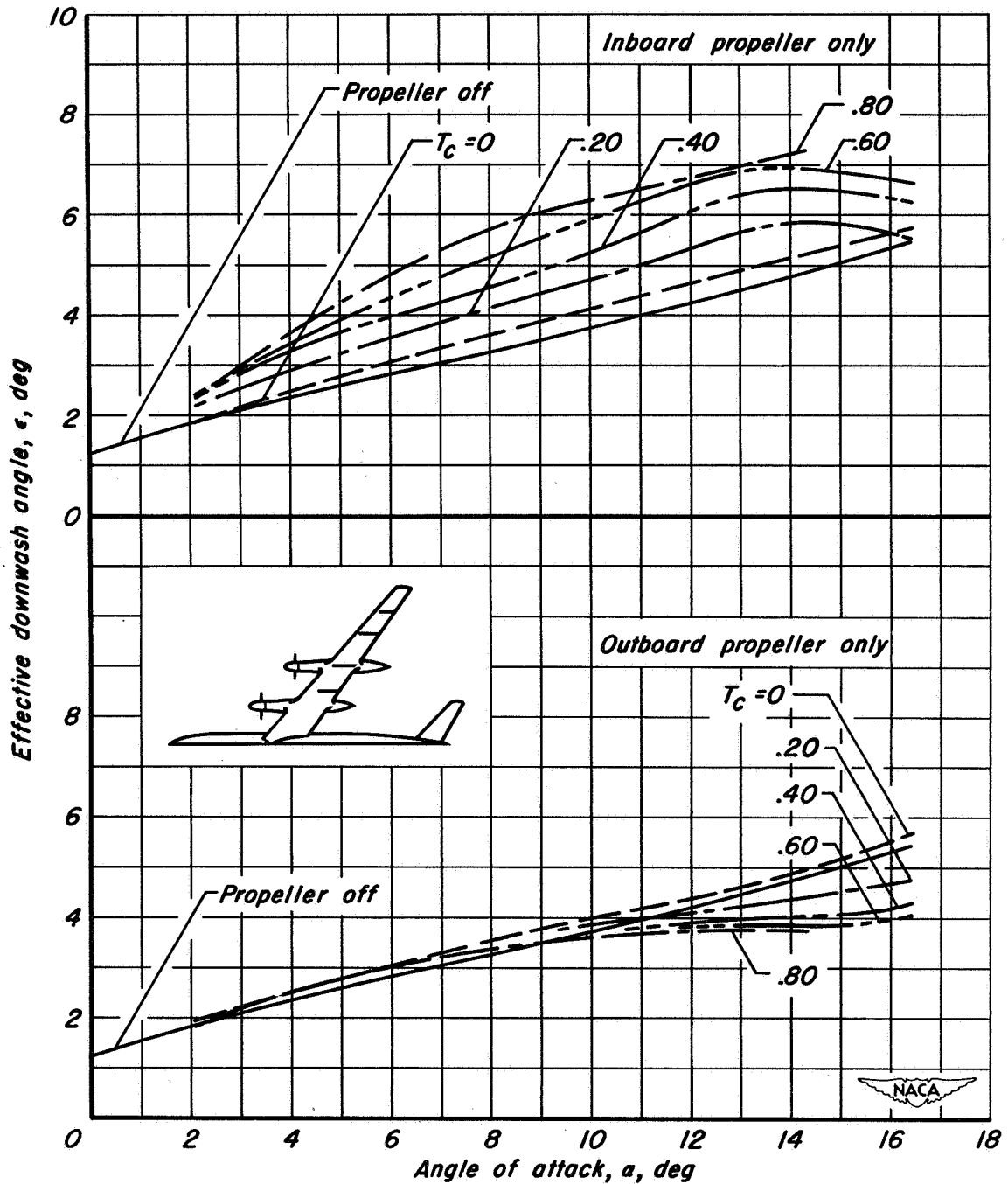
Figure 43.- The estimated effective downwash at the tail due to opera-
tion of each propeller; tail height = 0.10 b/2; flaps up; M = 0.082;
R = 4,000,000; β = 26°.
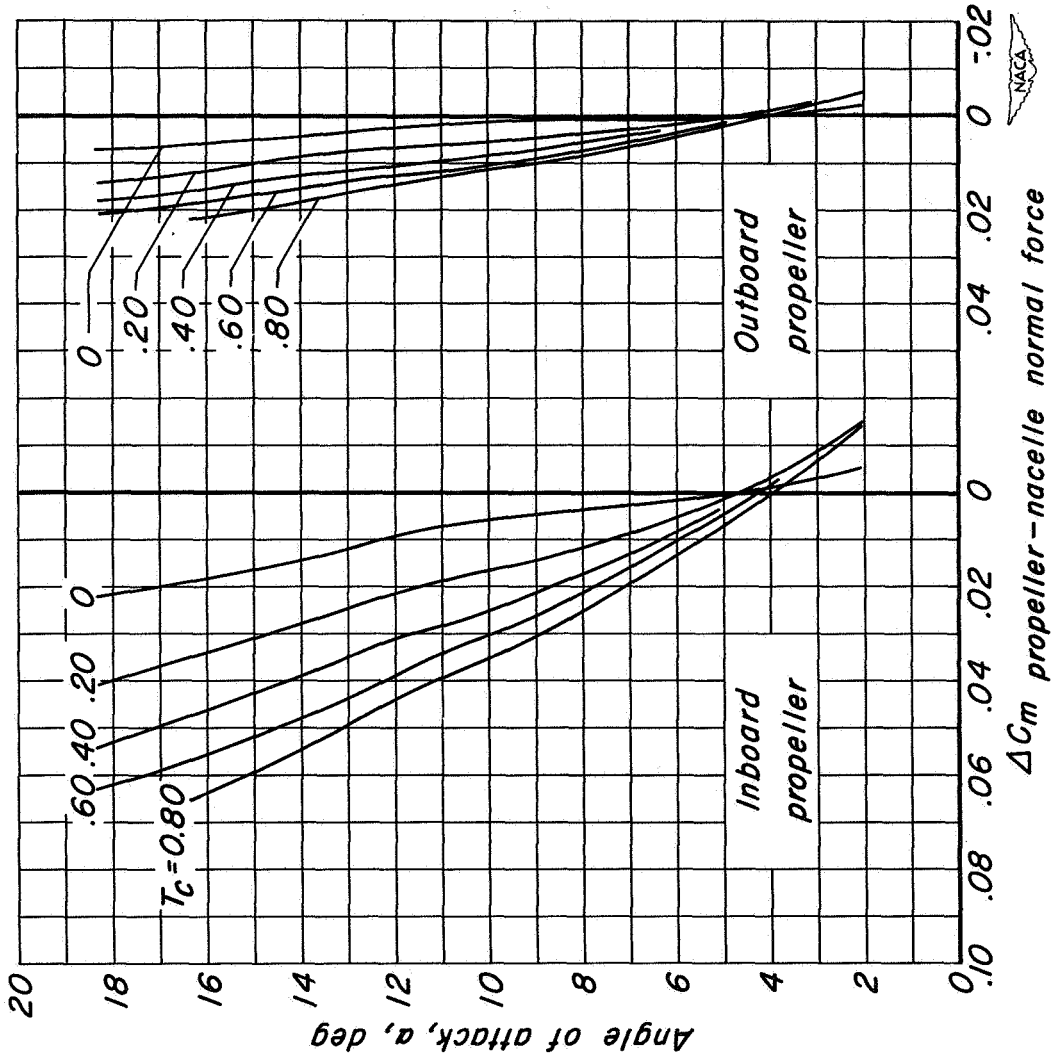
Figure 44.- The estimated increments of pitching-moment coefficient of the model due to the normal force of each propeller with the nacelles moved 0.1 b/2 outboard of their original positions; flaps up or deflected; M = 0.082; R = 4,000,000; β = 26°.
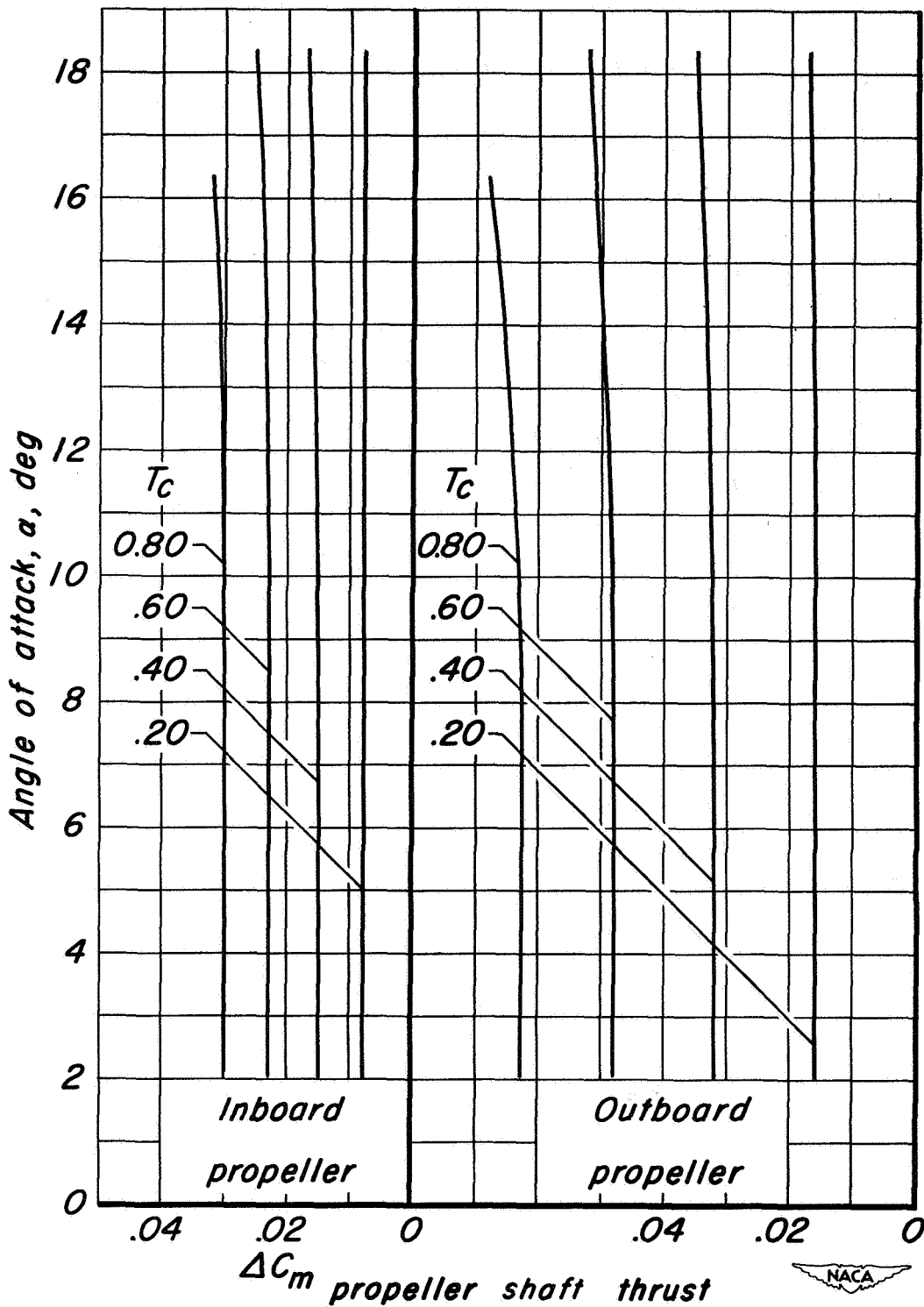
Figure 45.- The estimated increments of pitching-moment coefficient of the model due to the shaft thrust of each propeller with the nacelles moved 0.1 b/2 outboard of their original positions; M = 0.082; R = 4,000,000; β = 26°.
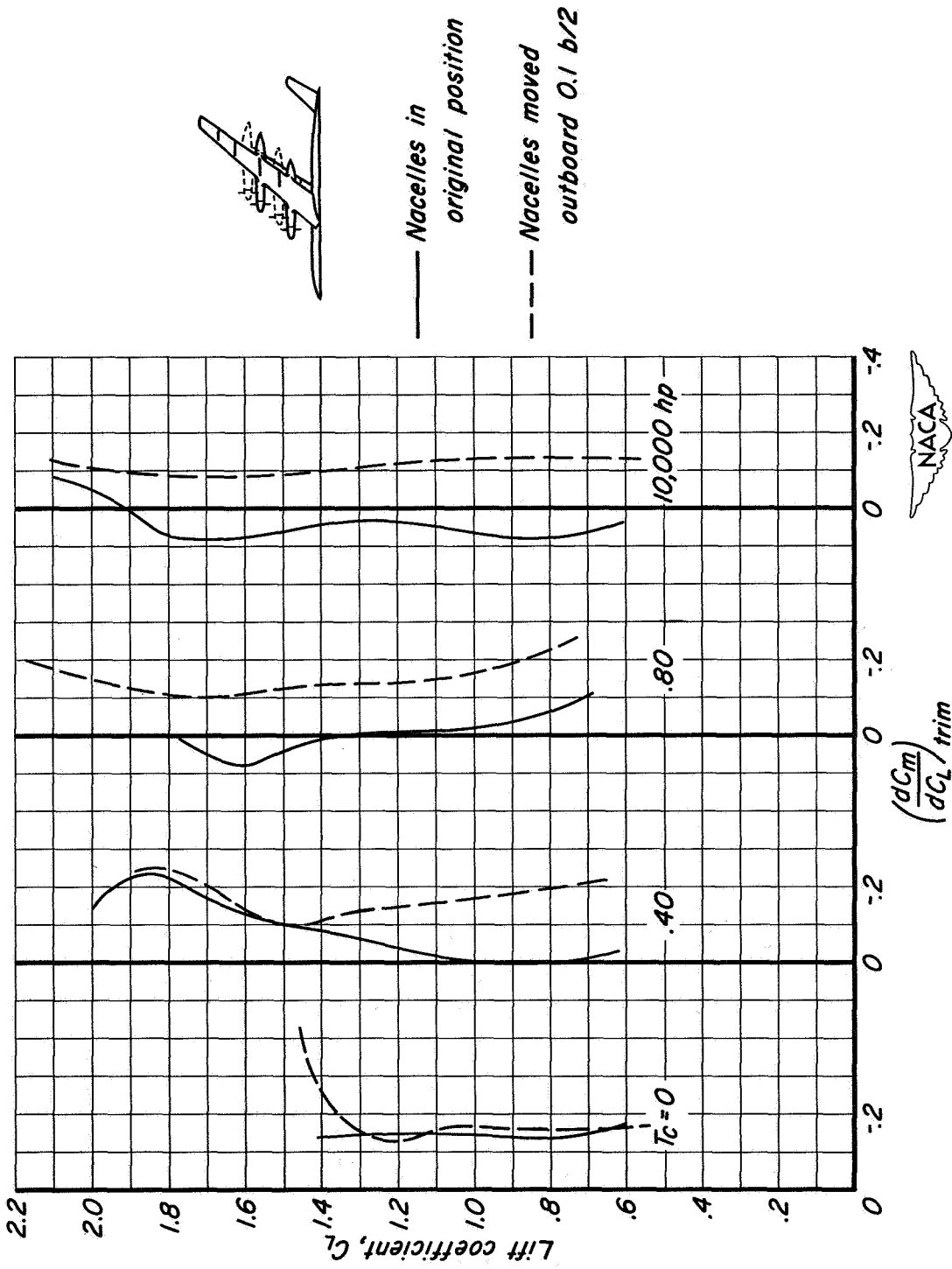
CO███████AL
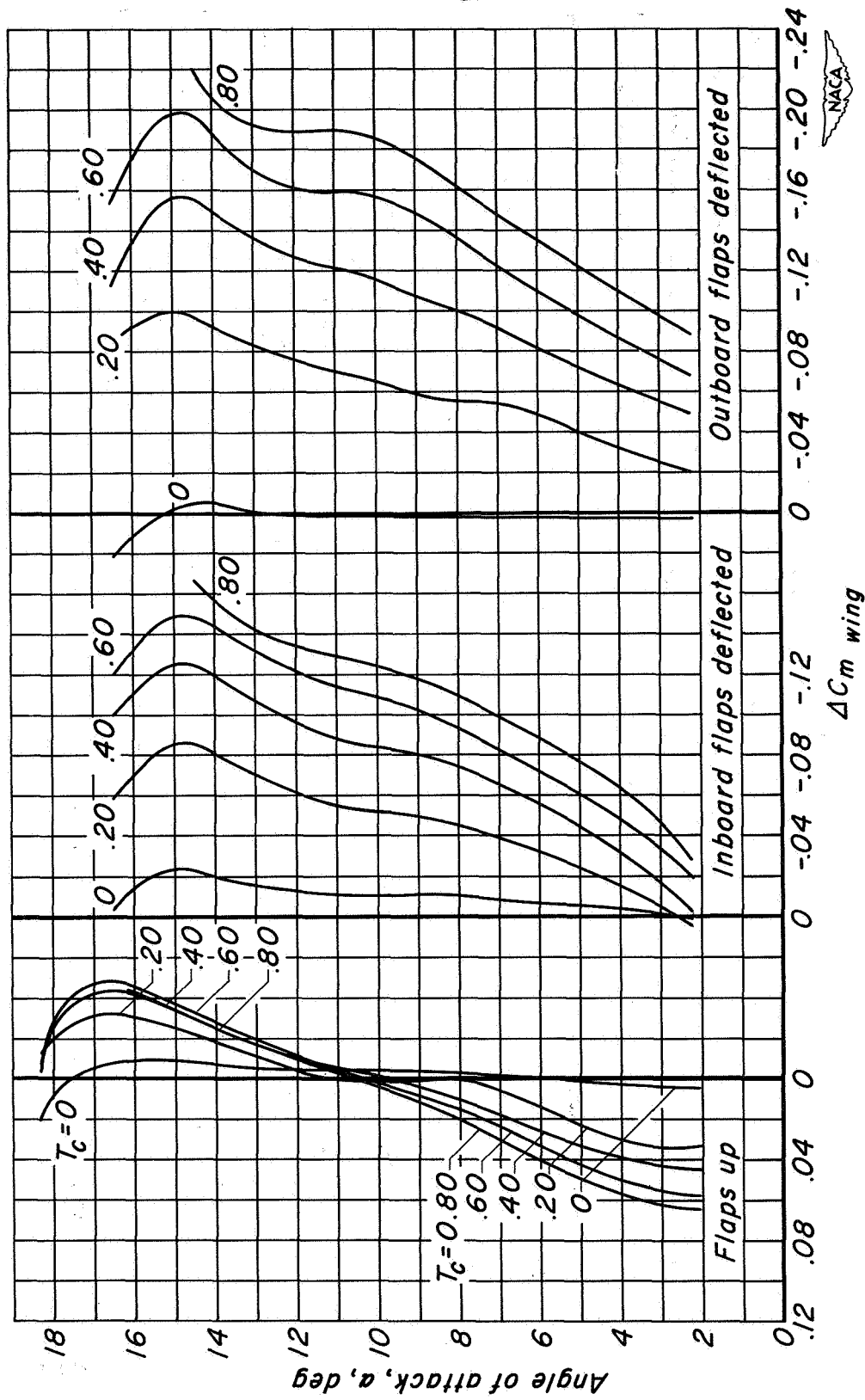
Figure 46.— The estimated increments of pitching-moment coefficient of the model due to the slip-streams on the wing with the nacelles moved 0.1 b/2 outboard of their original positions; M = 0.082; R = 4,000,000; β = 26°.
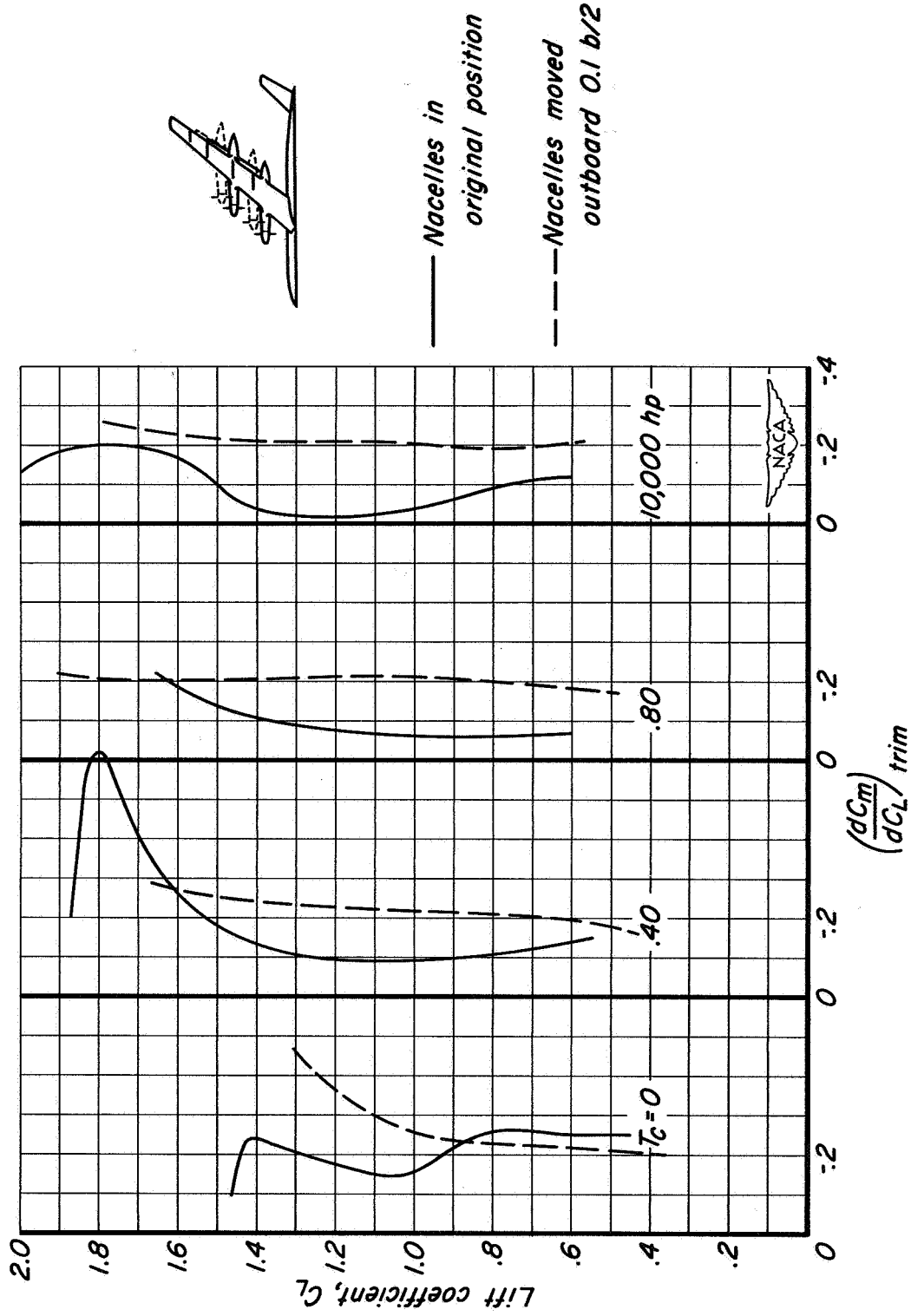
CO███████AL

Nacelles in
original position

Nacelles moved
outboard 0.1 b/2
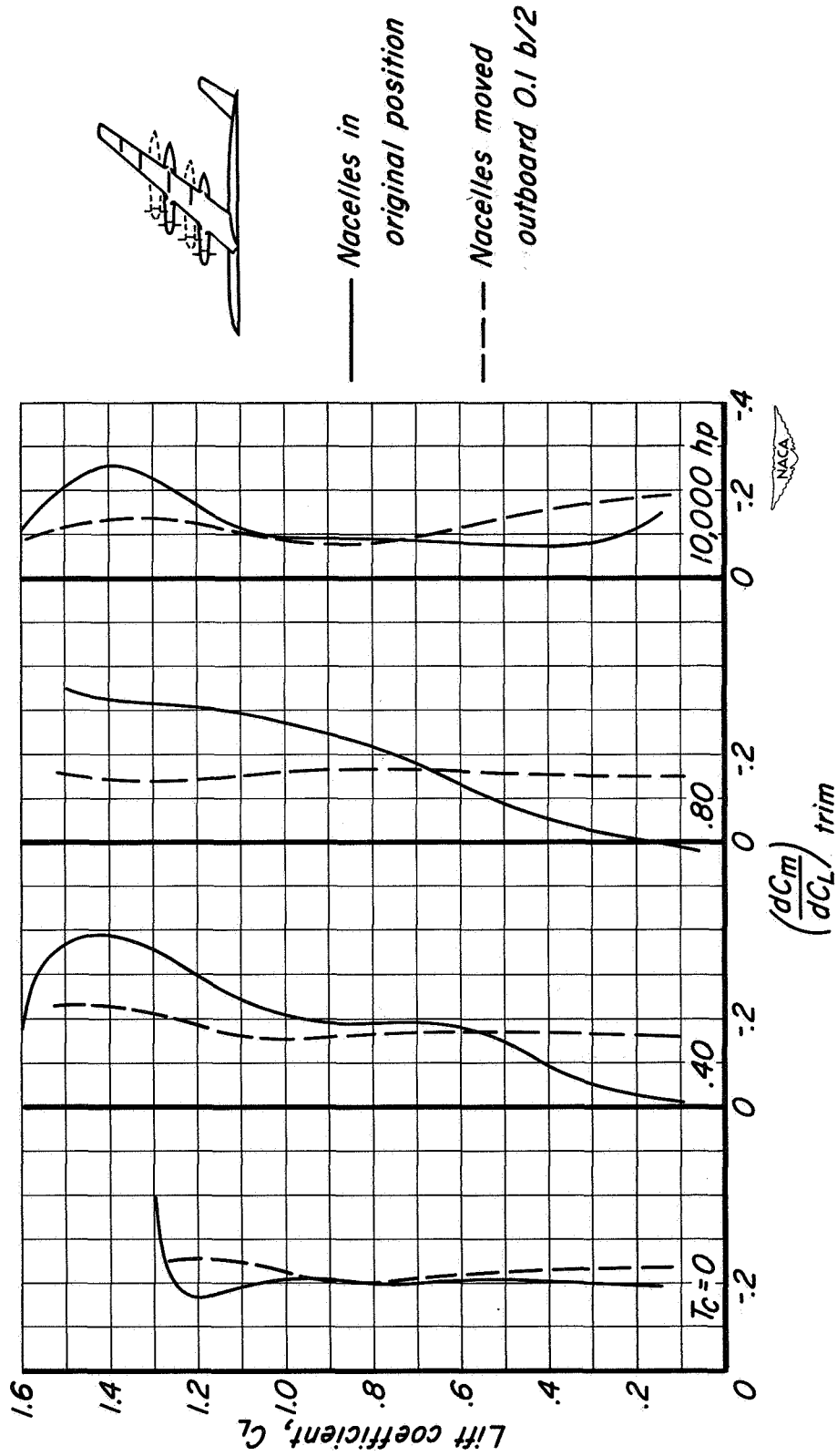
(a) Flaps up.

Figure 47.- The estimated effects on the longitudinal stability of the model of moving the nacelles 0.1 b/2 outbgard of their original positions; tail height = 0.10 b/2; M = 0.082; R = 4,000,000; β = 26°.

(b) Inboard flaps deflected.

Figure 47.- Continued.

Nacelles in original position

Nacelles moved outboard 0.1 b/2

$\left(\dfrac{dC_m}{dC_L}\right)$ trim

Lift coefficient, C_L

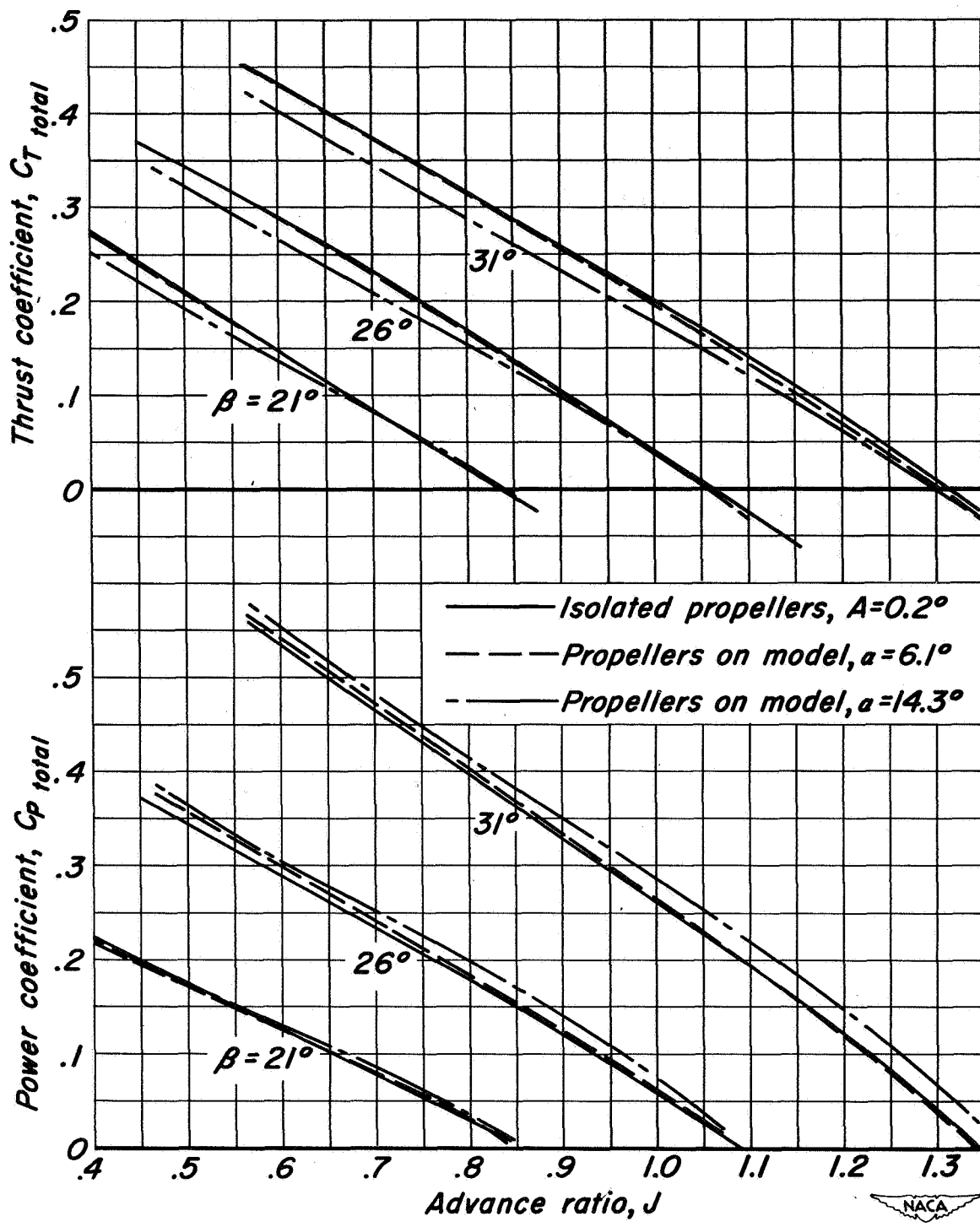(c) Outboard flaps deflected.

Figure 47.- Concluded.
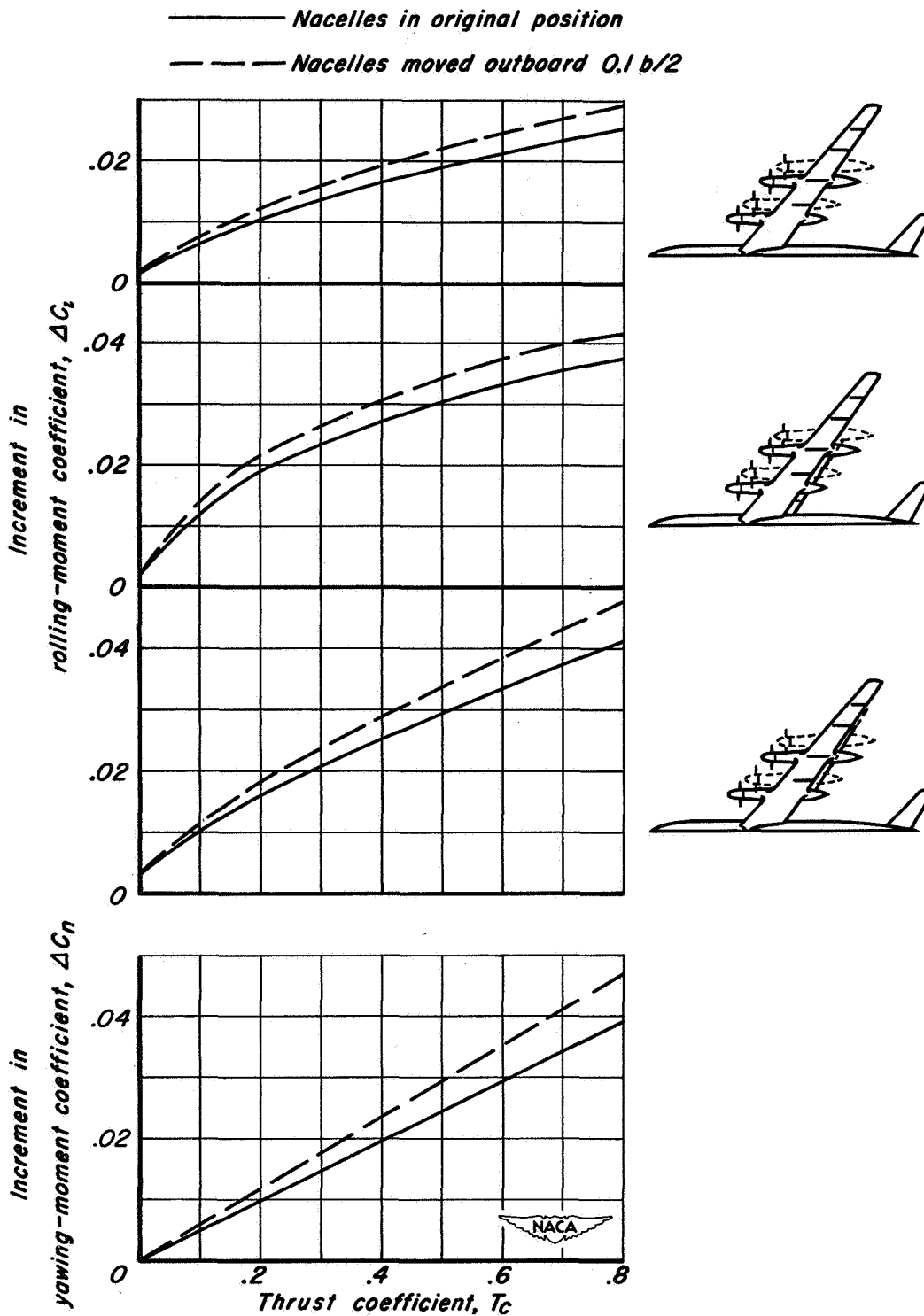
Figure 48.- The estimated increments of rolling-moment coefficient and yawing-moment coefficient resulting from loss of thrust on the right outboard propeller; M = 0.082; R = 4,000,000; β = 26°; α = 14°.
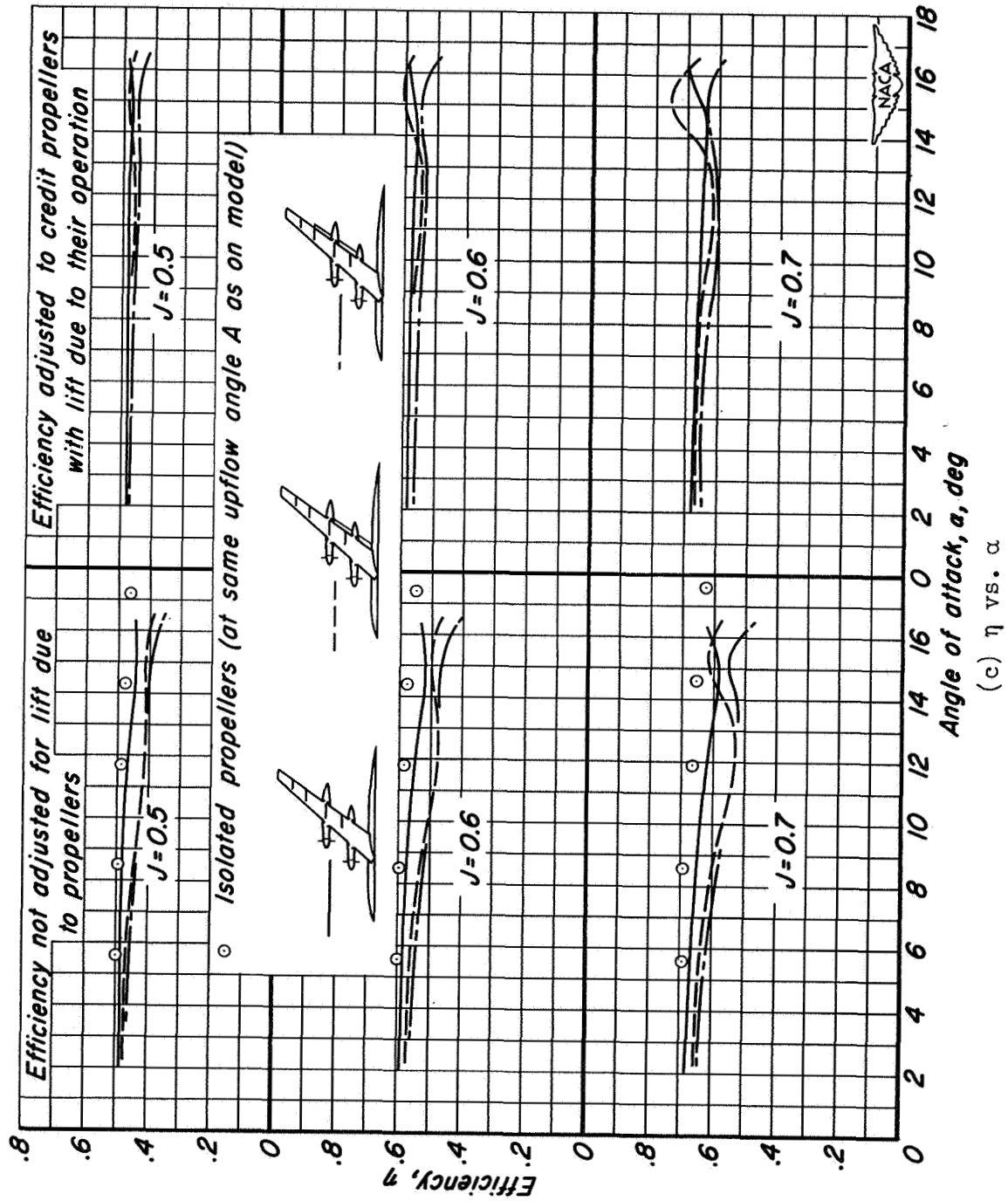
(a) Thrust and power characteristics.

Figure 49.- A comparison of propulsive characteristics of the model with
    isolated-propeller characteristics; tail removed; flaps up; M = 0.082;
    R = 4,000,000.
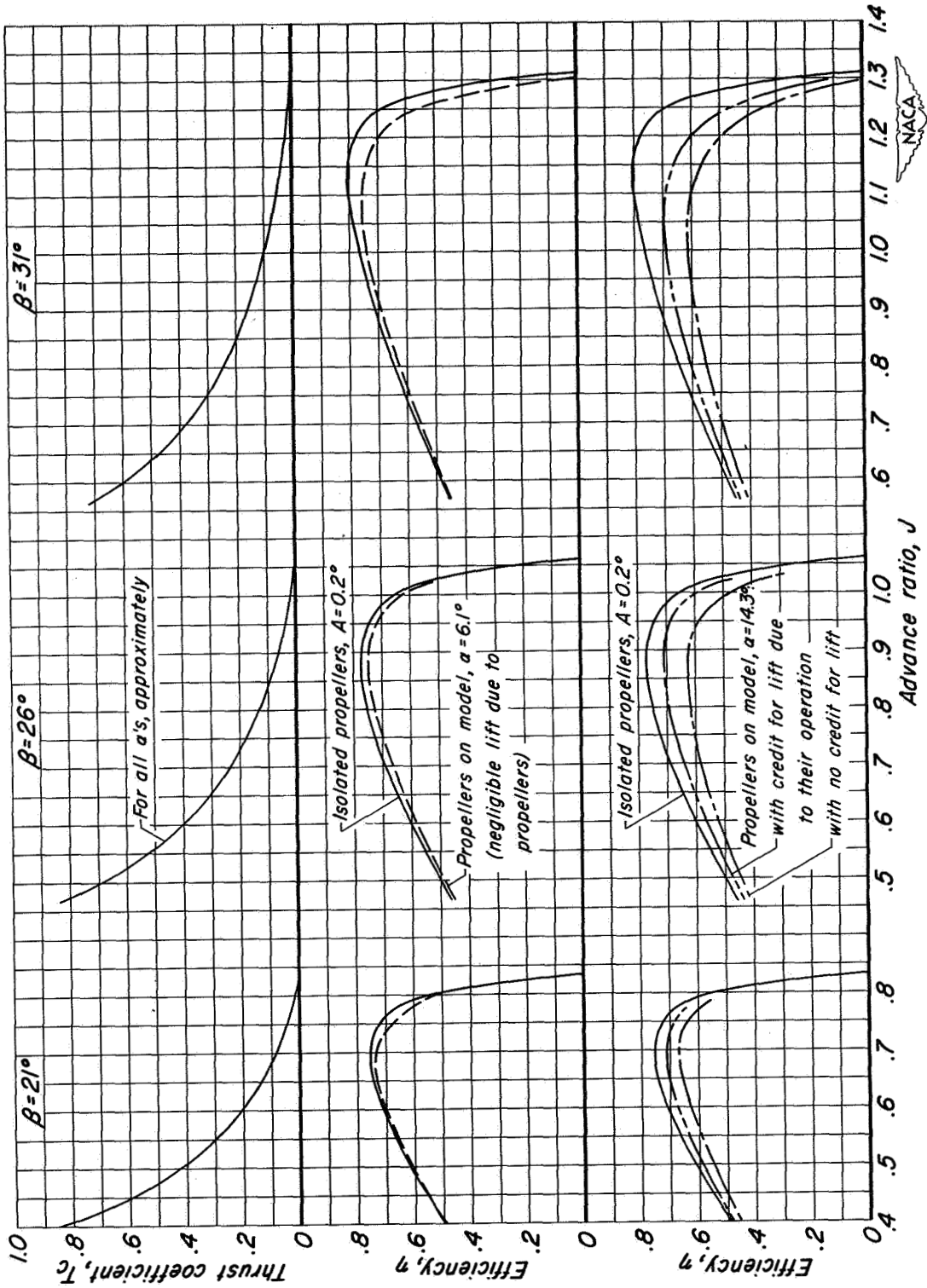
(b) η and T_c vs. J

Figure 49.- Continued.

(c) η vs. α

Figure 49.- Concluded.